

LEABHARLANN CHOLÁISTE NA TRÍONÓIDE, BAILE ÁTHA CLIATH | TRINITY COLLEGE LIBRARY DUBLIN
Ollscoil Átha Cliath | The University of Dublin

Terms and Conditions of Use of Digitised Theses from Trinity College Library Dublin

Copyright statement

All material supplied by Trinity College Library is protected by copyright (under the Copyright and Related Rights Act, 2000 as amended) and other relevant Intellectual Property Rights. By accessing and using a Digitised Thesis from Trinity College Library you acknowledge that all Intellectual Property Rights in any Works supplied are the sole and exclusive property of the copyright and/or other IPR holder. Specific copyright holders may not be explicitly identified. Use of materials from other sources within a thesis should not be construed as a claim over them.

A non-exclusive, non-transferable licence is hereby granted to those using or reproducing, in whole or in part, the material for valid purposes, providing the copyright owners are acknowledged using the normal conventions. Where specific permission to use material is required, this is identified and such permission must be sought from the copyright holder or agency cited.

Liability statement

By using a Digitised Thesis, I accept that Trinity College Dublin bears no legal responsibility for the accuracy, legality or comprehensiveness of materials contained within the thesis, and that Trinity College Dublin accepts no liability for indirect, consequential, or incidental, damages or losses arising from use of the thesis for whatever reason. Information located in a thesis may be subject to specific use constraints, details of which may not be explicitly described. It is the responsibility of potential and actual users to be aware of such constraints and to abide by them. By making use of material from a digitised thesis, you accept these copyright and disclaimer provisions. Where it is brought to the attention of Trinity College Library that there may be a breach of copyright or other restraint, it is the policy to withdraw or take down access to a thesis while the issue is being resolved.

Access Agreement

By using a Digitised Thesis from Trinity College Library you are bound by the following Terms & Conditions. Please read them carefully.

I have read and I understand the following statement: All material supplied via a Digitised Thesis from Trinity College Library is protected by copyright and other intellectual property rights, and duplication or sale of all or part of any of a thesis is not permitted, except that material may be duplicated by you for your research use or for educational purposes in electronic or print form providing the copyright owners are acknowledged using the normal conventions. You must obtain permission for any other use. Electronic or print copies may not be offered, whether for sale or otherwise to anyone. This copy has been supplied on the understanding that it is copyright material and that no quotation from the thesis may be published without proper acknowledgement.

Synthesis, Functionalization and Applications of Silver Nanoparticles



A thesis submitted to the University of Dublin for the degree of Doctor of Philosophy

by

Deirdre Ledwith B.A. (Mod.)

Under the supervision of

Prof. John M. Kelly

School of Chemistry

Trinity College Dublin

Dublin

April 2009

TRINITY COLLEGE
10 AUG 2009
LIBRARY DUBLIN
Thesis
8810

Declaration

I declare that this work has not been submitted as an exercise for degree at this or any other university, and that it is entirely my own work. Due acknowledgements and references are given to the work of others. The library is granted permission to lend or copy this thesis upon request.

To my family

Mam, Dad, David, Sinéad, Louise and John

The aim of the work described in this thesis is to investigate various different methods for synthesis, functionalization and surface-enhanced Raman spectroscopy applications of silver nanoparticles.

The thesis begins with an examination of the methods reported in literature for the synthesis of silver nanoparticles. Particular emphasis is placed on the preparation of anisotropic silver nanostructures. The current accepted explanations of the growth mechanisms associated with each of the different morphologies are also presented.

The thesis continues with a description of the work carried out on the preparation of silver nanoparticles. The synthesis of silver nanoparticles of tuneable colour via a seed mediated method involving trisodium citrate and a polymer such as poly(vinylpyrolidone) (PVP) is described. The effects of different parameters for example time, temperature and concentration of citrate are investigated. The colour of the sols may be tuned by varying the concentration of citrate. Sols prepared at room temperature exhibit a blue- shift of the longitudinal band with time. As the temperature at which the reaction is carried out is increased from room temperature, well-defined triangular plates with enhanced stability are produced. However the procedure does lead to mixture of shapes. Experiments carried out to improve the reproducibility of an existing synthesis of silver nanoparticles developed within the group which employs poly(vinylalcohol), are outlined as are experiments that have been carried out to investigate the importance of including the anionic polymer poly(4-styrene sulfonate) sodium salt (PSSS) during the synthesis of the seed particles.

Various routes for the synthesis of silica coated silver nanoparticles are presented with two new methods for the production of coated particles being developed. Both new methods involve a two-step procedure, initially priming the silver nanoparticle surface followed by growth of the silica shell by a modified Stöber procedure. The primers used are 3-mercaptopropyltriethoxysilane and 1,3-diaminopropane. Using the latter primer, silica shells of tuneable thickness can be produced. The stability of silver nanoparticles is also examined and their functionalization via the layer-by-layer method is also reported.

Finally the use of highly shaped silver nanoprisms as substrates for Surface Enhanced Raman Scattering (SERS) is presented. Large SERS enhancements were found for aggregated silver nanoprisms in solution. The aggregation process, which is vital to the observation of the SERS phenomenon, is monitored by UV-vis spectroscopy and TEM, and in particular the effect of the aggregating agent on the morphology on the nanoprisms used as the SERS substrates is monitored. Maximum SERS intensities are observed when there was an overlap between excitation wavelength and the maximum absorbance of the aggregated substrate.

Acknowledgments

First and foremost, I would like to express my sincere thanks to my supervisor, Prof. John Kelly, for all his guidance and support throughout the past four years. I would also like to thank Dr. Steven Bell in Queen's University Belfast for allowing me to carry out all the SERS measurements in his lab.

To Dr. Margaret Brennan-Fournet and Dr. Patrick Fournet. Thank you for allowing me to spend time writing this thesis when I should have been working away in the lab!

To all the members of the Kelly group, past (Suresh, Aine, Susan, Damian and most recently Sibu) and present (Dave, Ger, Gemma, Kyra, Paraic, Suni and Michael.) What can I say guys?! We've definitely had some memorable experiences!

To the staff of the Centre for Microscopy and Analysis, especially Neal Leddy for all his help with the TEM.

To all the technical staff, especially Patsy, Martin and Brendan and to Fred and Eddie (R.I.P.) in stores.

To my lunchtime buddy Eimear. I don't think I would have made it this far without all those cups of tea!

To my family and my non-chemist friends. Thanks for listening to me raving about things you don't have a clue about! This thesis would not have been possible without all your support.

Finally this research would not have been possible without financial support from Enterprise Ireland and the School of Chemistry.

Table of Contents

List of Abbreviations ..... **viii**

List of Figures ..... **x**

List of Tables ..... **xxi**

List of Schemes ..... **xxiii**

Chapter 1

1. Introduction **2**

1.1 Optical properties of metal nanoparticles **3**

1.1.1 The origin of surface plasmon resonance in metal nanoparticles 3

1.1.2 Effect of size 5

1.1.3 Effect of shape 6

1.2 Characterization of nanoparticles: **7**

1.2.1 Transmission Electron Microscopy 8

1.2.2 Dynamic Light Scattering (DLS) 9

1.2.3 Zeta-potential 10

1.3 Nucleation and Stabilization of nanoparticles **11**

1.3.1 Burst Nucleation and Diffusional Growth Theory 11

1.3.2 Stability of electrostatically stabilized nanoparticles 12

1.3.3 Stability of sterically stabilized nanoparticles 14

1.4 Preparation of spherical silver nanoparticles **14**

1.4.1 Aqueous synthetic methods 14

1.4.1.1 Chemical Reduction 14

1.4.1.2 Physical methods 16

1.4.2 Organic Solvents 18

1.4.2.1 Reduction by the solvent 18

1.4.2.2 Microemulsion methods 19

1.4.2.3 Thiol stabilized nanoparticles 20

1.5 Synthesis of Anisotropic Silver Nanoparticles 22

1.5.1 Nanorods and nanowires 22

1.5.1.1 Aqueous surfactant based methods 23

1.5.1.2 Organic (polyol based) methods 25

1.5.2 Cubes 29

1.5.2.1 Aqueous surfactant based methods 29

1.5.2.2 Organic polyol based methods 29

1.5.3 Other morphologies prepared by the polyol process 31

1.5.3.1 Right Bipyramids 31

1.5.3.2 Nanobeams 31

1.5.3.3 Nanobars and Nanorice 32

1.6. Nanoplates and Nanoprisms 32

1.6.1 Photochemical methods: 33

1.6.2 Thermal methods 37

1.7 Functionalization of Nanoparticles 43

1.8 Applications 47

1.9. Conclusion 47

1.10 References 50

Chapter 2

2. Introduction 60

2.1 Preparation of silver nanoparticles via the 'added citrate' method. 61

2.1.1 Changing the concentration of TSC used in the growth step: 64

2.1.2 Effect of reaction temperature 66

2.1.3 Stability of particles 70

2.1.4 Separation of nanoparticles 74

2.1.4.1 Centrifugation in a sucrose concentration gradient: 74

2.1.4.2 Disc Centrifugation: 76

2.1.5 Summary of the 'added citrate' method 79
2.1.6 Role of poly(vinylpyrrolidone) (PVP) 79
2.1.6.1 Changing the molecular weight of PVP used in the growth step 79
2.1.5.2 Changing the concentration of PVP used in the growth step 80
2.1.7 PVP as an etching agent: 82
2.1.8 Importance of the method of seed preparation 87
2.1.9 Discussion of added citrate method: 90
2.1.9.1 Growth mechanism of particles of controlled shape 92
2.1.9.2 Stability of particles prepared by the added citrate method: 100
2.1.9.3 Effect of Reaction Temperature 102
2.1.10 Conclusion of the 'added citrate' method 104

2.2 The reproducible preparation of PVA stabilized silver sols: 105
2.2.1 Introduction 105
2.2.2 Results: 107
2.2.2.1 Light vs dark 111
2.2.2.2 Method of seed preparation: 112
2.2.2.3 Water quality issues: 115
2.2.3 Discussion of the PVA method: 117

2.3 The importance of PSSS in the preparation of seed particles: 119
2.3.1 No added citrate preparation of silver nanoparticles: 119
2.3.2 Results: 120
2.3.3 Discussion of the role of PSSS: 128

2.4 General Conclusions 130

2.5 References 132

Chapter 3

3 Introduction: 136

3.1 Silica coated silver nanoparticles 136
3.1.1 Results 138

3.1.1.1 Method 1: Ung *et al.* 138
3.1.1.2 Method II: Graf *et al.* 141
3.1.1.3 Method III: Kobayashi *et al* 145
3.1.1.4 MPTES primed method:..... 147
3.1.1.5 1,3-diaminopropane primed method: 148
3.1.1.5 Reproducibility:..... 153
3.1.2 Discussion of the silica coating of silver nanoparticles: 153
3.1.2.1 Stöber chemistry..... 153
3.1.2.2 Methods used for the silica coating of silver nanoparticles 156
3.1.3 Conclusions from the silica coating of silver nanoparticles:..... 160

3.2 Other methods for functionalizing silver nanoparticle: 161
3.2.2 Results 161
3.2.2 Discussion: 170

3.3 General Conclusions on the Functionalization and Stability of Silver Nanoparticles:..... 175

3.4 References: 176

Chapter 4

4.1 Introduction to Surface Enhanced Raman Spectroscopy 179
4.1.1 Factors affecting Surface Enhanced Raman Spectroscopy (SERS)..... 181
4.1.1.1 Electromagnetic enhancement mechanism: 181
4.1.1.2 Chemical Enhancement Mechanism: 182

4.2 Results 184
4.2.1 Preliminary results using 'added citrate' nanoparticles 184
4.2.2 Detailed study using 'no added citrate' nanoparticles 188
4.2.2.1 Part 1: Nanoprisms with λ_{max} between 485-615 nm..... 188
4.2.2.1.1 Crystal Violet 189
4.2.2.1.2 4-Mercaptopyridine..... 191
4.2.2.1.3 Adenine 193

4.2.2.1.4 Adenosine 193
4.2.2.1.5 Comparison with Lee and Meisel colloids 193
4.2.2.1.6 532 nm laser excitation 194
4.2.2.2 Part 2: Nanoprisms with λ_{max} between 510-925 nm 196
4.2.2.2.1 Study of the aggregation process 196
Effect of the addition of 30 μM 4-aminothiophenol: 199
Effect of the addition of 30 μM 4-methylthiophenol and thiophenol: 201
Effect of the addition of 30 μM 4-mercaptopyridine 203
4.2.2.2.2 SERS study 204
Thiophenol (30 μM) 204
4-Methylthiophenol (30μM) 206
4-Aminthiophenol (30 μM) 208
4-mercaptopyridine (30 μM) 210
Ethanol peaks 211
Varying the substrate concentration 212

4.2 Discussion: 213
4.3.1 Discussion of the Preliminary study: 215
4.3.2 Discussion of the Detailed Study: Part 1:
Nanoprisms with λ_{max} between 485-615 nm 216
4.3.3 Discussion of the Detailed Study: Part 2:
Nanoprisms with λ_{max} between 510-925 nm 219

4.4 Conclusions 223

4.5 References 224

Chapter 5

5.1 Chemicals used in the preparation and functionalization of silver nanoparticles. 228

5.2 Instrumentation/Characterization 229

5.3 Preparation of 'added citrate' silver nanoplates 230

5.3.1 Preparation of seed particles 230
5.3.2 Growth from seeds 230

5.4 Acetone precipitation of PVP 230

5.5 Preparation of seed particles by other methods from the literature 231

5.6 Preparation of silver nanoparticles by the PVA method 232
5.6.1 Preparation of seeds 232
5.6.2 Growth from seeds: 232

5.7 Sols prepared by the added citrate method and

PVA method in the presence of PSSS: 232
5.7.1 Preparation of seed particles 232
5.7.2 Growth from seeds: 232

5.8 Preparation of silver nanoprisms by the 'no added citrate' method 233
5.8.1 Preparation of seed particles: 233
5.8.2 Growth from seeds 233

5.9 Silica coating procedures 233
5.9.1 Ung *et al.* 233
5.9.1.1 Preparation of the silver sol: 233
5.9.1.2 Priming of the surface with APTES: 233
5.9.1.3 Coating with sodium silicate: 234
5.9.3 Graf *et al.* 234
5.9.3.1 Synthesis of the particles: 234
5.9.3.2 Synthesis of the Silica Shell: 234
5.9.3.3 Volhard titration 235
5.9.4 Kobayashi *et al* 235
5.9.4.2 Preparation of the nanoparticles 235
5.9.4.3 Coating procedure 235
5.9.5 Mercaptopropyltriethoxysilane (MPTES) primed method 235
5.9.5.1 Preparation of the nanoparticles 235
5.9.5.2 Coating procedure 236

5.9.6: Diaminopropane primed method 236

5.9.6.1 Preparation of the nanoparticles 236

5.9.6.2 Coating procedure 236

5.10 Anion etching experiments 236

5.11 Functionalization with Gelatin 237

5.12 LbL functionalization 237

5.13 Ion exchange of the poly(allylamine hydrochloride) 237

5.14 SERS experiments 238

5.15 References: 239

Chapter 6

6.1 Preparation of silver nanoparticles 241

6.2 Functionalization of silver nanoparticles 242

6.3 Applications of shaped silver nanoparticles 243

6.4 Future work 243

6.5 References 245

List of Abbreviations

ADCA = 1,3-acetonedicarboxylic acid

Ag@SiO_2 = Silica coated silver nanoparticles

APTES = 3-aminopropyltriethoxysilane

AOT = bis(2-ethylhexyl)sulfosuccinate

AR = Aspect ratio

BPEI = Branched poly(ethylenimine)

BSPP = bis(p-sulfonatophenyl)phenylphosphine dihydrate dipotassium salt

CCD = Charge coupled device

CT = Charge Transfer

CTAB = Cetyltrimethylammonium bromide

CTAT = Cetyltrimethylammonium tosylate

CV = Crystal Violet

DDA = Discrete Dipole Approximation

DLS = Dynamic Light Scattering

DMF = Dimethylformamide

DMSO = Dimethylsulfoxide

EDS = Energy Dispersive X-ray Spectroscopy

EDTA = Ethylenediaminetetraacetic acid

EELS = Electron Energy Loss Spectroscopy

EF = Enhancement Factor

EG = Ethylene glycol

EM = Electromagnetic

FT-Raman = Fourier Transform Raman

FWHM = Full width at half maximum

HEPES = 4-(2-hydroxyethyl)-1-piperazineethanesulfonic acid

HOMO = Highest Occupied Molecular Orbital

HOPG = Highly oriented pyrolitic graphite

HRTEM = High Resolution TEM

IR = Infrared

LED = Light Emitting Diode

LSPR = Localized Surface Plasmon Resonance

LUMO = Lowest Unoccupied Molecular Orbital

MHA = 16-Mercaptohexadecanoic Acid

MTP = Multiply Twinned Particles

NIR = Near Infrared

NMR = Nuclear Magnetic Resonance

PAM = Poly(acrylamide)

PCS = Photon Correlation Spectroscopy

PSSS = Poly(styrenesulfonate) sodium salt

PVA = Poly(vinylalcohol)

PVP = Poly(vinylpyrrolidone)

RT = Room Temperature

SAED = Selected Area Electron Diffraction

SDS = Sodium dodecylsulfate

SEM = Scanning Electron Microscope

SERS = Surface Enhanced Raman Scattering

SERRS = Surface Enhanced Resonance Raman Scattering

SPR = Surface Plasmon Resonance

TEM = Transmission Electron Microscope

TEOS = Tetraethyl orthosilicate

TOPO = Trioctylphosphine oxide

TSA = Tungstosilicate acid

TSC = Trisodium citrate

TGA = Thermogravimetric Analysis

UV-vis = Ultraviolet-visible

XPS = X-ray Photocorrelation Spectroscopy

XRD = X-ray Diffraction

List of Figures

Figure 1.1: Diagram depicting the increase in publications on silver nanoparticles in the last decade. Source: Scifinder Scholar December 2008..... **2**

Figure 1.2: Origin of the surface plasmon resonance due to the coherent oscillation of the conduction electrons with the incoming electromagnetic field..... **4**

Figure 1.3: Diagrams depicting the electric field lines of the A) dipole B) quadrupole and C) octupole resonances..... **6**

Figure 1.4: Calculated UV-vis extinction spectra (black), absorption spectra (red) and scattering spectra (blue), depict the effect of nanoparticle shape on the spectral characteristics..... **7**

Figure 1.5: Comparison of the optical set-up of a traditional light microscope and a transmission electron microscope..... **8**

Figure 1.6: Schematic of DLS equipment..... **9**

Figure 1.7: Schematic representation of the concept of zeta potential..... **10**

Figure 1.8: La Mer theory diagram..... **11**

Figure 1.9: Electrostatic stabilization of nanoparticles..... **13**

Figure 1.10: A) Assembly of spherical silver nanoparticles prepared by the microemulsion method on HOPG. B) Sample after annealing at 50°C at atmospheric pressure for 8 days..... **20**

Figure 1.11: TEM image of bimodal superlattice consisting of 8 and 3 nm thiol stabilized silver nanoparticles..... **22**

Figure 1.12: Mechanism proposed for the surfactant directed growth of metallic nanorods. The single crystalline seeds develop facets to which there is differential adsorption of the surfactant. Addition of metal ions and a weak reducing agent leads to preferred growth on the exposed facets
resulting in growth in a one-dimensional fashion..... **24**

Figure 1.13: Reduction of Ag^+ by ethylene glycol produces small nuclei. The structure of these nuclei can fluctuate due to the available thermal energy. As the nuclei grow they become stuck in a given morphology. The morphology of the nanostructures produced depends on the structure of the seed particles..... **26**

Figure 1.14: Schematic depicting the nucleation and growth process of polyhedral nanoparticles..... **30**

Figure 1.15: Bimodal growth. a) TEM image of Ag nanoprisms formed by single-beam excitation b&c) SEM images of stacked type I and type II nanoprism. Note the thicknesses are nearly identical d) Schematic illustrating the fusion process.....**33**

Figure 1.16: The proposed growth mechanism of silver nanoprisms from spherical nanoparticles under photomediated control.....**35**

Figure 1.17: UV-vis-NIR absorption spectra of nanoplates prepared by varying the concentration of seed added a) 0.1 mL b) 0.25 mL c) 0.5 mL d) 1 mL e) 2 mL f) 3 mL. TEM images of sols a-d.....**39**

Figure 1.18: A&B) TEM images of nanoprisms prepared with a) 0.30 mM b) 0.80 mM $NaBH_4$, showing a decreasing in nanoprism thickness on increasing $NaBH_4$ concentration. C) Schematic detailing the preparation of silver nanoprisms.....**41**

Figure 1.19: TEM images of a) bare silver nanoprisms and silica-coated silver nanoprisms with an average shell thickness of b) 15 ± 1 nm, c) 30 ± 2 nm, and d) 45 ± 3 nm, respectively.....**46**

Figure 2.1: a) UV-vis spectrum of seeds prepared by the reduction of $AgNO_3$ by $NaBH_4$ in the presence of citrate. b) DLS measurements of the seeds shown above in a). **62**

Figure 2.2: Structure of ascorbic acid and dehydroascorbic acid.....**62**

Figure 2.3: a) UV-vis spectrum b) TEM image of a typical green sol prepared by the added citrate method given above in Scheme 1. Scale bar is 500 nm.....**63**

Figure 2.4: UV-vis spectra and photograph of different coloured sols prepared by varying only the concentration of TSC in the growth step. TSC concentrations used are A) 0.7 mM; B) 0.35 mM; C) 0.175 mM; D) 0.07 mM; E) 0.024 mM; F) 0.012 mM; G) 0.004 mM. Also included is the chemical structure of trisodium citrate.....**65**

Figure 2.5: TEM images of sols from figure 4 above. a) sol D prepared with 0.175 mM TSC b) sol G prepared with 0.004 mM TSC. Scale bar is 100nm.....**66**

Figure 2.6: TEM images of sols prepared with 0.7 mM TSC at a) room temperature; b) 50°C; c) 100°C. All scale bars shown are 500 nm. d) UV-vis spectra of sols prepared with 0.7 mM TSC at A) room temperature; B) 50°C; C) 100°C immediately after preparation.....**68**

Figure 2.7: TEM image of a single silver trinagular nanoparticle and it's corresponding Selected Area Electron Diffraction Pattern (SAED) **68**

Figure 2.8: Histograms of the shape distribution of particles in sols prepared at room temperature, 50°C and 100°C. Key: Sharp Triangles: well-defined apices, Truncated Triangles: apices missing, Discs: diameter ≥35nm, Small Spheres: diameter ≤35nm, Sharp Triangles: well-defined apices with edge length <35 nm.....**69**

Figure 2.9: FT-IR spectra of particles prepared at RT, 50°C and 100°C in KBr discs. ... **70**

Figure 2.10: UV-vis spectra of the blue-shift experienced by the in-plane dipole resonance of sols prepared at room temperature with 0.7mM TSC, with time. Spectra were taken at 5 minute intervals for 1 hour. ... **71**

Figure 2.11: UV-vis spectra of a sol prepared with 0.7 mM TSC (black) and stored overnight for 24 hours in the dark (red) and in ambient light (blue). ... **72**

Figure 2.12: UV-vis spectra of a red sol prepared with 0.3 mM TSC over a period of one week when additional TSC was added to the sol. ... **73**

Figure 2.13: Plots of the position of the in-plane dipole SPR, of a green sol prepared with 0.74 mM TSC , versus time, in the a) absence and
b) presence of TSC respectively ... **73**

Figure 2.14: Diagram depicting the layering of the various concentrations of sucrose in the centrifuge tube and the separation of the sol after centrifugation. ... **75**

Figure 2.15: UV-vis spectra of the original sol and the fractions after centrifugation in the sucrose gradient. ... **75**

Figure 2.16: Schematic of the disc centrifuge. ... **76**

Figure 2.17: Results of the disc centrifugation of sols prepared by the added citrate method with 0.7 mM TSC at RT and 50°C. ... **77**

Figure 2.18: UV-vis spectra of sols prepared with 0.7 mM TSC at room temperature with PVP molecular weight 10 k (black) and 55 k (red). Spectra taken 1 hour after sol preparation ... **80**

Figure 2.19: UV-vis spectra of sols prepared with 0.7 mM TSC at room temperature with varying concentrations of PVP (from 1 wt% to 0 wt%). Spectra were taken 1 hour after the preparation of the sols. ... **80**

Figure 2.20: UV-vis spectra of silver nanoparticles prepared at room temperature with 0.7 mM TSC using PVA (1wt %). ... **81**

Figure 2.21: UV-vis spectra of sol prepared with 0.7 mM TSC at 50°C redispersed in a) H_2O b) 1 wt% PVP solution over the period of one week. ... **83**

Figure 2.22: TEM images of a sol prepared with 0.7 mM TSC at 50°C redispersed in a) Millipore water b) 1 wt% PVP solution, 1 week after redispersion. ... **83**

Figure 2.23: Relationship between the concentration of PVP used and the magnitude of the hypsochromic shift. Spectra were recorded 24 hours after redispersion in PVP. ... **84**

Figure 2.24: The 400 MHz ^{1}H NMR spectrum in D_2O of a) PVP purified and b) impurity isolated by acetone precipitation.....**85**

Figure 2.25: Stability of particle redipsersed in a) H2O b) purified PVP
c) pink impurity **85**

Figure 2.26: Sol prepared with 0.7 mM TSC at 50°C redispersed in a) H_2O b) N-vinylpyrrolidone c) N-methylpyrrolidone and d) pyrrolidone after 3 days. **86**

Figure 2.27: a) UV-vis spectra of the seeds prepared by the various methods listed above, immediately prior to use. b) UV-vis spectra of the sol grown from these seeds by the standard added citrate room temperature method.....**88**

Figure 2.28: a) UV-vis spectra of sols prepared by the added citrate RT method using 0.7 mM TSC when the seeds are prepared in the presence (black) and absence of PSSS (red). Also included is the chemical structure of PSSS. **89**

Figure 2.29: a&b) TEM images of added citrate sol prepared at room temperature with 0.7 mM TSC, in the presence and absence of PSSS respectively. **89**

Figure 2.30: Histogram of the shape distribution of the sols grown by the added citrate RT method when PSSS is included in the seed synthesis.....**90**

Figure 2.31: A) TEM image of <111> oriented silver nanoprism. B) Electron diffraction pattern of an individual silver nanoprism showing the assigned reflection indices. C) Edge-on-view of silver nanoprisms.
D) Typical XRD pattern for a sample of nanoprisms. **93**

Figure 2.32: Face centred cubic lattice showing
a) {111} b) {100} and c) {110} planes **93**

Figure 2.33: Diagram of a truncated octahedral seed particle **94**

Figure 2.34: a) untwinned or perfect fcc crystal b) single twinned crystal c) pentagonally twinned crystal **94**

Figure 2.35: Chemcial structures of 1) citrate 2) carballylate 3) citramallate
4) isocitrate. **96**

Figure 2.36: A) Silver halide model for a single twin plane containing type A and type B faces. Type A faces contain re-entrant grooves which facilitate the rapid growth of these faces while type B faces consist of a convex like surface. The growth of the nanoprism is arrested when the fast growing type A sides grow themselves out to meet the slow growing type B faces. B) Silver halide model for a particle with two parallel twin planes. The second twin plane causes all six sides to contain A-type faces with re-entrant grooves. This leads to rapid growth in two dimensions as each A-type face regenerates another A-type face adjacent to it as it grows out.....**97**

Figure 2.37: A) TEM image of a stack of vertically oriented silver nanoprisms. B) HRTEM image of the nanoprism on the right hand side of A, showing defect structure. This nanoprism is oriented such that the {110} plane is in the plane of the image, that is, the electron beam is along <110>. C) Analysis of the internal structure of the prism shown in B. A series of intrinsic stacking faults has resulted in a hexagonally close packed pattern emerging and gives rise to an arrangement of atoms that is aligned perpendicular to the surface with a spacing of 2.5 Å. The correct spacing of 2.35 Å has been obtained for the {111} planes and also for the alternative ABAB.... layers of the hcp region.. ..... **98**

Figure 2.38: Schematic presentation of the surface complexation of a nucleophile (N) followed by oxidation of the particle by O_2. ..... **101**

Figure 2.39: Red-shift of the plasmon band on detection of a-IgG. [53] **107**

Figure 2.40: Typical red sol prepared by the a) heating method b) irradiation method described above **108**

Figure 2.41: UV-vis spectra highlighting the irreproducibility of the PVA method upon scaling up the volume at which sols are prepared. **109**

Figure 2.42: UV-vis spectra of sols prepared on a 100 mL scale using the same seeds and the same reagents, again highlighting the irreproducibility of the PVA method. **109**

Figure 2.43: Sols prepared by the PVA method, with the growth step carried out in the dark. **112**

Figure 2.44: Seeds prepared by different methods from the literature. **113**

Figure 2.45: Sols grown by the PVA method, in the dark from seeds above in Figure 2.44. ..... **114**

Figure 2.46: Structure of poly(sodium 4-styrenesulfonate) sodium salt (PSSS). **115**

Figure 2.47: Six different batches of sols prepared under identical conditions, in the presence of PSSS, using six different sets of seed particles **116**

Figure 2.48: A) TEM image of silver nanoprisms prepared with 60 µL seeds B) Normalized spectra of a series of as-prepared samples obtained using different volumes of seed solution: 1) 650 µL, 2) 500 µL, 3) 400 µL, 4) 260 µL, 5) 200 µL, 6) 120 µL, 7) 90 µL, 8) 60 µL, 9) 40 µL, 10) 20 µL **119**

Figure 2.49: Seeds prepared in the a) absence b) presence of PSSS **121**

Figure 2.50: UV-vis spectra of sols prepared from the seeds shown above in Figure 2.49 by the a) added citrate method b) PVA method. **122**

Figure 2.51: UV-vis spectra of the sols prepared by the no added citrate method from the seeds shown above in Figure 2.49. ..... **123**

Figure 2.52: UV-vis spectra of seeds prepared when PSSS was added at various stages throughout the preparation of the seeds. **124**

Figure 2.53: UV-vis spectra of sols prepared from the seeds shown above in Figure 2.52 using the a) added citrate method b) no added citrate method. **125**

Figure 2.54: UV-vis spectra of seeds prepared using different concentrations of PSSS. **125**

Figure 2.55: UV-vis spectra of sols prepared from the seeds shown above in Figure 2.54. The position of the in-plane dipole is given above in Table 2.8 ..... **126**

Figure 2.56: UV-vis spectra of sols prepared from seeds shown above in Figure 2.54 using a modification of the added citrate method in which no TSC was used in the growth step. **127**

Figure 2.57: A) Ag nanoprisms grown from seeds produced with PSSS present. B) and C) Ag nanoparticles grown from seeds produced without PSSS present. Sample consists of nanoprisms of a wide range of sizes and ''spherical'' particles of various sizes with 5-fold symmetry present. D) UV-vis spectra of nanoprisms in (A) grown from seeds produced in the presence of PSSS (grey) and nanoparticles in (B) and (C) grown form seeds produced in the absence of PSSS (black). **126**

Figure 2.58: Chemical Structure of bis (p-sulfonatophenyl) phenylphosphine dehydrate dipotassium salt (BSPP) **130**

Figure 3.1: a) Schematic of the procedure used for the silica coating of silver or gold nanoparticles. b)TEM image of $Au@SiO_2$ prepared by this procedure. **139**

Figure 3.2: Structure of 3-aminopropyltriethoxysilane (APTES) and tetraethylorthosilicate (TEOS). **139**

Figure 3.3: a) UV-vis spectra of sol a various stages during the silica coating procedure. b) TEM image of silver nanoparticles after the coating procedure. **140**

Figure 3.4: a)UV-vis spectra b)TEM image of $Ag@SiO_2$ prepared when the pH of the solution was varied. **141**

Figure 3.5: Schematic of general procedure for coating Ag particles with silica **142**

Figure 3.6: UV-vis spectrum and TEM image of $Ag@SiO_2$ prepared by the method outlined above with 4 mM TEOS. **143**

Figure 3.7: a) UV-vis spectrum and b) TEM image of $Ag@SiO_2$ prepared at 2 mM TEOS. **143**

Figure 3.8: a) UV-vis spectrum and b)TEM image of $Ag@SiO_2$ prepared with 64 μM TEOS. **144**

Figure 3.9: UV-vis spectra before coating of a sol prepared by the added citrate method using 0.7 mM TSC (black) and after the coating procedure as reported by Kobayashi *et al.* **146**

Figure 3.10: Structure of 3-mercaptopropyltriethoxysilane (MPTES). **146**

Figure 3.11: Normalized UV-vis spectra of a sol prepared by the added citrate method with 0.7 mM TSC before (black) and after (red) silica coating using 3-mercaptopropyltriethoxysilane as a surface primer. **147**

Figure 3.12: TEM images of a sol prepared by the added citrate method with 0.7 mM TSC after silica coating using 3-mercaptopropyltriethoxysilane as a surface primer and 1 mM TEOS. **147**

Figure 3.13: Normalized UV-vis spectra of a sol prepared by the added citrate method with 0.7 mM TSC at 50°C before (black) and after (red) silica coating by the method shown above in Scheme 3.1when additional catalyst (DMA) is added. **149**

Figure 3.14: TEM images of silver nanoparticles prepared by the added citrate method with 0.7 mM TSC at 50°C after silica coating. **149**

Figure 3.15: Normalized UV-vis spectra of silver nanoparticles prepared by the added citrate method at 50oC using 0.7 mM TSC before (black) and after coating with 0.5 mM TEOS (red) and 0.25 mM TEOS (blue). **150**

Figure 3.16: TEM images of silver nanoparticles prepared by the added citrate method at 50°C using 0.7 mM TSC after coating with a) 0.5 mM TEOS b) 0.25 mM TEOS. **150**

Figure 3.17: TEM images of a sol prepared by the added citrate method with 0.7 mM TSC at 50°C when diaminopropane a)10 μM b) 20 μM c) 40 μM d) 80 μM and e) 200 μM is used in the coating procedure. **151**

Figure 3.18: The variation in the thickness of silica shell formed as the concentration of diaminopropane primer is varied at constant TEOS concentration. **152**

Figure 3.19: TEM images of the results of the silica coating process as described above when a) ethylenediamine b) diaminopropane and c) diaminobutane were used as primers. **152**

Figure 3.20: Structure of the positively charged poly(allylamine hydrochloride) and negatively charged poly(styrene sulfonate sodium salt). **161**

Figure 3.21: UV-vis spectra taken over the period of 1 day of a green 'added citrate' sol redispersed in 1 mg/mL poly(allylamine hydrochloride). **162**

Figure 3.22: UV-vis spectra taken over the period of 1 day of a green 'added citrate' sol in the presence of NaCl (1 mM). **163**

Figure 3.23: UV-vis spectra taken over the period of 1 day of a green 'added citrate' sol in the presence of NaBr (1 mM). **163**

Figure 3.24: UV-vis spectra taken over the period of 1 day of a green 'added citrate' sol in the presence of NaI (1 mM). **163**

Figure 3.25: UV-vis spectra recorded at 30s intervals over the period of 15 minutes of a sol prepared by the added citrate method (with seeds prepared in the presence of PSSS), a) as prepared tested with NaCl (1 mM) b) stabilized by 0.1 wt% gelatin, tested with NaCl (10 mM). **165**

Figure 3.26: UV-vis spectra recorded at 30s intervals over the period of 15 minutes of a sol prepared by the added citrate method (with seeds prepared in the presence of PSSS) in the presence of gelatin after a) 48 hours b) 96 hours tested with 10 mM NaCl. **166**

Figure 3.27: UV-vis spectra recorded at 30s intervals over the period of 15 minutes of a sol prepared by the added citrate method (with seeds prepared in the presence of PSSS) in the presence of a) 0.1 wt% b) 0.05 wt% and c) 0.01wt% gelatin and left to stand for 4 days, tested with 10 mM NaCl. **167**

Figure 3.28: TEM images of the sols shown above in Figure 3.27 before stability testing with NaCl (10 mM) was carried out. a) 0.1 wt% b) 0.05 wt% c) 0.01 wt% gelatin..... **168**

Figure 3.29: Normalized UV-vis spectra of a sol prepared by the added citrate method from seeds maded with PSSS after functionalization with gelatin (black), nitrate modified PAH (red), PSSS (blue). **169**
Figure 4.1: Schematic of the scattering processes. Adapted from reference [1] **179**

Figure 4.2: UV-vis spectrum of a green sol prepared by the 'added citrate' method using 0.7 mM TSC at room temperature. **184**

Figure 4.3: SERS spectra of the green added citrate sol shown above in Figure 4.2, after aggregation with $MgCl_2$ before (black) and after (red) centrifugation. **185**

Figure 4.4: SERS spectra of crystal violet (5 μM) using nanoparticles before (black) and after (red) centrifugation. Also shown is the structure of crystal violet. **186**

Figure 4.5: Sols prepared by the 'no added citrate' method using, from A-G, 1 mL, 800 μL, 750 μL, 600 μL, 500 μL, 400 μL and 250 μL seeds. **188**

Figure 4.6: a) SERS spectra of crystal violet added to each of the sols shown above in Figure 4.5, after aggregation with $MgSO_4$ b) a plot of the change in intensity of 1173cm^{-1} peak against the initial SPR λ_{max} of each sol c) UV-vis spectra of each of the sols shown above in Figure 4.5 after aggregation with $MgSO_4$. **189**

Figure 4.7: SERS spectra of CV added before aggregation and plot of the change in intensity of 1173cm^{-1} peak against the initial SPR λmax..... **190**

Figure 4.8: SERS spectra of 4-mercaptopyridine (30 μM) using sols from Figure 4.5 as substrates. **191**

Figure 4.9: Plot of the Raman intensity of the 1004 cm^{-1} band of 4-mercaptopyridine in Figure 4.8 against SPR λ_{max}. **192**

Figure 4.10: SERS spectra of adenine using sols shown above in Figure 4.5 as substrates. **193**

Figure 4.11: SERS spectra of 4-cerpatopyridine (30 μM) using Lee and Meisel colloid (black) and $SolG_{615}$ from Figure 4.5 (red) as the substrates..... **194**

Figure 4.12: Normalized UV-vis spectra of sols prepared by the 'no added citrate method' from A-K with 650 μL, 500 μL, 400 μL, 260 μL, 200 μL, 120 μL, 90 μL, 60 μL, 40 μL, 20 μL, 10 μL seeds..... **196**

Figure 4.13: UV-vis spectra of sols A-H after aggregation with $MgSO_4$. **196**

Figure 4.14: TEM images of Sol B520 from Figure 4.12 a) before b) after aggregation with $MgSO_4$ (0.1 M)..... **197**

Figure 4.15: TEM images of Sol H775 from Figure 4.12 a) before b) after aggregation with $MgSO_4$ (0.1 M)..... **197**

Figure 4.16: Normalized UV-vis spectra of sols prepared by the 'no added citrate' method from A-E with 650 μL, 400 μL, 200 μL, 60 μL and 10 μL seeds. **199**

Figure 4.17: UV-vis spectra monitoring the aggregation process of sols in the presence of 4-aminothiophenol (30 μM). Spectra were recorded every 30 seconds for 15 minutes. a)A_{500} b) B_{550} c) C_{590} d) D_{765} e) E_{980} f) TEM image of Sol E_{595} from Figure 4.12 in the presence of 30 μM 4-aminothiophenol.
Red lines indicate the laser excitation wavelength..... **200**

Figure 4.18: a) UV-vis spectra monitoring the aggregation process of $SolD_{590}$ from Figure 4.16 in the presence of 4-methylthiophenol (30 μM). Spectra were recorded every 30 seconds for 15 minutes. b) TEM image of $SolE_{595}$ from Figure 4.12 after aggregation. Red lines indicate the laser excitation wavelength..... **202**

Figure 4.19: a) UV-vis spectra monitoring the aggregation process of $SolD_{590}$ from Figure 4.16 in the presence of thiophenol (30 μM). Spectra were recorded every 30 seconds for 15 minutes. b) TEM image of $SolE_{595}$ from Figure 4.12 after aggregation. Red lines indicate the laser excitation wavelength. **202**

Figure 4.20: a) UV-vis spectra monitoring the aggregation process of SolD590 from in the presence of 4-mercaptopyridine (30 μM) and $MgSO_4$ (0.1 M). Spectra were recorded every 30 seconds for 15 minutes. b) TEM image of SolE595 from Figure 4.12 after aggregation. Red lines indicate the laser excitation wavelength. **203**

Figure 4.21: SERS spectra of thiophenol (30 μM) using the sols from Figure 4.12 as substrates. **204**

Figure 4.22: Raman intensities of the band at a) 1574 b) 1000 cm^{-1} of thiophenol versus the initial λ_{max} of each sol. **205**

Figure 4.23: SERS spectra of 4-methylthiophenol (30 μM) using the sols from Figure 4.12 as substrates, ... **206**

Figure 4.24: Raman intensities of the band at a) 1594 b) 1080 cm^{-1} in 4-methylthiophenol versus the initial λ_{max} of each sol. **206**

Figure 4.25: SERS spectra of 4-aminothiophenol (30 μM) using the sols from Figure 4.12as substrates. **208**

Figure 4.26: Raman intensities of the band at a) 1594 b) 1080 cm^{-1} of 4-aminothiophenol versus the initial λ_{max} of each sol. **208**

Figure 4.27: SERS spectra of 4-mercaptopyridine (30 μM) using the sols from Figure 4.12 as substrates. Sols were aggregated with $MgSO_4$ (0.1M) after the addition of the analyte. **210**

Figure 4.28: Raman intensities of the band at 1004 cm^{-1} of 4-mercaptopyridine versus the initial λmax of each sol. **210**

Figure 4.29: Spectrum of ethanol (3.4M) **212**

Figure 4.30: SERS spectra of 4-aminothiophenol (30 μM) when the concentration of substrate was lowered. Φ denotes the EtOH peaks. **212**

Figure 4.31: SERS spectra of 4-mercaptopyridine (30 μM) when the concentration of substrate was lowered. Φ denotes the EtOH peaks. **213**

List of Tables

Table 2.1: Typical concentrations of TSC used to prepare sols of different colours. **65**

Table 2.2: Mean size of triangular plates prepared at different temperatures **67**

Table 2.3: Comparison of the sizes calculated from TEM and disc centrifugation. **78**

Table 2.4: ^{1}H NMR (400 MHz, D_2O) shifts of the family of pyrrolidone compounds analysed. **87**

Table 2.5: Variables associated with the preparation of silver nanoparticles by the PVA method. **111**

Table 2.6: FWHM of the seeds prepared in the absence and presence of PSSS **122**

Table 2.7: FWHM of the seeds shown above in Figure 2.52. ..... **124**

Table 2.8: FWHM of seeds shown above in Figure 2.54. ..... **126**

Table 3.1: The stability of silver nanoparticles prepared by the added citrate method at 50°C using 0.7mM TSC against various anions. **164**

Table 3.2: Zeta potential measurements of silver nanoparticles at various stages in theLbL coating procedure. **169**

Table 4.1: Assignment of the Raman signals observed in Figure 4.3, from a green added citrate sol prepared at room temperature using 0.7 mM TSC. **185**

Table 4.2: Assignments of SERS signals of crystal violet δ= bending, ν=stretching γ = out-of-plane deformation. **186**

Table 4.3: Assignments of SERS signals of 4-mercaptopyridine from δ= bending, ν=stretching, ring=ring breathing. **192**

Table 4.4: Assignment of the Raman intensities of thiophenol above in Figure 4.21 ... **205**

Table 4.5: Assignment of the Raman intensities of 4-methylthiophenol above in Figure 4.23 ..... **207**

Table 4.6: Assignment of the Raman intensities of 4-aminothiophenol above in Figure 4.25 ..... **209**

Table 4. 7: Assignment of the Raman intensities of 4-mercaptopyridine above in Figure 4.27 ..... **211**

Table 4.8: Enhancement factors calculated by equation 4.2 above for the band at 1000 cm^{-1} in the SERS spectrum of thiophenol (from Figure 4.21).....**222**

List of Schemes

Scheme 2.1: Preparation of citrate stabilized green sol. **63**

Scheme 2.2: The oxidation of citrate to acetonedicarboxylate in the presence of silver ion and heat. **103**

Scheme 2.3: Synthesis of the silver nanoparticles prepared by the PVA stabilized method. **106**

Scheme 3.1: New proposed method for the preparation of silica coated silver nanoprisms..... **148**

Scheme 3.2: Hydrolysis and Condensation reaction of a silicon alkoxide precursor ($R=CH_2CH_3$)..... **154**

Scheme 3.3: Mechanism of the base-catalysed hydrolysis of silicon alkoxide precursor ($R=CH_2CH_3$)..... **155**

Scheme 3.4: Nucleophilic Attack to form siloxane bond in the condensation reaction ($R=CH_2CH_3$)..... **155**

Chapter 1: Introduction

1. Introduction

In recent years there has been an explosion in the interest of silver nanoparticles. This is noticeable by the dramatic increase in the number of publications regarding silver nanomaterials. Metal nanoparticles and in particular silver nanoparticles have proved to be good candidates for use in such areas as optoelectronics[1-3], surface-enhanced Raman scattering (SERS)[4-6] and more recently metal enhanced fluorescence[7, 8]. Controlling the size, shape and surrounding media of metal nanoparticles is important because many of their intrinsic properties are determined by these factors. Particular emphasis has recently been placed on the control of shape because in many cases it allows the properties to be fine tuned with a greater versatility than can be achieved otherwise. It is only within the past decade that it has become possible to control the shape of silver nanoparticles synthesized in solution and numerous methods have been developed. The surface modification of nanoparticles has become an area of rapid development in the past few decades, mainly due to the fact that modification of the nanoparticle surface can significantly alter both the physical and chemical behaviour of the colloid.

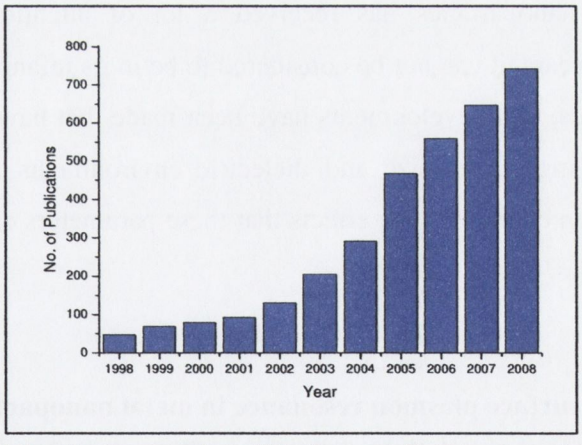


Figure 1.1: Diagram depicting the increase in publications on silver nanoparticles in the last decade. Source: Scifinder Scholar December 2008.

In this chapter approaches to the synthesis of both spherical and anisotropic silver nanoparticles will be discussed. Various different approaches that have been taken to prepare silver nanoparticles of various sizes and morphologies by solution based chemical methods are presented. The advantages of these methods over physical techniques such as

lithography are that no specialized equipment is necessary and scale-up of the procedure is relatively easy. This is important when the possibility of incorporating such nanoparticles into devices is considered. The functionalization of silver nanoparticles, specifically their encapsulation within silica shells will also be discussed. There are a myriad of reasons why the functionalization of nanoparticles is attractive. One of the most important of these is that conjugation of other molecules and biomolecules can be carried out by building on the wealth of knowledge that already exists about the surface chemistry of silica. Finally, some applications of silver nanoparticles will be briefly highlighted.

1.1 Optical properties of metal nanoparticles

It has been known as far back as the Middle Ages that beautifully coloured glass could be produced by adding gold to the melt, with vivid reds and purples being generated. However, it was not until the middle of the 19th century, that the true origin of the observed colours could be explained. Michael Faraday attributed these bright colours to the presence of finely divided colloidal gold.[9] With this in mind although the study of the optical properties of metal nanoparticles has received a lot of attention from the research community in recent years, it can not be considered to be in its infancy. However, it is only in the past few decades, that developments have been made that have enabled noble metal nanoparticles of varying shape, size and dielectric environments to be produced, thus renewing the interest in examining the effects that these parameters can have on the optical spectra of such particles.

1.1.1 The origin of surface plasmon resonance in metal nanoparticles

The optical properties of nanosized metallic particles are significantly different to those of bulk metals. For elements such as Pb, Sn and Cd, absorption bands are present in the UV part of the spectrum and nanoparticles do not display strong colours,[10] while for the noble metals, in particular Ag and Au this absorption is pushed out into the visible part. The origin of such absorption is the interaction of the 'free' electrons of the nanoparticles

with electromagnetic radiation. When the wavelength of light is much larger than the nanoparticle size a situation as depicted below in Figure 1.2 develops.[11] When the light is incident on a spherical particle, the oscillating electric field generates a force on the mobile conduction electrons in the metal. Because there is a Coulombic force of attraction between the electrons and nuclei, the electron cloud oscillates relative to the nuclear framework. The frequency of this oscillation is determined by four factors: the density of the electrons, the effective electron mass and the size and shape of the charge distribution. This collective oscillation of the electrons is called the surface plasmon resonance of the particle and more correctly the dipole plasmon resonance.[12-17] Higher modes of plasmon excitation can also occur. For example, when half the electron cloud moves parallel to the applied field, and the other half moves antiparallel, this is known as the quadrupole mode.[13]

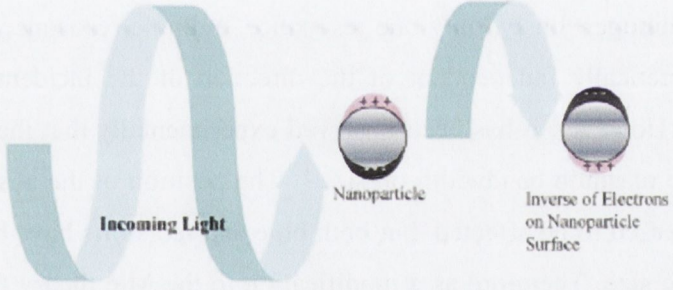


Figure 1.2: Origin of the surface plasmon resonance due to the coherent oscillation of the conduction electrons with the incoming electromagnetic field. Reproduced from reference 11.

Gustav Mie originally presented a solution to Maxwell's equations in 1908, that describes the extinction spectra of small spheres interacting with an electromagnetic field, where extinction = scattering + absorption.[18] This theory is the only simple exact solution to Maxwell's equations that is relevant to particles and remains of great interest to this day. It is given by the following equation:

$$k = \frac{18\pi NV\varepsilon_m^{3/2}}{\lambda} \frac{\varepsilon_2}{[\varepsilon_1 + 2\varepsilon_m]^2 + \varepsilon_2^2} \quad \textbf{Equation 1.1}$$

where k is the extinction coefficient, N is the number of particles, V is the volume of the nanoparticle, λ is the wavelength of the absorbing radiation and ε_m the dielectric constant of

the surrounding medium (assumed to be frequency independent). ε_1 and ε_2 represent the real and imaginary parts of the material dielectric function, respectively. It must be noted that the above equation 1.1 is only valid for small spherical particles and as such is under dipolar limitations. When larger nanoparticles or shaped nanoparticles are under consideration, higher order multipolar resonances become important. This will be discussed further in the following sections.

1.1.2 Effect of size

For small spherical particles (<10 nm), the electric field can be taken to be constant over the entire nanoparticle. This is known as the quasi-static approximation[12]. This model assumes that the response of a metal nanoparticle can be found by first considering the influence of external forces on one free electron alone and then multiplying the effect of the single electron by the total number of conduction electrons. Since the displacement of charges is done homogeneously, only one resonance, a dipole resonance is produced. This resonance is theoretically independent of the direction of the incident light and of the nanoparticle size. However, it has been observed experimentally that there is a strong size dependence of the plasmon bandwidth on size.[12] The position of the absorption maximum has also been observed to be affected, but both blue and red shifts have been reported with decreasing particle size. Therefore as a modification to the Mie theory for small particles, the dielectric function of the metal nanoparticles itself is assumed to become size dependent. This size dependence of the dielectric function is introduced when the diameter of the particle becomes smaller than the mean free path of the conduction electrons.

When the size of the spherical nanoparticle is increased, radiation effects become more and more important. These are also known as retardation effects.[12] As the size is increased, scattering i.e. radiation damping, causes dramatic shifts, broadening and increases of the amplitude of the surface plasmon resonance.[19] The displacement of the electron cloud is no longer homogeneous and higher order resonances are induced[13, 14, 19, 20]. For example for Ag nanoparticles, with an average diameter of 215 nm, dipolar, quadrupolar, octupolar and hexadecapolar resonances have been observed.[21] Higher order multipolar resonances are always located at higher energy with respect to dipolar ones.

Additionally, dipolar resonances can also be red-shifted by the presence of the electric filed generated by the higher multipolar charge distribution.[19]

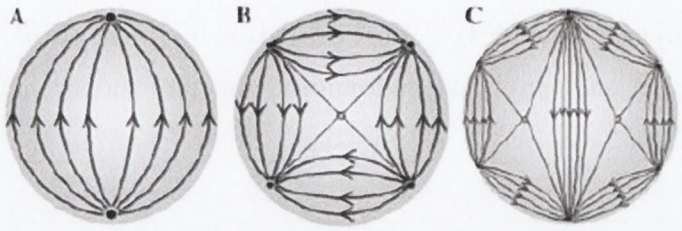


Figure 1.3: Diagrams depicting the electric field lines of the A) dipole B) quadrupole and C) octupole resonances. Reproduced from reference 20.

1.1.3 Effect of shape

One drawback associated with the Mie theory (and the modifications that have been made to include nonspherical particles such as spheroids and infinite cylinders) is that it cannot be used to yield exact solutions to Maxwell's equations, thereby predicting the extinction spectra, of nanoparticles with other arbitrary shapes. In the past few years, numerical methods have been developed which overcome this problem. Such methods include the discrete dipole approximation (DDA), the T-matrix, spectral representation and finite differences methods. The most commonly used method is the DDA. Briefly, this method is based on portioning a particle into a number N, of elementary polarizable units called dipoles. The electromagnetic response of the dipoles to the local electric field is assumed to be known. The field exciting a dipole is a superposition of the external field and the fields scattered by all other dipoles. A system of N linear equations for N linear fields exciting the N dipoles may be written. The numerical solution of this system is used to compute the partial fields scattered by the dipole and thus the total scattered field.[14, 22]

One area in which the DDA method is particularly useful is in determining the optical properties of triangular nanoprisms of silver. Recent advances in colloid chemistry and of lithographic techniques have made it possible to synthesize triangular prisms of silver. However, the distribution of sizes and shape generated so far is fairly broad and many of the particles have missing tips.

Schatz *et al.*[13] have used the DDA method to model spectra for both perfectly triangular particles and truncated triangles. Wiley *et al.* have carried out calculations which illustrate the effect of nanoparticle shape on the optical properties of various shapes of silver nanoparticles (see Figure 1.4).[22] Work carried out by Noguez *et al.* also highlights the influence of shape and physical environment on the surface plasmons of metal nanoparticles.[14, 19, 23]

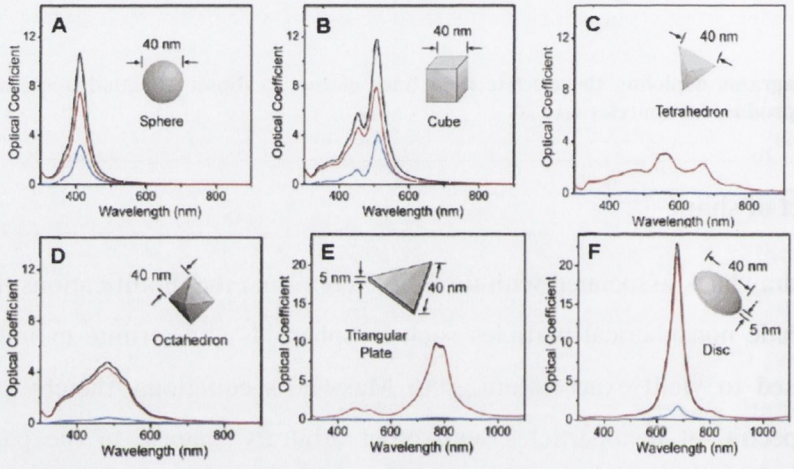


Figure 1.4: Calculated UV-vis extinction spectra (black), absorption spectra (red) and scattering spectra (blue), depict the effect of nanoparticle shape on the spectral characteristics. Adapted from reference 22

1.2 Characterization of nanoparticles:

As already highlighted above, UV-vis spectroscopy is a useful tool for the characterization of silver nanoparticles. However, in order to understand the functional properties of nanoparticles, it is necessary to characterize their structural and surface properties in detail. Since nanoparticles are too small to be visualized with conventional optical microscopes, several experimental techniques have been developed that can be used either simultaneously or by themselves to characterize nanoparticles. These techniques include TEM (transmission electron microscopy), XRD (X-ray diffraction), DLS (dynamic light scattering) and zeta-potential measurements and will be described briefly in the following section.

1.2.1 Transmission Electron Microscopy

TEM is a high spatial resolution structural and chemical characterization tool. The first practical TEM was built in 1938 at the University of Toronto by Albert Prebus and James Hillier[24], but in recent years the technique has been developed so that individual atoms in a crystal lattice can be imaged at resolutions close to 0.1 nm. TEM is based on the interaction of a beam of electrons with a specimen, as it passes through the sample. The image formation process is as follows. The thin sample is illuminated by a parallel (or nearly parallel) beam of electrons. This beam is diffracted by the lattices of the crystal. The diffracted beams are then focussed by the objective lens system.

A modern TEM consists of an illumination system, a specimen holder, an objective lens system, a magnification system, a data recording system and a chemical analysis system.[25] The illumination system is usually composed of a LaB_6 thermionic source or a field emission source. The objective lens system is the heart of the TEM as it determines the limit of image resolution, while the magnification system consists of a series of intermediate and projection lenses which determine the extent of the magnification. The data is collected digitally with the use of a charge coupled device (CCD). Information of the chemical composition of the sample can be obtained by using energy-dispersive X-ray analysis (EDX) of electron energy loss spectroscopy (EELS).

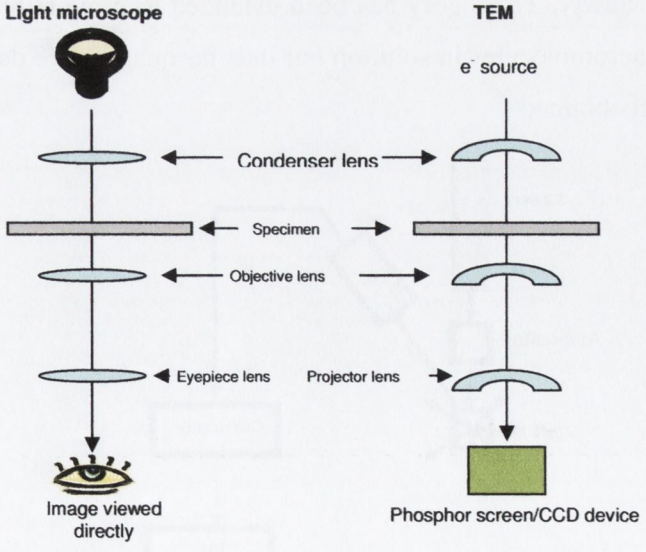


Figure 1.5: Comparison of the optical set-up of a traditional light microscope and a transmission electron microscope.

1.2.2 Dynamic Light Scattering (DLS)

DLS is also known as PCS - Photon Correlation Spectroscopy. This technique measures Brownian motion and relates this to the size of the particles. DLS measures the time dependent fluctuations in the scattering intensity to determine the translational diffusion coefficient. When particles are small compared with the wavelength of light, light is scattered in all directions. If the light source used is monochromatic *i.e.* a laser source, a time dependent fluctuation in the intensity can be observed due to the Brownian motion of the particles. The scattered light undergoes constructive or destructive interference, which is realized by an intensity fluctuation. A size measurement is obtained from an autocorrelation of the intensity trace recorded during the experiment, using the relationship between the size of a particle and its speed due to Brownian motion, defined in the Stokes-Einstein equation.

$$D_H = \frac{kT}{3\pi\eta D} \qquad \textbf{Equation 1.2}$$

where D_H is the hydrodynamic diameter, k is the Boltzmann constant, η is the solvent viscosity and D is the translational diffusion coefficient. The hydrodynamic diameter is defined as 'the size of a hypothetical hard sphere that diffuses in the same fashion as that of the particle being measured.' In simple terms, small particles move quickly while larger particles move more slowly. The theory has been extended to provide limited information about the shape of macromolecules in solution but thus far quantitative data for anisotropic materials has not been obtained.[26]

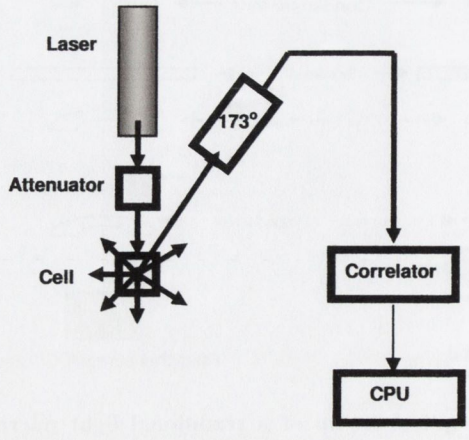


Figure 1.6: Schematic of DLS equipment. Adapted from reference 26.

1.2.3 Zeta-potential

This technique has been coupled with DLS in the Malvern Zetasizer™ system. The magnitude of the zeta potential gives an indication of the stability of the colloidal system. As will be described below in Section 1.3.2, an electrical double layer exists around each particle in solution. The innermost part of this layer is known as the Stern region, where the ions are strongly bound. Outside this, a diffuse layer exists, where the ions are less firmly bound. Inside this diffuse layer there is a boundary, called the surface of hydrodynamic shear or the slipping plane. Ions within this boundary move with the particle when it undergoes Brownian motion, whereas ions outside the boundary do not. The potential that exists at this point is known as the zeta potential.

Particles with zeta potentials greater than +30 mV or less than -30 mV are generally considered to be stable.[27] They tend to repel each other and there is no tendency towards aggregation. However, if the zeta potential of the particles does not meet the above criteria, there is no driving force to keep the particles away from each other and aggregation will occur. As the stability of particles is highly dependent on the pH of the solution, the zeta potential value is also highly dependent on pH. A zeta potential value quoted on its own with a corresponding pH is a meaningless number.

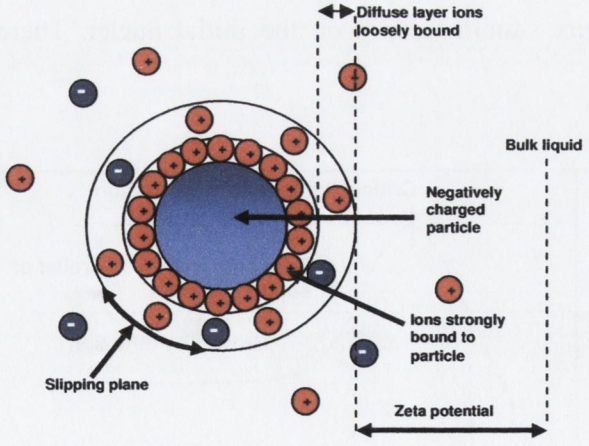


Figure 1.7: Schematic representation of the concept of zeta potential. Adapted from reference 27.

The zeta potential of a colloid is actually measured by applying an electric field across a dispersion of particles. The particles will move towards the electrode of opposite charge with a constant velocity. This velocity or electrophoretic mobility is dependent on four factors; the strength of the electric field, the dielectric constant of the medium, the viscosity of the medium and the zeta potential. The zeta potential can be calculated by the application of the Henry equation,

$$U_E = \frac{2\varepsilon z f(ka)}{3\eta} \quad \textbf{Equation 1.3}$$

where U_E is the electophoretic mobility, ε is the dielectric constant, z is the zeta potential, η is the viscosity and f(ka) is Henry's function (a theoretical approximation based on the size of particles and the dielectric constant of the dispersing medium.)[26]

1.3 Nucleation and Stabilization of nanoparticles

1.3.1 Burst Nucleation and Diffusional Growth Theory

One key theory which explains the nucleation and growth of nanoparticles is the La Mer model.[28] It is based on the premise that the conditions of the chemical reaction must be tailored in such a way that the nucleation event occurs in one short single burst, and that all subsequent growth occurs simultaneously on the initial nuclei. There are three distinct stages to this model.

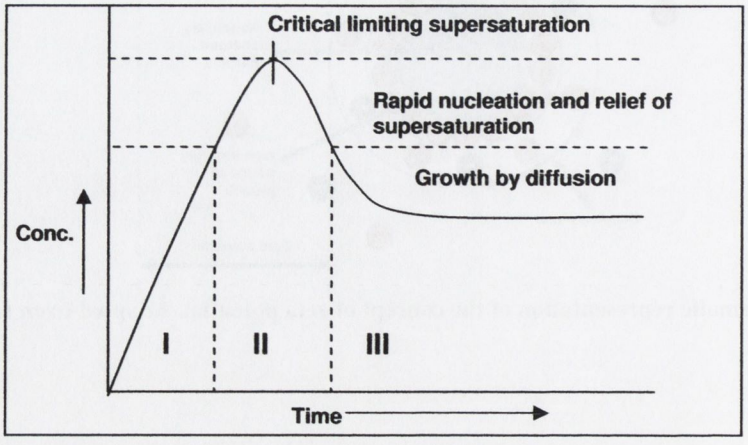


Figure 1.8: La Mer theory diagram. Adapted from reference 29.

During stage I, the concentration of the reactants is increased until some critical concentration is reached. In stage II, nucleation occurs. The degree of supersaturation is high enough to overcome the energy barrier for nucleation, thus resulting in the formation of stable nuclei. The monomer concentration is reduced, because the rate of its consumption resulting from nucleation and growth exceeds supply, until the net nucleation rate is zero. After this, the system enters stage III, in which nucleation is nonexistent and the particles keep growing by diffusion, until all the monomers are consumed.[29]

This process is also known as the burst nucleation process and is characterized by the separation of the nucleation and growth processes of the particles so that highly monodisperse, uniform crystals are produced.[30] One area in which the separation of nucleation and growth has been applied successfully is the seed mediated growth method. In this method, preformed nuclei are introduced into the reactant solution and then monomers are supplied to precipitate on the surface of the existing nuclei. The monomer concentration is carefully controlled so as to suppress a further nucleation process. Growth of the seed particles is then diffusion controlled *i.e.* the growth rate depends solely on the flux of the monomers supplied to the seed particles. In order to produce monodisperse nanoparticles by this method, the seed crystals need to be themselves uniform and monodisperse. Recently Robb and Privman have presented a model for this process which realizes the qualitative explanation of La Mer in a form which allows for a full analytical and numerical treatment of the process.[31]

There are two methods by which the nanoparticles remain as individual particles and are prevented from agglomeration; electrostatic and steric stabilization.

1.3.2 Stability of electrostatically stabilized nanoparticles

The stability of a dispersion of particles depends upon the interplay of repulsive and attractive interactions between the particles. The attractive interaction, V_A, between particles arises form van der Waals interactions, while the repulsive interaction, V_R, can arise either from the electric double layer of charged particles or from the steric repulsion

from an organic layer surrounding the particles. If there is an energy barrier between particles that is greater than ~2kT then the dispersion is stable, otherwise the dispersion is unstable and the particles flocculate out of solution.

Particles that are charged attract ions of the opposite polarity towards the particle's surface to maintain electrical neutrality. The concentration of these ions decays exponentially with distance away from the surface. This is known as the electric double layer.

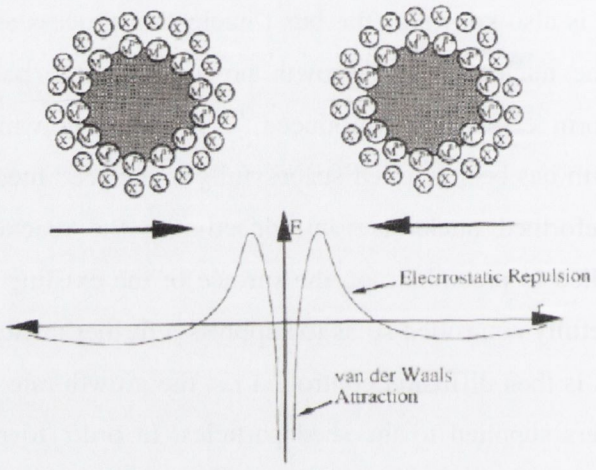


Figure 1.9: Electrostatic stabilization of nanoparticles. Reproduced from reference 32.

The repulsive interaction between two particles, V_R, arises from the interactions between these double layers which includes the repulsion between the like charges on the particles, thus $V_R = V_{ELEC}$. V_{ELEC} decays exponentially with interparticle separation. V_{ELEC} can be decreased by increasing electrolyte concentration and/or increasing the charge on the counter-ions.

$$V_{TOT} = V_A + V_{ELEC} \qquad \textbf{Equation 1.4}$$

A common example of particles that are stabilized due to electrostatic repulsion is negatively charged citrate stabilized gold or silver nanocrystals in water.[32]

1.3.3 Stability of sterically stabilized nanoparticles

An organic monolayer gives rise to a repulsive interaction between particles, called a steric repulsion. There are two contributions to the steric repulsion. Firstly, an osmotic term, V_{OSM}, takes into account the thermodynamics associated with the exclusion of solvent molecules from interdigitating alkane chains on colliding particles (osmotic pressure). This depends greatly on the solvent. Secondly, an elastic term, V_{ELAS}, considers the thermodynamics associated with the loss of possible configurations of the interdigitating alkane chains due to reduced available volume (entropy). The attractive interaction, V_A, between particles arises from van der Waals interactions.

$$V_{TOT} = V_A + V_{OSM} + V_{ELEC} \qquad \textbf{Equation 1.5}$$

A good example of particles stabilized by a monolayer of organic capping ligands is silver nanocrystals capped with dodecanethiol.[32] In the following sections, some approaches that have been taken for the preparation of both isotropic and anisotropic silver nanoparticles will be reviewed.

1.4 Preparation of spherical silver nanoparticles

1.4.1 Aqueous synthetic methods

1.4.1.1 Chemical Reduction

This method was first introduced by Turkevich and co-workers in the early 1950s for the preparation of gold nanoparticles.[33] It basically involves the heating of a dilute solution of $HAuCl_4$ to its boiling point followed by reduction by trisodium citrate. The resulting nanoparticles were very uniform, ca. 20 nm in diameter. This method was further studied by other groups[34-36]. By varying the reaction conditions such as the ratio of trisodium citrate to gold salt, control over the diameter of the resulting nanoparticles could be achieved. The same procedure can be used to reduce silver salt but the particles formed are larger, less uniform, with a greater degree of polydispersity. This has been attributed to the fact that fewer seeds are formed initially and the growth of these seed particles is slow leading to the formation of larger nanocrystals of varying shape and size. Despite this, or

maybe even because of it, this type of colloid is a popular substrate for surface enhanced Raman spectroscopy (SERS).

Another successful procedure is to use sodium borohydride. As it is a strong reducing agent, a larger number of nuclei are formed when it is used to reduce metal salts and therefore the resulting particles are typically small (< 10 nm). Silver nitrate is reduced by sodium borohydride in the presence of trisodium citrate. The citrate acts solely as the capping agent. These particles can then be used as seeds or nucleation centres for the preparation of nanoparticles with larger sizes and different shapes. This will be discussed in further detail below in Section 1.5. Briefly, these seed particles act as catalysts for the reduction of silver ion by weaker reducing agents such as ascorbic acid. The reaction conditions, especially the ratio of seed particles to metal ion, must be controlled carefully so as to avoid any secondary nucleation events. The advantage of using seeding to prepare larger spherical particles is that greater control over the size of the grown nanoparticles can be achieved.

Other reducing agents such as hydrazine[37] and hydroxylamine[38, 39] have been used to prepare spherical silver nanoparticles in aqueous solution. Again, similar to the case of the citrate reduction, particles larger than 20 nm with a high degree of polydispersity were formed. It was reported that poly(vinylpyrrolidone) (PVP) can act as a reducing agent. By varying the ratio of metal salt to PVP, the size and shape of the nanoparticle can be tuned.[40] In addition to this, the reduction process is explained by two main reactions: direct abstraction of hydrogen atoms from the polymer by the metal ion and then reduction of the metal ion by the organic radical formed by the former process. Another mechanism in which the end hydroxyl groups of PVP reduce silver ion has also been proposed by Washio *et al.*[41] Moreover, this mechanism has been used to explain the anisotropic growth of silver nanoplates and is discussed again in Section 1.6.2.

Various sugars have also been used as reducing agents to prepare silver nanoparticles with controllable sizes ranging from 45 to 380 nm.[42] The nanoparticles were prepared by the reduction of the $[Ag(NH_3)_2]^+$ complex with four structurally different

sugars: xylose, glucose, fructose and maltose. It was shown that the size distribution of the resulting particles was strongly dependent on the concentration of ammonia present and also on the nature of the reducing sugar.

1.4.1.2 Radiation based methods

The γ-radiolysis method for the preparation of spherical metal nanoparticles was pioneered by Henglein and co-workers. This technique is based on the formation of hydrated electrons and organic radicals in solutions through γ-radiolysis. These species then act as reducing agents for the metal ions in the presence of trisodium citrate, yielding metal atoms which then coalesce into larger nanoparticles.[43] The nanoparticles formed by this method are typically small, but these small nanoparticles can again be used as seeds to produce larger particles by the same technique.[44] The authors proposed two possible growth mechanisms: the condensation of small silver clusters, and the reduction of silver ions onto silver particles via radical to particle electron transfer.

More recently Liu *et al.* have demonstrated that the quantity and dimensions of the Ag nanoparticles can be controlled by varying the γ-radiation dose applied to the silver nitrate solution with good batch to batch reproducibility.[45] The authors also highlight the fact that the nanoparticles produced are "clean", that is, no polymer or surfactant is required to stabilize them.

In a similar method, the trisodium citrate can be replaced by the polymer poly(vinylpyrrolidone) (PVP). In a study carried out by Shin *et al.*[46], TEM results showed that both the amount and the molecular weight of the PVP in the irradiated solution affect the average size of the nanoparticles produced. A three-step mechanism for the formation of these nanoparticles has been postulated. Firstly the silver ions interact with the PVP, then nearby silver atoms that have been reduced by γ-radiation aggregate to form primary particles. Finally, nearby primary particles coalesce to form larger aggregates which are termed secondary particles.

Another report which involves the use of PVP describes the comparison of silver nanoparticles prepared by γ-radiation and by chemical reduction.[47] It was reported that the γ-radiation strategy produced silver nanoparticles with a narrower size distribution. The final size could also be tuned by varying the concentration of silver nitrate precursor. The chemical reduction method does not allow such ease in tuning the size.

Bogle *et al.* have recently reported a method for the synthesis of silver nanoparticles of different sizes in the range 60-100 nm using electron irradiation of silver nitrate in the presence of poly(vinyl alcohol) (PVA).[48] The process of formation of the silver nanoparticles appeared to be initiated at an electron fluence of approx. 2×10^{13} e cm^{-2}. By varying this electron fluence the size of the nanoparticle could be controlled. Larger nanoparticles (in the 100-200 nm range) could be produced by removing the PVA and thereby promoting coalescence of the particles.

Microwave irradiation has also been used to prepare silver nanoparticles in a paper by Yin *et al.* They describe a method for the large scale production of silver nanoparticles from a silver nitrate and trisodium citrate solution in the presence of formaldehyde as the reducing agent.[49]

A method for the size control of silver nanoparticles involving the UV-irradiation of argentine-tungstosilicate acid solution (Arg-TSA) was recently reported with spherical nanoparticles between several nanometres and several hundred nanometres being produced.[50] This size control is achieved by variation of the reaction conditions such as molar ratio of silver nitrate to TSA, pH and reaction temperature. The authors propose that the Arg-TSA colloidal particles are a new kind of organic-inorganic template for the synthesis of silver nanoparticles with the Arg-TSA complex acting as a UV-switchable reducing agent.

Tan *et al.* have recently reported the UV-assisted reduction of silver ion in polyamine solutions, namely branched poly(ethylenimine) (BPEI), at low concentrations of HEPES that results in the formation of positively charged Ag nanoparticles.[51] It was

reported that the BPEI:silver nitrate:HEPES molar ratio had a dramatic effect on the nanoparticle size. An increase in BPEI:silver nitrate led to a decrease in particle size. The size of the resulting nanoparticles could also be controlled by the BPEI molecular weight, with an increase in particle diameter with increasing molecular weight of the polymer. It is suggested that the formation of the silver nanoparticles involves the oxidative cleavage of BPEI chains, resulting in the formation of fragments with both primary amine and amide groups. During this fragmentation process, formaldehyde is formed and it is this species that reduces the silver nitrate and not the polyamine as has been suggested by others.

1.4.2 Organic Solvents

1.4.2.1 Reduction by the solvent

Pastoriza-Santos *et al.* reported the ability of dimethylformamide (DMF) to behave as a reducing agent. In the absence of any additional reducing agent and even at room temperature, DMF was shown to be able to reduce silver nitrate in the presence of 3-aminopropyltrimethoxysilane (APTES) to yield stable, silver nanoparticles.[52] It was demonstrated that the rate of reduction of silver ions by DMF is strongly temperature dependent. It was also shown that if the reaction was carried out at reflux, the silver nanoparticles were found to be passivated by a thin layer of silica. In a later paper, the same group replace APTES with poly(vinylpyrrolidone) which resulted in the formation of stable, PVP protected silver nanoparticles.[53] This reaction was also carried out under microwave irradiation and it was shown that greater control could be achieved when compared with conventional refluxing. A one pot procedure for the preparation of titania coated silver nanoparticles has also been descibed.[54] Liu *et al.* have also reported the preparation of silver nanoparticles using DMF as the reducing agent. In this case, the authors investigate the effectiveness of various macrocyclic compounds at capping the prepared nanoparticles.[55] They demonstrated that macrocyclic, multidentate thiol ligands are more effective at capping stable silver nanoparticles than monodentate ligands with similar structures, resulting in the production of smaller, more stable nanoparticles.

Dimethylsulfoxide (DMSO) has also been used in the preparation of silver nanoparticles. Very stable capped nanoparticles of average diameters close to 4.4 nm with narrow size distribution were prepared by the addition of silver 2-ethylhexanoate to DMSO in the presence of trisodium citrate.[56] It is proposed that reduction takes place through the formation of a silver-DMSO complex precursor with both DMSO and trisodium citrate acting as reducing agents.

The polyol process, which has been used widely to prepare anisotropic silver nanoparticles (see Section 1.5.1.2), has also been used to prepare stable dispersions of spherical silver nanoparticles.[57] In general, silver nitrate is reduced by ethylene glycol in the presence of PVP. In a recent paper by Kim *et al.*, the experimental set-up in the polyol process was found to be important. For example the precursor injection rate and the temperature ramping rate, were found to be key factors in the production of monodisperse silver nanoparticles.[58].

1.4.2.2 Microemulsion methods

This type of approach is also known as the soft templating method and is typically carried out in aqueous surfactant systems such as cetyltrimethylammonium bromide (CTAB), sodium dodecylsulfate (SDS), or bis(2-ethylhexyl) sulfosuccinate (AOT). The Pileni group, in particular, has carried out significant work in this area. Highly monodisperse silver nanoparticles were produced in the liquid phase which starts from an initial synthesis in functionalized AOT micelles.[59, 60] Size selective precipitation is then carried out using dodecanethiol to cap the particles, with ethanol being added to induce aggregation. In this manner, highly monodisperse samples could be prepared.

Initially it was postulated that due to the very small size of the micelles, they could act as microreactors capable of controlling the size of the particles as well as preventing them from aggregating. In more recent years, the trend of thought has moved away from these micelles behaving as physical templates towards the possibility of them acting as growth directing adsorbates. This will be discussed again in the section dealing with

anisotropic particles. However, the exact nature of the growth mechanism is still a source for debate.

The spherical nanoparticles prepared by the AOT reverse micelle method by the Pileni group have been shown to undergo a morphological evolution.[61, 62] The silver nanocrystals were deposited on a copper TEM grid, covered either by amorphous carbon or highly oriented pyrolitic graphite (HOPG). When annealed at 50°C under atmospheric pressure triangular single crystal nanoparticles were produced. The size of these triangular nanocrystals depends on the initial order of the small spherical nanoparticles on the substrate. The single-crystal size is larger on HOPG than on amorphous carbon as the ordering on the carbon substrate is local whereas it is more extended on the HOPG. In recent years, this microemulsion method has evolved into the use of supercritical fluids for the preparation of silver nanoparticles.[63-65]

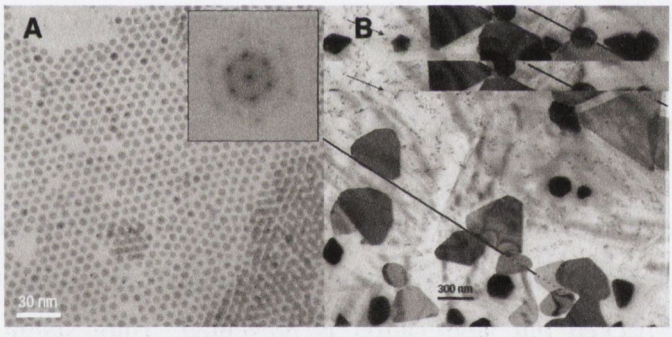


Figure 1.10: A) Assembly of spherical silver nanoparticles prepared by the microemulsion method on HOPG. B) Sample after annealing at 50°C at atmospheric pressure for 8 days. Adapted from reference 61.

1.4.2.3 Thiol stabilized nanoparticles

This method for the synthesis of highly monodisperse gold nanoparticles was first developed by Brust *et al.*[66, 67] It has since been adapted to prepare silver nanoparticles and involves the reduction of silver nitrate by sodium borohydride in a two phase system, in the presence of an alkanethiol and a phase transfer agent such as tetraoctylammonium bromide.[68, 69] Size selective precipitation using a solvent/non-solvent pair can then be carried out to narrow the particle size distribution. A polar solvent is added to the

nanoparticle dispersion resulting in the preferential precipitation of larger particles. This method has received considerable attention because it allowed, for the first time, the easy synthesis of small silver nanoparticles (<10 nm), which could be repeatedly isolated and resuspended in organic solvents without aggregation or decomposition. The other advantage to particles prepared by this method is that the resulting nanoparticles can be treated and handled as common organic compounds. Ligand exchange reactions have been utilized to introduce various different molecules such as thiol functionalized oligonucleotides[70, 71], dithiols[72] and thioalkyated poly(ethylene glycol) compounds bearing amino or alcohol moieties.[73]

A disadvantage of this method, however is that the size of the nanoparticles produced is limited to below 25 nm. Also in some cases the thiol ligands may be hard to displace making further surface functionalization difficult. Other groups have overcome these problems by preparing silver nanoparticles in a single phase process in the presence of alkylamines,[74] fatty acids[75] and carboxylates.[76-79] Nanoparticles up to 32 nm have been prepared and because the ligands are weaker they are easily displaced by thiols bearing whatever functional group that may be required.

An important area of research involving nanoparticles prepared by the methods described above is the assembly of two- and three-dimensional arrays, in which the nanoparticles are closely packed but aggregation is prevented. Thiol stabilized silver nanoparticles in particular tend to spontaneously form highly ordered, hexagonal packed, superlattices when the solvent is slowly evaporated on a suitable substrate.[69, 80-82]

It has been proposed that the hydrocarbon chains of the thiol ligands are necessary in the formation of superlattices through the interdigitation of chains on adjacent particles as the separation of the spheres is linearly dependent on the length of the alkyl chain.[83] Bimodal systems have also been produced in which thiol stabilized silver nanoparticles of 8 and 3 nm formed a two dimensional structure analogous to NaCl crystal structure (see Figure 1.11). Further to this a superlattice containing both gold and silver thiol stabilized nanoparticles has also been prepared.[84]

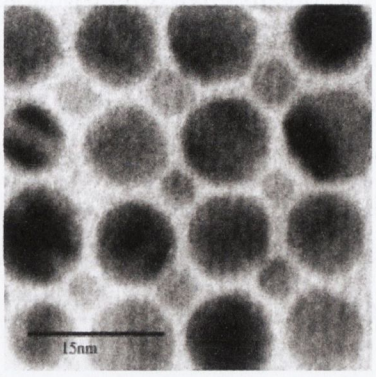


Figure 1.11: : TEM image of bimodal superlattice consisting of 8 and 3 nm thiol stabilized silver nanoparticles. Reproduced from reference 68.

1.5 Synthesis of Anisotropic Silver Nanoparticles

The synthesis of non-spherical silver nanoparticles has attracted a lot of interest in recent years. As already discussed above in Section 1.1.3, the optical properties of silver nanoparticles are strongly dependent on shape. Controlling the morphology of the nanoparticle provides an easy route for controlling the optical properties. In this section general strategies for the synthesis of silver nanoparticles of various morphologies via solution based methods are discussed. For a general review on the shape control of colloidal metal nanocrystals, readers are directed to a recent article by Tao *et al.*[85]

1.5.1 Nanorods and nanowires

To begin with it is necessary to differentiate between nanorods and nanowires. The aspect ratio of a shape is defined as the length of the major axis divided by the width of the minor axis. Nanorods are a class of material that have a width of between 1 and 100 nm and an aspect ratio of greater than 1 but less than 20. Nanowires are similar materials but with an aspect ratio of greater than 20.[86] Although this definition is by no means uniform in the literature it is nevertheless a good guideline to use.

In the following pages, the main focus will be on the preparation of nanorods and nanowires via synthesis in solution. Firstly the surfactant based aqueous method will be

discussed followed by the polyol, organic based preparation. In both of these approaches the most important concept to understand is the preferential binding of an organic species or ion to a specific crystal face, usually a less stable, higher energy face. Calculations generally agree that the sequence of surface energies for low-index facets is $\gamma_{(111)} < \gamma_{(100)} < \gamma_{(110)}$.[87] Therefore the species interacts more strongly with crystal faces such as {100} (and in some cases the {110} if present) promoting growth at the less protected {111} faces and yielding one dimensional structures.

1.5.1.1 Aqueous surfactant based methods

A large amount of work in this area has been performed by the Murphy group,[86, 88-91] with the majority of work being carried out on the synthesis of gold nanowires and rods. Typically, a metal salt of gold or silver is initially reduced by a strong reducing agent such as sodium borohydride ($NaBH_4$) to form spherical nanoparticles. These seed particles are then used to grow the nanorods.

In the presence of more metal salt, surfactant cetyltrimethylammonium bromide (CTAB) and an additional, milder reducing agent such as ascorbic acid, the metal reduced on the seeds grows into nanowires or rods. The surfactant is critical to achieving nonspherical shapes. By changing various different synthetic parameters, control over the aspect ratio can be achieved. For example, the lower the seed to metal ion ratio, the higher the aspect ratio of the resulting material. The final state of the nanocrystals depends on a number of factors working synergistically and dynamically.[92] Thus the nature of the counter-ion, the size of the surfactant head group, the length of the surfactant tail group, the relative concentrations of all the reagents, pH, temperature, and the strength of the reducing agent are all expected to play important roles, although a detailed study has yet to be carried out.

A number of different mechanisms have been proposed to explain the growth of 1D structures from apparently spherical seed particles. Initially it was suggested that the surfactant, cetyltrimethylammonium bromide (CTAB) forms rod like micelles in aqueous

solution, creating dimensionally constrained water pools, which act as microreactors for controlled synthesis.[88, 93] However, more recently it has been proposed that the surfactant molecules potentially bind to specific crystal faces and direct nanocrystal growth in one dimension.[92, 94]

From work carried out on gold nanorods and wires the following has been postulated. The initial seed particles appear to be single crystals. At an early stage in the growth process, the face-centred cubic symmetry of the gold or silver is broken by twinning events that occur to these seeds as the additional metal salt is reduced, to produce multiply twinned particles. At this stage, preferential binding of the surfactant CTAB on the {100} side faces leads to the blocking of these faces and the elongation of the rods.[88, 92, 94]

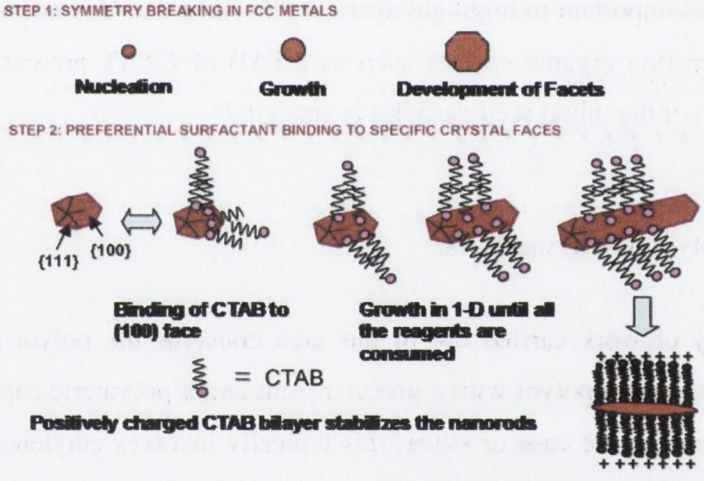


Figure 1.12: Mechanism proposed for the surfactant directed growth of metallic nanorods. The single crystalline seeds develop facets to which there is differential adsorption of the surfactant. Addition of metal ions and a weak reducing agent leads to preferred growth on the exposed facets resulting in growth in a one-dimensional fashion. Adapted from reference 92.

In a similar synthesis, cetyltrimethylammonium tosylate (CTAT) has been used to produce pentagonal silver nanorods.[95] It is worth mentioning here that only seed particles which had a multiple twinned decahedral structure could grow to form rods. In the fcc lattice, the {111} planes have the highest atomic density and are therefore less open to the binding of the hydrophobic ends of the CTAT molecule. The {100} planes have a lower atomic density and the centres of octahedral interstitial sites offer more open sites to pin

surfactant molecules. The {100} faces are passivated by the CTAT molecules leaving the {111} planes, which have the lowest surface energy, accessible to adatoms.

Another mechanism, also coming from the growth of gold nanorods and wires has been suggested by Perez-Juste *et al.*[96] In this case the gold (I) ions are bound to the CTAB micelles and are transported to the growing seed particles. The transport is determined by the double layer interaction and is therefore dependent on the electric field surrounding the particles. The field at the tip of the nanorods is larger, which leads to preferential binding of the ions on the tips, causing elongation of the particles. This mechanism does not explain the initial change in morphology of the seeds and it is suggested that it may be that a stacking fault or twinning plane in the seed is also necessary to create the initial electric field asymmetry. It is important to highlight again at this stage that it is not only necessary to have a shape directing organic species such as CTAB of CTAT present, but that the appropriate structure of the initial seed particles is also vital.

1.5.1.2 Organic (polyol based) methods

The majority of work carried out in this area concerns the polyol process. This synthesis involves heating a polyol with a precursor salt and a polymeric capping agent to generate metal colloid. In the case of silver, this typically involves ethylene glycol (EG), silver nitrate ($AgNO_3$) and poly(vinylpyrrolidone) (PVP) respectively. The ethylene glycol acts as both the solvent and reducing agent. Early work involved the use of platinum seeds[97] but further work found that such seeds were dispensable. When the silver ions are reduced to atoms, they come together to form nuclei. When the nuclei are sufficiently small (<5 nm in diameter), the available thermal energy is enough to cause the structure to fluctuate, allowing defects to form.[98] Twinned crystals are readily formed in silver and gold as well as in silver halides, as the stacking fault energy is lower than in most metals, decreasing the energy required to form a twin plane.[99] Formation of the twin defects is also thermodynamically favoured at small sizes because they enable a greater surface coverage of the lowest energy {111} facets.[100] As the nuclei grow, they become stuck in a given morphology when changes to the defect structure become too costly relative to the thermal

energy. This process results in a distribution of multiply twinned, singly twinned and single crystal seeds, with the five-fold twinned decahedron being the lowest in free energy. These five-fold twinned particles are therefore the most abundant morphology. By manipulating the structure of the seed particles and the growth conditions, one shape of particle can be formed as the dominant product.[101] The possible seed structures are shown schematically below in Figure 1.13

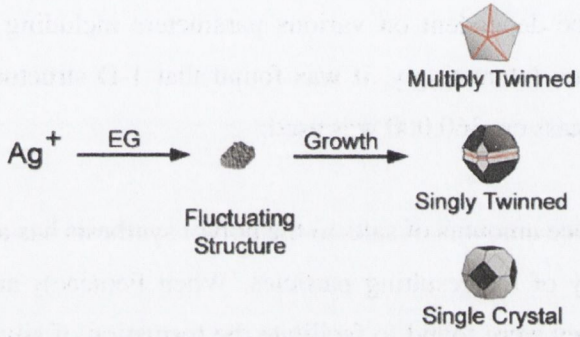


Figure 1.13: Reduction of Ag^+ by ethylene glycol produces small nuclei. The structure of these nuclei can fluctuate due to the available thermal energy. As the nuclei grow they become stuck in a given morphology. The morphology of the nanostructures produced depends on the structure of the seed particles. Adapted from reference 101.

Multiply twinned decahedra are the most chemically reactive of the seed structures listed above.[102] This can be taken advantage of when trying to produce a single dominant morphology and will be discussed in further detail below. Silver atoms add preferentially to the twin defects of the decahedra leading to elongation of the seeds in one direction. As the seeds grow into pentagonal rods, PVP interacts more strongly with the {100} side facets than with the {111} ends.[103] The sides of the nanorods are therefore tightly passivated by the PVP while the ends remain accessible for the addition of atoms.

An additional reason for the one dimensional growth of the decahedral seed particles is that the seed particles are strained. The twin boundaries represent areas of high energy because the preferred angle between them is 70.5° yet 72° is available.[99] This means that there is 7.5° that needs to be filled. This may promote growth at the unpassivated ends in order to reduce the overall surface energy of the crystal.

As mentioned above, it was found that silver nanowires could be produced by the polyol process in the presence of platinum seeds. In a recent paper by Tsuji *et al.*, using Pt seeds, the polyol method was carried out under microwave irradiation instead of reflux conditions.[104] Although the product of this reaction was a mixture of both one dimensional nanorods and wires and three dimensional spherical and triangular-bipyramidal particles, the reaction time was considerably shorter, taking just minutes, and the 1-D and 3-D structures could be separated easily by centrifugation. The final morphology of particles produced was found to be dependent on various parameters including concentrations of reactants and heating time. Interestingly, it was found that 1-D structures were favoured when PVP with a molar mass ca. 360,000 was used.

The addition of trace amounts of salts to the polyol synthesis has also been shown to influence the morphology of the resulting particles. When $Fe(acac)_3$ and $Fe(NO_3)_3$ were added to the synthesis, they were found to facilitate the formation of silver nanowires.[105] It was deduced that the Fe(II) added directly to the preparation or resulting from the reduction of Fe(III) by ethylene glycol acted as an efficient oxygen scavenger, preventing the etching of the multiply twinned particles by atomic oxygen and thus favouring the production of silver nanowires. It is proposed that the higher number of defects on the surface of twinned particles lead to their greater activity for oxidative etching. In a similar manner CuCl and $CuCl_2$ were found to facilitate the formation of the nanowires.[106] In this case both the chloride anion and copper cation were found to be necessary for the successful formation of the wires, whereas the role of the counter-ion (be it nitrate or acac) in the Fe case discussed above was found to be negligible. The Cu(I) acts in a similar manner to the Fe(II), as an oxygen scavenger, while the chloride ion helps to reduce the initial concentration of Ag(I) , effectively acting as a sink and controlling the rate of release of Ag(I), thereby promoting the formation of the more stable multiply twinned seed particles.

Work carried out by Chen *et al*, also highlights the role of additives in the polyol process.[107] Silver nanowires with adjustable diameters were synthesized by introducing certain control agents into the conventional polyol process. These control agents were classified into three groups: inorganic anions, metal cations and molecules. The authors

presume that these species influence the size of the initial seed by forming silver salt colloids or by varying the rate of silver ion reduction.

In another variation on the polyol process, Zhang *et al.* have recently described a steel-assisted method for the production of silver nanowires.[108] It is proposed that *in situ* acidic etching of multiply twinned particles by nitric acid is one of the most harmful factors affecting the preparation of silver nanowires by the polyol process. By including the steel pieces in the synthesis, the nitric acid generated *in situ* is decomposed. Consequently the MTP seed particles are not etched and the yield of nanowires is increased.

To investigate the nature of the interaction of PVP with nanowires and rods, the nanowires were incubated in a dilute solution of 1,12-dodecanedithiol for 1 hour and then with gold nanoparticles (prepared by the Turkevich method) for 10 hours.[103] The dithiol molecules allow the gold nanoparticles to attach to the surface of the Ag nanowires. It was found that the Ag nanowires were decorated with the Au nanoparticles only on their ends but not on their sides, suggesting that the PVP interacts more strongly with the {100} [109] faces than with the {111} faces. Further investigations were carried out by other groups using FT-Raman, XPS and TGA to elucidate the spatial conformation of the PVP molecules on the surface of the nanowires.[109, 110] Results indicate that one monolayer of PVP is probably adsorbed on the surface of the nanowire through Ag-O coordination. Results from SERS indicate the skeletal chain of the PVP is lying on the surface of the nanowire and the pyrrolidone ring might be tilted on the surface of the Ag nanowire.

1.5.2 Cubes

1.5.2.1 Aqueous surfactant based methods

To the best of our knowledge there is only one aqueous synthesis of silver nanocubes in the literature.[111] It involves the reduction of Ag^+ with glucose in the presence of the surfactant cetyltrimethylammonium bromide (CTAB). This reaction occurs in one pot and there is no separate seeding step. The CTAB is the key ingredient in this procedure. The final morphology of the particles is strongly dependent on the ratio CTAB:Ag^+. It is proposed that firstly, the bromide ion (from the CTAB) combines with the silver ion to produce AgBr. This AgBr effectively acts as a reservoir for Ag^+, maintaining a low concentration in solution. Secondly, the CTAB stabilizes the higher energy {100} faces (similar to the way PVP does in the polyol synthesis of silver nanowires. Lastly, it stabilizes the prepared nanocubes and prevents agglomeration.

1.5.2.2 Organic polyol based methods

As in the synthesis of nanowires, the key to producing highly monodisperse nanocubes is controlling the structure of the seed particles during the initial nucleation stage of growth. As mentioned in Section 1.5.1.2 above, the polyol process results in a distribution of multiply twinned, singly twinned and single crystal seeds being formed. When trace amounts of salts are added to this process, the structure of the seeds can be controlled.[22, 102, 105, 112-116] Twinned particles are more active towards oxidative etching due to the greater density of surface defects present.[115] These particles are dissolved and a situation develops where this oxidative etching competes with the reduction of Ag^+ by the ethylene glycol. This competing reaction slows down the rate of nucleation, favouring the formation of single crystal seeds.

These single crystal seeds have a cubooctahedral geometry, which means they consist of a mixture of {111} and {100} faces. The higher energy {100} faces are stabilized by the preferential binding of PVP to them, promoting growth on the {111} faces.[117] Again the structure of the initial seed, as well as the presence of an organic species capable of

specifically binding to one face is of vital importance. The PVP here is acting in a similar manner to when it is used to prepare silver nanowires. However cubooctahedral seeds will not grow to form 1D structures, under the same conditions and herein lies the difference between the two polyol procedures.

The final morphology of the cubes produced, that is, whether they are truncated or not depends on the kinetics of the reduction process.[22] Sharp cubes are formed when the reduction rate is relatively fast. These cubes are bounded almost entirely by {100} facets and are the most kinetically favoured shape. When the reduction rate is reduced, truncated cubes are the dominant product. These cubes take longer to form because time is required for surface reconstruction to occur. The driving force behind surface reconstruction is the need to reduce the surface coverage of the high energy {100} faces by replacing them with the lowest energy {111} facets on the corners. These truncated cubes are the most thermodynamically favoured shape.

In modification of the synthetic procedure described above, Tao *et al.* have reported a procedure in which nanocrystals with regular polyhedral shapes, bounded entirely by either the {100} and {111} faces are produced.[118] In this case the metal salt is reduced by a diol solvent at near reflux temperatures in the presence of PVP. By extending the polyol reaction for a given period of time, cubes, truncated cubes, cuboctahedra, truncated octahedra and octahedra can be obtained in high yield as shown in the schematic below in Figure 1.14.

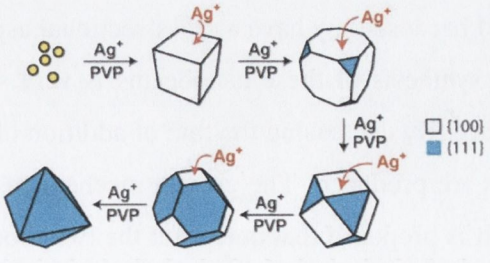


Figure 1.14: Schematic depicting the nucleation and growth process of polyhedral nanoparticles. Adapted from reference 118.

It may be mentioned that the authors state that the stability of both {100} and {111} planes in the presence of PVP, especially for the cubooctahedral and octahedral particles indicates that shape control may not be explicitly dictated by the capping polymer. Preferential growth is favoured by a kinetically limited equilibrium influenced by the reaction conditions.

1.5.3 Other morphologies prepared by the polyol process

1.5.3.1 Right Bipyramids

This novel type of nanostructure consists of two right tetrahedra placed base-to-base and are formed from seeds with a single twin. To selectively produce seeds with a single twin plane, the extent of etching is controlled. In fact, the only difference between the synthesis of these right bipyramids and those that produce wires and cubes as discussed above is the incorporation of Br^- instead of Cl^- or Fe^{3+}. Br^- is less corrosive than Cl^-, so there is enough etching to remove the multiply twinned seeds, while those containing only a single twin remain intact. Growth then continues as with the previous nanostructures. The PVP binds preferentially to the {100} surfaces thereby promoting growth on the {111} faces. The presence of the single twin plane is significant because it is the only factor that differentiates the bipyramid synthesis from that of the nanocube.[119]

1.5.3.2 Nanobeams

Single twinned crystals can also be grown into nanobeams. This type of silver nanostructure is so named because they have a cross-sectional aspect ratio similar to that of a beam of wood.[120] The synthesis of these nanobeams is very similar to that of the right bipyramids described above. By decreasing the rate of addition of silver atoms to the single crystal seeds, nanobeams are produced. The growth mechanism of these nanostructures is not fully understood but it is proposed that defects at the twin boundary provide favourable sites for atomic addition. If there was a greater density of defects on one side of the seed particle, beams could be produced.

1.5.3.3 Nanobars and Nanorice

The final type of nanostructure that can be prepared by the polyol synthesis to date is nanobars. Unlike rods, the nanobars are single crystals bounded by the {100} faces. In essence they are elongated cubes displaying the sharp corners and edges of a cube. These nanobars are produced by increasing the concentration of Br^- added to the synthesis. The question as to how the single crystal seeds grow anisotropically has not been answered fully but it is suggested that all multiply twinned and single twinned crystals are etched away by the Br^-.[121] In addition to promoting the production of the single crystal seeds, oxidative etching could cause anisotropic growth if it removed material from one side of the seed more than the others. It is also possible that due to the increased concentration of Br^-, AgBr is formed, and that this has a critical effect on the growth as has been suggested in the growth of silver nanoplates. In a post synthetic step, the corners and edges of the nanobars can be rounded to transform them into nanorice, by immersing them in a solution of PVP.

1.6. Nanoplates and Nanoprisms

Nanoplates, a term which includes nanodisks and nanoprisms, are a classification of material in which the lateral dimensions are larger than their height. Nanoprisms in particular, usually have an equilateral triangle shape. In recent years, they have received considerable attention due to the ability to tune the position of the in-plane dipole SPR across the entire visible spectrum and into the near-infrared region, by controlling the edge length and thickness.

In general, the synthetic approaches used to prepared silver nanoplates can be split into two categories: photochemical and thermal. There are advantages and disadvantages associated with both procedures. The photochemical methods have prepared probably the most monodisperse, highest quality samples but the process usually requires days for completion. Thermal methods, while rapid, often produce samples with a large range of shapes and sizes.

1.6.1 Photochemical methods:

The first report of the photochemical preparation of silver nanoprisms was published in 2001 and consists of a photoinduced method for converting large quantities of silver nanospheres into triangular nanoprisms on exposure to a white light source.[122] This method consists of photoconverting citrate-capped Ag spherical nanoparticles (<10 nm) into larger triangular particles (edge length ~100 nm) through the irradiation of the small seeds with visible light in the presence of bis(p-sulfonatophenyl)phenylphosphine dihydrate dipotassium salt) (BSPP). The exact mechanism is a subject of some controversy. It was suggested that the BSPP plays an important part in a two step process, where the initial Ag seeds are converted into small clusters concurrently with the formation of small nanoprism. These small nanoprisms then grow at the expense of the small clusters through a light induced Ostwald ripening process. When all the spherical particles and small nanoclusters are consumed the reaction is terminated. However, the presence of BSPP was not found to be vital as when it was replaced by PVP similar results were obtained. Further to this, Sun and Xia claim that it is in fact the presence of citrate ions that promote this morphological evolution.[123]

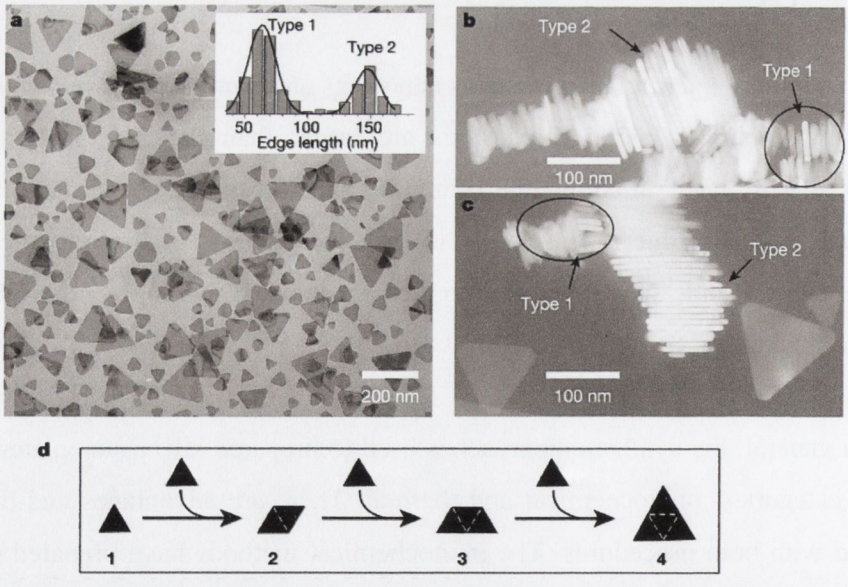


Figure 1.15: Bimodal growth. a) TEM image of Ag nanoprisms formed by single-beam excitation b&c) SEM images of stacked type I and type II nanoprism. Note the thicknesses are nearly identical d) Schematic illustrating the fusion process. Reproduced from reference 124.

A deeper understanding of this process was gained through subsequent experiments carried out by Jin *et al.* using narrow band light sources.[124] It was found that the excitation wavelength controlled the particle size, so that when longer wavelengths were used, particles with a larger edge length were produced. In this work, dual beam illumination was used. When excitation with a single wavelength was carried out, a bimodal distribution of nanoprism size was produced (Type I and Type II nanoprisms). These two types of nanoprism can be seen in Figure 1.15 above. This situation also arises when an inappropriate secondary beam was chosen. The observed bimodal growth process occurs through an edge selective nanoprism fusion mechanism with four type I nanoprisms coming together in a step-wise fashion to form a type II nanoprism and is shown schematically above. When excitation of the samples with a secondary light source (corresponding to the λ_{max} of the in-plane or out-of-plane quadrupole SPR) was carried out, nanoprism fusion was suppressed and only a unimodal growth process was observed. Nanoprisms with a monodisperse size distribution are produced. Recently, the same group has reported that this process can be controlled by adjusting the pH.[125]

The suggested growth mechanism for the photoconversion process is that the secondary beam excitation suppresses the fusion of preformed type I nanoprisms, by inducing charge redistribution on the particles surface caused by the excitation of the dipole plasmon. (It was also suggested that plasmon excitation could facilitate ligand dissociation at the particle edges where the local fields are the most intense allowing type I prisms to grow.) It is therefore easy to see how this nanoprism fusion process might also be controlled by pH, in that electrostatic repulsive forces encountered by the nanoprisms may be tuned by varying the pH.

Building on this work, the most recent paper from the Mirkin group concerning a mechanistic study of photomediated triangular silver nanoprism growth, suggests that the photochemical process is driven by a silver redox cycle.[126] This involves the reduction of silver nitrate on the surface of the seed particles and the concomitant dissolution of some seed particles facilitated by BSPP. The small seed particles and the BSPP act as a buffer to the keep the Ag^+ concentration constant, which facilitates the deposition of silver ion on the

seed particle surface under photochemical control. In effect, the seed particles serve as photocatalysts. Dipole interaction favours the formation of silver nanoprisms with well defined tips, by localising energy at the tips thereby promoting growth at the tips. Quadrupole excitation facilitates the growth of truncated prisms as the energy is localised on the edges instead of the tips. Higher concentrations of silver ion can promote the growth of the thickness of the prism. It is proposed that, when the Ag^+ concentration is increased a thermal process is favoured over the photochemical process and as a result there is significant silver deposition on the {111} faces of the prism. This mechanistic study was carried out using single beam excitation, as described above. The use of secondary beam excitation has not yet been fully investigated.

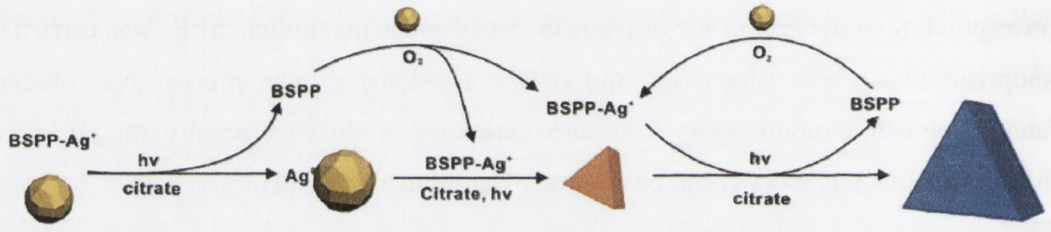


Figure 1.16: The proposed growth mechanism of silver nanoprisms from spherical nanoparticles under photomediated control. Reproduced from reference 126.

Another mechanism for the photoconversion of spherical seed particles into nanoprisms has been proposed by Callegari *et al.*[127] In this case, a two step irradiation process is involved. Initially, the seed particles are irradiated by a conventional fluorescent tube for one hour. Then different illumination conditions are assigned by fitting coloured glass filters in front of the fluorescent tube. According to this mechanism, in the initial irradiation period large spherical particles are formed by the aggregation of the smaller seed particles, when the excess borohydride present is photooxidized creating weak attractive forces around the Ag seeds. In the second irradiation period, light induces coalescence of these loose aggregates into solid particles with subsequent growth. The transformation from aggregated into solid particles works by excitation of the SPR, with the illumination conditions determining the end size of the nanoprisms.

Recently, Bastys *et al.*, have used LED illumination to prepare silver nanoprisms with high absorption coefficients well within the near infrared red region.[128] Similar to previous work, illumination wavelength was observed to determine particle edge length. The mechanism proposed is different to those discussed above in that although the Ag nanoprisms are formed via the consumption of seed particles, Ostwald ripening is not thought to play a role as no incomplete triangular plates are evident during the growth process. The type I/type II nanoprism fusion mechanism is also ruled out as TEM analysis did not reveal the presence of any dimer or trimer intermediates.

In another plasmon-driven synthesis developed by Xue *et al.*, triangular core-shell nanoprisms from gold seeds have been produced.[129] In a typical experiment, spherical gold and silver nanoparticles with diameters of 11 and 5 nm respectively are mixed together and irradiated with 550 nm light. TEM analysis reveals that the resulting product consists of nanostructures with a single gold particle core that have triangular silver shells with average edge length ~70 nm. During the initial irradiation period, the Au seeds are coated with silver shells of irregular shapes. On increased irradiation time, the shells develop a triangular shape. As discussed above, the edge-length of the hybrid nanostructure is determined by the excitation wavelength and growth stops when the dipole plasmon resonance becomes red-shifted with respect to the plasmon excitation.

A recent paper by An *et al.*, describes the photoinduced shape evolution of triangular nanoplates to hexagonal nanoplates.[130] Citrate stabilized silver seeds were irradiated with a conventional 70 W sodium lamp. The initial silver seeds were first converted into triangular silver nanoplates (type I) with average edge length of 76 nm. Some small silver nanoparticles (~8 nm) were also present. On further irradiation, the type I particles evolved to a hexagon shape, with a concurrent increase in diameter and shape change of the small spherical particles to disks. The hexagonal plates now have an edge length of 26 nm while the disks have a diameter of 11 nm. The mechanism of the formation of the triangular nanoplates suggested here is thought to be similar to that described in references 124 and 127, however a detailed understanding of the truncation process is not given.

Another different light induced method for Ag nanoprism formation is photoinduced growth. The difference between this method and those described above is that the seeds are irradiated in the presence of additional Ag ions and trisodium citrate. This method was devised by Maillard *et al.*[131] The proposed mechanism is as follows. At the beginning of the reaction, the seeds absorb light isotropically. As some inhomogeneity occurs in the deposited silver layer, the particle starts to become ellipsoidal like and the plasmon resonance splits in the longitudinal and transverse modes. It is assumed that reduced atoms are deposited in proportion to the near field intensity enhancement at the surface position and the longer axis grows preferentially.

This process accelerates until the position of the longitudinal band shifts beyond the irradiation wavelength. A disk shape is produced because it is suggested that a disk has a larger rotationally averaged absorption coefficient at the exciting wavelength than a rod. It is the concentration of silver ions that determines the final particle size and not the excitation wavelength. The aspect ratio is however determined by the irradiation wavelength. For a more in depth analysis into this growth mechanism the reader is directed to two recent papers by Rocha *et al.*,[132, 133] in which the formation kinetics and the role of structural defects in the growth of silver nanoprisms are discussed. It is proposed here that although SPR excitation plays an important role in determining the final edge length of the nanoprisms, it is likely that a combination of suitable capping agents and the initial seed nanoparticles' structure can be a crucial factor in determining the end morphology of nanoparticles prepared by this method.

1.6.2 Thermal methods

In a method similar to the polyol synthesis discussed earlier, one of the early approaches to successfully prepare silver nanoplates involved the reduction of silver nitrate by dimethylformamide (DMF) in the presence of poly(vinylpyrrolidone) (PVP) under reflux.[134] The mechanism proposed by Liz-Marzan and co-workers involved the formation of small spheres which aggregate and then through a melting process recrystallise into particles with well-defined edges. A similar approach was used by Jiang *et al.* except

instead the reaction was exposed to high-intensity ultrasound irradiation instead of reflux conditions.[135] Seeds formed in the initial stage of the reaction quickly grew into larger crystals via Ostwald ripening. The presence of PVP is reported to be a key factor in the growth of silver nanoplates through a selective adsorption/desorption process. Such preparations usually result in a mixture of shapes being prepared which can be separated by careful centrifugation. More recently, Yang *et al.* have reported that control of the mole ratio of silver ion to PVP can increase the percentage of one particular shape and in the case of triangular plates a yield of 95% was reported.[136] Silver ions were first reduced into small Ag seeds, which then grew into circular then hexagonal and finally triangular plates, in the presence of PVP.

Xiong *et al.* have reported a method in which the polyol method described above was directly modified to prepare Ag nanoplates instead of nanowires.[137] In this procedure silver ions are reduced by ethylene glycol when the PVP is replaced by poly(acrylamide) (PAM). In this protocol, the PAM has a dual role as it can act as a steric stabilizer, protecting the particles from aggregation while also complexing the silver ions through its amido group. This coordination effect serves to significantly reduce the rate of reaction, thereby dictating the end shape of the nanoparticles by kinetic means.

Although the first reported method for the preparation of silver nanoplates was by Jin *et al.* and involved a photochemical route as discussed above, the first literature report of a thermal method was by Chen and Carroll.[138, 139] This solution phase, method is based on the reduction of silver ions with ascorbic acid on silver seeds in the presence of an alkaline solution of highly concentrated cetyltrimethylammonium bromide (CTAB). The end product of this synthesis is truncated triangles, which can be converted to circular disks through aging at higher temperatures. They further showed that by adjusting the CTAB concentrations and silver seed amounts, the lateral dimensions of these nanoplates can be systematically controlled from 40 to 300 nm (see Figure 1.17).[140] The growth mechanism suggested by the authors involves the selective adsorption of CTAB on the (111) plane of the silver seeds, along with the formation of silver bromide on the seed particles. The exact mechanism is unclear. It was suggested earlier, in Section 1.5.1.1, that in the case of

nanorods and wires that the CTAB selectively adsorbs on the {100} crystal faces thus promoting growth in the <111> direction, contradicting the growth mechanism suggested for the case of nanoprisms.

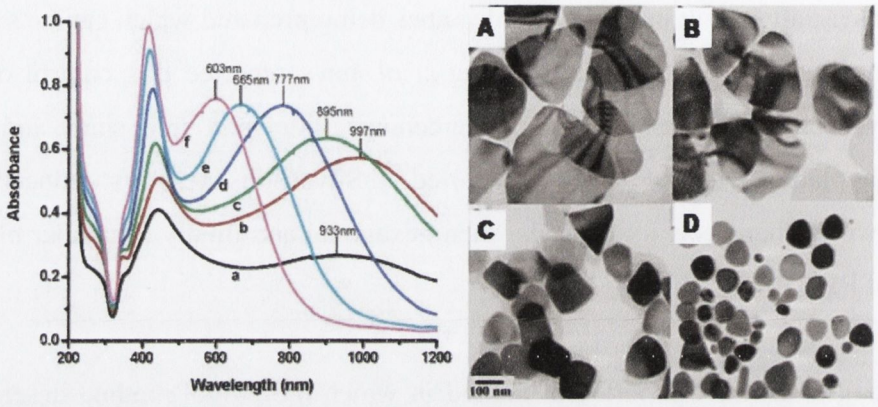


Figure 1.17: UV-vis-NIR absorption spectra of nanoplates prepared by varying the concentration of seed added a) 0.1 mL b) 0.25 mL c) 0.5 mL d) 1 mL e) 2 mL f) 3 mL. TEM images of sols a-d. Reproduced from reference 140.

Another group that makes use of the surfactant based methods is the Pileni *et al.*[141] In this case truncated silver nanoplates were produced by the sonication of two reverse micellar solutions consisting of silver di(2-ethyl-hexyl)sulfosuccinate (Ag(AOT)) and sodium di(2-ethyl-hexyl)sulfosuccinate (Na(AOT)) isooctane with Na(AOT) and hydrazine. The nanoplate size is tuned by the amount of reducing agent added during the synthesis.

In the above two syntheses, the particular products obtained were characterized as having wide size and shape distribution and also a low surface-to-volume ratio. Work carried out by Jiang *et al.*,[142] involving a self-seeding coreduction method in the presence of NaAOT saw an improvement in the quality of the triangular nanoplates and hence the circular nanodisks produced. Trace sodium borohydride was injected rapidly into a solution containing silver nitrate, ascorbic acid and citric acid resulting in the formation of a short burst of nuclei. Subsequent particle growth was then achieved by the combined reduction by the citric and ascorbic acids. The silver nanocrystal then developed facets and grew into the desired shape stabilized by the NaAOT through an Ostwald ripening process. It is predicted by molecular dynamic simulations that the NaAOT molecules are more apt to

bind at the {111} plane, leading to the preferential growth of the other crystalline faces. The morphology of the particles changes upon aging and after one hundred hours, the dominant product was circular nanodisks. The exact mechanism of this transformation is not completely understood but the authors suggest that the small difference of the interaction energies between AOT-Ag{110} and AOT-Ag{100} might result in a possibile atom migration with a reduction in the total surface free energy. In a later paper, the authors have also reported a method for stopping this morphological change by using thiols.[143] Thiols such as 1-hexanethiol, 1-octanethiol, 1-dodecanthiol and 1-hexadecanethiol were shown, by molecular dynamic simulations to exhibit larger interaction energies than AOT on the silver atomic surfaces and hence prevent the proposed atomic migration, thereby freezing the shape evolution.

The Xia group have also prepared triangular nanoplates by a thermal process.[144] Small seed silver nanoparticles prepared by the reduction of silver nitrate by sodium borohydride in the presence of both trisodium citrate and poly(vinylpyrrolidone) were refluxed in aqueous solution, under ambient conditions instead of undergoing irradiation. After ten hours the dominant product was triangular nanoplates with approximately 5% wirelike nanostructures present. The exact mechanism for this transformation process is not fully understood but it is thought that the thermal treatment provided a mild driving force to facilitate the transport of atoms from the spherical colloids to the anisotropic plates in a process similar to Ostwald ripening. A similar method involving photoconversion was also reported by the group.[123] The presence of citrate was found to be crucial to this transformation process, possibly by preferentially binding to the {111} planes, while the PVP served only as a particle stabilizer.

The same group have also prepared silver nanoplates with PVP playing a dual role as both the reductant and stabilizer.[41, 145] Silver nitrate and PVP were heated together in a capped vial to 60°C. The hydroxyl end groups of commercially available PVP reduced the silver nitrate at a slow enough rate so as to promote the growth of triangular plates, which are the kinetically favoured product. The edge length of the plates could be controlled by adjusting the reaction time. Unlike in the reflux method described above, light was found to

have a negligible effect and the presence of citrate was not vital for the production of nanoplates. This approach has been successfully adapted to prepare nanoplates of other noble metals such as gold, platinum and palladium.

In a recent paper, the Xia group also suggest another mechanism for the formation of these triangular plates.[146] Trimeric silver clusters, which are a common species in silver nitrate solutions act as nucleation sites for the addition of the newly reduced silver atoms. Mass spectrometry was used to identify the presence of silver clusters. It is worth mentioning at this point that the authors emphasized that the end morphology of a nanocrystal is determined by the interplay of many parameters all of which must be considered before an appropriate growth mechanism can be proposed.

The Mirkin group have developed a procedure for the production of triangular nanoplates in excellent yield through a solely thermal process.[147] In a typical experiment, silver nitrate, trisodium citrate, PVP and hydrogen peroxide were combined with sodium borohydride. The small nanoparticles formed initially (indicated by the presence of a pale yellow colour) were transformed into nanoprisms (indicated by a vivid blue colour) over a half hour period. The advantage of this procedure over other procedures is that it provides control (albeit limited) over the thickness of the nanoprism. This decrease in nanoprism thickness can be seen in the TEM images in Figure 1.18. The concentration of sodium borohydride used, not only controls the edge length of the particles but also the thickness. Again, similar to other procedures already discussed, the presence of citrate was found to be crucial to this transformation process and the PVP serves only as a stabilizer.

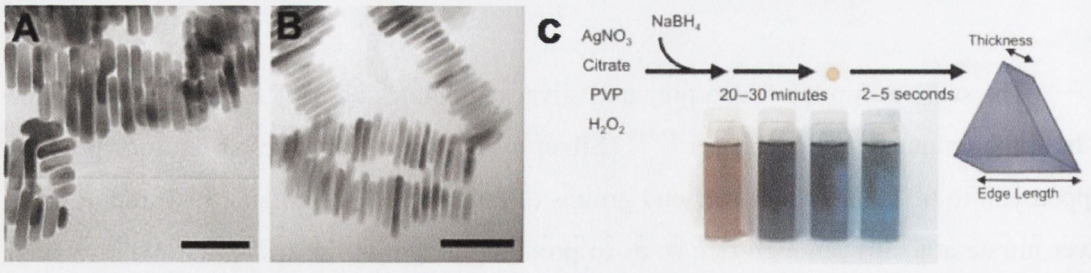


Figure 1.18: A&B) TEM images of nanoprisms prepared with a) 0.30 mM b) 0.80 mM $NaBH_4$, showing a decreasing in nanoprism thickness on increasing $NaBH_4$ concentration. C) Schematic detailing the preparation of silver nanoprisms. Adapted from reference 147.

Other aqueous procedures that produce nanoprisms with reasonable control over the size are discussed below. Zou and Dong's procedure involves the reduction of silver nitrate by hydrazine in the presence of seed particles and trisodium citrate.[6] The size of the nanoplates is simply controlled by adjusting the concentration of seed particles used. Larger nanoplates can be produced when a smaller number of seeds are used. The dominant morphologies present include truncated triangular, hexagonal and nanodisks.

Cao *et al.* have developed a method which involves reducing silver oxide with hydrazine in the presence of trisodium citrate and ethylenediaminetetraacetic acid (EDTA).[148] In this system, the citrate molecules serve only as colloid stabilizers, preventing aggregation while the EDTA molecules complex with the silver ion effectively acting as a bank for the silver ions. The ratio of EDTA to silver ion, therefore significantly affects the rate of reaction and the end particle morphology can be tuned as this chelation mediated process offers kinetic control over the growth with triangular particles being the favoured product.

Recently some procedures involving biomolecules have been reported to produce silver nanoplates. Yang *et al.* use the small biomolecule glycyl glycine to produce larger nanoplate (>100 nm) in a hydrothermal process.[149] Aqueous solutions of silver nitrate and glycyl glycine were heated together to 160°C for 24 hours. The authors suggest that the biomolecule can selectively adhere to the {111} planes of the Ag crystal thereby directing growth. Although the yield of nanoplates is lower (~80%) than in other reported procedures, the interest in this procedure lies in the ability of the biomolecule to direct growth. The authors also state that other similar peptides such as alanyl glycine can also be used to prepare such nanoplates.

Another paper recently published describes the synthesis of Ag nanoplates using proteins extracted from the unicellular green alga *Chlorella vulgaris*.[150] Hydroxyl groups in tyrosine residues and carboxyl groups in aspartic acid and/or glutamic acid residues were further identified as the most active functional groups for the reduction of Ag ion and for

also directing the anisotropic growth of the nanoplates. A simple bifunctional peptide was designed containing one tyrosine residue and two aspartic acid residues which was able to produce silver nanoplates in high yields. Similar to the case where the hydroxyl groups at the end of the PVP control the rate of reduction[41], the formation of nanoplates was found to be kinetically controlled. Again, the yield of nanoplates is lower than in other reported procedure but this is the first report of a biomolecule specifically designed to aid the production of silver nanoplates.

1.7 Functionalization of Nanoparticles

The design and production of nanomaterials with specific functional properties has been a cause of much interest in recent years. Given the small size of nanoparticles, it is not surprising that their properties are very dependent on the surface properties. Therefore, modification of the nanoparticle surface can significantly alter the properties and behaviour of metal nanoparticles. The principal benefits of the surface modification of colloidal particles are threefold. Firstly, the chemical and colloidal stability can be enhanced. Secondly the physical properties can be tuned and finally interparticle distance can be controlled to a greater extent. This is of vital importance when incorporating individual nanoparticles into assemblies or arrays.

Three different strategies may be employed in the synthesis of functionalized nanoparticles.

1. Direct synthesis where the functional group is directly introduced during the synthesis of the nanoparticles.
2. Ligand exchange where the functional group is exchanged for the existing stabilizing agent.
3. Post-synthetic modification where the functional group is introduced through modification of the existing stabilizing agent.

The most important factor to be considered in the functionalization of nanoparticles is that the desired functional group must be introduced without loss of stability of the colloid.
It must be noted at this point, that the majority of work carried out in this area has involved spherical gold nanoparticles. Examples of functionalized silver nanoparticles prepared by

the direct synthesis route and ligand exchange route have already been highlighted above in Section 1.4.2.3. One example of the post-synthetic modification of nanoparticles is the creation of core-shell materials. Particle coating is a versatile method for altering the charge, functionality and reactivity of the surface.[151] In the following section the preparation of silica coated metal nanoparticles will be discussed.

Silica coated colloidal particles are a class of materials widely used in the area of material science and as a result their surface chemistry is well developed. They are often used as model particles to study phase behaviour, rheology and diffusion. Various dyes have been incorporated into silica nanoparticles and this has enabled quantitative real-space studies with confocal fluorescence microscopy to be carried out. The advantages of using silica shells instead of organic stabilizers to functionalize metal nanoparticles are numerous. Silica is chemically inert. The shell is optically transparent so that chemical reactions can be monitored spectroscopically. As the position, and to some extent the intensity of the plasmon band of silver nanoparticles is dependent on the dielectric constant of the medium surrounding the particles, the silica shell can be used to modulate both.[152, 153] The shell provides the particles with enhanced colloidal stability so that concentrated dispersions can be prepared that remain stable over a much wider range of conditions, such as ionic strength.[154] A shell of silica also facilitates the introduction of versatile surface moieties (e.g. -COOH, or $-NH_2$) by readily available coupling agents, as the surface chemistry of silica is well established.[155] Further conjugation to other substrates and molecules is then possible which is useful for biological applications. This ease of functionalization is one of the major advantages of silica coating metal nanoparticles over functionalization with a simple thiol bond. This is used widely in nanoparticle chemistry to functionalize mainly gold and in some cases silver, but is not sufficient to accomplish a permanent linkage as an equilibrium is established with dynamic ligand exchange.

The methods for covering nanoparticles with silica can be roughly divided into two techniques. The first technique is used for aqueous based systems and is based on the sol-gel Stöber process. Briefly, this involves the hydrolysis of alkyl silicates and subsequent condensation of silicic acid in alcoholic solutions, using ammonia as the catalyst.[156]. The

second method is based on a microemulsion approach and is used to coat nanoparticles with hydrophobic surface ligands. The reverse micelle acts as a 'microreactor. The hydrolysis and condensation of the alkyl silicate precursor occurs in the water droplets to form a coating on the nanosized metal with the reverse micelle structure. Examples of this procedure are given in the following references.[157-159]

One of the first methods for the preparation of core-shell nanoparticles was reported by Liz-Marzan *et al.* in 1990s.[160] Gold colloids were homogenously coated with silica by means of a threes step process. Firstly, the surface of the gold was rendered vitreophilic by using the silane coupling agent (3-aminopropyl)trimethoxysilane (APTES) as a primer. A thin layer of silica was then deposited using sodium silicate before the thickness of the silica shells was increased by using the Stöber process. This method was then adapted for the preparation of silica coated silver nanoparticles.[161] The use of a surface primer to initiate the growth of the silica shell was believed to be the key to these coating procedures. Graf *et al.*[162] used the non-ionic polymer, poly(vinylpyrrolidone) (PVP), instead of a silane coupling agent as the surface primer, and although this method was simpler and faster, the quality of the coat was strongly dependent on the chain length of polymer used, which itself in turn was dependent on the size of the silver nanoparticles.

It was found later that surface primers were not necessary for the silica coating of gold or silver particles. Several groups have reported that a modified Stöber process could be applied directly, without the use of a poorly reproducible priming step.[155, 163-167] One disadvantage of these methods when considering the coating of silver nanoparticles is the use of ammonia as the catalyst. Silver nanoparticles are chemically unstable in the presence of ammonia and are readily oxidized to form complex ions. This problem was overcome by the Liz-Marzan group when they use dimethylamine as a catalyst for the hydrolysis and subsequent condensation of tetraethyl orthosilicate (TEOS).[168] By using this secondary amine, the silica coating process was successfully carried out while the physical integrity of the underlying silver core was maintained. These aqueous based methods will be discussed further in Chapter 3.

All of the methods mentioned above involve the silica coating of spherical gold or silver nanoparticles. The lack of methods for the preparation of coated, shaped silver nanoparticles is probably due to the fact that these structures have very high surface energies, especially at their tips, and are therefore easily oxidized. This leads to truncation or even complete dissolution of the silver core, especially in the presence of amines necessary in the silica coating process. To date, to the best of our knowledge, there is only one reported procedure for the coating of shaped silver nanoparticles. Xue *et al.* have reported a strategy for preparing triangular $Ag@SiO_2$ nanoprisms using 16-mercaptohexadecanoic acid (MHA) as a surface passivating agent (see Figure 1.19).[169] The silver nanoprisms are initially functionalized with MHA, which prevents them etching or aggregating when exposed to amine during the silica coating Stöber process. It was reported that a 15 nm coat is the critical thickness. Below this, incomplete coatings were obtained.

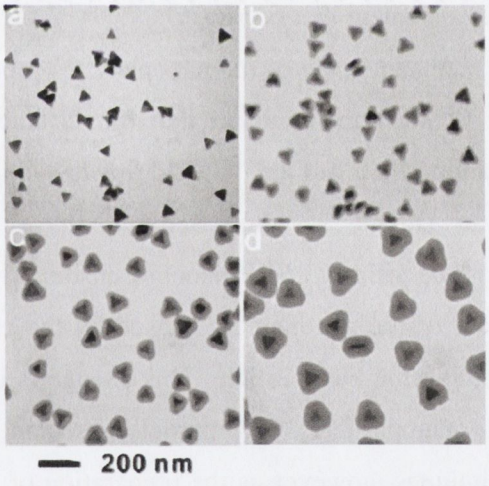


Figure 1.19: TEM images of a) bare silver nanoprisms and silica-coated silver nanoprisms with an average shell thickness of b) 15 ± 1 nm, c) 30 ± 2 nm, and d) 45 ± 3 nm, respectively. Reproduced from reference 169.

1.8 Applications

The improvements in the shape-controlled synthesis of silver nanomaterials have expanded the applications in which they can be used. Spherical nanoparticles, such as citrate reduced particles, have long been used as substrates for surface enhanced Raman spectroscopy (SERS).[4, 38, 39, 42] This enhancement is mainly due to the intense electromagnetic field exhibited by silver nanoparticles. The intensity of enhancement is strongly dependent on the shape of the nanostructure.[6, 136, 170, 171] The Raman spectrum of adsorbed molecules can be enhanced up to several million times and in some cases single molecule detection is possible. A brief introduction to SERS theory will be given subsequently in Chapter 6 Another area in which silver nanomaterials show promising behaviour is metal enhanced fluorescence (MEF). Many experiments have been carried out that highlight the importance of such parameters as nanoparticle shape and size, and the distance between the nanoparticle surface and the fluorophore that determine the degree of fluorescence quenching or enhancement that occurs.[7, 8, 166, 172, 173] Development of syntheses which have control over the size and shape of the nanoparticles produced, and also further work into functionalization of such material, so that the distance and position of the fluorophore relative to the nanoparticle surface, will aid the development of both the above mentioned technologies. Van Duyne[174-178] and Schatz[179] have pioneered use of Ag nanoprisms as sensitive nanoscale affinity LSPR nanobiosensors. These sensors operate on the basis of a shift in the SPR of the nanoparticle caused by the change in the refractive index of the medium surrounding the nanoparticle. This change is induced by the specific binding of an analyte to the nanoparticles. The particles used in these biosensors were prepared by lithographic techniques, however as the preparation of silver nanoparticles by solution based techniques has improved, it may provide a more cost effective option.

1.9. Conclusion

The synthesis of silver nanoparticles of well-defined shape and size is not a trivial matter. However, recent developments in the production of metal nanoparticles via solution

based methods have led to a remarkable range of morphologies with increasing control over their size being produced.

A range of methods for the preparation of spherical silver nanoparticles have been developed. Organic based procedures involving the steric stabilization of such nanomaterials with molecules such as alkanethiols have provided an easy route for the preparation of highly monodisperse, well ordered nanoparticles. The disadvantage to this method lies in the difficulty in producing larger (>25 nm) particles. Aqueous methods, such as citrate reduction can produce larger nanomaterials. However, control over the distribution of size is limited.

Control over the crystal structure of the seed is vital for producing monodisperse, well-defined, shaped nanomaterials in high yield. As shown above, a wide range of morphologies, for example cubes, right bipyramids and nanobeams can be produced via one synthetic process, with only small variations in the procedure required to alter the final morphology of the product. However, while the growth mechanism from the seeds for most of these nanostructures can now be explained, the processes determining the initial seed formation are not yet fully understood. Achieving a deeper understanding of this process would allow for greater control over the structure of the seed particles and may open up the possibility of new shapes with higher yield being produced.

In addition to the structure of the seed particles, the coordination of organic species is usually required to maintain the stability of the nanoparticles in solution. In many cases (but not all) these molecules may selectively bind to higher energy crystal faces, therefore reducing the energy of these faces and directing crystal growth onto the more stable crystal faces. In this way, the anisotropic growth of nanostructures such as nanorods and nanowires can be explained.

Mentioned above, are only some of the current application of silver nanoparticles of well-defined size and shape. Future work in this area must include the surface functionalization of nanoparticles. This will allow for the easier incorporation of nanoparticles into useful assemblies, and ultimately nanoscale devices.

The aims of the work presented in this thesis are:

1. To develop new aqueous based methods for the preparation of well-defined, monodisperse silver nanoparticles.
2. To functionalize these nanoparticles with a view towards further biofunctionalization
3. To examine some applications of the prepared nanoparticles.

A brief outline of subsequent chapters is given below.

In Chapter 2, two new methods for the preparation of silver nanoparticles are discussed. Both procedures are based on the seed mediated reduction of silver nitrate by ascorbic acid. In the first case, the growth step is carried out in the presence of the neutral polymer poly(vinylpyrrolidone) (PVP) and trisodium citrate (TSC). The second method was a further development of this procedure so that no additional capping agent or polymer was required for the growth of highly monodisperse silver nanoprisms. Modifications to an existing method for the preparation of silver nanoparticles using the polymer poly(vinylalcohol) are also presented. Different approaches taken to functionalize the prepared silver nanoparticles with silica are discussed in Chapter 3. In Chapter 4 experiments using the silver nanoparticles as substrates for surface enhanced Raman spectroscopy (SERS) are presented. Details of all the materials, experimental procedures and instrumentation are provided in Chapter 5. Finally, the conclusions drawn from the work presented in this thesis along with directions that future work could take are detailed in Chapter 6.

1.10 References

1. P. V. Kamat, *J. Phys. Chem. B*, 2002, **106**, 7729-7744.
2. S. V. Karpov, V. S. Gerasimov, I. L. Isaev and V. A. Markel, *Phys. Rev. B*, 2005, **72**, 205425.
3. A. M. Whelan, M. E. Brennan, W. J. Blau and J. M. Kelly, *J. Nanoscience Nanotech.*, 2004, **4**, 66-68.
4. S. E. J. Bell and N. M. S. Sirimuthu, *J. Am. Chem. Soc.*, 2006, **128**, 15580-15581.
5. D. Graham, K. Faulds and W. E. Smith, *Chem. Commun.*, 2006, 4363-4371.
6. X. Zou and S. Dong, *J. Phys. Chem. B*, 2006, **110**, 21545-21550.
7. R. L. Stoermer and C. D. Keating, *J. Am. Chem. Soc.*, 2006, **128**, 13243-13254.
8. K. Aslan, J. R. Lakowicz and C. D. Geddes, *J. Phys. Chem. B*, 2005, **109**, 6247-6251.
9. M. Faraday, *Philos. Trans. R. Soc. London*, 1857, **147**, 145.
10. L. M. Liz-Marzan, *Langmuir*, 2006, **22**, 32-41.
11. S. Eustis and M. A. El-Sayed, *Chem. Soc. Rev.*, 2006, **35**, 209-217.
12. U. Kriebig and M. Vollmer, *Optical Properties of Metal Clusters*, Springer-Verlag, Berlin, 1996.
13. K. L. Kelly, E. Coronado, L. L. Zhao and G. C. Schatz, *J. Phys. Chem. B*, 2003, **107**, 668-677.
14. I. O. Sosa, C. Noguez and R. G. Barrera, *J. Phys. Chem. B*, 2003, **107**, 6269-6275.
15. A. Moores and F. Goettmann, *New J. Chem.*, 2006, **30**, 1121-1132.
16. W. A. Murray and W. L. Barnes, *Adv. Mater.*, 2007, **19**, 3771-3782.
17. M. E. Stewart, C. R. Anderton, L. B. Thompson, J. Maria, S. K. Gray, J. A. Rogers and R. G. Nuzzo, *Chem. Rev.*, 2008, **108**, 494-521.
18. G. Mie, *Ann. Phys.(Leipzig)*, 1908, **25**, 377–442.
19. C. Noguez, *J. Phys. Chem. C*, 2007, **111**, 3806-3819.
20. D. D. Evanoff Jr and G. Chumanov, *ChemPhysChem*, 2005, **6**, 1221-1231.
21. A. S. Kumbhar, M. K. Kinnan and G. Chumanov, *J. Am. Chem. Soc.*, 2005, **127**, 12444-12445.
22. B. J. Wiley, S. H. Im, Z.-Y. Li, J. McLellan, A. Siekkinen and Y. Xia, *J. Phys. Chem. B*, 2006, **110**, 15666-15675.

23. A. L. Gonzalez, J. A. Reyes-Esqueda and C. Noguez, *J. Phys. Chem. C*, 2008.
24. http://en.wikipedia.org/wiki/Transmission_electron_microscope.
25. Z. L. Wang, *J. Phys. Chem. B*, 2000, **104**, 1153-1175.
26. Malvern Instruments, *Zetasizer nanoseries user manual*, 2.2 edn., 2005.
27. http://www.malvern.co.uk/LabEng/technology/zeta_potential.
28. V. K. LaMer and R. H. Dinegar, *J. Am. Chem. Soc.*, 1950, **72**, 4847-4854.
29. C. N. R. Rao, A. Muller and A. K. Cheetham, *Nanomaterials Chemistry*, Wiley-VCH, 2007.
30. J. Park, J. Joo, S. G. Kwon, Y. Jang and T. Hyeon, *Angew. Chem. Int. Ed.*, 2007, **46**, 4630-4660.
31. D. T. Robb and V. Privman, *Langmuir*, 2008, **24**, 26-35.
32. J. S. Bradley, in *Clusters and Colloids*, ed. G. Schmid, Wiley-VCH, 1994, pp. 469-473.
33. J. Turkevich, P. C. Stevenson and J. Hillier, *Discuss. Faraday Soc.*, 1951, **No. 11**, 55-75.
34. G. Frens, *Nature Phys. Sci*, 1973, **241**, 20-22.
35. S. Biggs, M. K. Chow, C. F. Zukoski and F. Grieser, *J. Colloid Interface Sci.*, 1993, **160**, 511-513.
36. M. K. Chow and C. F. Zukoski, *J. Colloid Interface Sci.*, 1994, **165**, 97-109.
37. U. Nickel, K. Mansyreff and S. Schneider, *J. Raman Spectrosc.*, 2004, **35**, 101-110.
38. M. V. Canamares, J. V. Garcia-Ramos, J. D. Gomez-Varga, C. Domingo and S. Sanchez-Cortes, *Langmuir*, 2005, **21**, 8546-8553.
39. N. Leopold and B. Lendl, *J. Phys. Chem. B*, 2003, **107**, 5723-5727.
40. C. E. Hoppe, M. Lazzari, I. Pardinas-Blanco and M. A. Lopez-Quintela, *Langmuir*, 2006, **22**, 7027-7034.
41. I. Washio, X. Xiong, Y. Yin and Y. Xia, *Adv. Mater.*, 2006, **18**, 1745-1749.
42. L. Kvitek, R. Prucek, A. Panacek, R. Novotny, J. Hrbac and R. Zboril, *J. Mater. Chem.*, 2005, **15**, 1099-1105.
43. A. Henglein and M. Giersig, *J. Phys. Chem. B*, 1999, **103**, 9533-9539.
44. A. Henglein, *Langmuir*, 2001, **17**, 2329-2333.
45. F.-K. Liu, Y.-C. Hsu, M.-H. Tsai and T.-C. Chu, *Mater. Lett.*, 2007, **61**, 2402-2405.

46. H. S. Shin, H. J. Yang, S. B. Kim and M. S. Lee, *J. Colloid Interface Sci.*, 2004, **274**, 89-94.
47. T. Li, H. G. Park and S. H. Choi, *Mater. Chem. Phys.*, 2007, **105**, 325-330.
48. K. A. Bogle, Dhole, S. D., Bhoraskar, V., N., *Nanotech.*, 2006, **17**, 3204-3208.
49. H. Yin, T. Yamamoto, Y. Wada and S. Yanagida, *Mater. Chem. Phys.*, 2004, **83**, 66-70.
50. L. B. Yang, Y. H. Shen, A. J. Xie and B. C. Zhang, *J. Phys. Chem. C*, 2007, **111**, 5300-5308.
51. S. Tan, M. Erol, A. Attygalle, H. Du and S. Sukhishvili, *Langmuir*, 2007, **23**, 9836-9843.
52. I. Pastoriza-Santos and L. M. Liz-Marzán, *Pure Appl. Chem*, 2000, **72**, 83-90.
53. I. Pastoriza-Santos and L. M. Liz-Marzan, *Langmuir*, 2002, **18**, 2888-2894.
54. I. Pastoriza-Santos, D. S. Koktysh, A. A. Mamedov, M. Giersig, N. A. Kotov and L. M. Liz-Marzan, *Langmuir*, 2000, **16**, 2731-2735.
55. J. Liu, W. Ong, A. E. Kaifer and C. Peinador, *Langmuir*, 2002, **18**, 5981-5983.
56. G. Rodriguez-Gattorno, D. Diaz, L. Rendon and G. O. Hernandez-Segura, *J. Phys. Chem. B*, 2002, **106**, 2482-2487.
57. P.-Y. Silvert, R. Herrera-Urbina, N. Duvauchelle, V. Vijayakrishnan and K. T. Elhsissen, *J. Mater. Chem.*, 1996, **6**, 573-577.
58. D. Kim, S. Jeong and J. Moon, *Nanotech.*, 2006, **17**, 4019-4024.
59. A. Taleb, C. Petit and M. P. Pileni, *Chem. Mater.*, 1997, **9**, 950-959.
60. C. Petit, P. Lixon and M. P. Pileni, *J. Phys. Chem.*, 1993, **97**, 12974-12983.
61. A. Courty, A. I. Henry, N. Goubet and M. P. Pileni, *Nature Mater.*, 2007, **6**, 900-907.
62. A. I. Henry, A. Courty, N. Goubet and M. P. Pileni, *J. Phys. Chem. C*, 2008, **112**, 48-52.
63. Y. P. Sun, P. Atorngitjawat and M. J. Meziani, *Langmuir*, 2001, **17**, 5707-5710.
64. H. Ohde, F. Hunt and C. M. Wai, *Chem. Mater.*, 2001, **13**, 4130-4135.
65. C. A. Fernandez and C. M. Wai, *Small*, 2006, **2**, 1266-1269.
66. M. Brust, M. Walker, D. Bethell, D. J. Schiffrin and R. Whyman, *Chem. Commun.*, 1994, **1994**, 801-802.

67. M. Brust, J. Fink, D. Bethell, D. J. Schiffrin and C. Kiely, *Chem. Commun.*, 1995, **1995**, 1655-1656.

68. J. R. Heath, C. M. Knobler and D. V. Leff, *J. Phys. Chem. B*, 1997, **101**, 189-197.

69. B. A. Korgel, S. Fullam, S. Connolly and D. Fitzmaurice, *J. Phys. Chem. B*, 1998, **102**, 8379-8388.

70. J. Zhang, J. Malicka, I. Gryczynski and J. R. Lakowicz, *J. Phys. Chem. B*, 2005, **109**, 7643-7648.

71. J. Zhang and J. R. Lakowicz, *J. Phys. Chem. B*, 2006, **110**, 2387-2392.

72. C. Jiang, D. J. Cardin and S. C. Tsang, *Chem. Mater.*, 2008, **20**, 14-16.

73. R. C. Doty, T. R. Tshikhudo, M. Brust and D. G. Fernig, *Chem. Mater.*, 2005, **17**, 4630-4635.

74. H. Hiramatsu and F. E. Osterloh, *Chem. Mater.*, 2004, **16**, 2509-2511.

75. N. R. Jana and X. Peng, *J. Am. Chem. Soc.*, 2003, **125**, 14280-14281.

76. Y. Kashiwagi, M. Yamamoto and M. Nakamoto, *J. Colloid Interface Sci.*, 2006, **300**, 169-175.

77. X. Z. Lin, X. Teng and H. Yang, *Langmuir*, 2003, **19**, 10081-10085.

78. S. Charan, N. Singh, P. K. Khanna and K. R. Patil, *J. Nanoscience Nanotech.*, 2006, **6**, 2095-2102.

79. K. J. Lee, B. H. Jun, J. Choi, Y. I. Lee, J. Joung and Y. S. Oh, *Nanotech.*, 2007, **18**, 335601.

80. S. Connolly, S. Fullam, B. Korgel and D. Fitzmaurice, *J. Am. Chem. Soc.*, 1998, **120**, 2969-2970.

81. B. A. Korgel and D. Fitzmaurice, *Adv. Mater.*, 1998, **10**, 661-665.

82. S. A. Harfenist, Z. L. Wang, M. M. Alvarez, I. Vezmar and R. L. Whetten, *J. Phys. Chem.*, 1996, **100**, 13904-13910.

83. Z. L. Wang, S. A. Harfenist, R. L. Whetten, J. Bentley and N. D. Evans, *J. Phys. Chem. B*, 1998, **102**, 3068-3072.

84. C. J. Kiely, J. Fink, J. G. Zheng, M. Brust, D. Bethell and D. J. Schiffrin, *Adv. Mater.*, 2000, **12**, 640-643.

85. A. R. Tao, S. Habas and P. Yang, *Small*, 2008, **4**, 310-325.

86. N. R. Jana, L. Gearheart and C. J. Murphy, *Chem. Commun.*, 2001, 617-618.

87. Y. Xia and N. J. Halas, *MRS Bull.*, 2005, **30**, 338-348.

88. C. J. Murphy, T. K. Sau, A. Gole and C. J. Orendorff, *MRS Bull.*, 2005, **30**, 349-355.

89. K. K. Caswell, C. M. Bender and C. J. Murphy, *Nano Lett.*, 2003, **3**, 667-669.

90. C. J. Murphy and N. R. Jana, *Adv. Mater.*, 2002, **14**, 80-82.

91. C. J. Orendorff, L. Gearheart, N. R. Jana and C. J. Murphy, *Phys. Chem. Chem. Phys.*, 2006, **8**, 165-170.

92. C. J. Murphy, T. K. Sau, A. M. Gole, C. J. Orendorff, J. Gao, L. Gou, S. E. Hunyadi and T. Li, *J. Phys. Chem. B*, 2005, **109**, 13857-13870.

93. N. R. Jana, *Small*, 2005, **1**, 875-882.

94. C. J. Murphy, A. M. Gole, S. E. Hunyadi and C. J. Orendorff, *Inorg. Chem.*, 2006, **45**, 7544-7554.

95. C. Ni, P. A. Hassan and E. W. Kaler, *Langmuir*, 2005, **21**, 3334-3337.

96. J. Pérez-Juste, L. M. Liz-Marzán, S. Carnie, D. Y. C. Chan and P. Mulvaney, *Adv. Funct. Mater.*, 2004, **14**, 571-579.

97. Y. Sun, Y. Yin, B. T. Mayers, T. Herricks and Y. Xia, *Chem. Mater.*, 2002, **14**, 4736-4745.

98. J. L. Elechiguerra, J. Reyes-Gasga and M. J. Yacaman, *J. Mater. Chem.*, 2006, **16**, 3906-3919.

99. C. Lofton and W. Sigmund, *Adv. Funct. Mater.*, 2005, **15**, 1197-1208.

100. P. M. Ajayan and L. D. Marks, *Phys. Rev. Lett.*, 1988, **60**, 585.

101. B. Wiley, Y. Sun and Y. Xia, *Acc. Chem. Res.*, 2007, **40**, 1067-1076.

102. H. Im Sang, T. Lee Yun, B. Wiley and Y. Xia, *Angew. Chem. Int. Ed.*, 2005, **44**, 2154-2157.

103. Y. Sun, B. Mayers, T. Herricks and Y. Xia, *Nano Lett.*, 2003, **3**, 955-960.

104. M. Tsuji, K. Matsumoto, N. Miyamae, T. Tsuji and X. Zhang, *Cryst. Growth Des.*, 2007, **7**, 311-320.

105. B. Wiley, Y. Sun and Y. Xia, *Langmuir*, 2005, **21**, 8077-8080.

106. K. E. Korte, S. E. Skrabalak and Y. Xia, *J. Mater. Chem.*, 2008, **18**, 437-441.

107. C. Chen, L. Wang, G. Jiang, J. Zhou, X. Chen, H. Yu and Q. Yang, *Nanotech.*, 2006, **17**, 3933-3938.

108. W. Zhang, P. Chen, Q. Gao, Y. Zhang and Y. Tang, *Chem. Mater.*, 2008, **20**, 1699-1704.

109. P. Jiang, S.-Y. Li, S.-S. Xie, Y. Gao and L. Song, *Chem. Eur. J.*, 2004, **10**, 4817-4821.

110. Y. Gao, P. Jiang, D. F. Liu, H. J. Yuan, X. Q. Yan, Z. P. Zhou, J. X. Wang, L. Song, L. F. Liu, W. Y. Zhou, G. Wang, C. Y. Wang, S. S. Xie, J. M. Zhang and D. Y. Shen, *J. Phys. Chem. B*, 2004, **108**, 12877-12881.

111. D. Yu and V. W.-W. Yam, *J. Am. Chem. Soc.*, 2004, **126**, 13200-13201.

112. A. R. Siekkinen, J. M. McLellan, J. Chen and Y. Xia, *Chem. Phys. Lett.*, 2006, **432**, 491-496.

113. Y. T. Lee, S. H. Im, B. Wiley and Y. N. Xia, *Chem. Phys. Lett.*, 2005, **411**, 479-483.

114. B. Wiley, Y. Sun, B. Mayers and Y. Xia, *Chem. Eur. J.*, 2005, **11**, 454-463.

115. B. Wiley, T. Herricks, Y. Sun and Y. Xia, *Nano Lett.*, 2004, **4**, 1733-1739.

116. S. E. Skrabalak, L. Au, X. Li and Y. Xia, *Nat. Protocols*, 2007, **2**, 2182-2190.

117. Y. Sun and Y. Xia, *Science*, 2002, **298**, 2176-2179.

118. A. Tao, P. Sinsermsuksakul and P. Yang, *Angew. Chem. Int. Ed.*, 2006, **45**, 4597-4601.

119. B. J. Wiley, Y. Xiong, Z.-Y. Li, Y. Yin and Y. Xia, *Nano Lett.*, 2006, **6**, 765-768.

120. B. J. Wiley, Z. H. Wang, J. Wei, Y. D. Yin, D. H. Cobden and Y. N. Xia, *Nano Lett.*, 2006, **6**, 2273-2278.

121. B. J. Wiley, Y. C. Chen, J. M. McLellan, Y. J. Xiong, Z. Y. Li, D. Ginger and Y. N. Xia, *Nano Lett.*, 2007, **7**, 1032-1036.

122. R. Jin, Y. Cao, C. A. Mirkin, K. L. Kelly, G. C. Schatz and J. G. Zheng, *Science*, 2001, **294**, 1901-1903.

123. Y. A. Sun and Y. N. Xia, *Adv. Mater.*, 2003, **15**, 695-699.

124. R. C. Jin, Y. C. Cao, E. C. Hao, G. S. Metraux, G. C. Schatz and C. A. Mirkin, *Nature*, 2003, **425**, 487-490.

125. C. Xue and C. A. Mirkin, *Angew. Chem. Int. Ed.*, 2007, **46**, 2036-2038.

126. C. Xue, G. S. Metraux, J. E. Millstone and C. A. Mirkin, *J. Am. Chem. Soc.*, 2008, **130**, 8337-8344.

127. A. Callegari, D. Tonti and M. Chergui, *Nano Lett.*, 2003, **3**, 1565-1568.

128. V. Bastys, I. Pastoriza-Santos, B. Rodriguez-Gonzalez, R. Vaisnoras and L. M. Liz-Marzan, *Adv. Funct. Mater.*, 2006, **16**, 766-773.

129. C. Xue, J. E. Millstone, S. Li and C. A. Mirkin, *Angew. Chem. Int. Ed.*, 2007, **46**, 8436-8439.

130. J. An, B. Tang, X. Ning, J. Zhou, S. Xu, B. Zhao, W. Xu, C. Corredor and J. R. Lombardi, *J. Phys. Chem. C*, 2007, **111**, 18055-18059.

131. M. Maillard, P. Huang and L. Brus, *Nano Lett.*, 2003, **3**, 1611-1615.

132. T. C. R. Rocha, H. Winnischofer, E. Westphal and D. Zanchet, *J. Phys. Chem. C*, 2007, **111**, 2885-2891.

133. T. C. R. Rocha and D. Zanchet, *J. Phys. Chem. C*, 2007, **111**, 6989-6993.

134. I. Pastoriza-Santos and L. M. Liz-Marzan, *Nano Lett.*, 2002, **2**, 903-905.

135. L. P. Jiang, S. Xu, J. M. Zhu, J. R. Zhang, J. J. Zhu and H. Y. Chen, *Inorg. Chem.*, 2004, **43**, 5877-5883.

136. Y. Yang, S. Matsubara, L. M. Xiong, T. Hayakawa and M. Nogami, *J. Phys. Chem. C*, 2007, **111**, 9095-9104.

137. Y. Xiong, A. R. Siekkinen, J. Wang, Y. Yin, M. J. Kim and Y. Xia, *J. Mater. Chem.*, 2007, **17**, 2600-2602.

138. S. H. Chen and D. L. Carroll, *Nano Lett.*, 2002, **2**, 1003-1007.

139. S. H. Chen, Z. Y. Fan and D. L. Carroll, *J. Phys. Chem. B*, 2002, **106**, 10777-10781.

140. S. Chen and D. L. Carroll, *J. Phys. Chem. B*, 2004, **108**, 5500-5506.

141. M. Maillard, S. Giorgio and M.-P. Pileni, *Adv. Mater.*, 2002, **14**, 1084-1086.

142. X. Jiang, Q. Zeng and A. Yu, *Nanotech.*, 2006, **17**, 4929-4935.

143. X. C. Jiang, Q. H. Zeng and A. B. Yu, *Langmuir*, 2007, **23**, 2218-2223.

144. Y. G. Sun, B. Mayers and Y. N. Xia, *Nano Lett.*, 2003, **3**, 675-679.

145. Y. J. Xiong, I. Washio, J. Y. Chen, H. G. Cai, Z. Y. Li and Y. N. Xia, *Langmuir*, 2006, **22**, 8563-8570.

146. Y. Xiong, I. Washio, J. Chen, M. Sadilek and Y. Xia, *Angew. Chem. Int. Ed.*, 2007, **46**, 4917-4921.

147. G. S. Metraux and C. A. Mirkin, *Adv. Mater.*, 2005, **17**, 412-415.

148. H. F. Zongwei Cao, Longtian Kang, Liwei Huang, Tianyou Zhai, Ying Ma and Jiannian Yao, *J. Mater. Chem.*, 2008, **23**, 2673-2678.

149. J. H. Yang, L. H. Lu, H. S. Wang, W. D. Shi and H. J. Zhang, *Cryst. Growth Des.*, 2006, **6**, 2155-2158.

150. J. Xie, J. Y. Lee, D. I. C. Wang and Y. P. Ting, *ACS Nano*, 2007, **1**, 429-439.

151. F. Caruso, *Adv. Mater.*, 2001, **13**, 11-22.

152. L. M. Liz-Marzan and P. Mulvaney, *J. Phys. Chem. B*, 2003, **107**, 7312-7326.

153. P. Mulvaney, L. M. Liz-Marzan, M. Giersig and T. Ung, *J. Mater. Chem.*, 2000, **10**, 1259-1270.

154. L. M. Liz-Marzan, in *Colloids and Colloid Assemblies*, ed. F. Caruso, Wiley-VCH, 2004, pp. 216-245.

155. S. H. Liu, Z. H. Zhang and M. Y. Han, *Anal. Chem.*, 2005, **77**, 2595-2600.

156. W. Stöber, A. Fink and E. Bohn, *J. Colloid Interface Sci.*, 1968, **26**, 62-69.

157. T. Li, J. Moon, A. A. Morrone, J. J. Mecholsky, D. R. Talham and J. H. Adair, *Langmuir*, 1999, **15**, 4328-4334.

158. Y. Han, J. Jiang, S. S. Lee and J. Y. Ying, *Langmuir*, 2008, **24**, 5842-5848.

159. N. R. Jana, C. Earhart and J. Y. Ying, *Chem. Mater.*, 2007, **19**, 5074-5082.

160. L. M. Liz-Marzan, M. Giersig and P. Mulvaney, *Langmuir*, 1996, **12**, 4329-4335.

161. T. Ung, L. M. Liz-Marzan and P. Mulvaney, *Langmuir*, 1998, **14**, 3740-3748.

162. C. Graf, D. L. J. Vossen, A. Imhof and A. van Blaaderen, *Langmuir*, 2003, **19**, 6693-6700.

163. V. V. Hardikar and E. Matijevic, *J. Colloid Interface Sci.*, 2000, **221**, 133-136.

164. E. Mine, A. Yamada, Y. Kobayashi, M. Konno and L. M. Liz-Marzan, *J. Colloid Interface Sci.*, 2003, **264**, 385-390.

165. D. D. Evanoff, R. L. White and G. Chumanov, *J. Phys. Chem. B*, 2004, **108**, 1522-1524.

166. K. Aslan, M. Wu, J. R. Lakowicz and C. D. Geddes, *J. Am. Chem. Soc.*, 2007, **129**, 1524-1525.

167. K. Aslan, M. Wu, J. R. Lakowicz and C. D. Geddes, *J. Fluorescence*, 2007, **17**, 127-131.

168. Y. Kobayashi, H. Katakami, E. Mine, D. Nagao, M. Konno and L. M. Liz-Marzan, *J. Colloid Interface Sci.*, 2005, **283**, 392-396.

169. C. Xue, X. Chen, S. J. Hurst and C. A. Mirkin, *Adv. Mater.*, 2007, **19**, 4071-4074.

170. L. Lu, A. Kobayashi, K. Tawa and Y. Ozaki, *Chem. Mater.*, 2006, **18**, 4894-4901.

171. J. M. McLellan, Z. Y. Li, A. R. Siekkinen and Y. N. Xia, *Nano Lett.*, 2007, **7**, 1013-1017.

172. J. R. Lakowicz, *Anal. Biochem.*, 2005, **337**, 171-194.

173. P. Anger, P. Bharadwaj and L. Novotny, *Phys. Rev. Lett.*, 2006, **96**, 113002-113004.

174. A. J. Haes and R. P. Van Duyne, *J. Am. Chem. Soc.*, 2002, **124**, 10596-10604.

175. J. C. Riboh, A. J. Haes, A. D. McFarland, C. Ranjit Yonzon and R. P. Van Duyne, *J. Phys. Chem. B*, 2003, **107**, 1772-1780.

176. A. J. Haes, W. P. Hall, L. Chang, W. L. Klein and R. P. VanDuyne, *Nano Lett.*, 2004, **4**, 1029-1034.

177. A. D. McFarland and R. P. VanDuyne, *Nano Lett.*, 2003, **3**, 1057-1062.

178. K. E. Shafer-Peltier, C. L. Haynes, M. R. Glucksberg and R. P. Van Duyne, *J. Am. Chem. Soc.*, 2003, **125**, 588-593.

179. M. D. Malinsky, K. L. Kelly, G. C. Schatz and R. P. Van Duyne, *J. Am. Chem. Soc.*, 2001,**123**,1471-1482.

Chapter 2:
Synthesis of Silver Nanoplates

2. Introduction

As previously mentioned in Chapter 1, silver nanoparticles have received a great deal of attention in recent years because they have proved to be useful in such applications as optics and photographic processes. In the past few years, the possibility of bioconjugation of silver particles has become an attractive area of research for a number of reasons. Firstly, Ag nanoparticles exhibit surface plasmon resonances (SPRs) that can be tuned from the visible into the near-IR region of the spectrum. Secondly, the extinction coefficient of the SPRs is up to four times larger than that of comparable gold nanoparticles. The aim of the work described in this chapter, was to develop new synthetic methods for the preparation of silver nanoparticles with well defined shapes. This work began in 2004 and entailed building upon existing knowledge within the group. Aine Whelan had previously developed a novel aqueous based method for the preparation of silver nanoparticles of tuneable colours. The method is based on the reduction of silver ion by ascorbic acid in the presence of citrate stabilized seed particles and the polymeric stabilizer poly(vinyl alcohol). By varying the concentration of the polymer and the molar ratio of silver ion to silver seed the morphology of the resulting particles and therefore the colour of the sol can be changed.[1]

One of the aims of the work described in this thesis was to prepare silver nanoparticles with a known surface functionality so that further conjugation of bio- or other molecules in the future could be facilitated. This chapter deals specifically with development of methods to allow the reproducible and controlled production of silver nanoparticles with well-defined shape. It is divided into three sections.

1. The preparation of silver nanoparticles via the 'added citrate' method.
2. Approaches that were taken to improve the reproducibility of the 'PVA method' (previously developed by Aine Whelan in the course of her doctoral studies)
3. The preparation of silver nanoparticles with poly(styrene sulfonate) sodium salt (PSSS) modified seeds.

2.1 Preparation of silver nanoparticles via the 'added citrate' method.

A new method for the preparation of silver nanoparticles of various colours has been developed. This method is based on the reduction of silver ion in the presence of citrate stabilized seeds, additional trisodium citrate and a polymeric stabilizer such as poly(vinylpyrrolidone).[2] The primary reason this method was adopted was to allow for the easy dispersion of the nanoparticles in ethanol. This is required for the silica coating step which will be discussed further in Chapter 3. Sols of various different colours, from yellow through to green have been prepared using this 'added citrate' procedure.

The method involves a two-step process. In the first stage seed silver particles are prepared. Silver ion is reduced by sodium borohydride in the presence of trisodium citrate to yield citrate stabilized silver nanoparticles (Equation 2.1). Trisodium citrate is known to be able to reduce metal ions at elevated temperatures.[3] Therefore the reduction is carried out in an ice-bath to ensure that the trisodium citrate acts only as a capping agent. $NaBH_4$ is used because it is a strong reducing agent (reduction potential: -1.48 V) and in this process it is desirable to have a rapid reduction of the silver ions resulting in the formation of a large number of relatively monodisperse seed particles

$$AgNO_3 + NaBH_4 + 3H_2O \rightarrow Ag + NaNO_3 + H_3BO_3 + 7/2H_2 \quad \textbf{Equation 2.1}$$

The seed particles were characterized by two methods, UV-vis spectroscopy and dynamic light scattering (DLS). A typical UV-vis spectrum and dynamic light scattering result (by volume) of the seed particles is given below. The seed particles typically exhibit one strong plasmon resonance, with the peak maximum between 390 and 400 nm. The presence of this single plasmon band indicates the presence of isotropic particles (see Section 1.1.3). DLS measurements indicate that the seeds are approximately 2 nm in diameter. TEM analysis was not carried out on the seed particles for two reasons. Firstly, the resolution of the electron microscope available in TCD when the experiments were being carried out was not sufficient and secondly it is known that the structure of small nanoparticles (< 5 nm) tends to fluctuate.[4] This change in structure would be accelerated by

the electron beam and therefore any data obtained would not be representative of the structure of the seeds in solution.

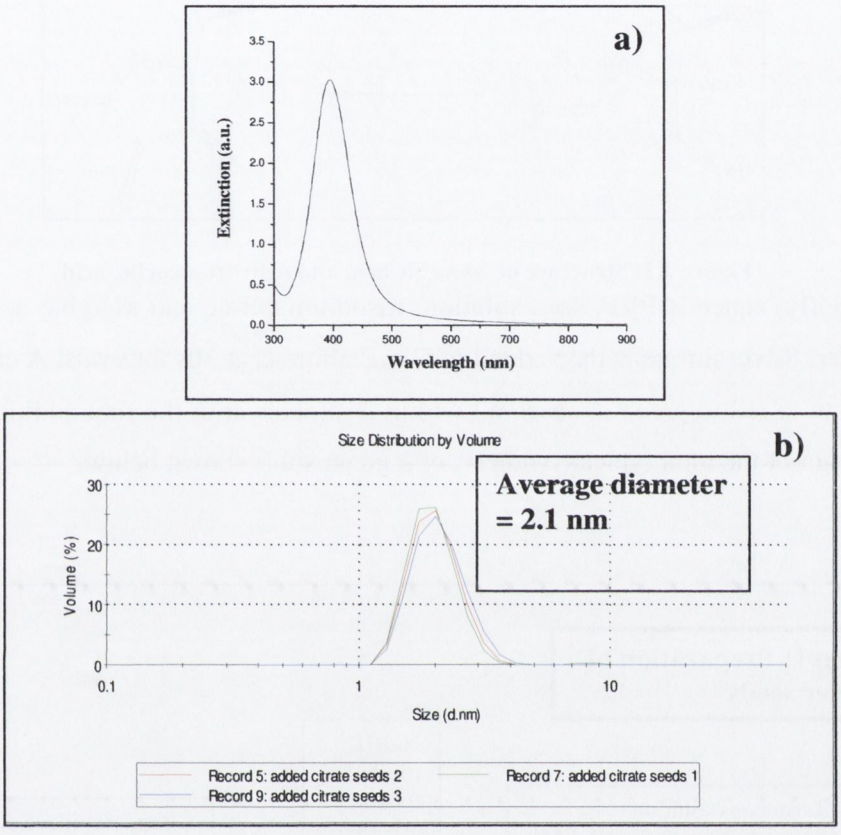


Figure 2.1: a) UV-vis spectrum of seeds prepared by the reduction of $AgNO_3$ by $NaBH_4$ in the presence of citrate. b) DLS measurements of the seeds, theUV-vis spectrum of which is shown above in a).

In the next step of the reaction, silver ion is reduced by ascorbic acid in the presence of the seed particles and a stabilizing agent, in this case TSC and poly(vinylpyrrolidone) (PVP). It is expected that the silver atoms formed are deposited on the seed particles. The equation for the reduction reaction is given below (Equation 2.2). The seed particles act as a catalyst for the reduction of the silver ion by the ascorbic acid. The reduction potential for the Ag^+/Ag (aqueous) systems is +0.7996 V while the reduction potential for the $C_6H_8O_6/C_6H_6O_6$ system is +0.17 V at pH 3.4 and is pH-dependent.[5, 6] Because of this, at room temperature, in the absence of seed particles at mildly acidic pH it will only reduce $AgNO_3$ very slowly.

$$C_6H_8O_6 + 2AgNO_3 \rightarrow C_6H_6O_6 + 2Ag + 2HNO_3 \qquad \textbf{Equation 2.2}$$

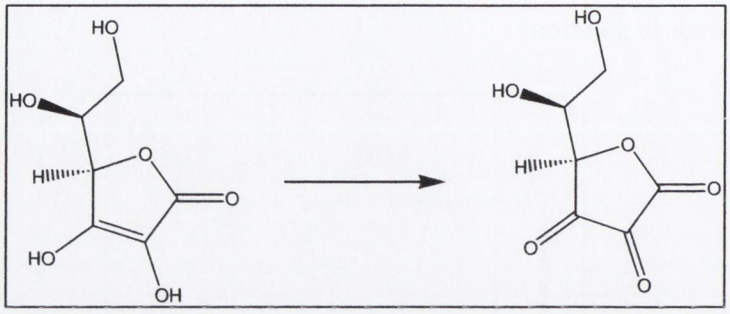
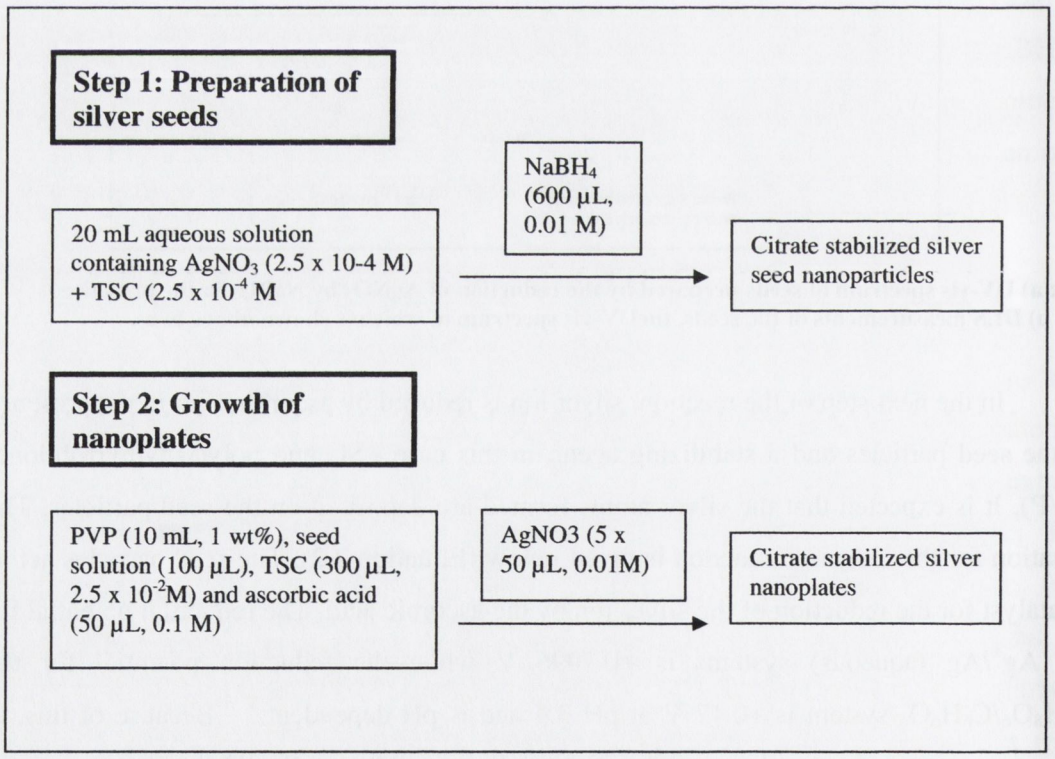


Figure 2.2: Structure of ascorbic acid and dehydroascorbic acid

Briefly, aqueous PVP, seed solution, trisodium citrate and ascorbic acid are left to stir together. Silver nitrate is then added in 50 μL aliquots at 30s intervals. A colour change from yellow to red to green is observed within 2 minutes after the first addition of Ag^{+}. A flow diagram of the total typical synthesis of a green sol is shown below.



Scheme 2.1: Preparation of citrate stabilized green sol.

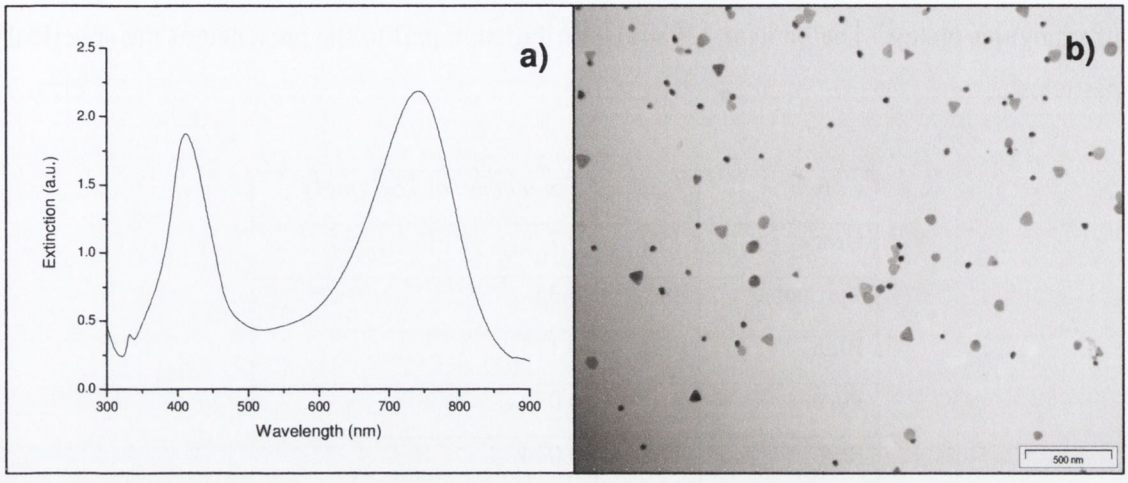


Figure 2.3: a) UV-vis spectrum b) TEM image of a typical green sol prepared by the added citrate method given above in Scheme 1. Scale bar is 500 nm.

An initial investigation of the importance of different parameters on the growth of the silver nanoplates was carried out by systematically varying the following parameters,

1) Concentration of trisodium citrate used in the growth step.
2) Temperature at which the growth step is carried out.

2.1.1 Changing the concentration of TSC used in the growth step:

Using the method described above the resultant colour of the sol can be tuned simply by using different concentrations of TSC (see Table 2.1 and Figure 2.4 below). Sols prepared with a relatively high concentration of TSC are typically green in colour. UV-vis analysis reveals three peaks in the spectrum located at approximately 760 nm, 410 nm and 330 nm (see Figure 2.3). Values similar to these have previously been reported for monodisperse triangular nanoplates and correspond to the in-plane dipole resonance, the out-of-plane dipole resonance and the out-of-plane quadrupole respectively.[7-12] However, it is very difficult to produce sols that have one distinct population of shaped particles by thermal methods. TEM analysis of the sol reveals that there is a range of morphologies present, both triangular and spherical particles. This is consistent with the UV-vis results as the intensity of the 410nm band is higher than expected for a monodisperse sol consisting

of triangular plates.[9] The band at 410nm is attributed in part to the presence of the spherical particles.

Colour	λ_{max}	*Final conc. of TSC (mM)*
Green	758	0.7
Turquoise	705	0.35
Blue	600	0.175
Purple	530	0.07
Red	495	0.024
Orange	468	0.012
Yellow	415	0.004

Table 2.1: Typical concentrations of TSC used to prepare sols of different colours.

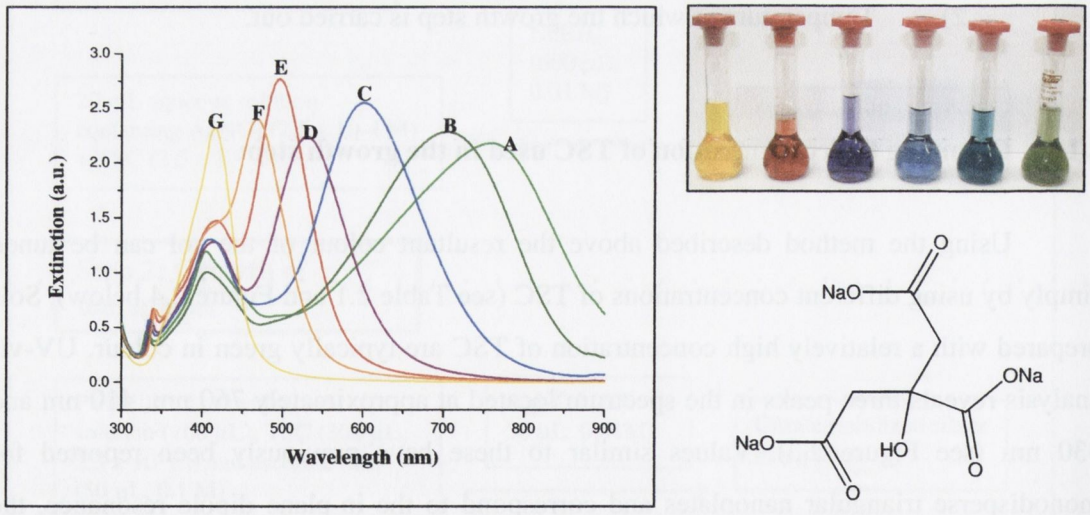


Figure 2.4 UV-vis spectra and photograph of different coloured sols prepared by varying only the concentration of TSC in the growth step. TSC concentrations used are A) 0.7 mM; B) 0.35 mM; C) 0.175 mM; D) 0.07 mM; E) 0.024 mM; F) 0.012 mM; G) 0.004 mM. Also included is the chemical structure of trisodium citrate.

As the final concentration of TSC is reduced from 0.7 mM to 0.04 mM the colour of the resultant sols may be tuned from green through to yellow. Green, purple, blue, red, orange and yellow sols have been prepared by this method (see Figure 2.4 above). It must be noted that all other parameters in the synthesis remain constant and only the concentration of TSC is varied. To the best of our knowledge, this is the first time a procedure has been reported in which the concentration of TSC alone determines the colour of the sol and therefore the shape of the nanoparticles.

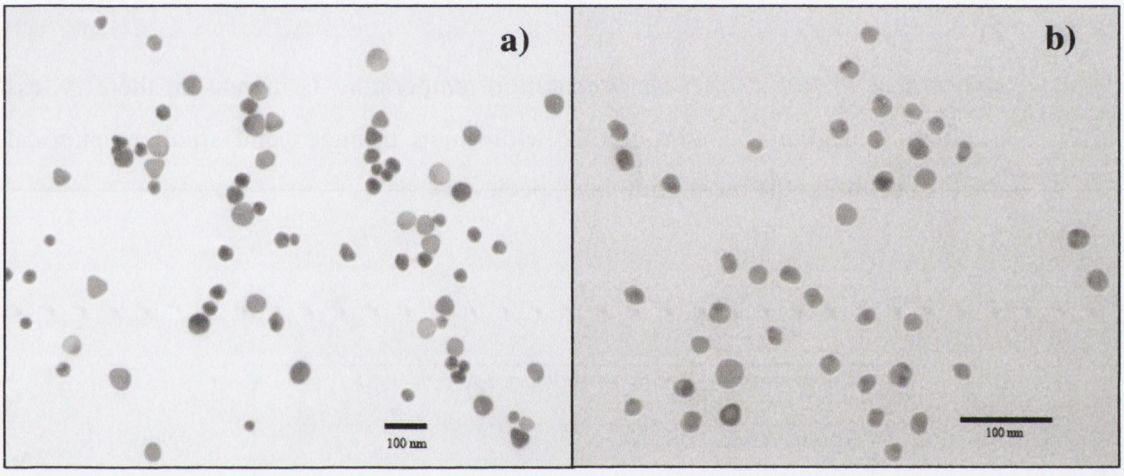


Figure 2.5: TEM images of sols from figure 4 above. a) sol D prepared with 0.175 mM TSC b) sol G prepared with 0.004 mM TSC. Scale bar is 100nm.

2.1.2 Effect of reaction temperature

The temperature at which the sol was prepared was varied. The standard procedure for the preparation of green sols (as per Scheme 2.1) was followed except that the PVP was first heated with stirring until the required temperature was reached. The seed solution, ascorbic acid and TSC were then added and the solution was stirred for 3 minutes. $AgNO_3$ was then added.

Increasing the temperature at which the growth step was carried out had three important effects.

a. The stability of sols prepared at elevated temperatures is enhanced. Sols prepared at 50°C and 100°C remain stable for periods in excess of 8 weeks, without the need for centrifugation and removal of the growth solution. This is in contrast to sols prepared at room temperature, which experience a movement of the out of plane dipole resonance to shorter wavelengths within the first 40 minutes after preparation, if the original growth solution is not removed by centrifugation. This process will be discussed in further detail below in Section 2.1.3.
b. The mean edge length of the triangular plates varies with temperature. (SeeTable 2.2)
c. As shown in Figure 2.6, as the preparation temperature is increased, there is less variation in the particle morphology with sharp triangles and smaller spherical particles becoming the most dominant species.

Temperature	*Mean particle edge length (nm)*
Room temp. (20°C)	54±10
50°C	63±10
100°C	81±15

Table 2.2: Mean size of triangular plates prepared at different temperatures

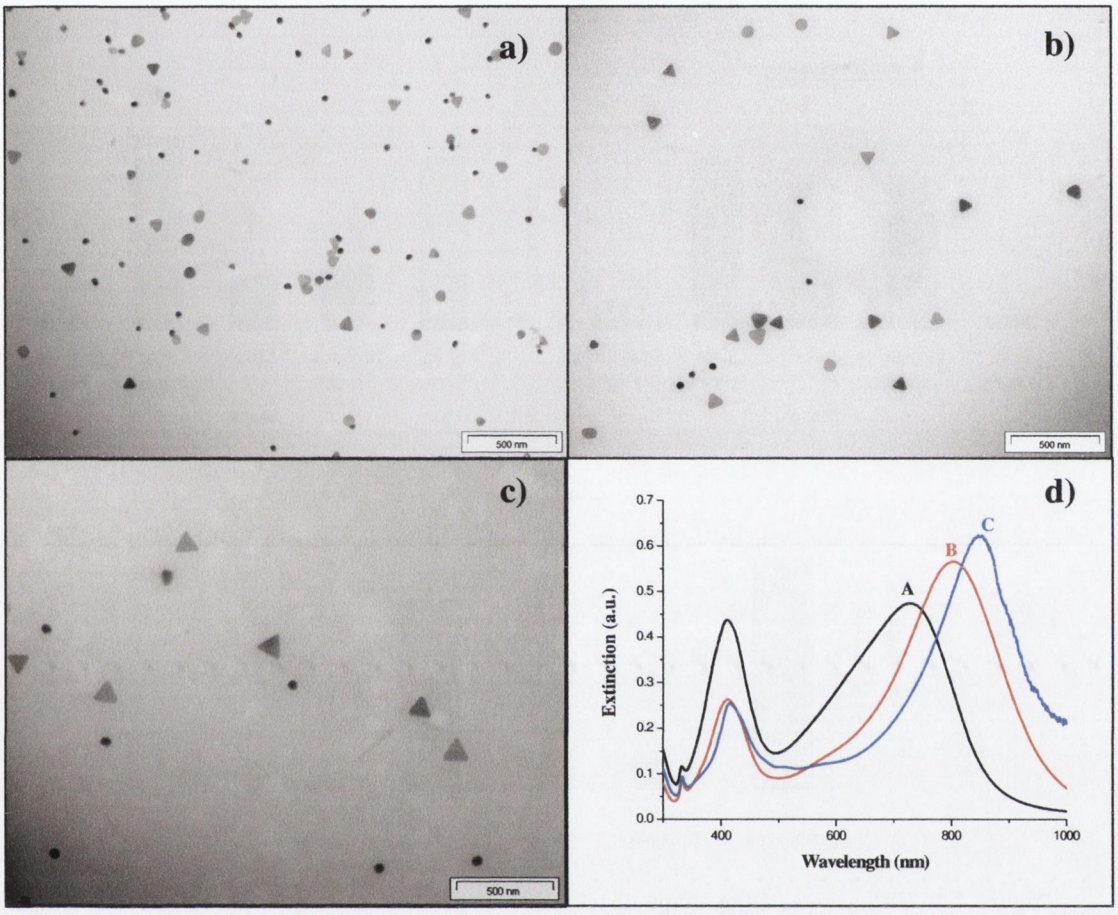


Figure 2.6:TEM images of sols prepared with 0.7 mM TSC at a) room temperature; b) 50°C; c) 100°C. All scale bars shown are 500 nm. d) UV-vis spectra of sols prepared with 0.7 mM TSC at A) room temperature; B) 50°C; C) 100°C immediately after preparation.

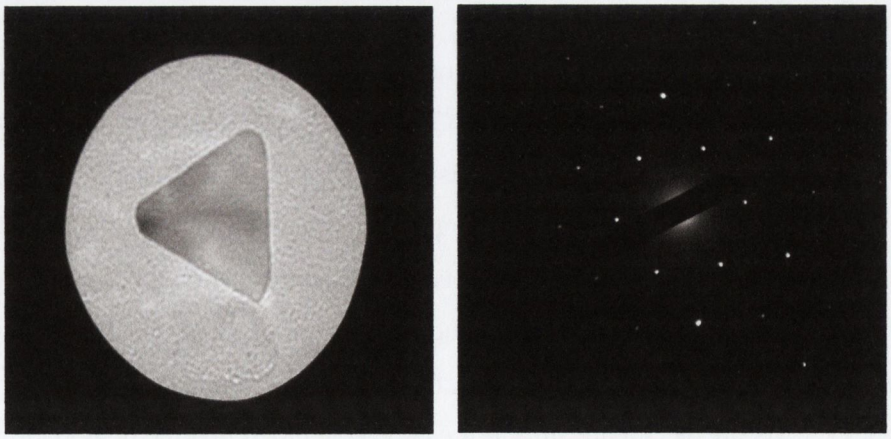


Figure 2.7: TEM image of a single silver trinagular nanoparticle and its corresponding Selected Area Electron Diffraction Pattern (SAED)

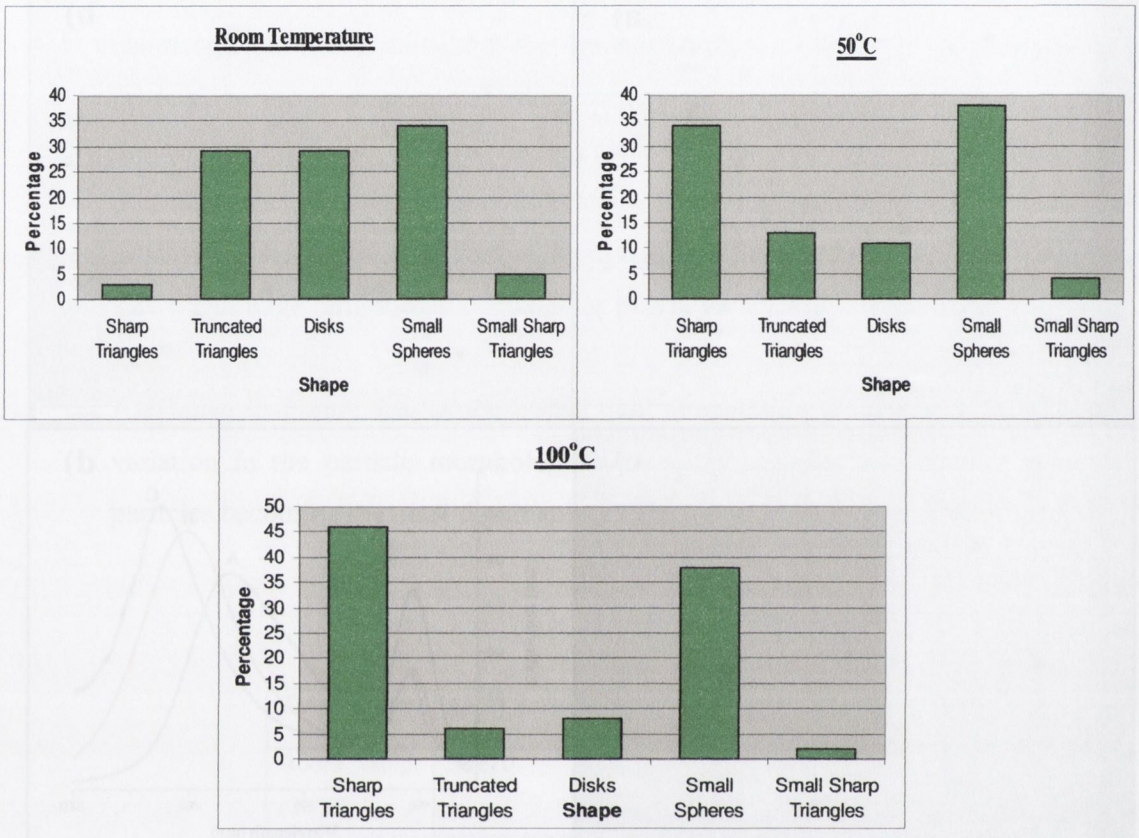


Figure 2.8: Histograms of the shape distribution of particles in sols prepared at room temperature, 50°C and 100°C. Key: Sharp Triangles: well-defined apices, Truncated Triangles: apices missing, Discs: diameter ≥35nm, Small Spheres: diameter ≤35nm, Sharp Triangles: well-defined apices with edge length <35 nm.

The effect of increasing the temperature was further investigated by IR analysis. 10 mL of sols prepared using 0.7 mM TSC at room temperature, 50°C and 100°C were centrifuged down and the pellets were redispersed in a final volume of 1 mL. The pellets were then dried in the speedy vac for 12 hours. The dried pellets were then crushed, mixed with KBr and made into discs for IR analysis. The results are shown below in Figure 2.9. It can be seen that although the growth solution was removed by both centrifugation and evaporation before preparing the KBr discs, the spectra are dominated by signals associated with the PVP.[13] As all spectra are similar it can be concluded that the degradation of PVP is not a factor in the added stability of sols prepared at temperatures greater than 50°C.

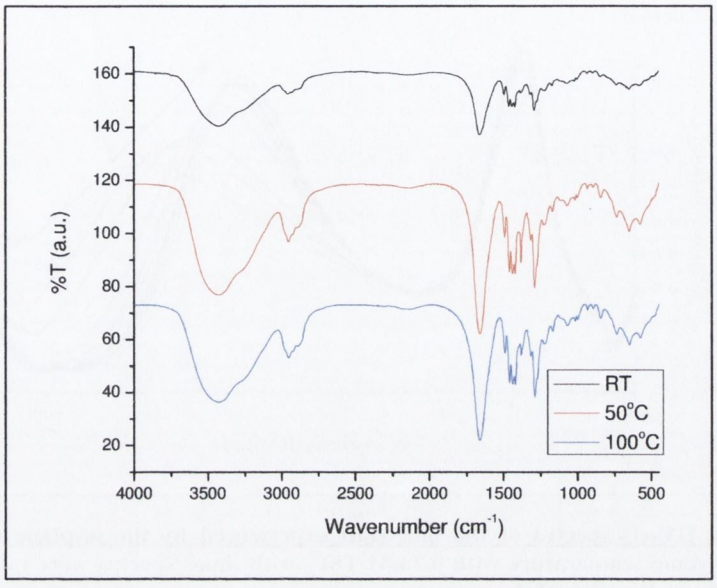


Figure 2.9: FT-IR spectra of particles prepared at RT, 50°C and 100°C in KBr discs.

2.1.3 Stability of particles

The sols that are prepared at room temperature are stable when centrifuged and redispersed in water. However, if the sol is left in its original growth solution, the in-plane dipole resonance experiences a hypsochromic shift within the first 24 hours after preparation. After further investigation it was noted that it is within the first 40 minutes after the last addition of Ag^+ that the majority of the movement of this band occurs. This is shown below in Figure 2.10. The magnitude of this blue-shift can be up to 100 nm. After this initial time period, the movement of the longitudinal band continues, but at a slower rate. The position of the band at ~410 nm (associated with both the out-of-plane dipole resonance, and the presence of isotropic particles) and the out-of–plane quadrupole remains relatively unchanged during this time period.

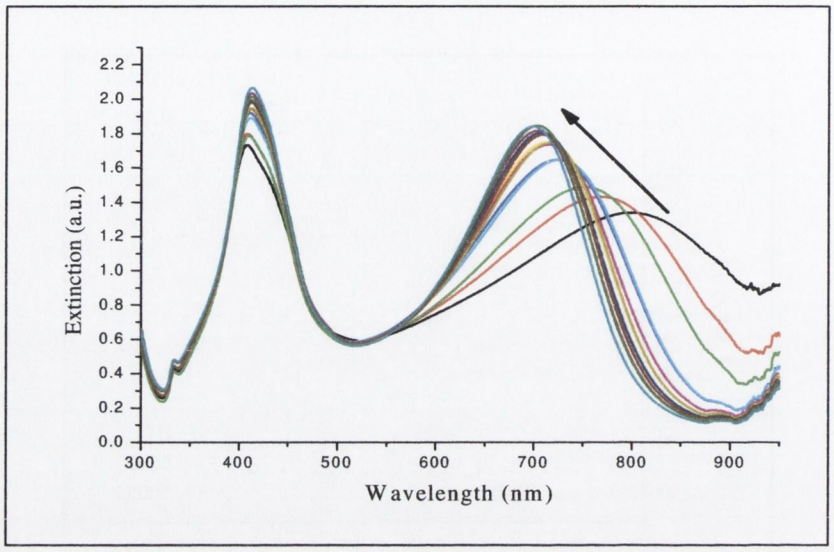


Figure 2.10: UV-vis spectra of the blue-shift experienced by the in-plane dipole resonance of sols prepared at room temperature with 0.7mM TSC, with time. Spectra were taken at 5 minute intervals for 1 hour in the direction of the arrow.

It was found that the magnitude of this shift is proportional to the position of the in-plane dipole resonance, and therefore the concentration of TSC used to prepare the nanoparticles. Thus sols prepared with 0.7 mM TSC experience the greatest blue-shift while sols prepared with 0.07 mM have a considerably smaller shift. Yellow sols, which are prepared with 0.004mM and exhibit only one SPR band at approximately 410 nm, experience little or no movement. The explanation for the occurrence of this hypsochromic shift is the truncation of the sharp triangles. The sharp apices of the triangles are being etched away to produce truncated triangles, hexagons and discs, with time. The effect of truncation of has been predicted by Kelly *et al.* using the discrete dipole approximation (DDA).[9] The results show that the in-plane dipole resonance of triangular nanoprisms is very sensitive to the truncation of the tips of the nanoprism. When 20 nm is snipped off each tip of prisms with an edge length of 100 nm, the SPR is blue-shifted by 100 nm.

Various different methods have been made to elucidate the cause of this blue-shifting process. All this work was carried out with green sols, prepared with 0.7 mM TSC because, of the samples prepared, the in-plane dipole SPR varies the most with time. The results are discussed below.

a) The role of light vs. dark

As already highlighted in Chapter 1, photoreduction and photoconversion methods have been used to prepare anisotropic silver nanoparticles. The mechanism by which light can effect the anisotropic growth of silver nanoparticles is becoming more understood; with the general trend of thought being that irradiation of small particles causes an uneven charge distribution over the particle surface. Therefore, some areas of the particles surface have better reducing abilities than others and anisotropic growth ensues. However it must be noted that the timescale over which these photoconversion/reduction processes occurs is of the order of hours and days. In the preparation described above the timescale on which growth and the subsequent etching process occurs is on the order of minutes. However, because of the wealth of literature on the effect of light on silver ions and nanoparticles it was decided that the possibility that the blue-shifting of the in-plane dipole was under photo mediated control could not be discounted.

Firstly, a green sol was prepared with 0.7 mM TSC, at room temperature. It was split in half, and one portion was stored in the dark while the second half was stored in ambient light. The sols were monitored by UV-vis spectroscopy and TEM after 24 hours (see Figure 2.11). Secondly, the whole procedure (including the preparation of the seed particles) was carried out in the dark. It was found, that despite these changes to the synthesis, the as prepared sol acted in a similar manner, regardless of whether they were or were not exposed to light. Again, as already stated above, because of the short timescale involved it is unlikely that light plays a role in either the growth or etching process.

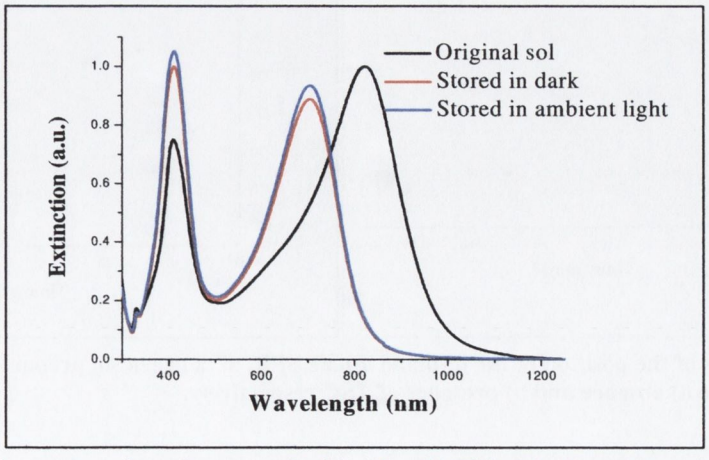


Figure 2.11: UV-vis spectra of a sol prepared with 0.7 mM TSC (black) and stored overnight for 24 hours in the dark (red) and in ambient light (blue).

b) Addition of TSC to the sol after it is prepared.

Sols prepared with a lower concentration of citrate, >0.3 mM, can be stabilized by adding extra citrate to them after the last addition of $AgNO_3$. This method can only be used to prevent the blue-shift of red sols. Addition of TSC to green sols after they had been prepared did not prevent or retard the etching process.

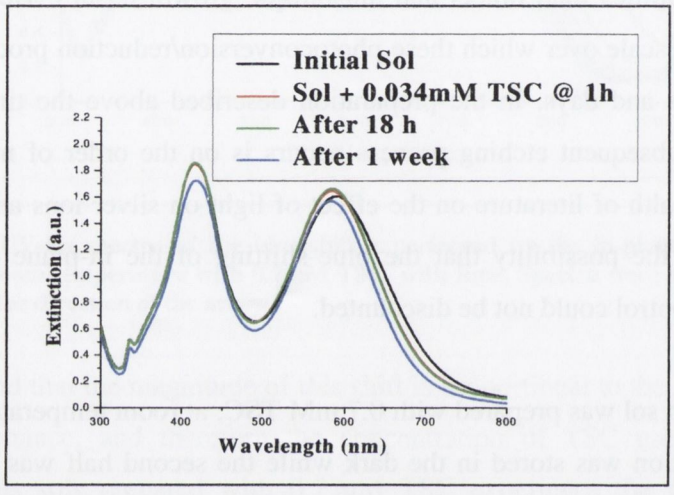


Figure 2.12: UV-vis spectra of a red sol prepared with 0.3 mM TSC over a period of one week when additional TSC was added to the sol.

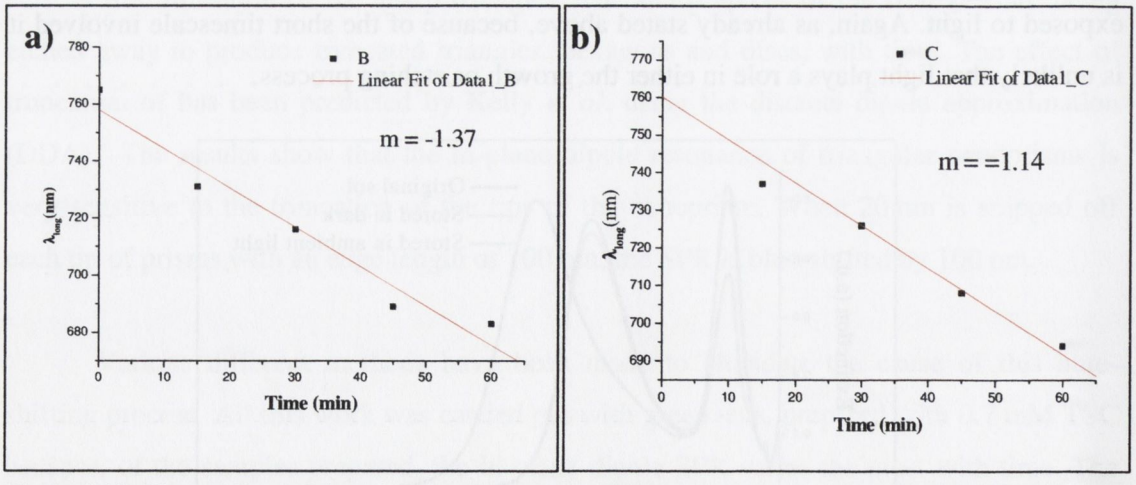


Figure 2.13: Plots of the position of the in-plane dipole SPR, of a green sol prepared with 0.74 mM TSC versus time, in the a) absence and b) presence of TSC respectively.

c) Centrifugation and redispersion

Removal of the growth solution by centrifugation greatly enhances the stability of green sols. The stability of green sols prepared at room temperature is improved by successive centrifugation and redispersion cycles. However, the enhanced stability is offset by the eventual loss of particles, as indicated by decreases in absorbance. The amount of time between centrifugation and redispersion is unimportant, provided that the supernatant is removed directly after centrifugation. At this point it was decided to attempt to separate the different shapes and sizes of particles present in a sol prepared by the added citrate method and the approach taken was through centrifugation.

2.1.4 Separation of nanoparticles

One of most of the important challenges that must be met when considering the use of nanoparticles is the separation of nanoparticles according to their size and in this case more importantly shape. Simple centrifugation has proved to be a useful tool in this area and nanorods have been successfully separated from spherical nanoparticles. It was anticipated that the shape separation of the sols described above would be possible by this method, (especially in the case of the sols prepared at 100°C containing two distinct populations of nanoparticles), however this did not prove to be the case. Because of this, other types of centrifugation processes were explored.

2.1.4.1 Centrifugation in a sucrose concentration gradient:

The sucrose density gradient was created by carefully layering lower concentrations of sucrose on top of higher concentrations in a centrifuge tube. The sample was then placed on top of the gradient and was centrifuged at 3000 rpm for 1 hour. The particles should travel through the gradient up until the point where their density matches the density of the sucrose surrounding them. A diagram depicting the before and after cases is shown below in Figure 2.14.

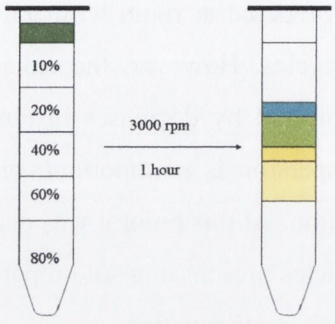


Figure 2.14: Diagram depicting the layering of the various concentrations of sucrose in the centrifuge tube and the separation of the sol after centrifugation.

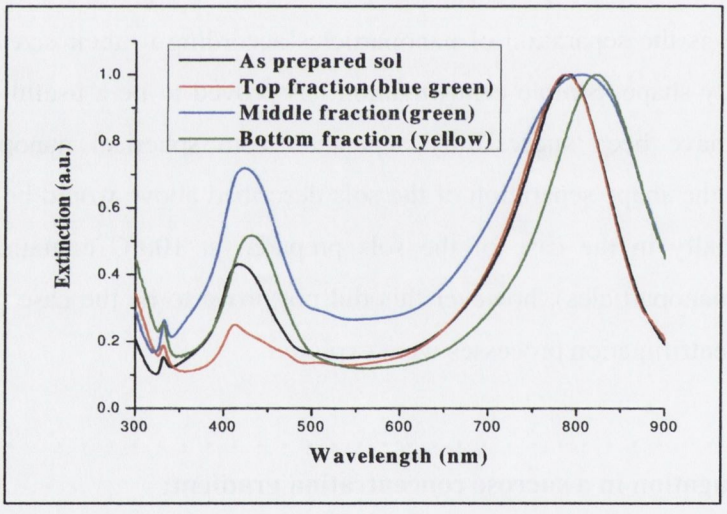


Figure 2.15: Normalized UV-vis spectra of the original sol and the fractions after centrifugation in the sucrose gradient.

From the UV-vis spectra above in Figure 2.15, it can be noted that as the intensity of the band at ~400 nm is reduced in the top fraction compared to the original sol, indicating that the percentage of spherical particles present is diminished. Because of this reduced ratio of the in-plane dipole resonance to the band centred at ~400 nm (thought to be largely due to the presence of spherical particles) it can be proposed that some shape separation has occurred. The broadening and red-shift of the in-plane experienced by the

middle and bottom fractions respectively can be explained by the presence of residual sucrose, which increases the dielectric constant of the medium surrounding the nanoparticles. On the whole a mixture of morphologies is present, in all three fractions so separation was not successful. Unfortunately TEM could not be carried out at this point because the electron microscope was not operational.

2.1.4.2 Disc Centrifugation:

During the time this work was carried out, an opportunity arose for the particles to be analysed by disc centrifugation. 5 mL of each sol that was to be analysed along with 100 mL 1 wt% PVP solution for the sucrose gradient were sent to Analytik Ltd for analysis by CPS Disc Centrifugation. The principle behind this technique is that particle size distributions can be measured by sedimentation. Sedimentation velocity increases as the square of particle diameter according to Stokes' Law. So particles that differ in size by only a few percent can be separated. If all the particles are the same size, then they settle at the same rate resulting in a thin band at the detector beam. The time needed for the particles to reach the detector is used to calculate the particle size.

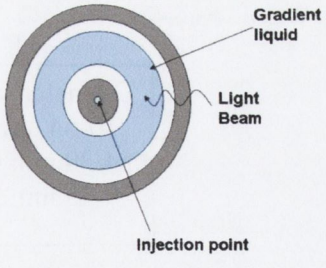


Figure 2.16: Schematic of the disc centrifuge.

For each sample that was analysed, a 0.1 mL injection volume was used. A sucrose gradient for the centrifugal disc was prepared using the 1 wt % PVP solution. The density gradient eliminates 'streaming' or the rapid settling of the particles without separation,

because at all times during the analysis the net density of the fluid (solvent + particles) increases continuously from top to bottom of the disc. The results of a sol prepared with 0.7 mM TSC at a) room temperature and b) 50°C are shown below in Figure 2.17.

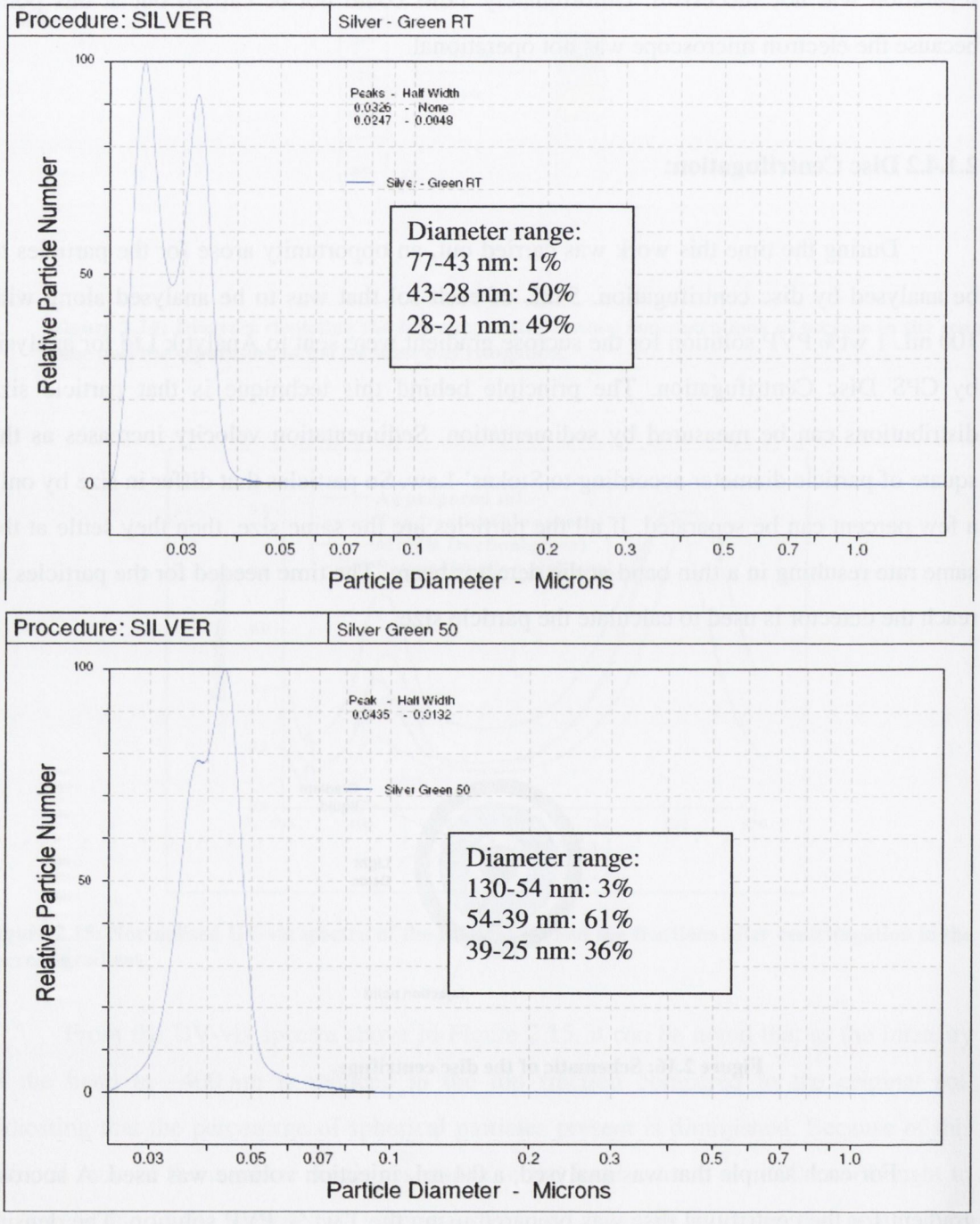


Figure 2.17: Results of the disc centrifugation of sols prepared by the added citrate method with 0.7 mM TSC at RT and 50°C.

The results from disc centrifugation correlate well with the measured sizes from TEM data. Firstly, the results indicate that as the preparation temperature of the sol is increased, the sol becomes more monodisperse. This is indicated by the presence of two distinct bands for the room temperature sol whereas only one band with a small shoulder is present for the sol prepared at 50°C. Secondly, as the temperature was increased the mean size increased. It must be noted that particle size is calculated from when Mie theory is applied to the intensity data from the detector beam. As already discussed in Chapter 1, Mie theory can only be directly applied to determine the size of spherical particles. As the particles in the samples above consist mainly of plate-like material, it is not surprising that the size value obtained from the disc centrifuge, deviate from those measured from TEM micrographs. A comparison of the average sizes by TEM analysis and by disc centrifugation is given below in Table 2.3.

	Size (nm)	
	TEM	**Disc Centrifugation**
Room temperature sol	54±10 nm	130-54 nm: 3% 54-39 nm: 61% 39-25 nm: 36%
50°C sol	63±10 nm	130-54 nm: 3% 54-39 nm: 61% 39-25 nm: 36%

Table 2.3: Comparison of the sizes calculated from TEM and disc centrifugation.

2.1.5 Summary of the 'added citrate' method

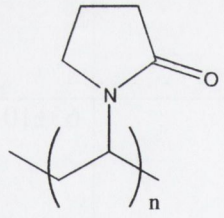
At this point, the results of the investigation thus far will be summarized.

1) Silver sols of various different colours have been produced by a seed mediated method involving the reduction of silver ion in the presence of trisodium citrate and PVP.
2) The colour of the sols can be tuned by varying the concentration of trisodium citrate.
3) The in–plane dipole resonance of the as prepared sols experiences a hypsochromic shift within the first 40 minutes after sol preparation.
4) The temperature at which sol preparation is carried out is important. As the temperature is increased the sols become more monodisperse and the particles become larger and the stability of the particles is increased.

Further investigation into the growth of silver nanoparticles via this seed mediated 'added citrate' method was carried out. The importance of the following parameters was examined.

a. Role of PVP
b. Role of the seed.

2.1.6 Role of poly(vinylpyrrolidone) (PVP)



2.1.6.1 Changing the molecular weight of PVP used in the growth step

The molecular weight of the PVP solution used in the growth step was varied from 10 k to 55 k. The growth step was then carried out at room temperature as described above in Scheme 2.1. It was found that when higher molecular weights of PVP are used, the in-plane dipole resonance becomes more blue-shifted. Again the positions of the transverse and quadrupole bands remain relatively unchanged (see Figure 2.18).

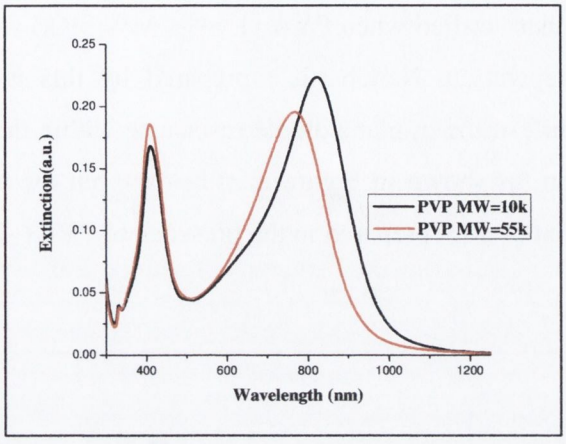


Figure 2.18: UV-vis spectra of sols prepared with 0.7 mM TSC at room temperature with PVP molecular weight 10k (black) and 55k (red). Spectra taken 1 hour after sol preparation.

2.1.5.2 Changing the concentration of PVP used in the growth step

The role of the PVP (MW 10 k) in the preparation of the sols was further investigated by varying the concentration from 1 wt% to no PVP, with a fixed TSC concentration of 0.7 mM. Triangular nanoplates were formed in each case and as the concentration of PVP was reduced in the sols and as can be seen in Figure 2.19, no trend was apparent in the UV-vis spectra. The morphology of the particles remained the same regardless of the concentration of PVP used. This result would indicate that PVP does not play a shape directing role in the growth process. This result agrees with the findings of Mirkin *et al.*, where in a similar synthesis it is proposed that PVP plays no role in the determination of the morphology of the particles but merely prevents nanoparticle aggregation.[14]

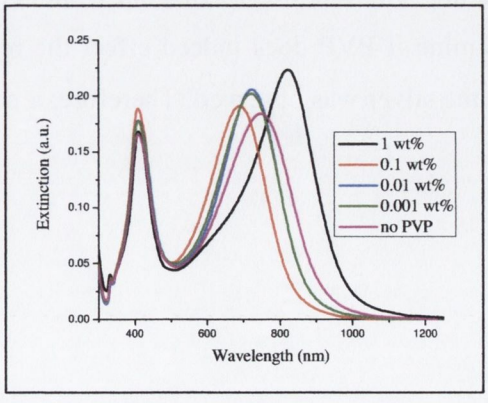


Figure 2.19: UV-vis spectra of sols prepared with 0.7 mM TSC at room temperature with varying concentrations of PVP (from 1 wt% to 0 wt%). Spectra were taken 1 hour after the preparation of the sols.

This result was further verified when PVA (1 wt%, MW 39 k) was substituted for PVP in the nanoparticle preparation. Nanoparticle prepared by this method, experience the aforementioned blue-shift of the in-plane dipole resonance within the first 40 minutes after nanoparticle preparation (as shown in Figure 2.20 below), but the magnitude of this shift (~80 nm) is less than that of a sol prepared in the presence of PVP (~200 nm).

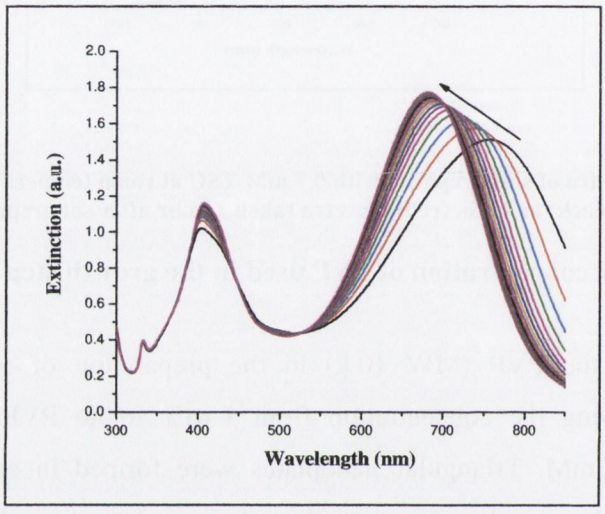


Figure 2.20: UV-vis spectra of silver nanoparticles prepared at room temperature with 0.7 mM TSC using PVA (1wt %). Spectra were taken at 5 minute intervals for 1 hour in the direction of the arrow.

Gold and silver nanoparticles have also been prepared using PVP alone as the reducing agent at low temperatures in aqueous solution.[15, 16] The size and shape of the resulting nanoparticles could be controlled by varying the ratio of silver ion to PVP. For this reason, the standard room temperature synthesis was carried out without the addition ascorbic acid, the reducing agent, to examine if PVP does indeed effect the reduction of the silver ion. However, no reduction of the silver was observed. Therefore, a possible role of the PVP as a reductant was ruled out.

2.1.7 PVP as an etching agent:

It is clear from the results presented above that the presence of PVP is not necessary for the production of silver nanoplates by the 'added citrate method'. As the removal of the growth solution via centrifugation greatly enhances the stability of the nanoparticles, it is clear that the process observed in the first 40 minutes after the preparation of sols resulting in the blue-shift of the in-plane dipole SPR is accelerated by the presence of some species in the growth solution. The reagent that is present in highest concentration is PVP (at 0.1 M, based on the molecular weight of the monomer). For this reason it was decided to test the stability of a green sol prepared with 0.7 mM TSC, at 50°C, against PVP. This sol was used because when redispersed in Millipore water after preparation, it does not experience a blue-shift with time. Any change in the position of the in-plane dipole resonance could be solely attributed to the presence of the PVP. A sol was prepared, centrifuged and the pellets were split in half. The first half (sol a) was redispersed in Millipore water while the second half (sol b) was redispersed in PVP (1 wt%). The sols were then monitored by UV-vis spectroscopy and TEM over a period of 1 week.

As shown in Figure 2.21, the spectrum of the sol redispersed in water did not change significantly with time, and TEM analysis of this sol immediately after redispersion and again after two weeks reveals very little change in the morphology of the particles. However, the spectrum of the pellets redispersed in 1 wt% PVP solution had blue-shifted by 170 nm in 24 hours and by a total of 240 nm in a period of 1 week. TEM analysis at this point showed that no triangular plates were present in the sample. All the sharp apices had been etched away resulting in circular discs remaining. A similar experiment was carried out in which the pellets were redispersed in various concentrations of poly(vinyl alcohol). No blue-shift with time of the in-plane dipole resonance was observed with this polymer.

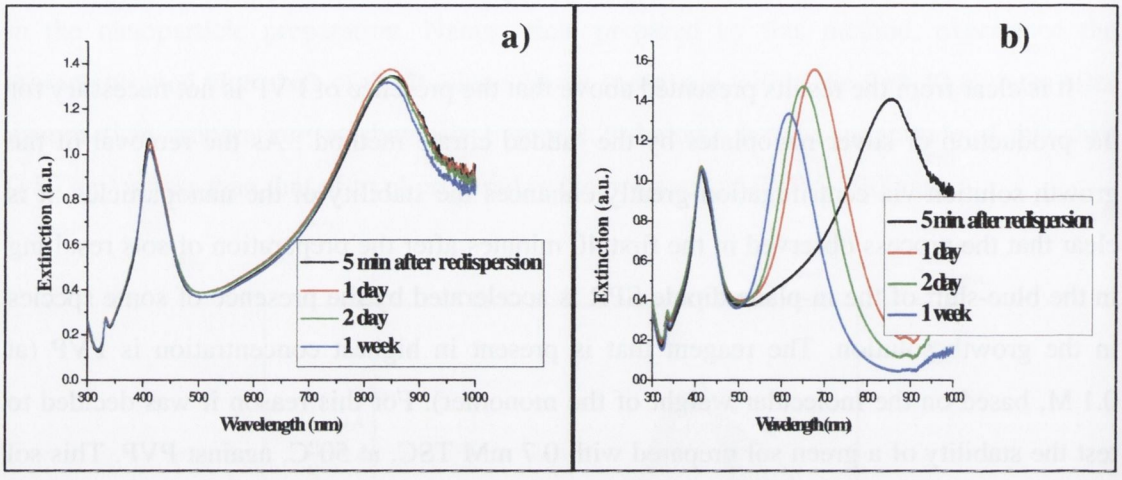


Figure 2.21 UV-vis spectra of sol prepared with 0.7 mM TSC at 50°C redispersed in a) H_2O b) 1 wt% PVP solution over the period of one week.

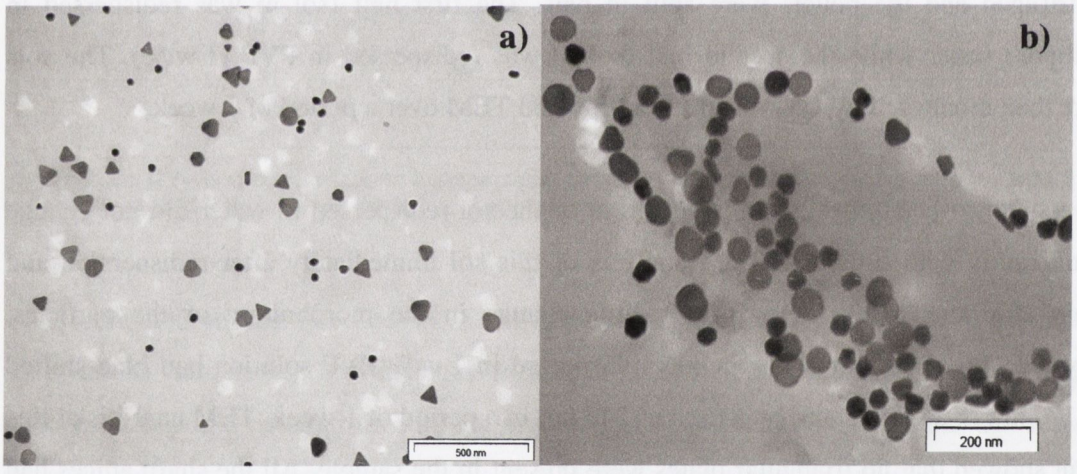


Figure 2.22: TEM images of a sol prepared with 0.7 mM TSC at 50°C redispersed in a) Millipore water b) 1 wt% PVP solution, 1 week after redispersion.

A linear relationship between the concentration of PVP and the magnitude of the hypsochromic shift after redipsersion was found.

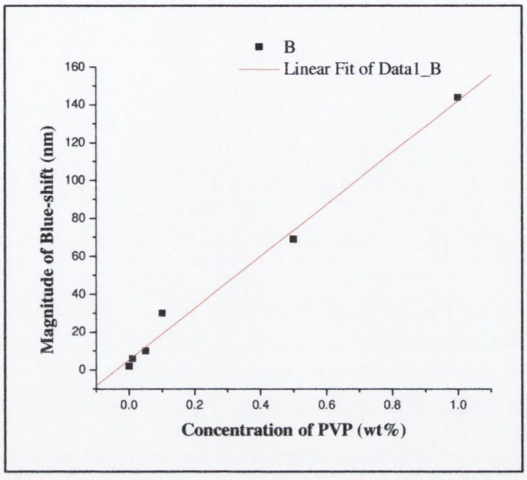


Figure 2.23: Relationship between the concentration of PVP used and the magnitude of the hypsochromic shift. Spectra were recorded 24 hours after redispersion in PVP.

It is believed that PVP is prepared by the free-radical polymerization of N-vinylpyrrolidone in water using hydrogen peroxide as the initiator. The stability of the particles prepared by the added citrate method was therefore tested against H_2O_2 and it was found that they were completely oxidised back to silver ion. It was proposed that the presence of trace amounts of H_2O_2 in the PVP used could be responsible for the etching process. For this reason, a PVP solution was boiled, to remove any trace of H_2O_2 present. It was then used to redisperse a sol prepared at 50°C but no increase in stability was observed.

The PVP was then purified by acetone precipitation. Briefly, acetone was added drop wise to an aqueous solution of PVP. The resulting white precipitate was washed with acetone three times and then dried. The acetone washings were also evaporated under reduced pressure to yield a pinkish powder. NMR analysis in D_2O was run on both compounds (Figure 2.24). Figure 2.24a corresponds well with the NMR spectra of PVP in the literature[17], however it is clear that an impurity not of polymeric nature, was isolated from the as received PVP (Figure 2.24b). (The peak at 2.175 ppm arises from the presence of residual acetone from the purification step.) A green added citrate sol was then prepared at 50°C. It was centrifuged and the pellets redispersed in Millipore water and a 1 wt % aqueous solution of the purified PVP and the impurity. The UV-vis spectra recorded 24 hours after redispersion are shown below in Figure 2.25.

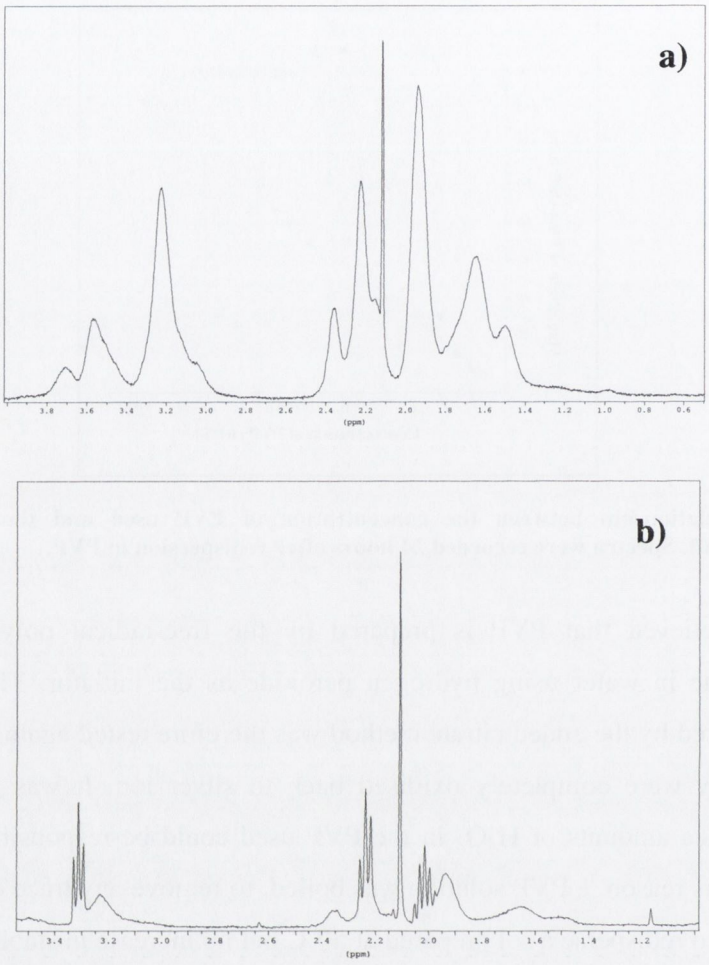


Figure 2.24: The 400 MHz ^{1}H NMR spectrum in D_2O of a) PVP purified and b) impurity isolated by acetone precipitation.

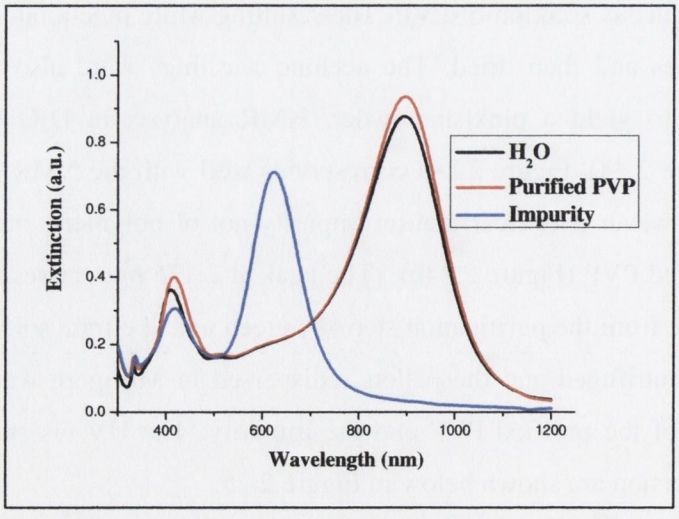
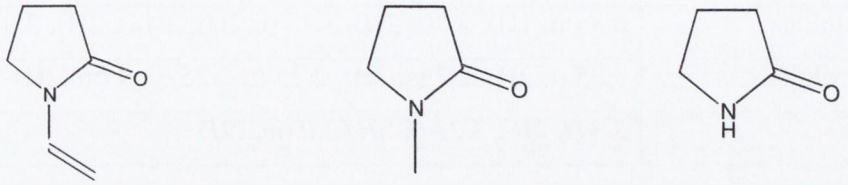


Figure 2.25: Stability of particle redipsersed in a) H_2O b) purified PVP c) pink impurity

This result indicates that it is not the PVP that acts as the etchant but an impurity present in it. The pyrrolidone ring is stable at temperatures up to ~230°C and it is believed that the decomposition takes place mostly on the backbone *i.e.* ring opening does not occur.[18] For this reason, to investigate this etching process further, it was decided to compare the effects of redispersing sols in a different pyrrolidone compounds. The materials used were: N-vinylpyrrolidone (1), N-methylpyrrolidone(2) and pyrrolidone (3).



(1) (2) (3)

Again a sol was prepared with 0.7 mM TSC at 50°C and the pellets were redispersed in Millipore water, and the above three pyrrolidone compounds. The results are shown below in Figure 2.26.

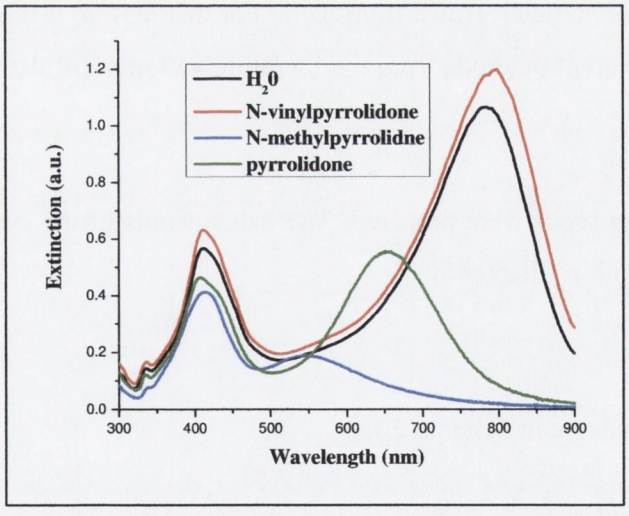


Figure 2.26: Sol prepared with 0.7 mM TSC at 50°C redispersed in a) H_2O b) N-vinylpyrrolidone c) N-methylpyrrolidone and d) pyrrolidone after 3 days.

The sol redispersed in N-methylpyrrolidone experienced the greatest blue-shift, while the sol redispersed in N-vinylpyrrolidone was stable with time, experiencing only a shift red-shift. This bathochromic shift can be attributed to the change in the refractive

index of the medium surrounding the particles. Comparison of the NMR spectra of the above compounds with the impurity isolated from the purification of PVP confirms the identity of said impurity to be pyrrolidone (see Table 2.4 below).

Compound	^{1}H NMR (400 MHz, D2O) δ (ppm)
Impurity (without residual polymer signals)	*3.3 (t, 2H), 2.22 (t, 2H) 2.0 (m, 2H).*
N-vinylpyrrolidone	6.8 (m, 1H), 4.5(t, 2H), 3.45 (t, 2H), 2.4 (t, 2H), 2.0 (t, 2H)
N-methylpyrrolidone	3.35 (t, 2H), 2.7 (s, 3H), 2.25 (t, 2.25). 1.9 (m, 2H)
pyrrolidone	*3.3 (t, 2H), 2.22 (t, 2H) 2.0 (m, 2H).*

Table 2.4: ^{1}H NMR (400 MHz, D_2O) shifts of the family of pyrrolidone compounds analysed.

2.1.8 Importance of the method of seed preparation

As can be noted from the discussion in Chapter 1, the structure of the seed particles is expected to be very important when considering the final morphology and monodispersity of the particles grown from them. For this reason, it was decided to prepare seeds by various different methods from the literature and monitor the effect on the grown nanoparticles.

The following seeds were prepared. The exact details of the syntheses are given in the experimental detail in Chapter 5.

1) Standard seeds

Prepared as detailed above in Scheme 2.1.

2) From Jana et al.[19]

Sodium borohydride was added in one rapid shot to a stirring aqueous solution of $AgNO_3$ and trisodium citrate. Stirring was stopped after 30 seconds and the seeds were aged for 4 hours under ambient conditions prior to use.

3) From Maillard et al.[20]

Sodium borohydride was added in one rapid shot to a stirring aqueous solution of $AgNO_3$ and trisodium citrate. Stirring was stopped after 5 minutes and the seeds were aged for 24 hours, under ambient conditions, prior to use.

4) From Chen et al.[21]

Sodium borohydride was rapidly injected into a stirring mixture containing $AgNO_3$ and trisodium citrate. The resultant sol was stirred for 3 hours and aged for 6 days under ambient laboratory conditions before use.

5) From Lu et al.[5]

An aqueous solution of $AgNO_3$ was rapidly mixed with trisodium citrate. Ice-cold sodium borohydride was added under vigorous stirring. The stirring was stopped after 30 seconds and the seeds were aged for 2 hours before use.

The UV-vis spectra of the seeds prior to use are shown below in Figure 2.27, as are the UV-vis spectra of sols prepared as described above in Scheme 2.1 at room temperature with 0.7 mM TSC. As can be seen from this data, small differences in the synthetic procedure of the seeds can lead to major differences in the sol grown from them. This result confirms the importance of controlling the nature of the seed particle, when considering a strategy for the growth of well-defined monodispersed sol followed a seed mediated process.

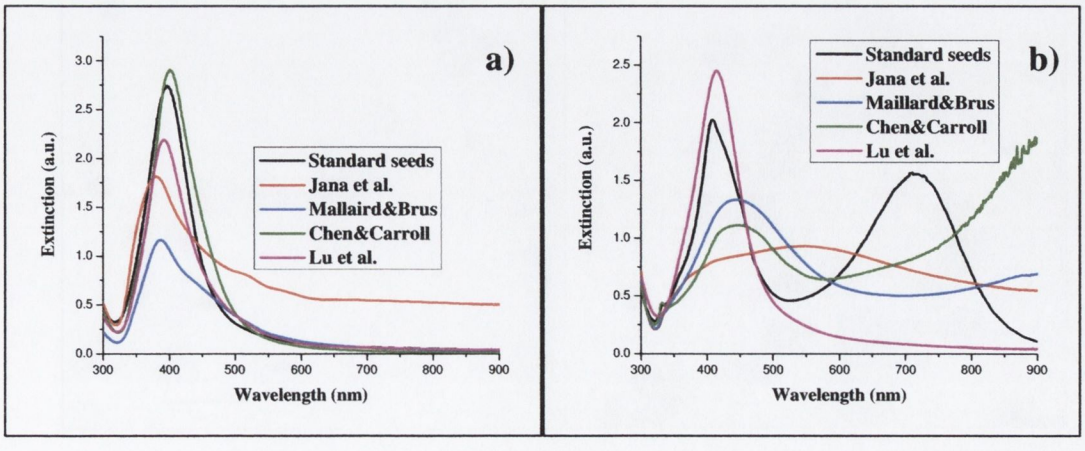


Figure 2.27: a) UV-vis spectra of the seeds prepared by the various methods listed above, immediately prior to use. b) UV-vis spectra of the sol grown from these seeds by the standard added citrate room temperature method.

During the course of the work carried out for this thesis, it was noted that the inclusion of poly(4-styrene sulfonate) sodium salt (PSSS) in the seed preparation, greatly increased the percentage of plate or prisms in the grown sol and the number of small spherical material as defined above in section was reduced immensely. The reason for the inclusion of PSSS in the growth of nanoparticles will be discussed further in Section 2.2 and 2.3 below. Figure 2.28 and Figure 2.29 below shows a typical UV-vis spectrum and TEM image of a sol prepared by the added citrate method using 0. 7 mM TSC at room temperature, using seeds prepared by the standard method as detailed above but with the Ag^{+}/TSC solution being made with a solution containing 20 mg/L PSSS instead of Millipore water.

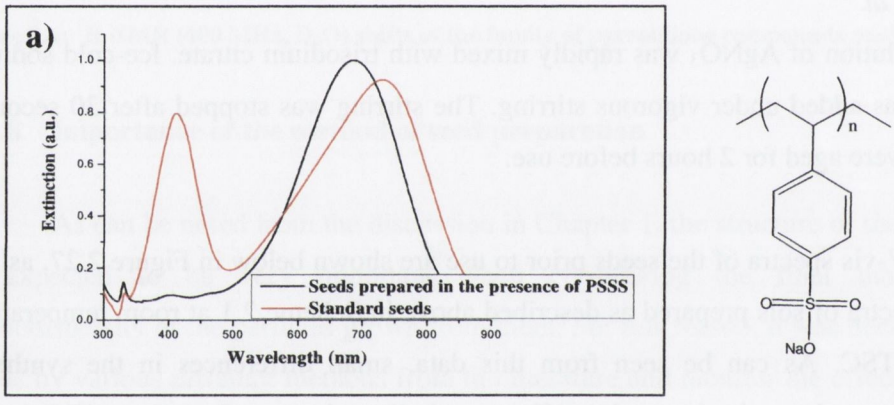


Figure 2.28: a) UV-vis spectra of sols prepared by the added citrate RT method using 0.7 mM TSC when the seeds are prepared in the presence (black) and absence of PSSS (red). Also included is the chemical structure of PSSS.

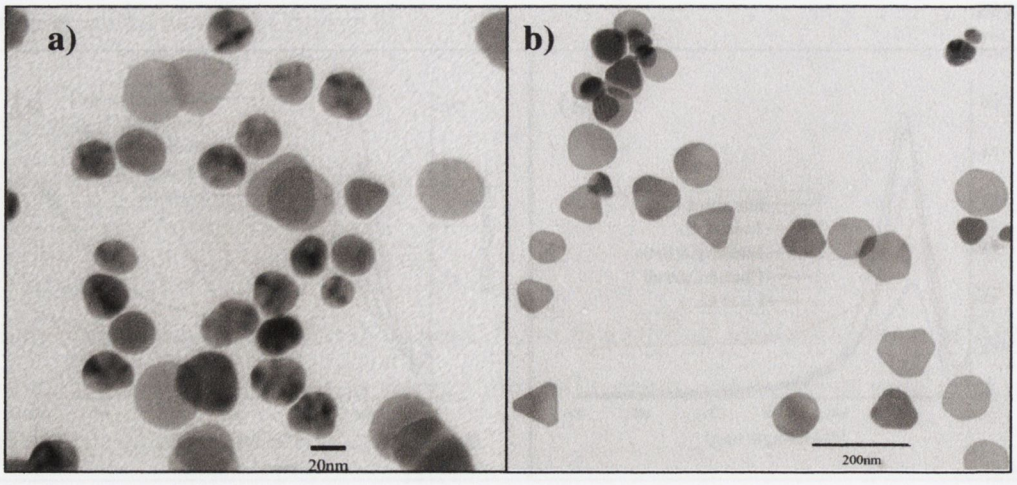


Figure 2.29: a&b) TEM images of added citrate sol prepared at room temperature with 0.7 mM TSC, in the presence and absence of PSSS respectively.

From the above result it is clear that the presence of PSSS in the preparation of seeds has a large effect on the morphology of the nanoparticles grown from the seeds. By comparing histograms of the shape distribution of the sols prepared in the presence (Figure 2.30) and absence of PSSS (Figure 2.8), at room temperature, it can be noted that the percentage of the plate-like morphology is enhanced by the presence of PSSS, while the population of spherical particles is diminished.

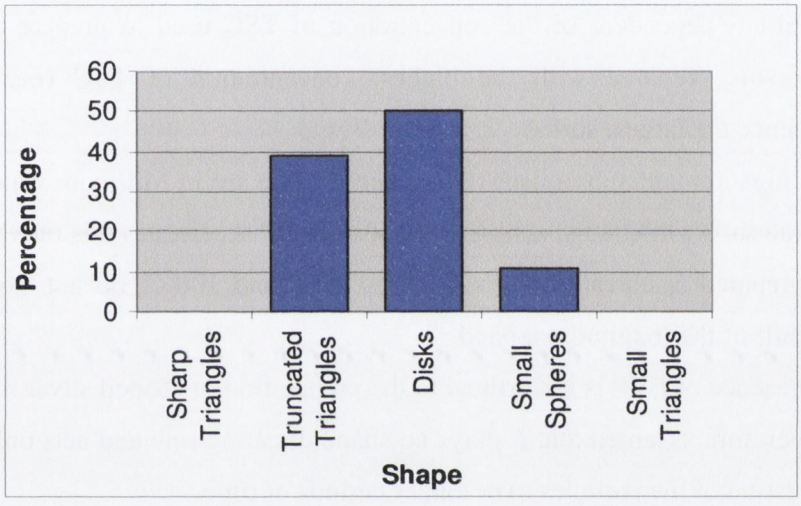


Figure 2.30: Histogram of the shape distribution of the sols grown by the added citrate RT method when PSSS is included in the seed synthesis.

2.1.9 Discussion of added citrate method:

As mentioned previously in the introduction to this chapter, the aim of the work described in this section was to develop a new synthetic method for the preparation of anisotropic silver nanoparticles. At this point it is beneficial to provide a summary of the findings of the experiments carried out. This is followed by a discussion of these results. Finally a possible growth mechanism is suggested.

1 Silver sols of various different colours have been produced by a seed mediated method involving the reduction of silver ion in the presence of trisodium citrate and PVP.

2 The morphology of the particles and therefore the colour may be tuned by varying the concentration of trisodium citrate.

3 The temperature at which the sol is prepared is important. As the temperature is increased the sols become more monodisperse and the particles become larger.

4 The in-plane dipole plasmon resonance of the sols blue-shifts with time. The biggest shift occurs within the first 40 minutes after the preparation of the sol. This blue-shift has been attributed to etching of the corners of the particles. The magnitude of this shift is dependent of the concentration of TSC used to prepare the particles. Those sols prepared with the highest concentration of TSC (i.e. green sols) experience the largest shifts.

5 Centrifugation and subsequent redispersion of the sol in Millipore water can retard this blue shift while redispersion of the sol in PVP accelerates this movement.

6 Sols prepared at elevated temperatures, i.e. 50 and 100°C, do not experience this blue shift of the longitudinal band.

7 The presence of PVP is not critical to the preparation of shaped silver nanoparticles. It is therefore assumed that it plays no shape directing role and acts only to prevent aggregation of the particles over longer periods of time.

8 Purification of the PVP by acetone precipitation yielded an impurity tentatively assigned as pyrrolidone by NMR analysis. It is this impurity that acts as an etchant and not the polymer as originally suspected.

9 The method used to prepare the seed particles is vital for the preparation of well-defined, relatively monodisperse silver sols. When other syntheses from the literature were used, the sols prepared where highly scattering with large FWHM of the in-plane dipole resonance, indicating that the shape and size of the particles present were polydisperse.

10 When PSSS is included in the seed synthesis, the resulting grown sols contain a higher percentage of plate-like materials and the number of isotropic particles present is greatly diminished.

2.1.9.1 Growth mechanism of particles of controlled shape

In order to propose any growth mechanism, it is of vital importance to understand the structure of nanoparticles. Extensive characterization, examples of which can be seen below in Figure 2.31, has shown that the large flat faces of the silver nanoprisms consist of the {111} fcc planes. X-ray diffraction (XRD) patterns show a dominant sharp peak for {111} indicating the presence of relatively large {111} planes in the sample. Electron diffraction patterns show spots corresponding to diffraction from the {220} and {422} planes of an fcc crystal. Also present are the signals arising from formally forbidden 1/3{422} reflections.[4, 7, 22-24] (The electron diffraction pattern shown above in Figure 2.7 corresponds well with this.) Lattice fringes associated with these forbidden reflections have also been seen in HRTEM studies as have lattice spacing from other crystallographic faces.[25-27] In summary the <111> orientation of silver nanoprisms is generally accepted, however the identity of the crystal faces at the edge of the nanoplates have yet to be confirmed.

It is also necessary to discuss the underlying fcc structure of silver. The surface energy of different crystal faces for this crystal structure is:{111}<{100}<{110}.[28, 29]As can be seen from Figure 2.32 below, the coordination number of atoms on the {111} face is 9 and they are arranged in close packed pattern, exhibiting a 6-fold hexagonal symmetry. This is the most energy efficient way of packing atoms and therefore the {111} face is the most stable. The {100} face, i.e. one side of the fcc unit cell, has a more open arrangement of atoms with a coordination number of 8 and exhibiting four-fold symmetry. The {110} face is the most unstable with a coordination number of 7.

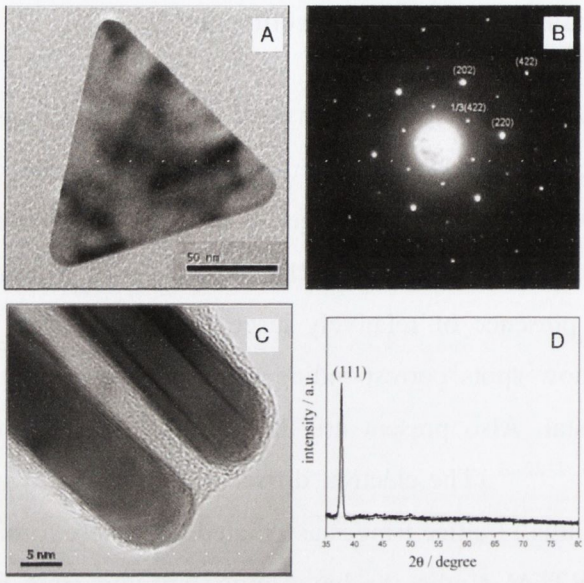


Figure 2.31: A) TEM image of <111> oriented silver nanoprism. B) Electron diffraction pattern of an individual silver nanoprism showing the assigned reflection indices. C) Edge-on-view of silver nanoprisms. D) Typical XRD pattern for a sample of nanoprisms. [25, 30]

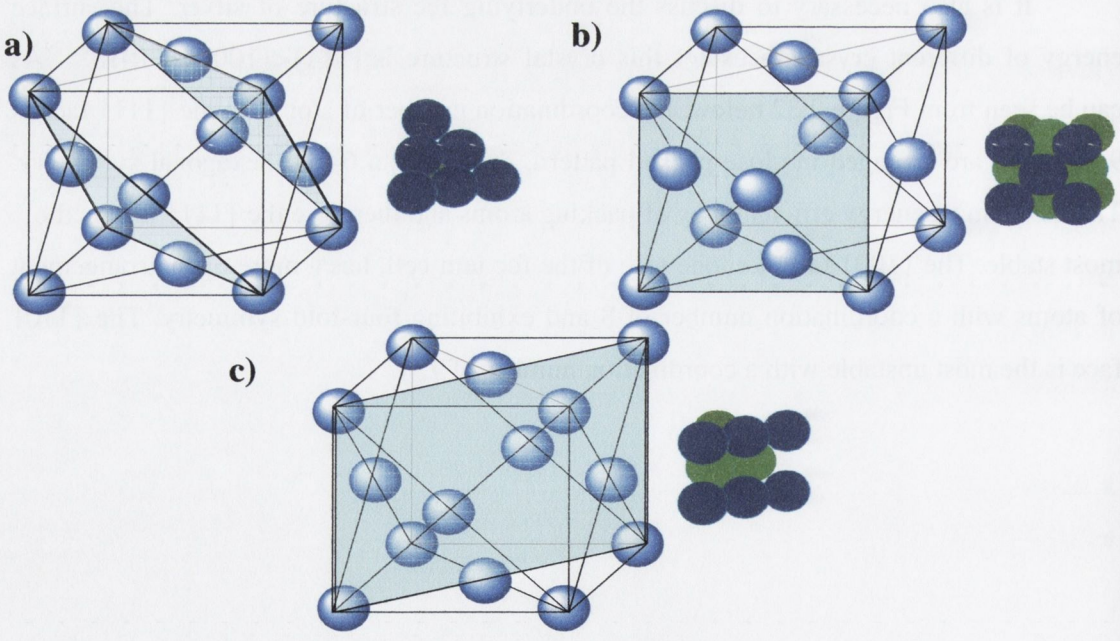


Figure 2.32: Face centred cubic lattice showing a) {111} b) {100} and c) {110} planes

The possibility of producing a particle that is 'perfect' in a crystallographic sense is unlikely as this would involve producing a structure whose surface contains high index-crystallographic planes, which are high in surface energy. To reduce this surface energy facets tend to form on particles that are smaller than 10 nm.[31] The most energetically favourable morphology for particles in this size regime is the truncated octahedral shown, below in Figure 2.33.[28] It can be seen that it is bounded by {111} and {100} facets and is based on a Wulff construction shape. A Wulff construction shape describes the equilibrium shape of a nanocrystal that minimizes the total surface energy for a given volume.

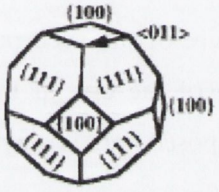


Figure 2.33: Diagram of a truncated octahedral seed particle.[28]

However real nanocrystals contain imperfections such as twins, or intrinsic or extrinsic stacking faults which form during crystal growth in materials where the stacking fault or twin boundary energy is low.[4] Although silver is an fcc metal as shown above in Figure 2.32 it can exhibit various different structural modification i.e. single crystal, single twinned or multiply twinned defects. This was already discussed in Chapter 1 and some examples of such defects are shown below in Figure 2.34.

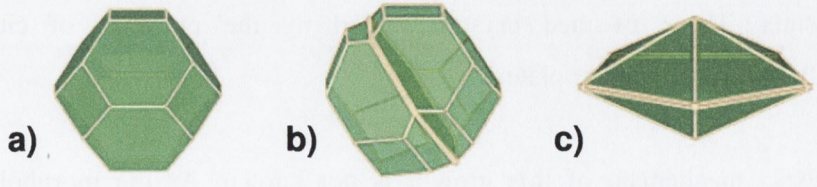


Figure 2.34: a) untwinned or perfect fcc crystal b) single twinned crystal c) pentagonally twinned crystal.[31]

There are a number of theories to explain the growth of anisotropic particles. As already discussed in Chapter 1, these theories include

1) templating by surfactant molecules
2) the preferential adsorption of organic stabilizers onto different crystallographic faces, leading to the addition of adatoms onto the more exposed faces, thus promoting growth in a certain direction.

In reality, the product of most synthetic procedures consist of a range of different morphologies and many different synthetic approaches can be used to prepare particles of the same morphology. For this reason it is more likely that the anisotropic growth that results from the preferential binding of organic species to certain crystal faces relies on the underlying twinned or defect structure of the seed particles since this is what ultimately determines the type and orientation of the crystal faces that are exposed to the growth medium. The growth mechanism proposed here is a hybrid of these two models.

The seed-mediated method described above allows the preparation of silver sols whose colour can be tuned by simply varying the concentration of one reagent (namely trisodium citrate). It is proposed that the mechanism is diffusion dependent. The silver ion and ascorbic acid must diffuse to the surface of the seed particle, where the silver ion is reduced to form silver atom. Reduction of silver ion by ascorbic acid will not occur in the absence of the seed particle. This atom is then incorporated into the structure of the seed particle.

The reliability of the method described above is certainly expected to be very dependent on the structure of the seed particles. The presence of a range of morphologies in the final sol suggests that the seed particles consist of a mixture of single crystal and twinned crystals. These twinned crystals, aided by the presence of citrate, grow anisotropically to form triangular plates.

The exact mechanism of this growth is not known. As the morphology of the particles produced is dependent on the concentration of TSC used in the growth step, TSC almost certainly plays some sort of shape directing role, probably due to its specific

adsorption on the {111} facets, inhibiting growth on this plane and therefore promoting anisotropic growth. Experiments carried out by various groups have established that citrate was the key component in the morphological evolution of spherical particles into thin plates bounded by the {111} facets in both photoinduced[7, 8, 23] and thermal[14, 32] syntheses. In fact in a recent paper by the Mirkin group it was stated that while other carboxylate-containing compounds, such as tricarballylate and citramalate were used in the photoconversion of silver nanospheres into nanoprisms, the only other carboxylate containing molecule that seems to effect prism formation is isocitrate.[33] Even in the case of isocitrate, although prisms form, other irregularly shaped large particles also are produced. Citrate is thought to preferentially adsorb on the {111} facets, inhibiting growth on this plane and therefore promoting anisotropic growth. Metraux and Mirkin have reported a synthesis in which, as the concentration of the reducing agent is increased, larger red-shifts of the in plane dipole surface plasmon have been observed.[14] In conjunction with this when the concentration of TSC is greater than 0.1 mM, nanoprisms were the major product. At concentrations lower than this, triangular and hexagonal structures were formed with a broad size distribution. To date, the procedure described above in Section 2.1 is the first and only reported, in which the concentration of TSC alone determines the shape of the nanoparticles and therefore the colour of the final sol.

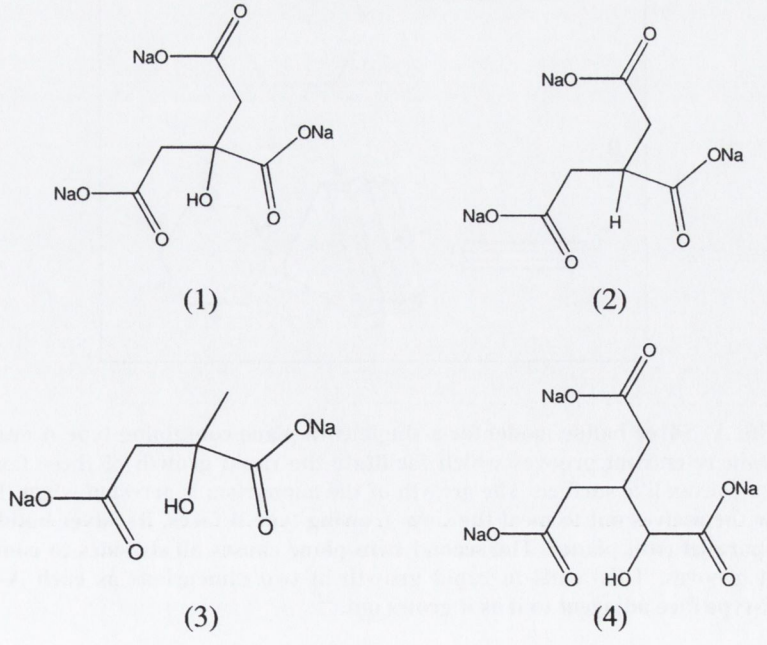


Figure 2.35: Chemcial structures of 1) citrate 2) carballylate 3) citramallate 4) isocitrate.

However, the presence of TSC cannot be the sole explanation for the anisotropic growth of the seed particles. A mechanism concerning the structure of the seed particle must also be considered. In recent years a few different approaches have been taken to understand this.

1) Pileni et al. showed the presence of 1/3{422} forbidden reflections in the {111} electron diffraction pattern; of silver nanoplates.[23] These signals were attributed to the presence of (111) stacking faults lying parallel to the {111} surface in the silver nanodiscs. It was suggested that these stacking faults occur in the initial nuclei of the particles and that further growth of the particles is accelerated along the (111) stacking fault so that the final particles have disc-like morphology.
2) The silver halide growth model has also been used.[4, 27] In this model, the presence of twin planes parallel to the flat {111} face is used to explain the anisotropic growth of particles. These twin planes are formed readily in gold and silver systems where the stacking fault energy is lower than in most metals, decreasing the energy required to form a twin plane. As shown in the diagram below, twin planes form re-entrant grooves which are favourable sites for the attachment of adatoms.

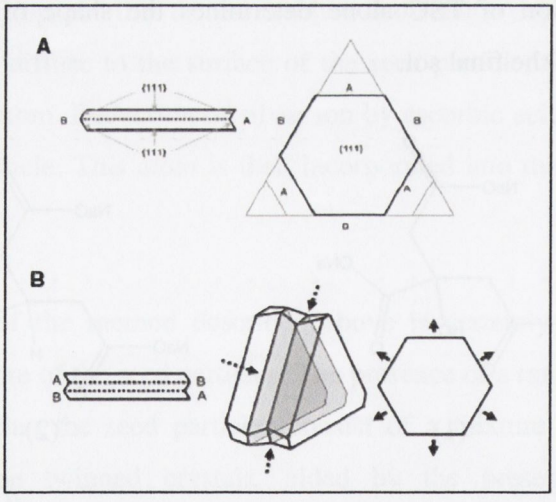


Figure 2.36: A) Silver halide model for a single twin plane containing type A and type B faces. Type A faces contain re-entrant grooves which facilitate the rapid growth of these faces while type B faces consist of a convex like surface. The growth of the nanoprism is arrested when the fast growing type A sides grow themselves out to meet the slow growing type B faces. B) Silver halide model for a particle with two parallel twin planes. The second twin plane causes all six sides to contain A-type faces with re-entrant grooves. This leads to rapid growth in two dimensions as each A-type face regenerates another A-type face adjacent to it as it grows out. [22]

3) Rocha and Zanchet have studied the defect structure of silver nanoprisms in detail and have shown that the internal structure can be very complex with many twins and stacking faults.[26] It was shown that defects which are parallel to each other and to the {111} face of the nanoprism can give rise to local hexagonally close-packed regions. This defect structure could also be observed in the seed particles. Recently our group has investigated this defect structure further in particles prepared by the 'no added citrate' method.[34] This will be discussed further below. TEM analysis provided direct evidence of a defect-induced arrangement of silver atoms that not only results in a hcp structure in the vicinity of the defects but also in multiple defects combining to yield a continuous hcp lamellar region (see Figure 2.37). The presence of this hcp region was also confirmed by XRD when two additional peaks, corresponding to predicted positions from theoretical diffractograms for a defect induced hcp arrangement of silver atoms, were observed. Due to this lamellar defect structure of the nanoprisms, it is at these edges that the hcp crystal structure is exposed to the growth solution and it is clear that the flat morphology of the nanoprisms arises from much faster growth here than on any other crystal face.

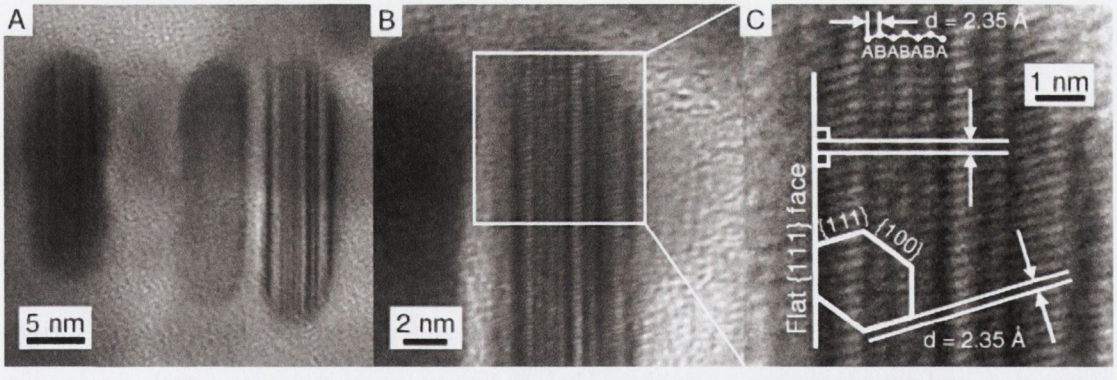


Figure 2.37: A) TEM image of a stack of vertically oriented silver nanoprisms. B) HRTEM image of the nanoprism on the right hand side of A, showing defect structure. This nanoprism is oriented such that the {110} plane is in the plane of the image, that is, the electron beam is along <110>. C) Analysis of the internal structure of the prism shown in B. A series of intrinsic stacking faults has resulted in a hexagonally close packed pattern emerging and gives rise to an arrangement of atoms that is aligned perpendicular to the surface with a spacing of 2.5 Å. The correct spacing of 2.35 Å has been obtained for the {111} planes and also for the alternative ABAB.... layers of the hcp region. From reference 34.

At this stage it should be clear that the growth mechanism for silver nanoprism is not fully understood. However it is also clear that growth of the nanoplates cannot be adequately explained by the surface binding model. Therefore, a defect structure is a more likely model to explain the growth mechanism. A mechanism similar to that described by Lofton and Sigmund is proposed.[22] It is based on the silver halide model in which the presence of twin planes creates favourable sites for the addition of atoms leading to anisotropic growth. The presence of both truncated and sharp triangular particles can also be explained by this model. The truncated triangular plates represent particles in which the tips have not grown out by the time the supply of Ag^+ had been consumed. The smaller spherical particles which are present are formed when single crystal seeds grow isotropically. It must be noted that at a small size there is enough thermal energy for the structure of the nuclei to fluctuate.[4] It is therefore almost impossible to effectively control the shape of small nanoparticles, such as seed particles in a complete way.

Let us now consider the case when poly(styrene sulfonate) sodium salt (PSSS) is present during the synthesis of the seed particles. The percentage of smaller spherical particles or multiple-twinned particles (MTP) is greatly reduced, with the dominant morphology being discs or truncated triangles. The exact nature of the interaction of the PSSS with the seed particle with the silver seed is unknown.

The role of PSSS will be further discussed below in Sections 2.2 and 2.3. It is clear however, regardless of the presence or role of PSSS, that the inherent structure of the seed particles is of vital importance when considering how these seed particles grow to yield plate-like structures. This importance of the nature of the seed particles has also been highlighted recently by Xia and co-workers when it was demonstrated that nanocubes, right bipyramids and nanowires can be produced by seed particles with single crystal, single twin crystal and multiple twinned morphologies respectively.[35-37]

Returning to the subject of the PVP, what role, if any, does it play? As reported above, sols containing triangular nanoplates are produced at various concentrations of PVP. However as it is reduced the particles become bigger and more polydisperse. It has been

proposed recently, that hydroxyl end groups present in commercial samples of PVP can reduce metal salts at a slow rate.[15, 16] However this is not the case in the procedure outlined above as growth occurs very rapidly. It appears that the PVP plays no role in the growth of the nanoplates but acts mainly to prevent particle aggregation. This observation is similar to that reported by Metraux and Mirkin.[14] Another point that backs up this observation is that Surface Enhanced Raman Spectroscopy (SERS) has previously been used to verify that PVP is adsorbed onto the surface of Pt nanoparticles.[18] When SERS spectra were obtained from these Ag particles, no signals from PVP were observed. This will be discussed again in detail in Chapter 4.

2.1.9.2 Stability of particles prepared by the added citrate method:

The sols prepared are stable when removed from excess growth mixture by centrifugation. However if they are not purified, a blue-shift of the in-plane dipole resonance with time is observed. A similar phenomenon has been reported recently by Jiang et al where triangular nanoplates were prepared by a self-seeded coreduction method in the presence of sodium bis(2-ethylhexyl) sulfosuccinate (NaAOT).[38, 39] The evolution from triangular plates to discs can reduce the total surface free energy through an atomic migration mechanism as the surface energy of different crystal faces for the fcc structure is : {111}<{100}<{110}.[28, 29] This would explain the initial blue-shift observed within the first 40 minutes after preparation of the sols prepared here. However it must be noted that commercially available PVP has an accelerating effect on this process (as is demonstrated in Section 2.1.7 above). A possible explanation for this observation is that PVP preferentially adsorbs to the {100} face of formed particles,[40, 41] thereby reducing the surface energy of this face relative to the {110} face. This promotes surface reconstruction to reduce the area of the {110} facets and increase the {100}. However, as shown above in Section 2.1.7, when the PVP is purified via acetone precipitation, this etching process can be prevented and it is only when the particles are exposed to the impurity (thought to be pyrrolidone) that etching occurs. This etching process in the presence of PVP has been reported previously on just one occasion. Wiley *et al.* converted silver nanobars to nanorice by storing them in an aqueous solution of PVP.[42] However no description of this process

was given. In fact, there is very little current literature on the subject of the shape or size evolution of silver nanoparticles due to etching. In the early 1990s Mulvaney *et al.* investigated the dissolution of small spherical silver nanoparticles (~5 nm) in the presence of nucleophiles such as chloride, cyanide and thiolate ions.[43, 44] This process is proposed to be initiated by the adsorption of a nucleophile (N) onto the surface of the silver nanoparticle. Because of this donation of electron density to the nanoparticle, the Fermi level is raised. This creates a situation were it is energetically favourable for an oxidising agent such as the O_2 dissolved in water to convert the Ag^0 to Ag^+. A surface layer of δ^+Ag---Nδ^- is formed which eventually leaves the surface as AgN. This process is shown schematically below in Figure 2.38.

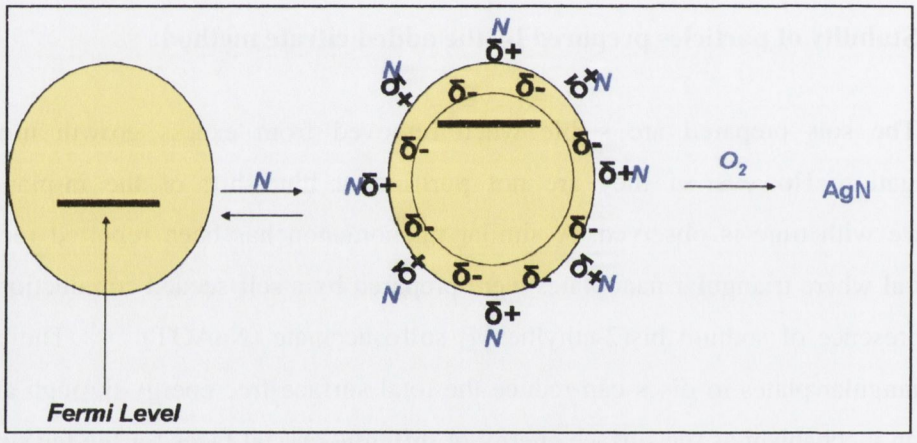


Figure 2.38: Schematic presentation of the surface complexation of a nucleophile (N), such as chloride, cyanide and thiolate ion, followed by oxidation of the particle by O_2.

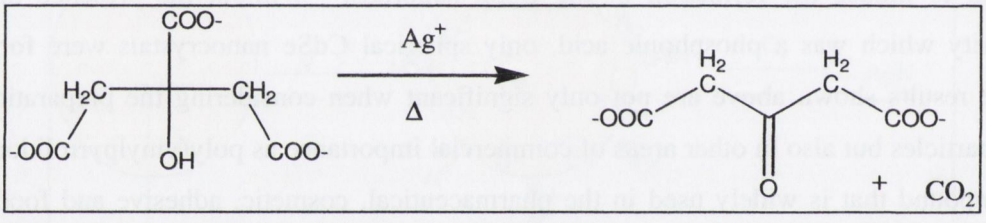
In the case of the etching of silver nanoparticles by the family of pyrrolidone compound described above, both pyrrolidone and N-methylpyrrolidone act as the nucleophile, raising the Fermi level, and thus making oxidation by O_2 more favourable. The degree of etching catalysed by N-methylpyrrolidone is greater than that of pyrrolidone because of the presence of the electron donating methyl group. Purified poly(vinylpyrrolidone) and N-vinylpyrrolidone do not cause etching when used at the same concentration of the aforementioned compounds, because of the steric hindrance around the lone pairs of electrons on the oxygen and nitrogen atoms. This bulk makes it more difficult for adsorption of these molecules on the nanoparticle surface. Oxidation does not occur because the Fermi level remains fixed.

The significance of these results lies in highlighting the importance of the quality and purity of compounds that are used in the synthesis of nanoparticles. A review of the literature concerning the preparation of nanoparticles reveals that the use of as received chemicals without further purification is commonplace. The following examples are the exception. A recent paper by Smith and Korgel,[45] reported that the yield of gold nanorods prepared by a seed mediated, surfactant assisted method[46] was highly dependent on the CTAB used. Ten different batches of CTAB were examined supplied by ten different manufacturers. The results indicate the presence of impurities in the CTAB from a particular supplier can vary from lot to lot and that this impurity in the surfactant can dramatically influence the colloid growth rate and thus nanorod formation. Another instance where the importance of an impurity in a reagent used was in the preparation of CdSe nanorods. Peng et al. noted that an impurity in trioctylphosphine oxide (TOPO), was needed to induce the formation of the CdSe nanorods.[47] Without the presence of this impurity which was a phosphonic acid, only spherical CdSe nanocrystals were formed. These results shown above are not only significant when considering the preparation of nanoparticles but also in other areas of commercial importance as poly(vinylpyrrolidone) is a compound that is widely used in the pharmaceutical, cosmetic, adhesive and food and drink industries.

2.1.9.3 Effect of Reaction Temperature

The temperature at which the preparation of silver nanoparticles (by the added citrate method as described above) is carried out is an important factor. As it is increased above room temperature, the monodispersity and stability of the particles is increased. It was shown above in Section 2.1.2, that analysis by FT-IR did not yield any conclusive insights into the effect of preparing the sols at elevated temperatures other than degradation of PVP was not observed. For this reason, and also because PVP does not appear to have any role in the growth of the particles it was decided to focus on the TSC. Citrate is known to reduce gold and silver at elevated temperatures.[3] It was initially postulated that as the temperature at which the synthesis is carried out is increased, the TSC may reduce Ag^+ as well as capping the resulting nanoparticles. If the TSC is playing a role in the reduction of

the Ag^+, its oxidation product, 1,3-acetonedicarboxylic acid (ADCA) could have some capping action and could possibly be a better stabilizer of the particles. Although ADCA is quite unstable and decomposes quickly to form acetoacetate it was decided to test this compound to see if it could be used to prepare shaped particles. The standard procedure was carried out substituting 1,3-acetonedicarboxylic acid for the TSC. Similarly, different coloured sols could be produced by changing the concentration of ADCA. These sols however, exhibited much more scattering than those prepared with citrate. The dipole resonance at longer wavelengths was much broader indicating a wide variation in both the size and shape of the nanoparticles. Importantly, these sols did not possess any extra stability and were subject to the aforementioned blue-shift. This indicates that ADCA is not a more efficient capping agent and does not play a role in the growth mechanism of particles prepared at temperature higher than room temperature.



Scheme 2.2: The oxidation of citrate to acetonedicarboxylate in the presence of silver ion and heat.

Further experiments to gain further insight into the possible role of ADCA in the preparation of silver nanoparticles would include varying the pH at which the synthesis is carried out. In the procedure described in the section above, the pH of the growth solution is between 5.5-6. At this pH the acid would exist in predominantly its protonated form. If the pH was increased, the deprotonation would occur and this would give a better system which could be directly compared with the TSC case.

Another explanation for the increased monodispersity of the sols as the temperature at which they are prepared is increased lies in the balance of thermodynamic vs kinetic control. As the temperature of the reaction is increased, the kinetics of the reduction of Ag^+ by ascorbic acid are also increased. By controlling the reduction kinetics, the propensity for thermodynamic control is reduced therefore reducing the formation of multiple twinned

particles which are the most thermodynamically favourable products.[12, 28, 31, 48] The kinetic regime then dominates. The role of the TSC becomes more important, and by adsorbing onto the {111} faces promotes growth on the other faces which are higher in energy. The final product can then take a shape deviating from these thermodynamically favourable ones. The presence of the small spherical particles can only be explained by the structure of the seed. Growth occurs more quickly on seeds with a twin defect because these sites are higher in energy.[12, 36, 49-53] The plates grow out through a mechanism similar to that described above, whereas growth on the single crystal seeds which is isotropic in nature does not occur as quickly.

But why the increased stability of particles prepared at temperatures greater than room temperature? When the synthesis is carried out at 100°C, the particles do not experience any blue-shift of the in-plane dipole resonance even when left in the original growth solution. As shown above, the biggest factor affecting the truncation of the particles with time is the presence of impurities in the PVP. However, these impurities are still present in the growth solution when the reaction is carried out at higher temperature. The boiling points of both pyrrolidone and N-methyl pyrrolidone are greater than 200°C and it is thought that the pyrrolidone ring remains intact. This would suggest that the capping ability of PVP becomes more efficient as the temperature is increased and the particles are protected from these species. This would also explain why the etching of Ag nanostructures prepared by the polyol method in which the reaction mixture is heated to temperatures in excess of 120°C has not been reported. It would be interesting to compare sols prepared at room temperature with those prepared at 100°C by X-ray photoelectron spectroscopy to investigate firstly, if PVP is adsorbed on the surface of the particles and secondly if the method of coordination varies with reaction temperature.

2.1.10 Conclusion of the 'added citrate' method

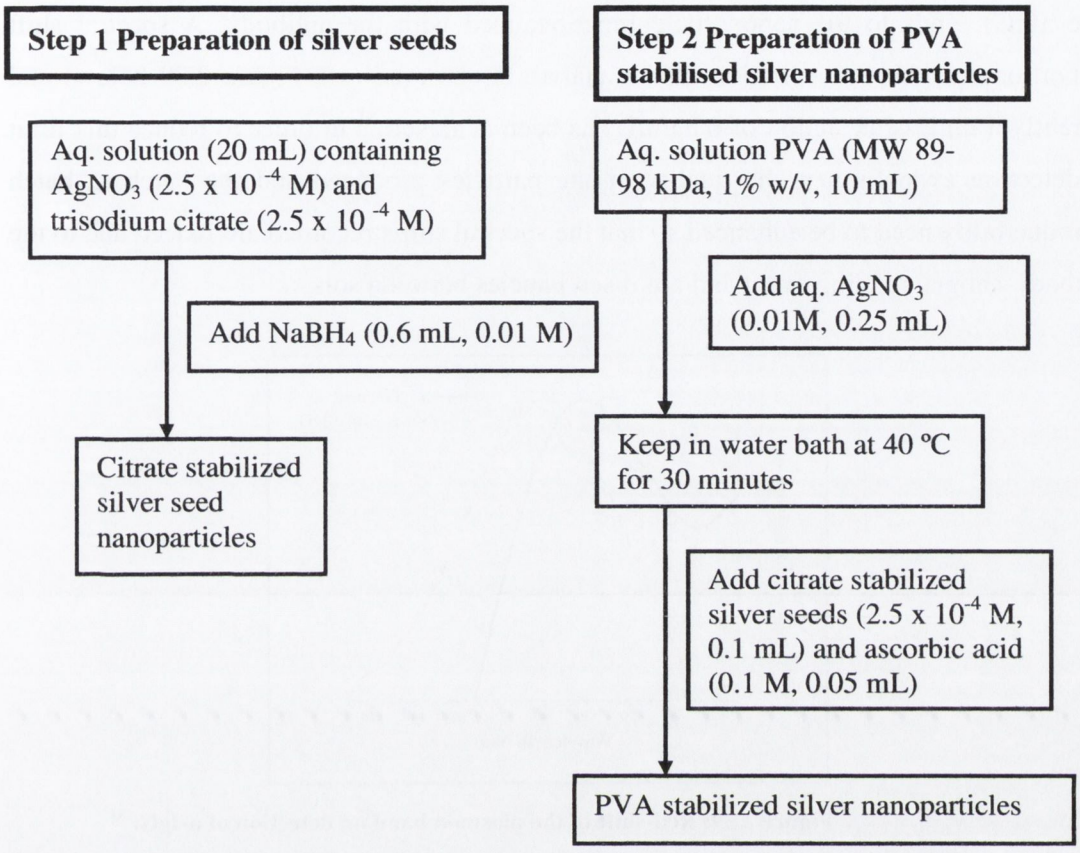
A new method to synthesise silver sols of various colours has been developed. It is a simple aqueous method where only the concentration of one reagent, the trisodium citrate, is changed. As the temperature at which the reaction is carried out is increased from room

temperature, well-defined triangular plates, with increased stability are produced. As PVP was not found to be a critical factor in determining the shape of the particles prepared by this method, it is assumed to be important only in preventing the aggregation of the particles once they are prepared. However, the stability of the particles prepared by this method was found to dependent on the presence of an impurity in the PVP. A growth mechanism highlighting both the role of the underlying structure of the seed particles and the presence of an organic molecule capable of adsorbing selectively onto one face of the seed particle has been suggested. The importance of the seed structure and reason why PSSS was added to the seed synthesis will be discussed in further detail in the following sections of this chapter.

2.2 The reproducible preparation of PVA stabilized silver sols:

2.2.1 Introduction

This procedure was the first synthetic method developed within the group and was pioneered by Dr. Aine Whelan as part of her PhD thesis.[1] At the time when this work was carried out the interest in silver nanoparticles was just beginning to increase and very few aqueous based syntheses for the preparation of anisotropic silver nanoparticles had been reported. It subsequently became the basis of a patent application for the use of the particles for biosensing.[54]. Briefly, in this procedure, aqueous PVA and silver nitrate are brought to 40°C and left to stir at this temperature for 30 minutes. Seed solution and ascorbic acid are then added sequentially. A colour change from colourless to yellow to red is observed. A flow diagram of a typical synthesis is shown below in Scheme 2.3.



Scheme 2.3: Synthesis of the silver nanoparticles prepared by the PVA stabilized method.

The colour of the resultant sol and therefore the morphologies of the nanoparticles can be changed from red to purple to blue to green by increasing the concentration of PVA. Originally, the preparation was carried out on a 10 ml scale and although there was some variation in the position of the SPR bands from batch to batch, the sols prepared in one single batch were similar i.e. there was very little variation in the UV-vis spectra and analysis of the sols by TEM showed that the size and shape distribution of particles very similar. However problems were encountered when larger volumes of sol were made. The in-plane dipole resonance could vary a much as 100 nm between different sols. This posed serious problems for collaborators in NUI Galway where the particles prepared by this method were being used for spectral sensing. Briefly, the particles were first functionalized by an antibody such as IgG. A shift of the in-plane dipole is observed because the dielectric constant of the medium surrounding the nanoparticles is changed by this binding event. A further change of the dielectric medium is recorded when the appropriate antigen (in this

case aIgG) binds to the nanoparticle functionalized with the antibody. A spectral shift proportional to the concentration of the analyte is observed (see Figure 2.39 below) and currently a limit of detection of 6 ng/mL has been achieved.[54] In order to reduce this limit of detection even further, the quality of the particles produced and the batch to batch reproducibility need to be enhanced so that the spectral shifts recorded are indeed due to the antibody-antigen binding event and not discrepancies between sols.

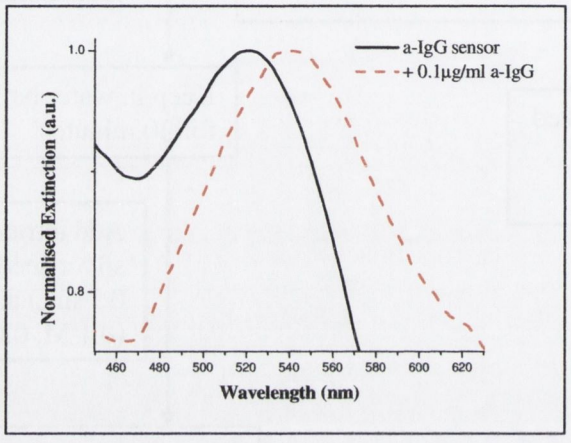


Figure 2.39: Red-shift of the plasmon band on detection of a-IgG. [53]

2.2.2 Results:

The starting point for the work described in the following section was the method for the preparation of particles as per Patent No: WO2004/086044. The synthesis as described above in Scheme 2.3 was carried out. It must be noted the TEM was not operational during the time this section of work was carried out so UV-vis spectroscopy was the sole means of characterizing both the seeds and nanoparticles grown from them. The preparation of the seed particles was described already above in Section 2.1. In the growth step, PVA (10 ml, 1 wt%) and $AgNO_3$ (0.01 M, 250 µL) were added to a boiling tube and heated to 40°C and maintained at this temperature for 30 minutes. Seed solution (100 µL) and ascorbic acid (0.1 M, 50 µL) were added simultaneously and the boiling tube was removed from the heat and shaken by hand. A gradual colour change from colourless to yellow to orange to red is observed over a period of 30 seconds.

The growth procedure described above was also carried out in front of a 75 W xenon lamp. In this case PVA (10 ml, 1 wt %) and $AgNO_3$ (0.01 M, 250 μL) were added to a boiling tube. Seed solution (100 μL) was added and the reaction vessel was placed 60 cm in front of the lamp. Ascorbic acid (0.1 M, 50 μL) was then added using a micropipette and the boiling tube was shaken to ensure mixing. A colour change from colourless to red was observed over a period of 30 seconds.

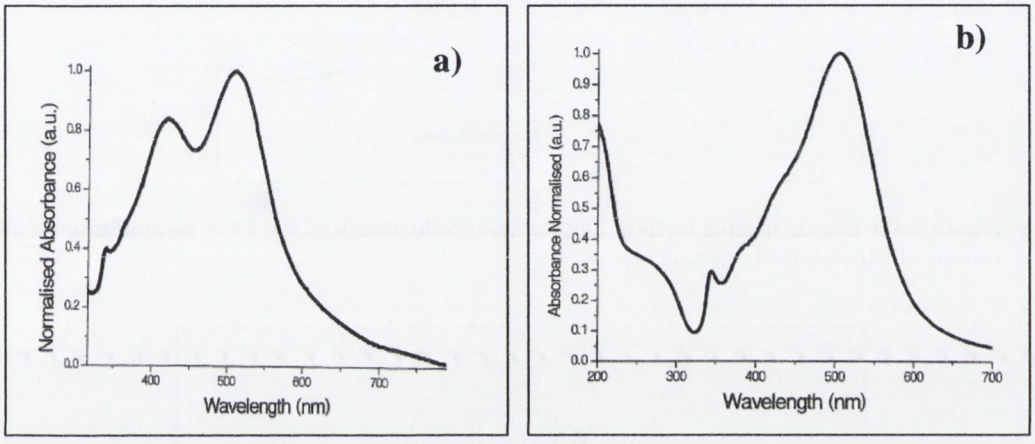


Figure 2.40: Typical red sol prepared by the a) heating method b) irradiation method described above.[53]

The above methods were used to prepare red sols on a 10 ml scale routinely. The batch to batch reproducibility was good and the resultant sols exhibited good spectral shifts when used for the antibody- antigen detection. It was decided to focus the scale-up efforts on the particles that were prepared in the absence of UV irradiation. The reason for this was mainly based on industry precedent. The use of UV irradiation is not favoured in large industrial processes and the growth of the particles by this method also requires a longer timeframe. However, when the thermal procedure was scaled up, the reproducibility of the preparation was diminished. As shown in Figure 2.41 below, simply by scaling up the volume at which the procedure was carried out from 10 ml to 100 ml a wide variety of coloured sols was produced. Further to this, when the method was repeated a number of times using the same seed particles and the same growth reagents, sols of the same colour could not be routinely produced. In some cases, the variation of the position of the in-plane dipole resonance could vary as much as 200 nm (see Figure 2.42).

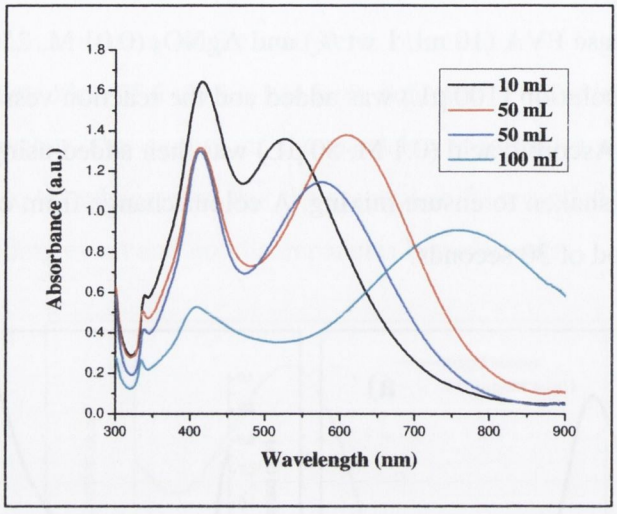


Figure 2.41: UV-vis spectra highlighting the irreproducibility of the PVA method upon scaling up the volume at which sols are prepared.

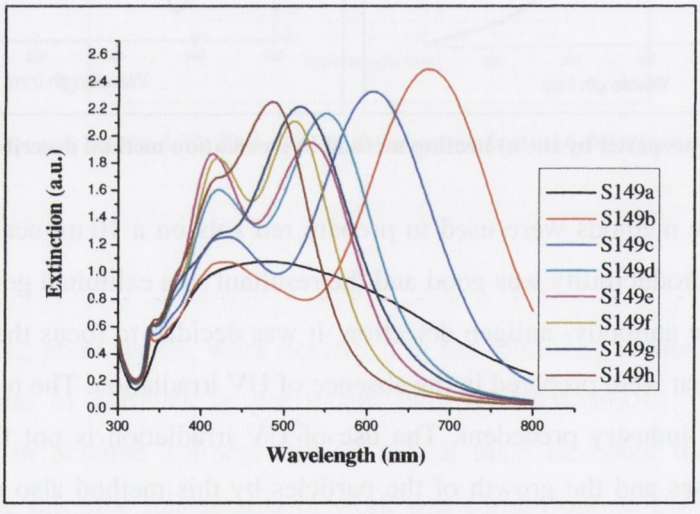


Figure 2.42: : UV-vis spectra of sols prepared on a 100 mL scale using the same seeds and the same reagents, again highlighting the irreproducibility of the PVA method.

Also these sols exhibited a higher degree of scattering than those prepared initially on a 10 mL scale. The following conclusions were drawn from the above results:

1. Reproducibility of the procedure was affected negatively by increasing the volume at which the nanoparticles were prepared at.

2. The particles were bigger than those prepared originally. This is indicated by more scattering.

3. There was a wider size distribution of particles present than in the earlier samples. This was indicated by an increased band width of the in-plane dipole resonance when compared to sols prepared in the earlier work.

Because of these factors, the nanoparticles produced by the scaled up method were not ideally suited for use in the spectral sensing.

It was decided to investigate the importance of various different parameters in the synthesis and in this way try to improve the reproducibility of batch-to-batch synthesis of the sols. The synthesis was broken down into four main steps.

Step 1: $AgNO_3$ is reduced in the presence of TSC by $NaBH_4$. The resultant seeds are aged for at least 2 hours prior to use.

↓

Step 2: $AgNO_3$ and PVA are heated together to 40°C and maintained at this temperature for a given period of time.

↓

Step 3: Seeds are added to the growth mixture.

↓

Step 4: Ascorbic acid is added to the growth mixture.

A thorough investigation of various different parameters including the nature of the silver seeds, the concentration of PVA used, the molar ratio of silver ion to elemental

silver, the molar ratio of ascorbic acid to silver ion, the molecular weight of PVA used and the chemical nature of the stabilizing agent used was carried out previously[55] and as such was deemed unnecessary to repeat. The purpose of the work described in this section was to improve the reproducibility of the *scaled up* preparation of the nanoparticles prepared by the PVA method. Because of this it was decided to focus on environmental factors affecting the synthesis. The variables associated with each step are summarized below in Table 2.5

Variables throughout the synthesis	*Light vs Dark*
Step 1:	Temperature Time at that temperature Rate at which that temperature is achieved
Step 2:	Method of preparing the seeds Whether the seeds and the ascorbic acid are introduced together or separately.
Step 3:	Rate of stirring on addition of the AA

Table 2.5: Variables associated with the preparation of silver nanoparticles by the PVA method.

2.2.2.1 Light vs dark

The most significant of these factors was found to be the presence or absence of light. From the work carried out by Aine Whelan it was known that because the nucleation and growth of seed particles occurs so rapidly, *i.e.* less than one minute, there is insufficient time for light effects to become important.[55] Therefore efforts were concentrated on investigating the effect of light on the growth process.

The standard procedure (as described above in Scheme 2.3) was carried out on a 50 mL scale with the following adjustment. The $AgNO_3$ and PVA solutions were combined together under ambient laboratory conditions. The rest of the growth step was carried out in

a darkroom. As can be seen from Figure 2.43 below, the reproducibility was greatly improved by carrying out the growth step in the absence of light.

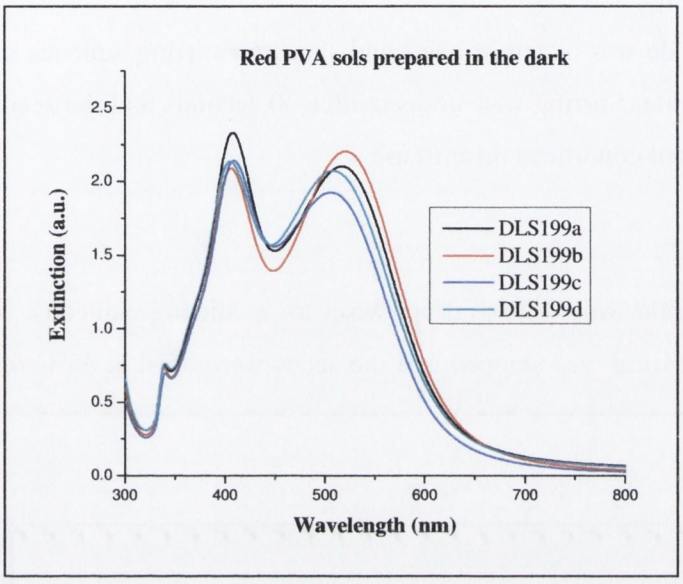


Figure 2.43: Sols prepared by the PVA method, with the growth step carried out in the dark.

2.2.2.2 Method of seed preparation:

Of the other factors listed above in Table 2.5, another one which has an important effect on the reproducibility of the procedure is the nature of the seed particles. As can be noted from the discussion in Chapter 1 and above in Section 2.1.8, the structure of the seed particles is expected to be very important when considering the final morphology and monodispersity of the particles grown from them. For this reason, it was decided to prepare seeds by various different methods from the literature and monitor the effect on the resultant nanoparticles.

The following seeds were prepared. The exact details of the syntheses are given in the experimental section in Chapter 5.

1) Standard seeds

Prepared as detailed above in Scheme 2.3.

2) From Jana et al.[19]

Sodium borohydride was added in one rapid shot to a stirring aqueous solution of $AgNO_3$ and trisodium citrate. Stirring was stopped after 30 seconds and the seeds were aged for 4 hours under ambient conditions prior to use.

3) From Ni et al.[56]

Sodium borohydride was added drop wise to a stirring aqueous solution of silver dodecylsulfate. Stirring was stopped and the seeds were aged at 35°C for 2 hours prior to use.

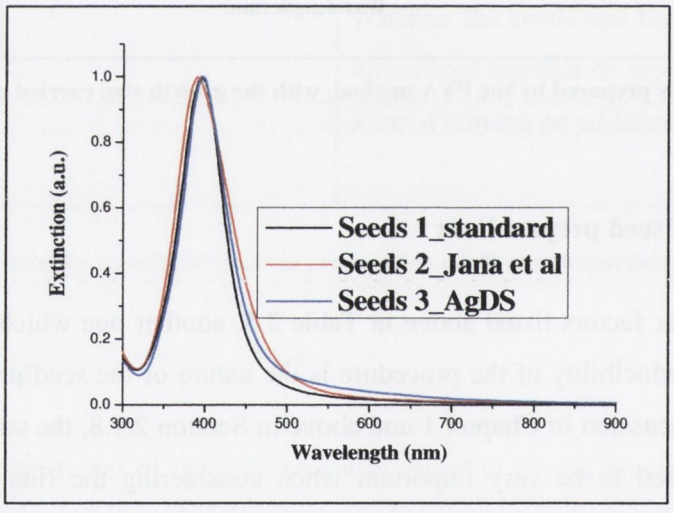


Figure 2.44: Seeds prepared by different methods from the literature.

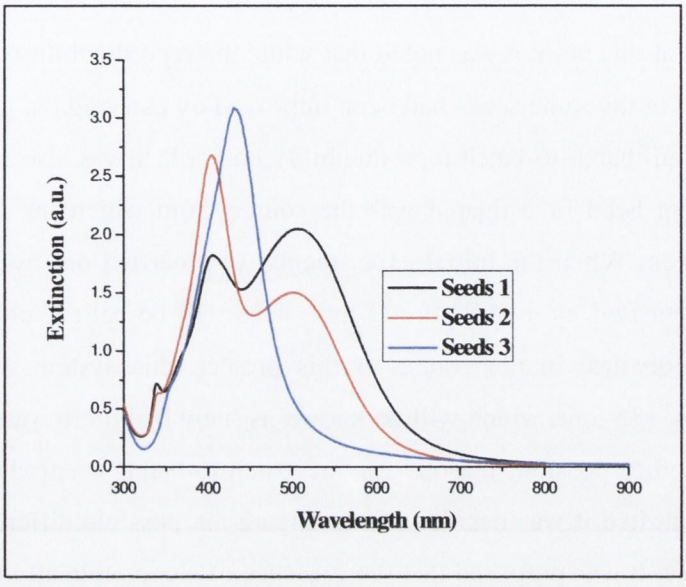


Figure 2.45: Sols grown by the PVA method, in the dark from seeds above in Figure 2.44.

Again similar to the case shown above in Section 2.1.8, small differences in the synthetic procedure of the seeds can lead to major differences in the sol grown from them. Another aspect to be noted from the above results is UV-vis spectroscopy alone is not sufficient to characterize whether or not the seeds prepared are suitable to be grown into highly shaped particles. While only small shifts were observed in the spectra of the seed particles, the UV-vis spectra were noticeably different. This result confirms the importance of controlling the nature of the seed particle, when considering a strategy for the growth of well-defined monodispersed sol followed a seed mediated process.

To summarize the results this far, it was found experimentally that small differences in the experimental procedure such as the rate of stirring etc did not increase the reproducibility of the PVA method. The quality of particles grown by this method is highly dependent on the method used to prepare the seed particles. The most important parameter effecting the growth of the particles was found to be the exclusion of light for the growth stage of the synthesis.

2.2.2.3 Water quality issues:

However, at this point it was noted that while the reproducibility of sols prepared in the same batch from the same seeds had been improved by carrying the growth stage out in the dark, the overall batch-to-batch reproducibility had not. It was also noted that the only factor that had not been investigated was the source from which the water used in this synthesis was taken. When the initial experiments were carried out by Aine Whelan, the water used was purified by a Millipore Q unit. This will be called 'old Millipore water' from this point forward. In the course of this project, this system was replaced by a Millipore Synergy 185 unit, which will be known as 'new Millipore water' from this point forward. As all other possible reasons for the batch-to-batch irreproducibility had been explored and exhausted it was decided to investigate the possible differences between the two water supplies. It was proposed that the presence of a contaminant in the old Millipore water, aided the growth of the nanoparticles prepared in the first instance and when the water purification system was changed, this contaminant was no longer present. In essence, the 'new Millipore water' was too pure!

The first step in identifying this compound was to contact the water purification section of Millipore. Unsurprisingly, they were unwilling to give any suggestion to what the nature of this compound might be. It was then decided to investigate compounds that could be used for ion-exchange applications. Poly(sodium 4-styrenesulfonate) is one such compound. The structure is shown below in Figure 2.46.

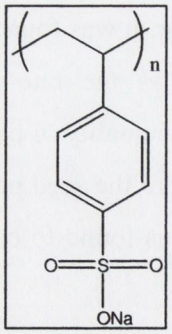


Figure 2.46: Structure of poly(sodium 4-styrenesulfonate) sodium salt (PSSS).

The standard procedure (as per Scheme 2.3 above) was carried out on a 100 mL scale, in the dark. All solutions used, both in the preparation of the seeds and the growth step, were prepared with an aqueous solution of PSSS, at a concentration of 20 mgL^{-1}. The graph below depicts the results of six individual experiments, where six batches of nanoparticles were prepared from six individual sets of seeds. The remarkable reproducibility, especially when compared with a similar experiment shown in Figure 2.41 above must be noted. Further investigations revealed that PSSS was necessary only in the preparation of the seed particles and could be eliminated from the growth step without having a detrimental effect on the repeatability of the method.

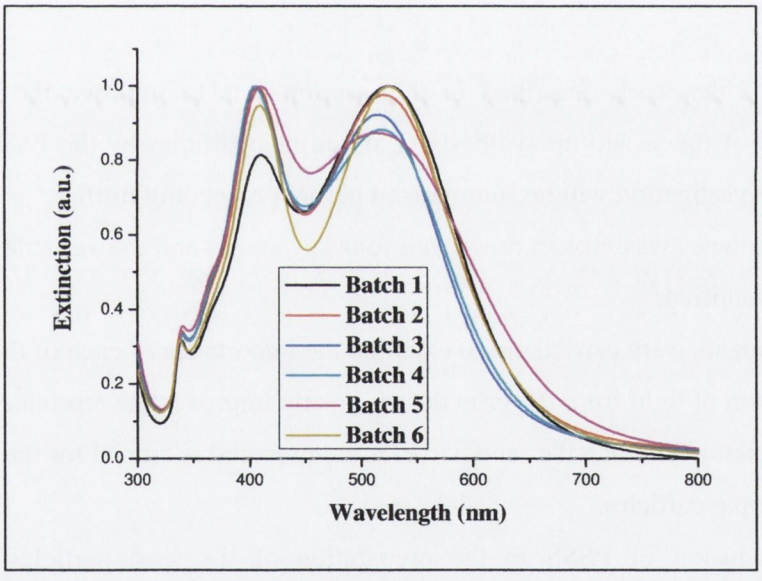


Figure 2.47: Six different batches of sols prepared under identical conditions, in the presence of PSSS, using six different sets of seed particles.

2.2.3 Discussion of the PVA method:

One of the biggest challenges encountered by material chemists is the scaled up synthesis of nanoparticles. Currently nanoparticles are produced in batch methods on a small scale which at best produces only quantities on the milligram to gram scale. As shown above, each batch of particles will have slightly different shapes and size distributions. By combining particles from different small volume batches the size distribution of the product is broadened. In order for nanoparticles to be used in applications such as sensing, larger batches (ultimately on a litre scale) with good batch to batch reproducibility need to be produced. The current production limitations also lead to a relatively high price which may be prohibitive to the development of technologies using nanoparticles.

The aim of the work described in this section was to improve the batch-to-batch reproducibility of the scaled up synthesis of silver nanoparticles by the PVA method. The results of the investigation will be summarized before proceeding further.

1. The synthesis was broken down into four key stages and the variables in each stage were identified.
2. Experiments were carried out to examine the importance of each of these variables.
3. Exclusion of light from the growth step greatly improves the reproducibility.
4. The method by which the seed particles are prepared is crucial for the preparation of anisotropic particles.
5. The inclusion of PSSS in the preparation of the seed particles enhances the reproducibility.

The reproducibility of the size and shape of PVA stabilised silver nanoparticles is affected by fluctuations in ambient light intensity. It is known that the photoreduction of silver ion in the presence of PVA is possible. It was previously shown by Aine Whelan in the course of her doctoral studies that seed particles can be produced which can grow in competition with the citrate stabilized seeds used in the synthesis. However it was previously shown that this photo-reduction was dependent on the concentration of PVA

used i.e. when 5 wt% PVA was used the formation of these 'seed' particles was increased. Recent work by Xia et al has shown that, the hydroxyl end groups of commercially available poly(vinylpyrrolidone) (PVP) are responsible for the reduction of noble metal salts l at temperatures greater than room temperature over periods of time of the order of 21 hours.[15, 16] It is therefore not unreasonable to suggest that in the above synthesis, the hydroxyl group of PVA are capable of reducing silver nitrate to form seed like nanoparticles. By performing the synthesis under the exclusion of ambient light, the possibility of the production of these seeds is reduced and therefore growth can only occur on the citrate stabilized seeds produced in the first step of above synthesis.

With regard to the importance of the method of production of seed particles, as stated above in section 2.1.8, the reliability of any method is expected to be very dependent on the structure of the seed particles. This is clear from Figure 2.45 above. In order to improve the reproducibility of the synthesis described above it clear that the reproducible synthesis of seeds needs to be addressed. Work carried out by the Brennan-Fournet group in NUI Galway has focussed on this and a microfluidic based method to produce seeds has been developed which in turn has greatly enhanced the routine reproducibility of the synthesis.

The inclusion of the cationic polymer poly(sodium 4-styrenesulfonate) (PSSS) during the production of the seed particles also greatly increased the reproducibility of the synthesis. In the following section, various different experiments carried out to investigate the role of PSSS in the two methods for the preparation of silver nanoparticles described above and also an additional third method, developed recently, will be presented.

2.3 The importance of PSSS in the preparation of seed particles:

2.3.1 No added citrate preparation of silver nanoparticles:

In the course of my PhD studies a third method, for the preparation of silver nanoparticles was developed in our lab in collaboration with Dr. Damian Aherne.[34] This method for silver nanoprism synthesis is another seed-based thermal synthetic procedure that *selectively* produces (>95%) silver nanoprisms in a rapid and reproducible manner; and under very mild conditions (room temperature and water as solvent, see the experimental section in Chapter 5 for details). The method involves the silver seed-catalyzed reduction of Ag^+ by ascorbic acid, and differs with previously reported procedures in that the concentration of spherical nanoparticles produced is minimal. The position of the in-plane dipole SPR can be tuned by controlling the size of the nanoprisms, with only a small variation in thickness. This can be achieved simply through adjustment of the number of seeds in the growth mixture (see Figure 2.48).

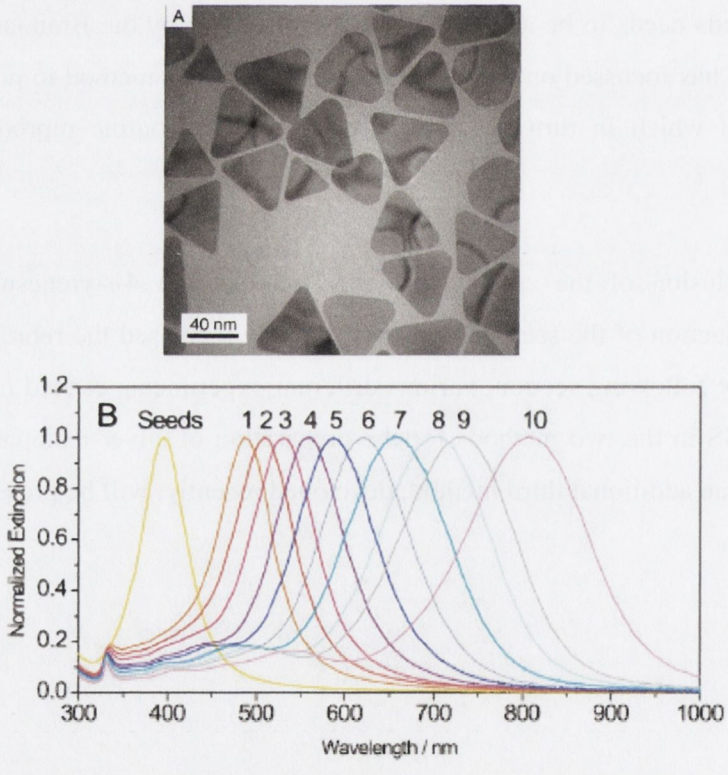


Figure 2.48: A) TEM image of silver nanoprisms prepared with 60 µL seeds B) Normalized spectra of a series of as-prepared samples obtained using different volumes of seed solution: 1) 650 µL, 2) 500 µL, 3) 400 µL, 4) 260 µL, 5) 200 µL, 6) 120 µL, 7) 90 µL, 8) 60 µL, 9) 40 µL, 10) 20 µL.[34]

Another difference between this procedure and those previously discussed above is that no shape directing agent *i.e.* no trisodium citrate (TSC) or polyvinylalchol (PVA) is used in the growth step. For this reason, it was proposed that it is the defect structure alone that determines the final morphology of the resultant particles.[34]

A key ingredient for the production of such high quality particles was found to be poly(sodium styrenesulphonate) (PSSS), which is used as a stabilizer in the seed production step. As shown above in Sections 2.1 and 2.2 the inclusion of PSSS in the synthesis of nanoparticles in both the added citrate method and the PVA method increases the monodispersity and reproducibility of the resultant sols respectively. The aim of the experiments described in the following section, was to determine the role of PSSS in preparing monodisperse, highly shaped silver nanoparticles.

2.3.2 Results:

As already mentioned above in Section 2.2, the presence of PSSS was only found to be necessary in the preparation of the seed particles. It was therefore decided to vary order of addition of the reactant in the seed growth step. Two sets of seed particles were prepared

1) In the absence of PSSS
2) In the presence of PSSS.

Briefly, the standard procedure for the preparation of seeds involves the drop wise addition of $AgNO_3$ using a peristaltic pump to a stirring solution containing citrate and sodium borohydride in the presence of PSSS. This procedure was varied as follows

Absence of PSSS

Seeds_1_no PSSS: $AgNO_3$ was added drop wise using the peristaltic pump to a stirring solution of TSC and $NaBH_4$.

Seeds_2_no PSSS: $AgNO_3$ was added drop wise using the peristaltic pump to a stirring solution of Millipore water and $NaBH_4$. No TSC was used.

Seeds_3_no PSSS: TSC was added to an aliquot of seeds_2 after the seed particles had been produced.

Presence of PSSS

Seeds_4_with PSSS: $AgNO_3$ was added drop wise using the peristaltic pump to a stirring solution of TSC and $NaBH_4$.

Seeds_5_with PSSS: $AgNO_3$ was added drop wise using the peristaltic pump to a stirring solution of Millipore water and $NaBH_4$. No TSC was used.

Seeds_6_with PSSS: TSC was added to an aliquot of seeds_2 after the seed particles had been produced.

The UV-vis spectra of the seeds prepared are shown below in Figure 46. These seeds were then used in all three methods described above for the synthesis of silver nanoparticles

1) added citrate method
2) PVA method
3) No added citrate method

It must be noted that the experiments carried out on the 'no added citrate' method were carried out at a preliminary stage in the development of the method. Therefore the sols prepared are not as monodisperse as those shown above in Figure 2.48. Subsequent development of the method, including controlling the rate of addition of $AgNO_3$ with a syringe pump instead of the peristaltic pump and controlling the efficiency of mixing yielded the monodisperse sol shown above.

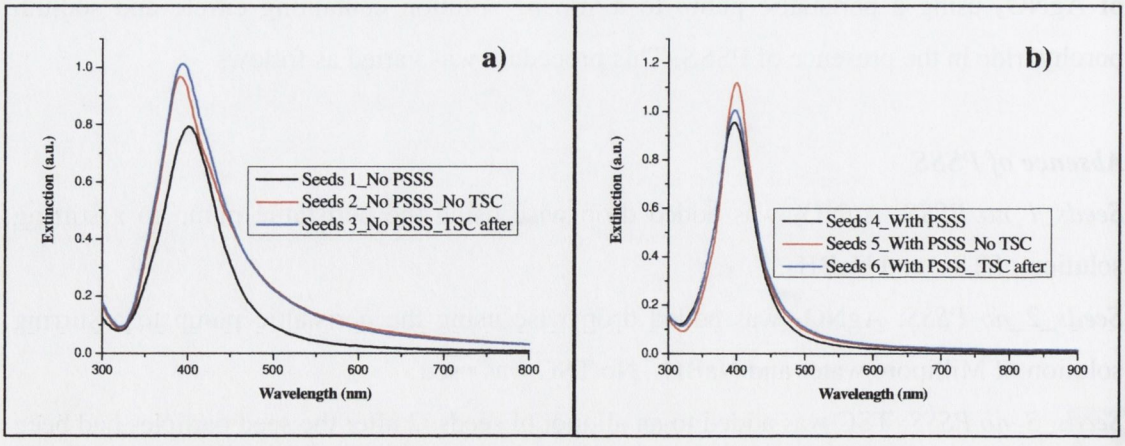


Figure 2.49: Seeds prepared in the a) absence b) presence of PSSS

The full width at half maximum (FWHM) was calculated for each of the above spectra using Gaussian analysis, as this has been found to be a measure of the monodispersity of the sol. The narrower the FWHM, the narrower the size distribution.

Seeds	*FWHM (nm)*
Seeds 1	75
Seeds 2	94
Seeds 3	90
Seeds 4	66
Seeds 5	69
Seeds 6	68

Table 2.6: FWHM of the seeds prepared in the absence and presence of PSSS

As can be seen, both from the spectra and the table above, the FWHM of the seeds prepared in the presence of PSSS is smaller than in those prepared in the absence of PSSS. Another thing to be noted from Figure 2.49 above is that the spectra of the seeds prepared in the absence of PSSS are unsymmetrical and exhibit a tail at longer wavelengths.

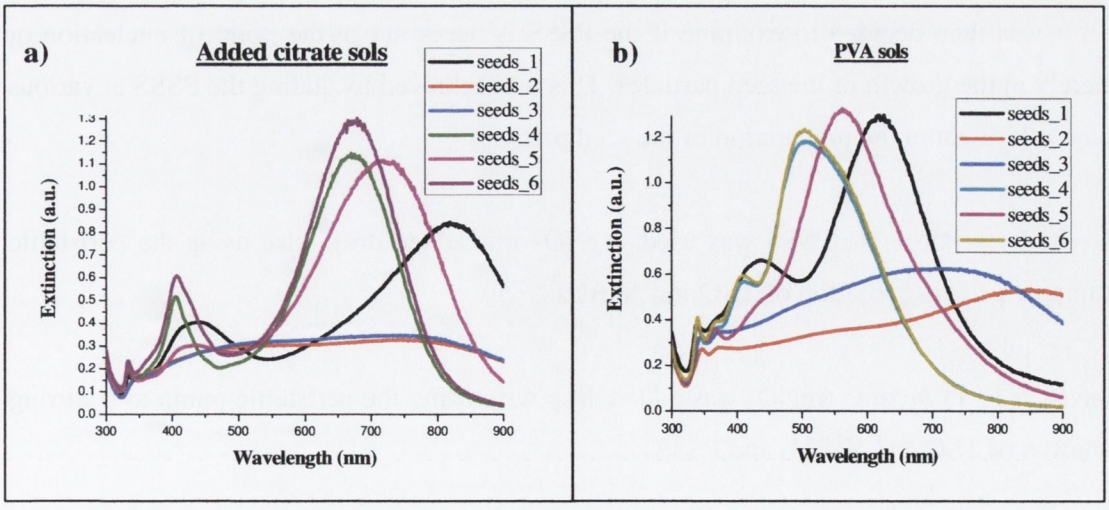


Figure 2.50: UV-vis spectra of sols prepared from the seeds shown above in Figure 2.49 by the a) added citrate method b) PVA method.

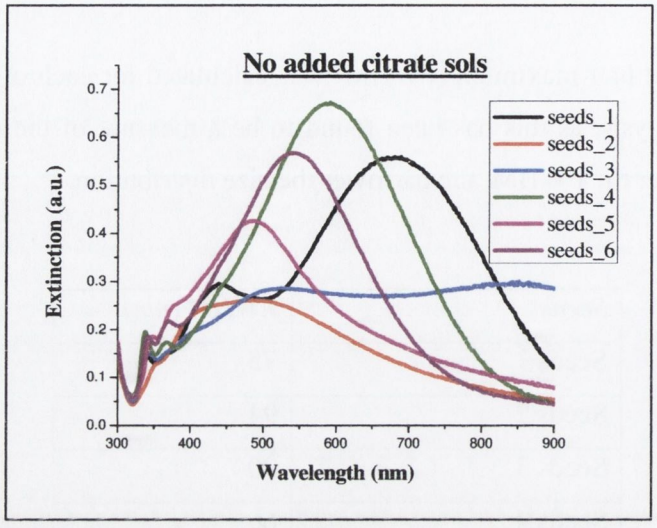


Figure 2.51: UV-vis spectra of the sols prepared by the no added citrate method from the seeds shown above in Figure 2.49.

From the above spectra the following points can be noted:

- PSSS is necessary to produce seeds which, when grown produce relatively monodisperse sols (as indicated by the relatively low absorbance of the SPR band at ~ 400nm).
- PSSS is more important than TSC in the preparation of the seeds. All seeds produced in the presence of PSSS produced monodisperse sols, regardless of the presence of TSC.

It was then decided to examine if the PSSS is necessary at the point of nucleation or merely in the growth of the seed particles. This was achieved by adding the PSSS at various stages throughout the preparation of the seed particles.

Seeds_1_no PSSS: No PSSS was used. $AgNO_3$ was added drop wise using the peristaltic pump to a stirring solution of TSC and $NaBH_4$.

Seeds_2_PSSS before: $AgNO_3$ was added drop wise using the peristaltic pump to a stirring solution of TSC and $NaBH_4$ and PSSS.

Seeds_3_PSSS during: $AgNO_3$ was added drop wise using the peristaltic pump to a stirring solution of TSC and $NaBH_4$. After approx 10 drops of $AgNO_3$ had been introduced, a faint yellow colour appeared. PSSS was then added.

Seeds_4_PSSS after: $AgNO_3$ was added drop wise using the peristaltic pump to a stirring solution of TSC and $NaBH_4$. After the addition of $AgNO_3$ was complete, PSSS was added.

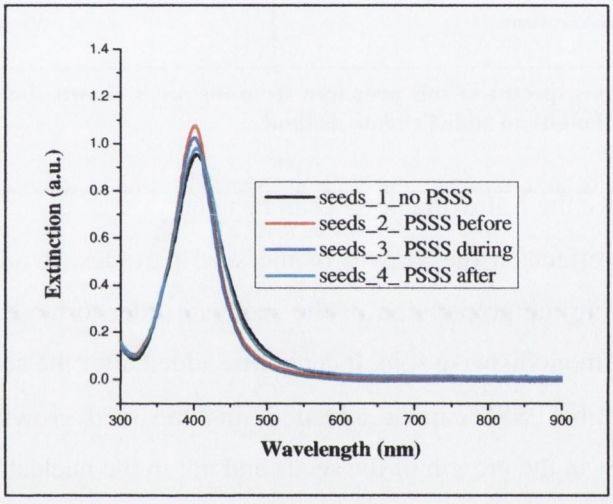


Figure 2.52: UV-vis spectra of seeds prepared when PSSS was added at various stages throughout the preparation of the seeds.

Seeds	*FWHM (nm)*
Seeds 1	80
Seeds 2	65
Seeds 3	64
Seeds 4	78

Table 2.7: FWHM of the seeds shown above in Figure 2.52.

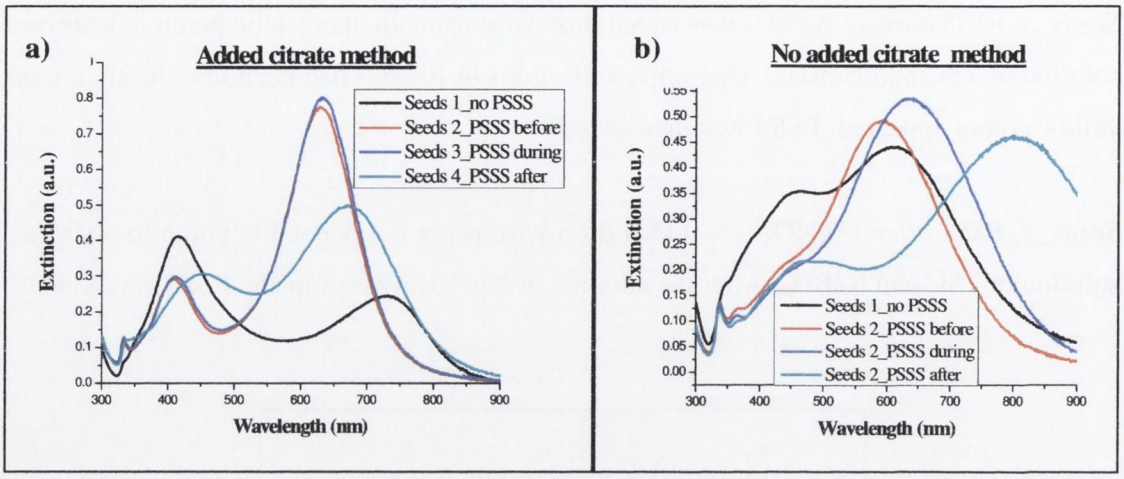


Figure 2.53: UV-vis spectra of sols prepared from the seeds shown above in Figure 2.52 using the a) added citrate method b) no added citrate method.

From the spectra above the following points can be noted:

- PSSS has an effect on the growth of the seed particles. It must be present either before or during the preparation of the seeds in order to have maximum effect for the growth of monodisperse sols. It cannot be added after the seed growth.
- The fact that the PSSS can be added during the seed growth suggests that it is important only in the growth of the seeds and not in the nucleation step.

The next set of experiments was carried out to investigate the importance of the concentration of PSSS used in the preparation of the seeds. PSSS was added to a stirring solution of TSC and $NaBH_4$. $AgNO_3$ was added slowly drop-wise using the peristaltic pump.

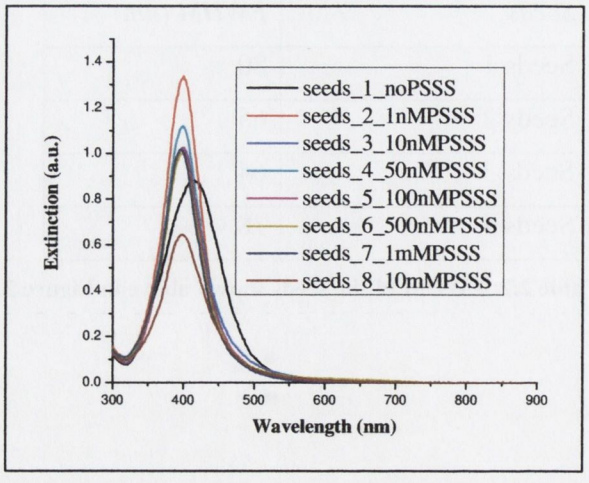


Figure 2.54: UV-vis spectra of seeds prepared using different concentrations of PSSS.

Seeds	*Conc. of PSSS*	*FWHM (nm)*	*λmax of grown sol (nm)*
Seeds 1	0 μM	83	700
Seeds 2	1 μM	58	765
Seeds 3	10 μM	66	820
Seeds 4	50 μM	61	758
Seeds 5	100 μM	62	739
Seeds 6	500 μM	63	689
Seeds 7	1 mM	61	647
Seeds 8	10 mM	65	617

Table 2.8: FWHM of seeds shown above in Figure 2.54.

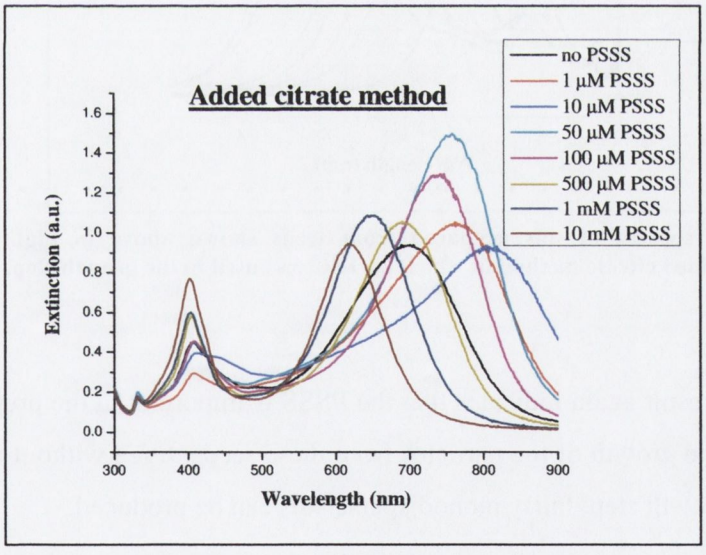


Figure 2.55: UV-vis spectra of sols prepared from the seeds shown above in Figure 2.54. The position of the in-plane dipole is given above in Table 2.8

The above results indicate that the optimal PSSS concentration is ~ 50 μM (based on the molecular weight of the monomer). By increasing the concentration of PSSS, the

relative ratio of the in-plane dipole and the band centred ~400 nm decreases *i.e.* the in-plane dipole is less dominant and the population of spherical particles is increased.

The following experiment was then carried out to examine if the concentration of PSSS alone is important in the growth of the particles, without the addition of TSC in the growth step. PVP, seed solution and ascorbic acid were stirred together. $AgNO_3$ was added drop wise with stirring. No additional TSC was used.

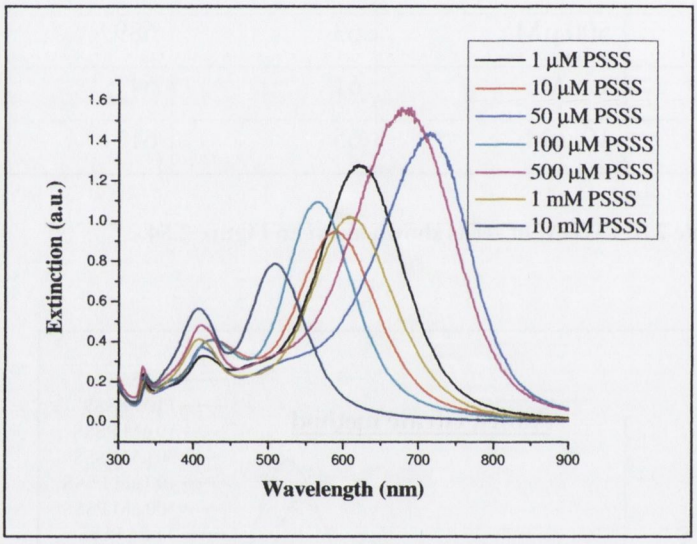


Figure 2.56: UV-vis spectra of sols prepared from seeds shown above in Figure 2.54 using a modification of the added citrate method in which no TSC was used in the growth step.

The above result again indicates that the PSSS is important in the preparation of the seeds, but also in the growth of the particles from these seeds. Even without the addition of extra TSC in the growth step, fairly monodisperse sols can be produced.

The culmination of the experiments described above was an experiment with the 'no added citrate' method when all parameters were optimized. If PSSS was left out or only added to the seed solution after seed production, then a diversity of nanoparticle shapes and sizes is produced as shown below in Figure 2.57.

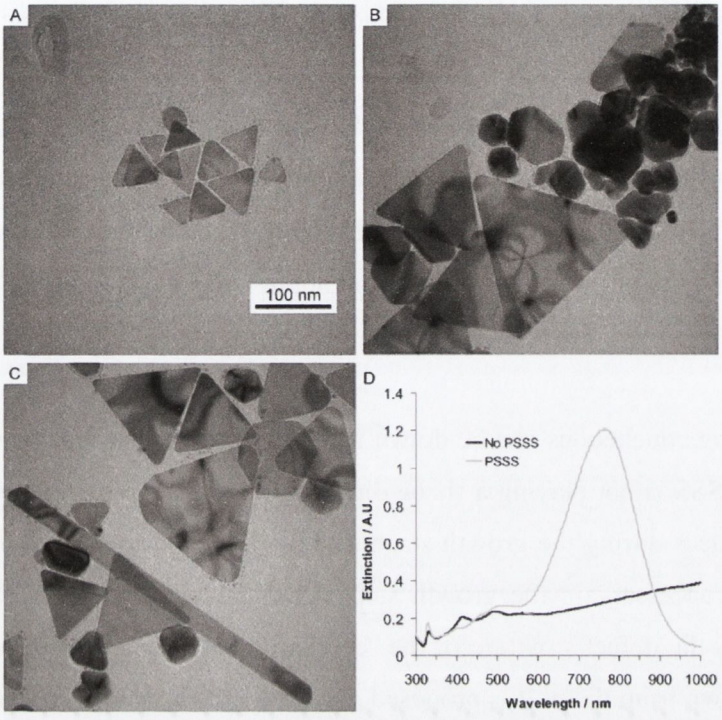


Figure 2.57: A) Ag nanoprisms grown from seeds produced with PSSS present. B) and C) Ag nanoparticles grown from seeds produced without PSSS present. Sample consists of nanoprisms of a wide range of sizes and "spherical" particles of various sizes with 5-fold symmetry present. D) UV-vis spectra of nanoprisms in (A) grown from seeds produced in the presence of PSSS (grey) and nanoparticles in (B) and (C) grown form seeds produced in the absence of PSSS (black). [34]

2.3.3 Discussion of the role of PSSS:

At this stage, the following points have been highlighted:

- PSSS is necessary to produce seeds which when grown produce relatively monodisperse sols (as indicated by a low absorbance of the band at 400 nm.)
- PSSS is more important than TSC in the preparation of the seeds.
- All seeds produced using PSSS exhibited less absorbance in the 400 nm region.
- When PSSS is not present, TSC does play a role in the growth of the sols.
- For the added citrate prep, the grown sols with the narrowest FWHM (145 nm) were produced with seeds where the TSC was present. However plasmon ~400 nm is

more visible when TSC is included indicating the presence of spherical nanoparticles.

- PSSS has an effect on the growth of the seeds. It must be present either initially or added during the growth of the seeds. It cannot be added after the seed growth.
- The fact that the PSSS can be added during the seed growth suggests that it is only important in the growth of the seeds and not in the nucleation step.

The following conclusions can be drawn from the set of experiments outlined above in Section 2.3.2. PSSS is not playing a shape directing role through preferential adsorption to certain crystal faces during the growth stage as experiments have shown that the presence of PSSS is not necessary in the growth step. As discussed previously above, it is now thought that it is the defect structure of the seed particle that determines the final shape of the particles grown from them. It is proposed that PSSS has a strong influence on the defect structure of the seeds however at this stage it is still unclear how PSSS achieves this.

Two possible explanations are given below.

1. The PSSS is interacting selectively with the surface of the seed. This concept of a polymer adsorbing preferentially onto a specific crystal face is not new. It has been shown previously by the Xia group, that PVP, an uncharged polymer, adsorbs preferentially on the {100} face of silver, preventing growth on this face and thereby promoting growth on the {111}, resulting in the formation of nanowires.[40] Therefore a strong interaction between PSSS, a charged polymer could be anticipated.

2. The PSSS is an important factor in controlling the growth kinetics of the seed particles with a defect structure, which when grown form triangular plates.

To date there has been no report in the literature of the use of PSSS in the growth of anisotropic silver nanoparticles. Mirkin *et al.*, have reported the use of another sulfonato

compound, bis(p-sulfonatophenyl)phenylphosphine dihydrate dipotassium salt (BSPP) in the photoconversion of spherical silver nanoparticles to silver nanoprisms.[7, 8, 33, 57]

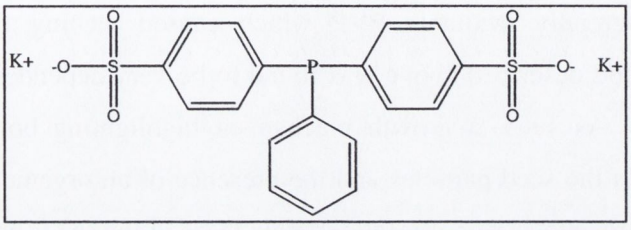


Figure 2.58: Chemical Structure of bis (p-sulfonatophenyl) phenylphosphine dehydrate dipotassium salt (BSPP).

In a mechanistic study, it was proposed that the BSPP acts as a buffer in the presence of seed particles, to keep the Ag^+ concentration constant, which facilitates the deposition of silver ion on the seed particle surface under photochemical control. In essence, the BSPP will coordinate with Ag^+ ion to form a coordination complex. It is proposed here that the PSSS can also coordinate with Ag^+ ion to form a coordination complex. This complex acts as a reservoir for silver ions in the preparation of the seed particles, slowing down the reduction and ultimately the formation of the seed particles. However, further experiments including the use of different compounds containing the SO_3^- moiety will need to be carried out to determine the exact nature of the interaction of PSSS with the seed particles and how this in turn affects the structure of the seed particles.

2.4 General Conclusions

The synthesis of silver nanoparticles by various routes has been described in this chapter. In Section 2.1 the synthesis of silver nanoparticles of tuneable colour via a seed mediated method involving trisodium citrate and a polymer such as poly(vinylpyrolidone) (PVP) has been described. The effects of different parameters for example time, temperature and concentration of citrate have been investigated. The colour of the sols may be tuned by varying the concentration of citrate. Sols prepared at room temperature exhibit a blue- shift of the longitudinal band with time. As the temperature at which the reaction is carried out is increased from room temperature, well-defined triangular plates with enhanced stability are produced. However the procedure does lead to mixture of shapes

being produced. The presence of the polymer PVP was not found to be an important factor in determining the final morphology of the nanoparticles produced. However, the purity of the PVP used was found to be crucial to the stability of the sols produced. An impurity was isolated from commercially available PVP which caused etching the particles. The reliability of the method described above was found to be very dependent on the structure of the seed particles. As such, a growth mechanism highlighting both the role of the underlying structure of the seed particles and the presence of an organic molecule capable of adsorbing selectively onto certain crystallographic faces of the seeds has been suggested.

In Section 2.2, experiments carried out to improve the reproducibility of an existing synthesis of silver nanoparticles developed within the group which employs poly(vinylalcohol), have been outlined. Two key factors which greatly enhance the batch-to –batch reproducibility have been identified namely the exclusion of light from the growth step of the synthesis and the inclusion of the anionic polymer poly(4-styrene sulfonate) sodium salt (PSSS) during the synthesis of the seed particles.

In Section 2.3, the role of PSSS in the seed preparation was explored in the two syntheses described above and also a third 'no added citrate' method. It was concluded that the presence of PSSS before or during the growth of the seed particles was necessary to prevent the formation of nanoparticles with a diversity of shapes and sizes. Possible explanations as to why the presence of PSSS in the growth of the seed particles is so important have been proposed

In the next chapter, the functionalization and stability of the anisotropic silver nanoparticles prepared above will be discussed.

2.5 References

1. A. M. Whelan, M. E. Brennan, W. J. Blau and J. M. Kelly, *J. Nanoscience Nanotech.*, 2004, **4**, 66-68.
2. D. M. Ledwith, A. M. Whelan and J. M. Kelly, *J. Mater. Chem.*, 2007, **17**, 2459-2464.
3. J. Turkevich, P. C. Stevenson and J. Hillier, *Discuss. Faraday Soc.*, 1951, **No. 11**, 55-75.
4. J. L. Elechiguerra, J. Reyes-Gasga and M. J. Yacaman, *J. Mater. Chem.*, 2006, **16**, 3906-3919.
5. L. Lu, A. Kobayashi, K. Tawa and Y. Ozaki, *Chem. Mater.*, 2006, **18**, 4894-4901.
6. Y. Wang, P. H. C. Camargo, S. E. Skrabalak, H. Gu and Y. Xia, *Langmuir*, 2008, **24**, 12042-12046.
7. R. Jin, Y. Cao, C. A. Mirkin, K. L. Kelly, G. C. Schatz and J. G. Zheng, *Science*, 2001, **294**, 1901-1903.
8. R. C. Jin, Y. C. Cao, E. C. Hao, G. S. Metraux, G. C. Schatz and C. A. Mirkin, *Nature*, 2003, **425**, 487-490.
9. K. L. Kelly, E. Coronado, L. L. Zhao and G. C. Schatz, *J. Phys. Chem. B*, 2003, **107**, 668-677.
10. I. O. Sosa, C. Noguez and R. G. Barrera, *J. Phys. Chem. B*, 2003, **107**, 6269-6275.
11. C. Noguez, *J. Phys. Chem. C*, 2007, **111**, 3806-3819.
12. B. J. Wiley, S. H. Im, Z. Y. Li, J. McLellan, A. Siekkinen and Y. A. Xia, *J. Phys. Chem. B*, 2006, **110**, 15666-15675.
13. H. Wang, X. Qiao, J. Chen, X. Wang and S. Ding, *Mater. Chem. Phys.*, 2005, **94**, 449-453.
14. G. S. Metraux and C. A. Mirkin, *Adv. Mater.*, 2005, **17**, 412-415.
15. I. Washio, X. Xiong, Y. Yin and Y. Xia, *Adv. Mater.*, 2006, **18**, 1745-1749.
16. Y. J. Xiong, I. Washio, J. Y. Chen, H. G. Cai, Z. Y. Li and Y. N. Xia, *Langmuir*, 2006, **22**, 8563-8570.
17. K. Dutta and A. S. Brar, *J. Polym. Sci. A*, 1999, **37**, 3922-3928.

18. Y. Borodko, S. E. Habas, M. Koebel, P. Yang, H. Frei and G. A. Somorjai, *J .Phys. Chem. B*, 2006, **110**, 23052-23059.
19. N. R. Jana, L. Gearheart and C. J. Murphy, *Chem. Commun.*, 2001, 617-618.
20. M. Maillard, P. Huang and L. Brus, *Nano Lett.*, 2003, **3**, 1611-1615.
21. S. Chen and D. L. Carroll, *J. Phys. Chem. B*, 2004, **108**, 5500-5506.
22. C. Lofton and W. Sigmund, *Adv. Funct. Mater.*, 2005, **15**, 1197-1208.
23. V. Germain, J. Li, D. Ingert, Z. L. Wang and M. P. Pileni, *J. Phys. Chem. B*, 2003, **107**, 8717-8720.
24. B. Rodriguez-Gonzalez, I. Pastoriza-Santos and L. M. Liz-Marzan, *J. Phys. Chem. B*, 2006, **110**, 11796-11799.
25. V. Bastys, I. Pastoriza-Santos, B. Rodriguez-Gonzalez, R. Vaisnoras and L. M. Liz-Marzan, *Adv. Funct. Mater.*, 2006, **16**, 766-773.
26. T. C. R. Rocha and D. Zanchet, *J. Phys. Chem. C*, 2007, **111**, 6989-6993.
27. Y. Yang, S. Matsubara, L. M. Xiong, T. Hayakawa and M. Nogami, *J. Phys. Chem. C*, 2007, **111**, 9095-9104.
28. Z. L. Wang, *J. Phys. Chem. B*, 2000, **104**, 1153-1175.
29. Y. Sun and Y. Xia, *Science*, 2002, **298**, 2176-2179.
30. X. Zou and S. Dong, *J. Phys. Chem. B*, 2006, **110**, 21545-21550.
31. A. S. Barnard, *J .Phys. Chem. B*, 2006, **110**, 24498-24504.
32. Y. G. Sun, B. Mayers and Y. N. Xia, *Nano Lett.*, 2003, **3**, 675-679.
33. C. Xue, G. S. Metraux, J. E. Millstone and C. A. Mirkin, *J. Am. Chem. Soc.*, 2008, **130**, 8337-8344.
34. D. Aherne, D. M. Ledwith, M. Gara and J. M. Kelly, *Adv. Funct. Mater.*, 2008, **18**, 2005-2016.
35. B. J. Wiley, S. H. Im, Z.-Y. Li, J. McLellan, A. Siekkinen and Y. Xia, *J. Phys. Chem. B*, 2006, **110**, 15666-15675.
36. B. Wiley, Y. Sun, B. Mayers and Y. Xia, *Chem. Eur. J.*, 2005, **11**, 454-463.
37. B. J. Wiley, Y. Xiong, Z.-Y. Li, Y. Yin and Y. Xia, *Nano Lett.*, 2006, **6**, 765-768.
38. X. C. Jiang, Q. H. Zeng and A. B. Yu, *Langmuir*, 2007, **23**, 2218-2223.
39. Y. Han, J. Jiang, S. S. Lee and J. Y. Ying, *Langmuir*, 2008, **24**, 5842-5848.
40. Y. G. Sun, B. Mayers, T. Herricks and Y. N. Xia, *Nano Lett.*, 2003, **3**, 955-960.

41. H. H. Huang, X. P. Ni, G. L. Loy, C. H. Chew, K. L. Tan, F. C. Loh, J. F. Deng and G. Q. Xu, *Langmuir*, 1996, **12**, 909-912.

42. B. J. Wiley, Y. C. Chen, J. M. McLellan, Y. J. Xiong, Z. Y. Li, D. Ginger and Y. N. Xia, *Nano Lett.*, 2007, **7**, 1032-1036.

43. P. Mulvaney, T. Linnert and A. Henglein, *J. Phys. Chem.*, 1991, **95**, 7843-7846.

44. T. Linnert, P. Mulvaney and A. Henglein, *J. Phys. Chem.*, 1993, **97**, 679-682.

45. D. K. Smith and B. A. Korgel, *Langmuir*, 2008, **24**, 644-649.

46. L. Gou and C. J. Murphy, *Chem. Mater.*, 2005, **17**, 3668-3672.

47. X. Peng, L. Manna, W. Yang, J. Wickham, E. Scher, A. Kadavanich and A. P. Alivisatos, *Nature*, 2000, **404**, 59-61.

48. B. Wiley, Y. Sun and Y. Xia, *Acc. Chem. Res.*, 2007, **40**, 1067-1076.

49. B. Wiley, T. Herricks, Y. Sun and Y. Xia, *Nano Lett.*, 2004, **4**, 1733-1739.

50. H. Im Sang, T. Lee Yun, B. Wiley and Y. Xia, *Angew. Chem. Int. Ed.*, 2005, **44**, 2154-2157.

51. B. Wiley, Y. Sun and Y. Xia, *Langmuir*, 2005, **21**, 8077-8080.

52. Y. Xiong, A. R. Siekkinen, J. Wang, Y. Yin, M. J. Kim and Y. Xia, *J. Mater. Chem.*, 2007, **17**, 2600-2602.

53. K. E. Korte, S. E. Skrabalak and Y. Xia, *J. Mater. Chem.*, 2008, **18**, 437-441.

54. WO/2004/086044.

55. A. M. Whelan, PhD, University of Dublin, 2004.

56. C. Ni, P. A. Hassan and E. W. Kaler, *Langmuir*, 2005, **21**, 3334-3337.

57. C. Xue and C. A. Mirkin, *Angew. Chem. Int. Ed.*, 2007, **46**, 2036-2038.

Chapter 3:
Functionalization and Stability of Silver Nanoparticles

3 Introduction:

As already mentioned in the previous two chapters, there has been tremendous interest in developing various procedures for the synthesis of nanoparticles and in particular noble metal nanoparticles in the past decade. This interest stems from the fact that the properties of such metallic nanoparticles are very dependent on size, shape and composition. It is envisaged that colloidal particles will be used as building blocks for more ordered and complex materials. However in order for this to happen the particles must be easily functionalized and the area of composite nanoparticles has flourished in order to cope with this demand. In fact the term used to describe the synthesis of composite materials, otherwise known as core-shell particles, with well-defined shape and properties is referred to as particle engineering.[1]

Various different approaches have been taken to prepare composite materials. On the whole a generic procedure that meets all the following requirements is needed

1) optical transparency
2) chemical inertness
3) photo stability
4) cheapness
5) high colloidal stability
6) easy transfer into a range of media

In this chapter, approaches that have been taken to modify the surface chemistry of the particles described in Chapter 2 while fulfilling these prerequisites will be presented. Firstly, various routes for the production of silica coated silver nanoparticles will be discussed, followed by an examination of the layer-by-layer method for the functionalization of nanoparticles.

3.1 Silica coated silver nanoparticles

Why silica? There are several advantages to using silica shells instead of organic stabilizers.

1. The silica shell is optically transparent so that chemical reactions can be monitored spectroscopically. The shell can also be used to modulate the position and intensity of the colloidal metal surface plasmon absorption bands.

2. Silica is chemically inert.
3. The shell prevents coagulation during chemical reactions.
4. The shell provides the particles with enhanced colloidal stability so that concentrated dispersions can be prepared that remain stable over a much wide range of solution conditions such as ionic strength, temperature and solvent polarity.
5. Well-known silane chemistry can be used to introduce other chemical moieties so that further functionalization is possible.

The aim of the work described in this section is to prepare silica-coated nanoparticles by developing methods reported in the literature. The reasons behind this are two-fold. Firstly, to prepare silver nanoparticles with *known* surface chemistry so that further functionalization is easier and secondly to impart extra stability to the nanoparticles. It will be shown in Section 3.2 of this chapter that the nanoparticles described in Chapter 2 are very sensitive to the presence of anions and in particular chloride ions. This is a serious issue when considering future uses of these particles in areas such as biosensing.

A number of routes have been developed to prepare $Ag@SiO_2$ particles. It should be noted that the routes reported to date use silver particles prepared by different methods. The surface chemistry of these particles is therefore different and this has to be taken into consideration when adapting a method to coat the silver nanoparticles described in Chapter 2.

Two general approaches have been taken to generate silica coatings on the surfaces of nanocrystalline particles. The first method relies on the well known Stöber process, in which silica is formed *in situ* through the hydrolysis and condensation of a sol–gel precursor in ethanol:water mixtures under alkaline conditions at room temperature. [2-13]The second method is based on a microemulsion synthesis, in which micelles or inverse micelles are used to confine and control the coating of silica on core nanoparticles.[14-17] It was decided to focus on the former method as it is most suitable for the preparation of core-shell particles from aqueous based nanoparticles.

For initial investigations three different literature methods were chosen. All involved the silica coating of spherical silver nanoparticles. It was hoped that once silica coated spherical silver nanoparticles were produced, the methods could be adapted to produce silica coated silver nanoprisms. The first method adopted was created by Ung *et al.*[3] It makes use of the silane-coupling agent 3-aminopropyltriethoxysilane (APTES) as a surface primer to render the surface of the citrate capped colloidal silver vitreophilic. This permits the deposition of a thin, dense silica coating in aqueous solution. The second method was developed by Graf *et* al.[5, 6] and uses poly (vinyl pyrrolidone) (PVP) as a coupling agent. The third method was developed by Kobayashi *et al.*[11] Citrate stabilized silver nanoparticles were coated directly with silica by means of a seeded polymerisation technique based on the Stöber method.[18]

3.1.1 Results

3.1.1.1 Method 1: Ung *et al.*[3]

The first method attempted was created by Ung *et al.* It makes use of the silane-coupling agent 3-aminopropyltriethoxysilane (APTES) as a surface primer to render the surface of the colloidal silver vitreophilic. This permits the deposition of a thin, dense silica coating in aqueous solution. After this Stöber growth is employed to tune the thickness of the silica coating to the required value. The procedure is as follows. The surface of silver particles is first activated by the adsorption of APTES, generating siloxy groups receptive to silicate ion deposition. Sodium silicate is added at supersaturated concentrations leading to an initial layer of silica one nanometre thick. The third step is the controlled precipitation of residual silicate by the addition of ethanol creating a homogeneous shell followed by Stöber growth of this shell to the required thickness.

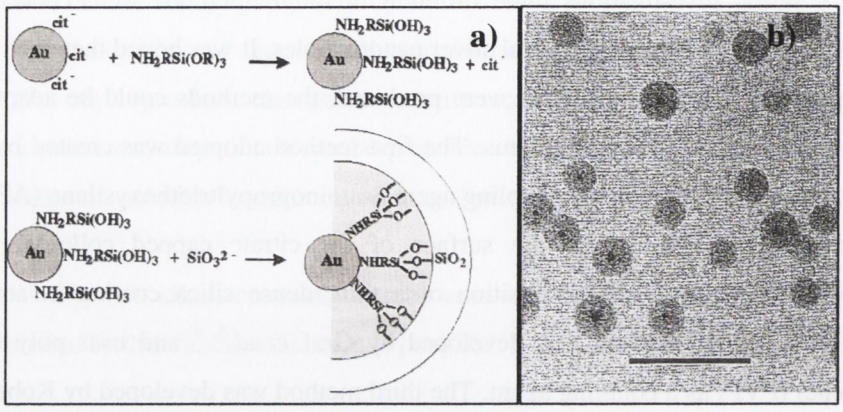


Figure 3.1: a) Schematic of the procedure used for the silica coating of aqueous silver or gold sols. b)TEM image of Au@SiO_2 prepared by this procedure.[2]

The method as reported in the above paper was followed and is given in detail in Chapter 5. Briefly, silver nanoparticles were prepared by the reduction of silver nitrate by sodium borohydride in the presence of trisodium citrate. To this as prepared sol, 3-aminopropyltriethoxysilane (APTES) (1.67 μM) was added under vigorous stirring and the sol was then allowed to stand for 15 minutes to ensure complete complexation of the amine groups with the nanoparticle surface. A solution of sodium silicate (0.54 wt %) was then added again under vigorous stirring and the sol was allowed to stand for 24 hours so that the active silica polymerizes onto the silver nanoparticle surface. After this period, the particles were transferred into ethanol/water (4:1) and ammonia (48 mM) and TEOS (1 mM) were then added to increase the thickness of the silica shell. The sol was then allowed to stir for 12 hours before being centrifuged at max speed for 30 minutes.

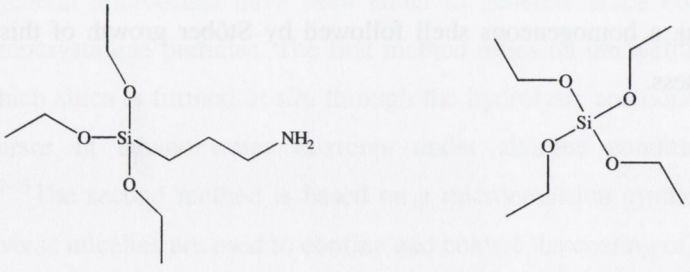


Figure 3.2: Structure of 3-aminopropyltriethoxysilane (APTES) and tetraethylorthosilicate (TEOS).

As shown in Figure 3.3 below, UV-vis spectroscopy indicated a red shift in the surface plasmon resonance. This was reported in the literature for coated particles and is due to an increase in refractive index around the particles. However, from the TEM images it is clear that there are no silica coated Ag nanoparticles present.

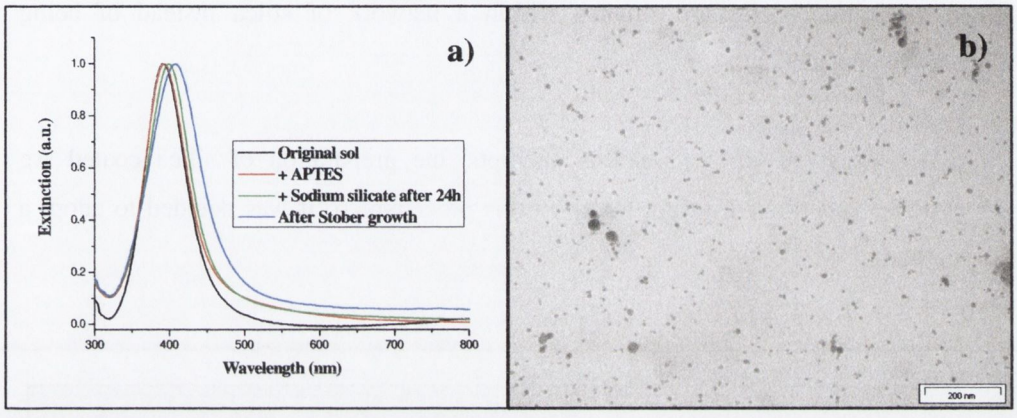


Figure 3.3: a) UV-vis spectra of sol a various stages during the silica coating procedure. b) TEM image of silver nanoparticles after the coating procedure.

pH dependence:

The adsorption of APTES onto the surface of the particles and the adsorption of the silicate is known to be affected by the pH of the solution. In the method described by Ung *et al.*, the pH of the sol was adjusted to certain values at certain stages in the coating process. The pH was adjusted to 5 prior to adsorption of the APTES as at this pH the particles were more homogeneously coated. The pH was again adjusted again prior to addition of the silicate to 11.5. It was reported that the system becomes more monodisperse with increasing pH and the quality and thickness of the shell was found to be optimised at this pH.[2, 3]

It was decided to monitor the pH values and adjust them accordingly. The method as given above was repeated. The pH of the sol prior to addition of APTES was 5. After addition of the APTES, and the 15 minutes stirring period, the pH of the sol was adjusted to 11 by drop wise addition of 2M NaOH. The reason for the high concentration of NaOH used was to limit any effects caused by dilution. Sodium silicate solution (0.54 wt %) was added and the dispersion left to stir for 24 hours.

The overall appearance of the sol was changed by the addition of NaOH. The sol changed from a bright yellow to a bronze colour suggesting aggregation. After the addition of the sodium silicate the colour did not change immediately but overnight it became an olive/brown colour. Again as in the previous sample, there was silica present however this time it was visible in the TEM images. As can been seen in Figure 3.4 below, the nanoparticles are situated within a network of silica instead of being individually coated.

At this stage, after numerous attempts, the preparation of silica coated Ag nanoparticles had proved unsuccessful by this procedure so it was decided to adopt a new method.

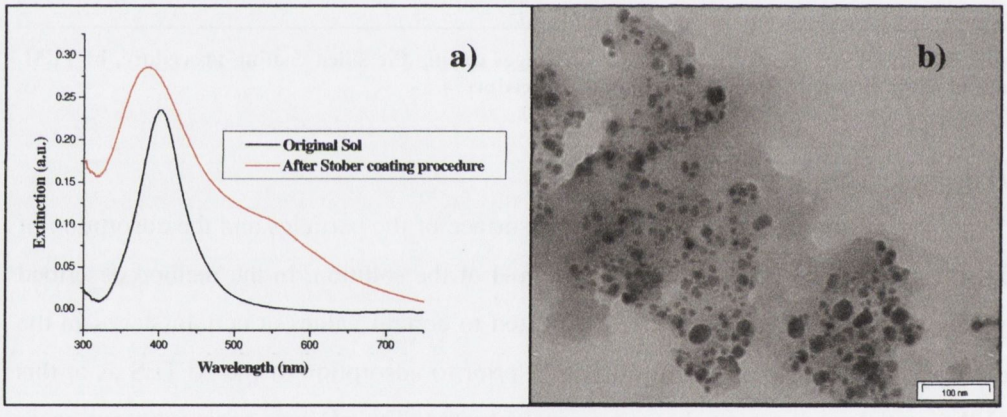


Figure 3.4: a)UV-vis spectra b)TEM image of Ag@SiO_2 prepared when the pH of the solution was varied.

3.1.1.2 Method II: Graf *et al.*[5]

The second method uses poly (vinyl pyrrolidone) (PVP) as a coupling agent. The presence of a highly polar amide group within the pyrrolidone ring and apolar methylene and methine groups in the ring and along its backbone enables it to stabilize colloidal particles in water and many nonaqueous solvents. Particles that are stabilized by PVP could be directly coated with a silica layer of variable thickness by addition of tetraethylorthosilicate (TEOS) to an ethanolic ammonia solution containing the particles as shown in the schematic below.

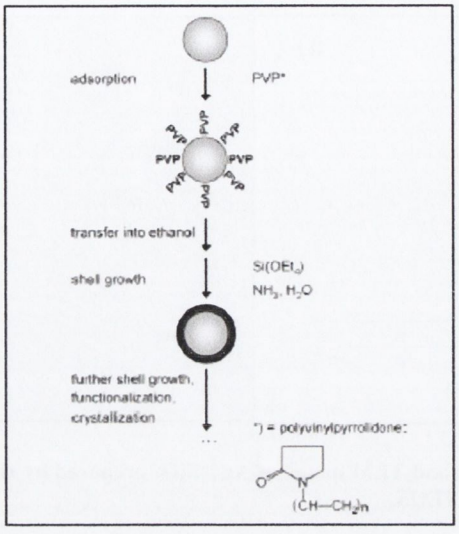


Figure 3.5: Schematic of general procedure for coating Ag particles with silica from reference[5]

The method as reported in the above paper was followed and is given in detail in Chapter 5. Briefly, silver nanoparticles were prepared by reduction of silver nitrate by ethylene glycol in the presence of PVP (MW 10k) at 120°C. After synthesis the particles were separated from ethylene glycol by the addition of acetone (500 mL/75 mL reaction mixture) to the reaction mixture. The particles were collected by centrifugation and were redispersed in ethanol. After further centrifugation the particles were redispersed in a solution of ammonia in ethanol (9 mM). Immediately after this an ethanolic solution of TEOS (4 mM) was added under stirring and the reaction mixture was stirred for 24 hours at room temperature. After this time the coated nanoparticles were collected by centrifugation and the precipitates were redispersed in EtOH. The UV-vis spectrum and TEM image of the resulting particles are shown below in Figure 3.6.

From the UV-vis spectra, it was expected that there was silica present in the sample as the surface plasmon resonance was red-shifted from the expected value of ~395 nm for Ag nanoparticles of this size. From the TEM micrograph it is clear that there were indeed some spherically coated Ag@SiO_2 particles. However, there was also a lot of free silica spheres present *i.e.* silica particles with no Ag core. It must be also noted that *all* the Ag nanoparticles present were coated with silica.

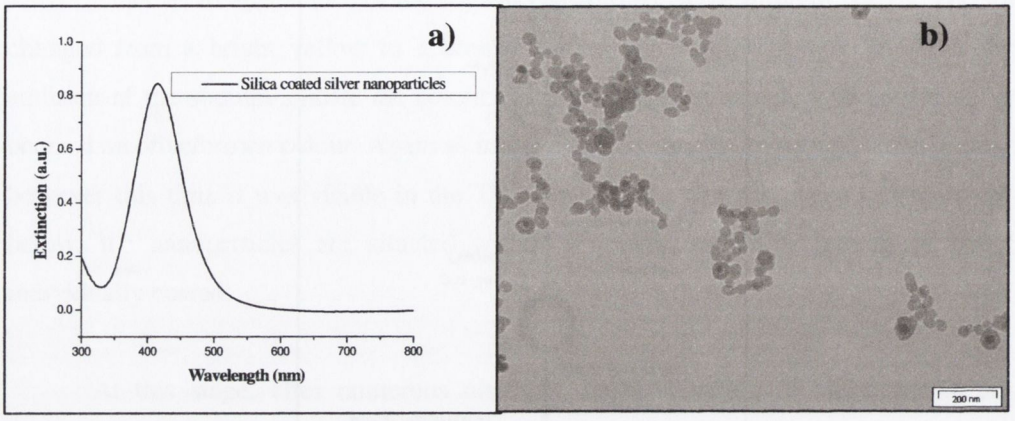


Figure 3.6: UV-vis spectrum and TEM image of $Ag@SiO_2$ prepared by the method outlined above from reference [5] with 4 mM TEOS.

For this reason a number of follow on experiments were carried out. Firstly, the concentration of TEOS was reduced by half to 2 mM.

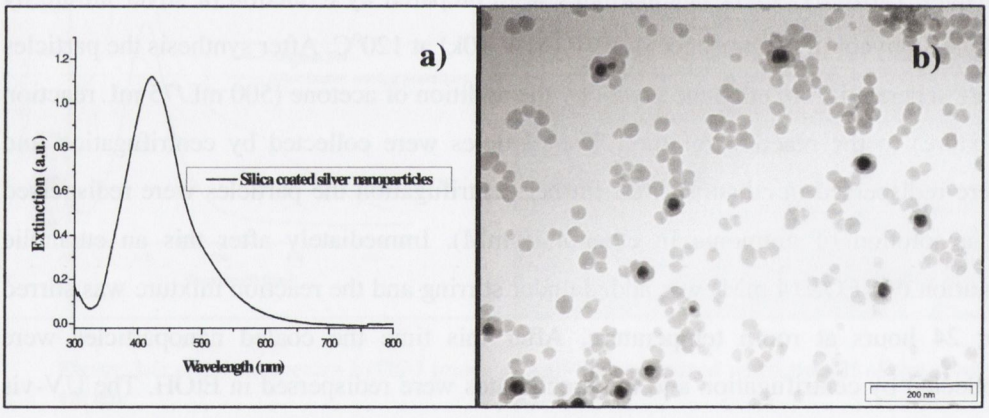


Figure 3.7: a) UV-vis spectrum and b) TEM image of $Ag@SiO_2$ prepared at 2 mM TEOS.

Again from the TEM images it can be seen that there are some coated particles present but also a lot of free silica spheres. However, again all the silver nanoparticles present appear to be coated.

It was then decided to calculate the amount of Ag^+ consumed to make the Ag nanoparticles. From this, the amount of nanoparticles produced could be calculated and therefore the amount of silica needed could also be calculated. The amount of Ag^+ consumed in the reaction was determined by the Volhard titration. From this experiment

and from the assumption that a molecule of TEOS had a surface area of 40Å^2 it was calculated that minimum concentration of TEOS that could be used during the coating process, so that discrete silica coats could be observed was 64 μM.

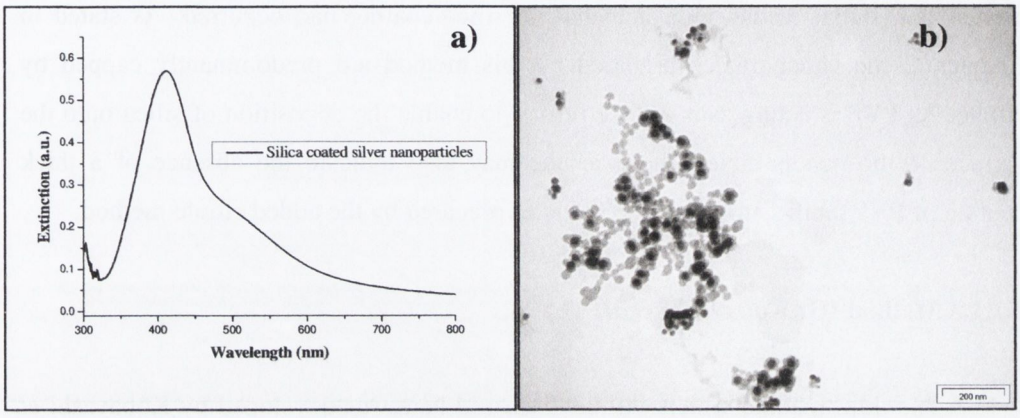


Figure 3.8: a) UV-vis spectrum and b)TEM image of Ag@SiO_2 prepared with 64 μM TEOS.

Again from the TEM images it could be seen that there were some coated Ag particles present but again a lot of free silica was also present. All the coated particles appeared to clump together. This was because there were no spherically coated Ag particles. The particles were linked together by their silica shells. Also in this experiment, there were some Ag particles that were not coated.

The experiment above was repeated but there were problems with the reproducibility of the experiments. In the first step (the synthesis of the particles) when the PVP, $AgNO_3$ and ethylene glycol were heated to 120°C and kept at this temperature, a silver mirror formed at the bottom of the reaction vessel. This indicated the presence of elemental silver. When this dispersion was centrifuged down, the precipitates redispersed in EtOH and when left to stand overnight a black precipitate was evident.

A disadvantage associated with the above method was that the synthesis of the particles was long and tedious. The Ag nanoparticles were removed from the ethylene glycol reaction mixture by the addition of 500 mL of acetone. This whole quantity had to be centrifuged down, redispersed in EtOH and centrifuged again prior to the silica

coating step. For this reason it was decided to use a different method for the preparation of the particles.

Green silver sols were prepared using the procedure discussed in Section 2. The sols were centrifuged down and the silica coating step taken from van Graf *et al.* was carried out. Initial results indicated that no silica coating had occurred. As stated in Chapter 2, the nanoparticles prepared by this method are predominantly capped by citrate. As PVP is acting as a surface primer to enable the deposition of silica onto the surface of the nanoparticles, these results may also indicate the absence of a thick coating of PVP on the surface of the particles prepared by the added citrate method.

3.1.1.3 Method III: Kobayashi *et al.*[11]

The third method which will be discussed here was developed by Kobayashi *et al.* Silver nanoparticles were coated directly with silica by means of a seeded polymerisation technique based on the Stöber method. Dimethylamine (DMA) was used as the catalyst instead of ammonia as it was found that the particles are more stable in the presence of DMA than in ammonia. In light of the conclusion drawn from Chapter 2 indicating that PVP is not involved in the growth or stabilization of the particles and that citrate plays an important role it was decided to attempt this method because $Ag@SiO_2$ particles has been prepared successfully from citrate stabilized silver nanoparticles.[11]

A green silver sol prepared by the 'added citrate' method using 0.7 mM TSC at 50°C was centrifuged down and the pellets were redispersed back to their original volume with Millipore water. EtOH was then added (so that the EtOH:water ratio was 4:1) followed by TEOS (1 mM) and DMA (0.8 M). The sol was left to stir overnight. From the UV-vis spectra of the sol before and after coating shown below in Figure 3.9, it is possible that silica coating has occurred, as a red shift of both the in-plane dipole and the band ~400 nm is evident. Unfortunately the TEM was not working therefore images to confirm this could not be taken. The red shift of the plasmon bands could simply be due to the change in the refractive index of the medium surrounding the particles caused by the addition of EtOH (refractive index 1.361).

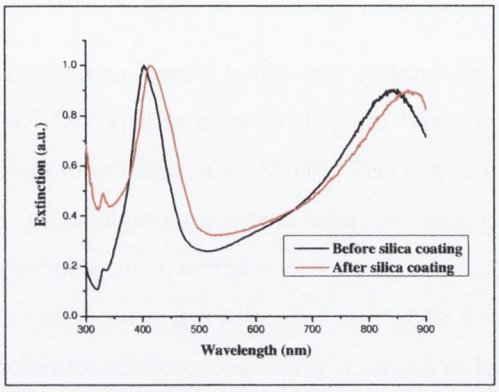


Figure 3.9: UV-vis spectra before coating of a sol prepared by the added citrate method using 0.7 mM TSC (black) and after the coating procedure as reported by Kobayashi *et al.*[11]

At this stage, although some progress had been made in producing silica coated silver nanoparticles it was clear that the above result was possibly the first time a sample of silver nanoplates had been coated. This was important as at the time the work was being carried, silica coated silver *nanoplates* had not been prepared. It was decided to persevere with this method where DMA was used to catalyse the silica shell growth instead of ammonia. The presence of ammonia is known to etch and/or cause aggregation of spherical silver nanoparticle and this problem is only heightened when silver nanoprisms are considered. This is because these structures have high surface energies especially at their tips and edges, where the silver atoms can be easily oxidised. The above method was repeated when access to the TEM was assured. However in this instance, no shift of the in-plane plasmon resonance was observed. It was then decided to prime the surface of the nanoprism with a surface primer to render it vitreophilic before carrying out the Stöber growth. Instead of using 3-aminopropyltriethoxysilane as described above, it was decided to use 3-mercaptopropyltriethoxysilane (MPTES) as the Ag-S bond is thought to be stronger than the Ag-N bond.

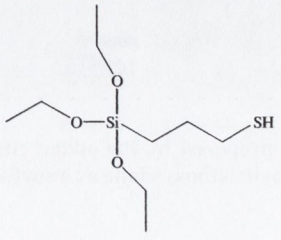


Figure 3.10: Structure of 3-mercaptopropyltriethoxysilane (MPTES).

3.1.1.4 MPTES primed method:

A green silver sol prepared by the 'added citrate' method using 0.7 mM TSC at 50°C was centrifuged down and the pellets were redispersed back to their original volume with Millipore water. MPTES (25 μM) was added with stirring and the sol was allowed to stand for 30 minutes to allow complete complexation of MPTES with the nanoparticle surface to occur. EtOH (4:1 to water) was then added followed by TEOS (1 mM) and finally DMA (0.8 M). The sol was left to stir overnight after which it was centrifuged and redispersed in EtOH. UV-vis spectra of the sol before and after coating and TEM images of the coated sol are shown below.

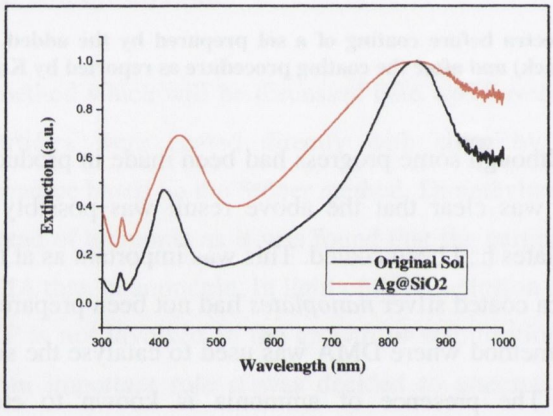


Figure 3.11: UV-vis spectra of a sol prepared by the added citrate method with 0.7 mM TSC before (black) and after (red) silica coating using 3-mercaptopropyltriethoxysilane as a surface primer.

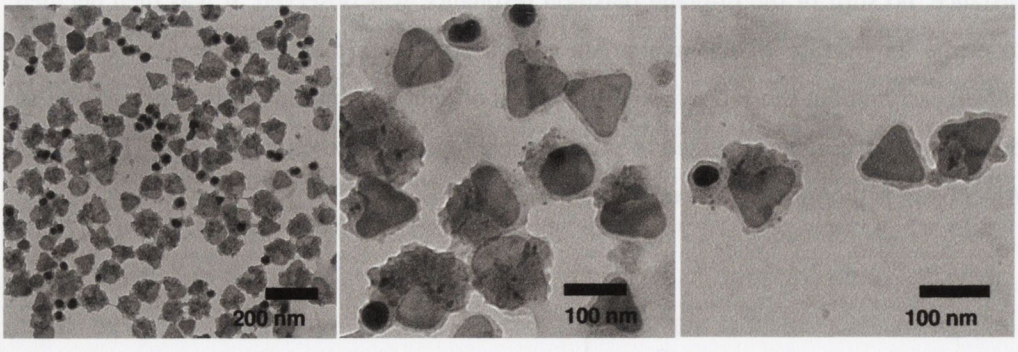
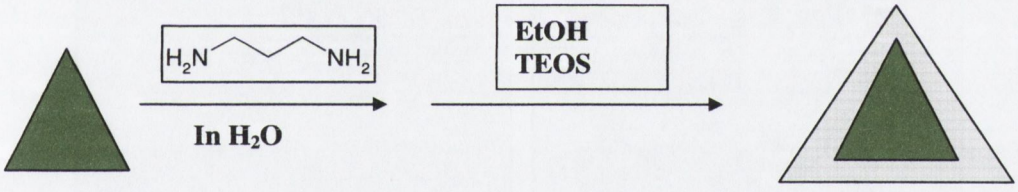


Figure 3.12: TEM images of a sol prepared by the added citrate method with 0.7 mM TSC after silica coating using 3-mercaptopropyltriethoxysilane as a surface primer and 1 mM TEOS.

From the TEM images above in Figure 3.12 it is clear that silica coating of the silver nanoprisms has occurred. However the quality of the coating is not homogenous and there is bridging of the coating between particles. Also on careful inspection, the edges and corners of the nanoprisms have been 'eaten' slightly and so the integrity of the particle is not maintained fully during the coating process. However in spite of this, the experiment shown above was a definite step forward towards the ultimate goal of preparing homogenously coated, well-dispersed silver nanoprisms.

3.1.1.5 1,3-diaminopropane primed method:

It was then decided to take a different approach. The possibility of catalysing the hydrolysis and condensation of TEOS on the surface of the nanoparticles was investigated. It was proposed that in this way the self nucleation of silica could be prevented. It was proposed that diaminopropane could facilitate this as shown in Scheme 3.1 below.



Scheme 3.1: New proposed method for the preparation of silica coated silver nanoprisms from aqueous sols.

A green sol was prepared by the added citrate method using 0.7 mM TSC at 50°C. It was centrifuged and redispersed in water. To this 1,3-diaminopropane (40 μM) was added and allowed to stir for 20 minutes. EtOH (4:1 to water) was then added followed by TEOS (1 mM). The sol was then allowed to stir overnight for 23 hours. However after this time no shift in the UV-vis spectrum was observed.

The method was then repeated but additional catalyst in the form of DMA (10 mM) was added 15 minutes after the addition of EtOH and TEOS in the above procedure. The UV-vis spectra of the sol before and after coating and TEM images of the coated sol are shown below in Figure 3.13 and Figure 3.14.

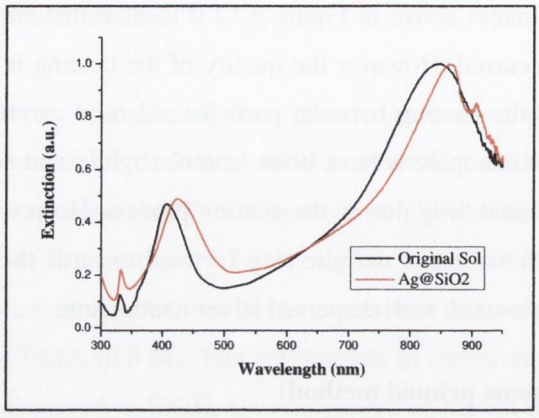


Figure 3.13: Normalized UV-vis spectra of a sol prepared by the added citrate method with 0.7 mM TSC at 50°C before (black) and after (red) silica coating by the method shown above in Scheme 3.1when additional catalyst (DMA) is added.

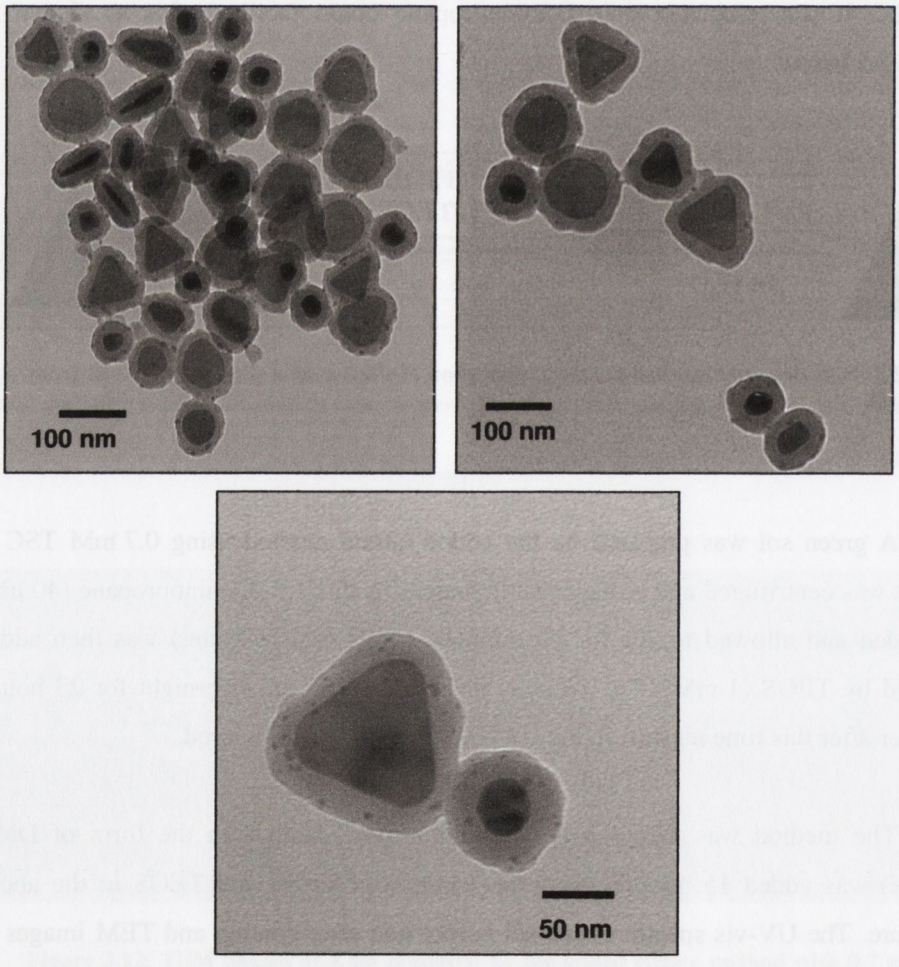


Figure 3.14: TEM images of silver nanoparticles prepared by the added citrate method with 0.7 mM TSC at 50°C after silica coating.

All Ag particles present are homogenously coated with a 20 nm silica shell. There are no uncoated or multiple core particles present and only a small amount of silica self nucleation is evident. The concentration of TEOS used was then reduced from 1 mM to 0.5 and 0.25 mM. The results are shown below.

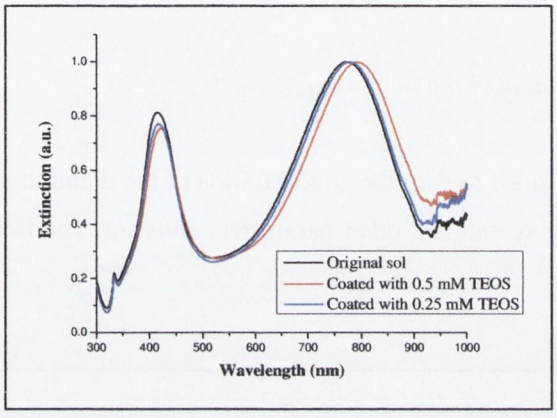


Figure 3.15: Normalized UV-vis spectra of silver nanoparticles prepared by the added citrate method at 50oC using 0.7 mM TSC before (black) and after coating with 0.5 mM TEOS (red) and 0.25 mM TEOS (blue).

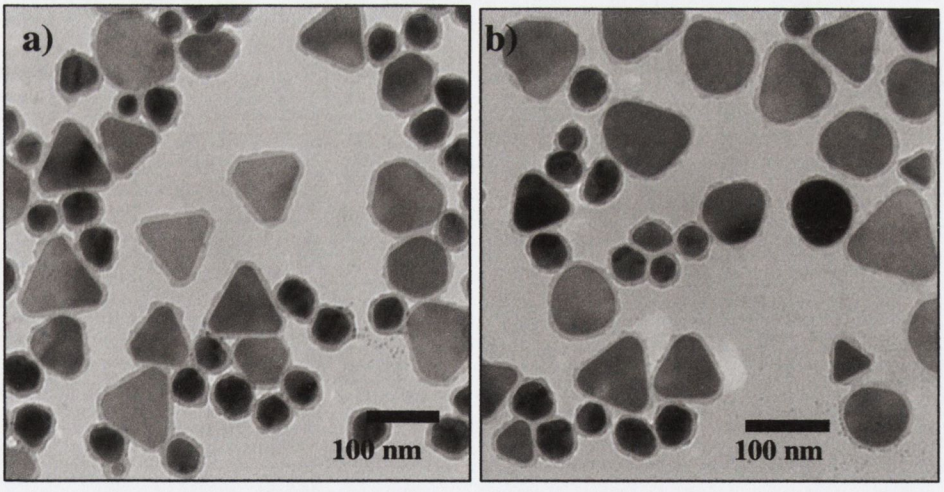


Figure 3.16: TEM images of silver nanoparticles prepared by the added citrate method at 50°C using 0.7 mM TSC after coating with a) 0.5 mM TEOS b) 0.25 mM TEOS.

As can be seen from the TEM images above in Figure 3.14, as the concentration of TEOS was decreased from 1 mM, 0.5 mM and 0.25 mM, the thickness of the resultant silica shell was decreased from 20 nm to 8 nm and 5 nm respectively. Another point to be noted is that as the thickness of the silica shell is decreased the homogeneity of the shell is also decreased.

Varying the concentration of diaminopropane used.

It was then decided to vary the concentration of the diaminopropane primer used in the synthesis while keeping all other parameters constant. The final concentration of TEOS was 0.5 mM.

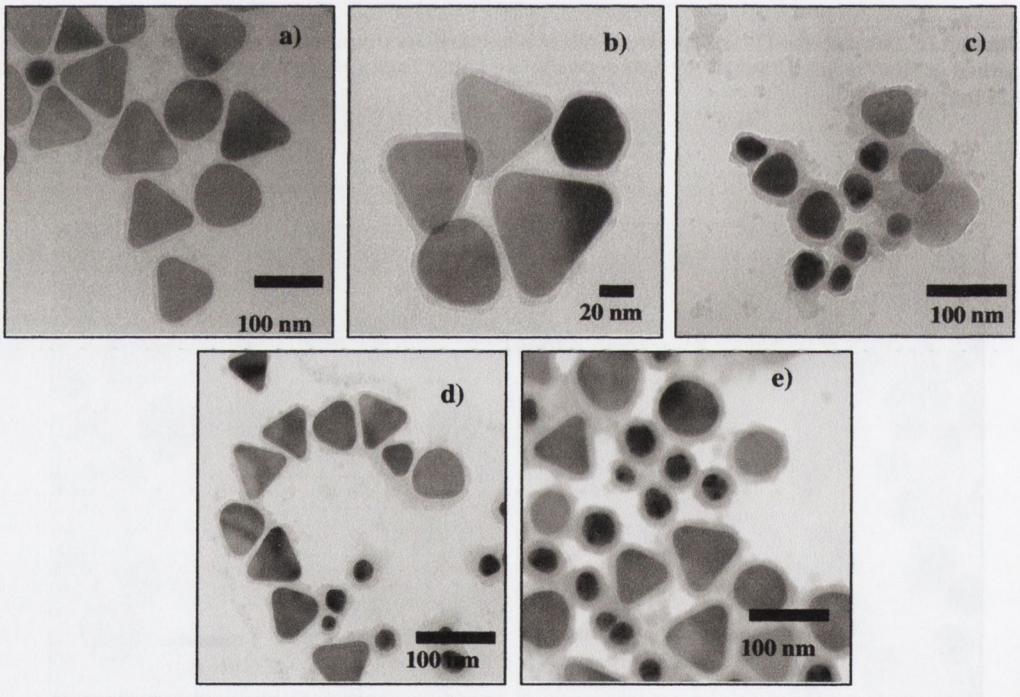
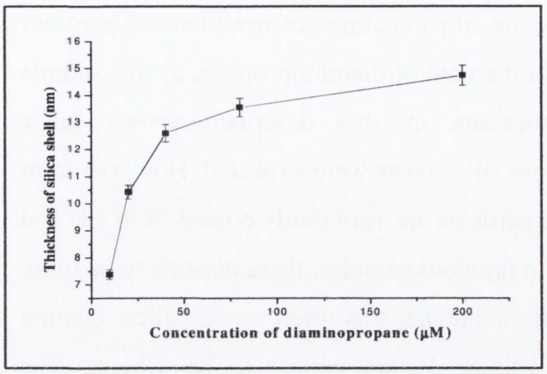


Figure 3.17: TEM images of a sol prepared by the added citrate method with 0.7 mM TSC at 50°C when diaminopropane a)10 µM b) 20 µM c) 40 µM d) 80 µM and e) 200 µM is used in the coating procedure.



$[NH_2(CH_2)_3NH_2]$ (μM)	*Shell Thickness (nm)*
10	7
20	10
40	13
80	14
200	15

Figure 3.18: The variation in the thickness of silica shell formed as the concentration of diaminopropane primer is varied at constant TEOS concentration.

As the concentration of diaminopropane is increased, the thickness of the silica shell is increased. The shells tend to be non-uniform, in that the thickness of silica around individual particles may vary. The best quality of shell was achieved with the highest concentration of diaminopropane (200 μM) but there was more silica self nucleation at this concentration.

Varying the chain length of diaminoalkane used:

The chain length of the diaminoalkane primer was varied using ethylenediamine, 1,3-diaminopropane and 1,4-diaminobutane. The concentrations of the reagents used were as follows: TEOS (0.5 mM), DMA (10 mM) and diaminoalkane (40 μM)

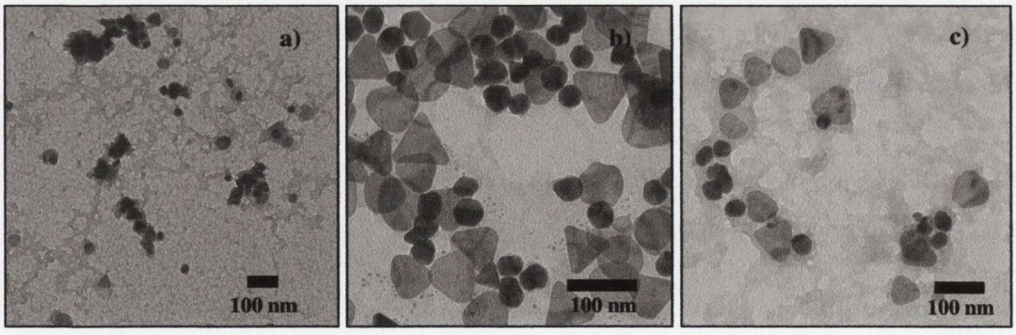


Figure 3.19: TEM images of the results of the silica coating process as described above when a) ethylenediamine b) diaminopropane and c) diaminobutane were used as primers.

When ethylenediamine was used some silica coating occurred but the particles seem to be joined together in a network. In the case of diaminopropane, as this sample was prepared following the same procedure as that described above, fairly homogeneously coated particles with ~12 nm silica coats were expected. However from the TEM image above it is clear that these particles are very thinly coated (if at all) and instead of the very obvious coat observed in previous samples, there appears to be more silica self nucleation. Finally when diaminobutane was used some silica coating occurred. However individually coated articles do not appear to be present. The particles seem to be situated in a silica network. In this instance the quality of the coating is better than that achieved with ethylenediamine.

3.1.1.5 Reproducibility:

It was decided to repeat this experiment, as the result above using the diaminopropane primer was not similar to those routinely observed previously using the same method of preparation. Unfortunately, silica coated silver nanoparticles were not obtained. In some cases the spherical particles present appeared to be preferentially coated while the prisms remained bare. Various different attempts were made to improve the reproducibility of the experiment for example:

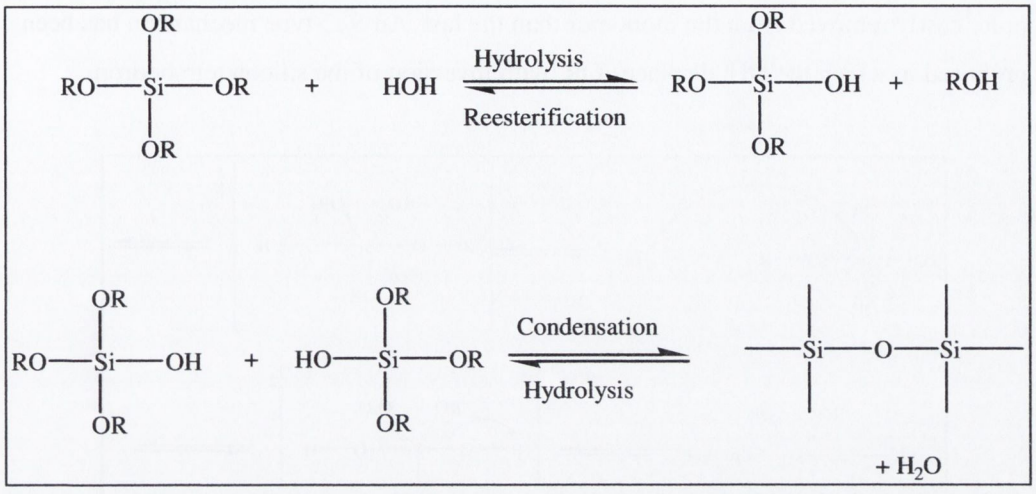
1. purification of the reagents used via distillation
2. carrying out the coating procedure in a polypropylene beaker instead of a standard pyrex beaker to decrease the possibility of the TEOS adhering to the sides of the glass thus preventing the condensation of silica on the particles

but homogeneously coated silver nanoparticles as shown above in Figure 3.14 were not observed again.

3.1.2 Discussion of the silica coating of silver nanoparticles:

3.1.2.1 Stöber chemistry

As all the methods described above make use of Stöber chemistry, the mechanism must be considered in further detail. The Stöber process involves the *base catalysed* hydrolysis and condensation of tetraethoxysilane (TEOS) as shown in Scheme 3.1 below. Hydrolysis occurs when TEOS and water are mixed together in a mutual solvent, in most cases alcohol.



Scheme 3.2: Hydrolysis and Condensation reaction of a silicon alkoxide precursor ($R=CH_2CH_3$).

It has been found that the following factors influence the hydrolysis and condensation reactions of the sol-gel process.[19]

a) pH
b) nature of the catalyst
c) H_2O/Si molar ratio

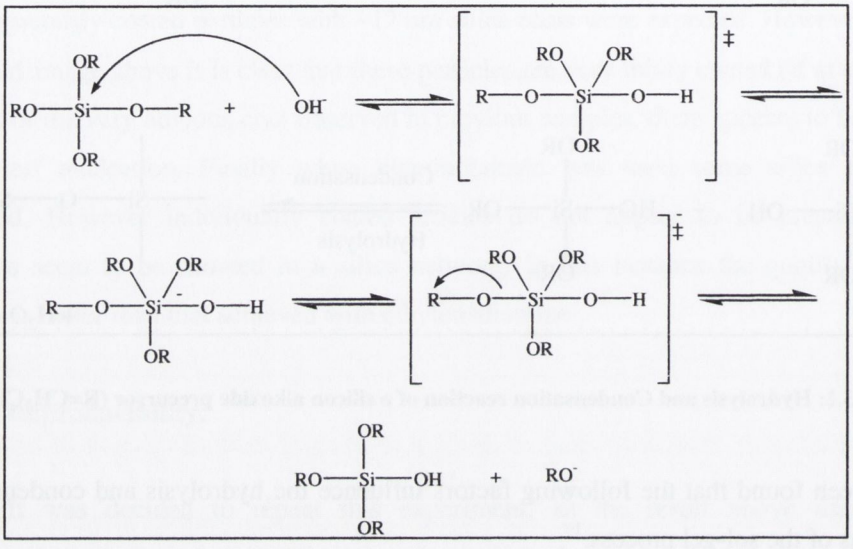
a) pH:

Hydrolysis of TEOS can occur by either an acid or base catalyzed mechanism. However as the work described in this chapter is concerned with Stöber chemistry, only the base catalysed mechanism will be considered. In polymerisations above pH 7, growth occurs through a process called Ostwald ripening. Particles grow in size and decrease in number as highly soluble small particles dissolve and reprecipitate on larger, less soluble particles.

b) Nature of the catalyst

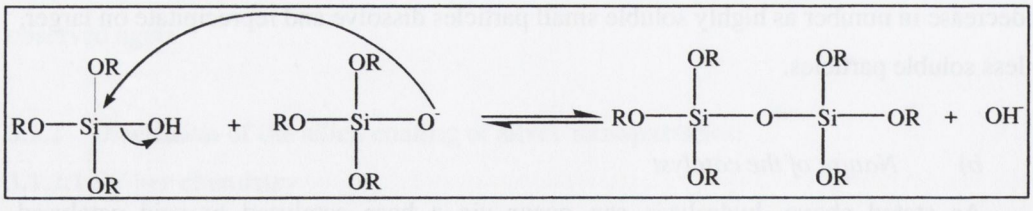
As stated above, hydrolysis can occur via a base catalysed or acid catalysed mechanism. Under acid catalysed conditions, linear or branched polymers are the dominant product while base catalysed reactions yield clusters or discrete particles. For this reason base-catalysed reactions alone will be discussed here. The basic alkoxide oxygens tend to repel the nucleophile, OH^-. However once an initial hydrolysis has occurred, following reactions proceed step-wise, with each subsequent alkoxide group

more easily removed from the monomer than the last. An S_N2-type mechanism has been proposed in which the OH^- displaces OR^- with inversion of the silicon tetrahedron.



Scheme 3.3: Mechanism of the base-catalysed hydrolysis of silicon alkoxide precursor ($R=CH_2CH_3$).

Condensation can also occur via a base catalysed or acid catalysed mechanism. The most widely accepted mechanism for the base-catalysed condensation reaction involves the attack of a nucleophile deprotonated silanol on a neutral silicic acid. It is generally accepted that the mechanism involves penta- or hexa- coordinated silicon transition state similar to that of a S_N2- type mechanism.



Scheme 3.4: Nucleophilic Attack to form siloxane bond in the condensation reaction ($R=CH_2CH_3$).

c) H_2O/Si Molar ratio (R):

Under basic conditions it has been observed that the hydrolysis of TEOS has a zero-order dependence on the water concentration. However, if R is increased while maintaining a constant solvent: silicate ratio, the silicate concentration is reduced, in turn reducing the hydrolysis and condensation rates. Also large values of R promote siloxane bond hydrolysis.

3.1.2.2 Methods used for the silica coating of silver nanoparticles

The synthesis of silica coated Ag nanoparticles has proven to be harder to reproduce than initially expected. The first method (by Ung *et al.*) attempted was unsuccessful. No coated Ag particles were produced. This has been attributed to a number of factors.

1. The presence of spectator ions in the sol prior to activation with APTES and again prior to growth of the silica shell with sodium silicate solution.
2. The lack of precise control of the pH of the sol in these steps.

The pH of the sol prior to the addition of the APTES is found to be very important in the determination of the surface orientation of the APTES molecules. APTES exists in a number of forms in aqueous solution. Around pH 2-4 APTES is positively charged, between pH 4 and 9 it is zwitterionic and above pH 9 it is negatively charged.[3]

$$^{+}H_3NC_3H_6Si(OH)_3 \leftrightarrow {}^{+}H_3NC_3H_6Si(O^-)_3 \leftrightarrow H_2NC_3H_6Si(O^-)_3$$

Due to the adsorbed citrate ions, the silver nanoparticles are themselves negatively charged. At pH greater than 9, the sol stability is maintained through increased ionisation of the surface citrate carboxyl groups. Nucleophilic attack by the APTES then occurs. However, at this pH APTES in its unprotonated form may also form cyclic hydrogen-bonded zwitterions between the amino and silanol groups, therefore locking the amine away and preventing it from surface complexation. A pH of 5 is therefore optimal with respect to these two competing requirements and the active complexing form is suggested to be $^{+}H_3NC_3H_6SiOH(O^-)_2$.[3] In spite of repeating the experiment as documented in the paper with the optimum conditions, silica coated spherical silver nanoparticles could not be produced. This method has also proved to be problematic for other researchers. The priming step involving the APS was found to be 'poorly

reproducible'[58] and in personal communication with Mulvaney (senior author on the paper describing the synthesis) he indicated that the procedure is 'very tricky'.

Silica coated silver nanoparticles were successfully prepared using the Graf *et al.* method. The limiting factor in this case was the actual preparation of the silver nanoparticles to be coated as the procedure to recover the nanoparticles prepared by the polyol method was long and tedious. However, the particles, once produced were coated with silica. The quality of the silica shell was not as good as expected from the reported procedure and there was a lot of free silica present that did not take part in the coating. However, of the literature methods used to prepare silica coated spherical silver nanoparticles this method, where PVP is used as a primer, was the most reproducible. The fact that particles prepared by the 'added citrate' method were not successfully coated with silica is another confirmation that PVP plays no role in the growth of these particles and acts merely to prevent particle aggregation. Because it is the PVP that effectively 'anchors' the silica onto the surface of the nanoparticles it is not surprising that Yin et al have reported the coating of Ag nanowires prepared by the polyol process, with silica.[20] It is proposed that this method could be adapted to coat the numerous morphologies of silver nanoparticles prepared by the polyol method (discussed in Chapter 1).

The third method used to prepare $Ag@SiO_2$ particles was adapted from Kobayashi *et al.* The main advantage of using this method is that DMA does not have the same aggregation/etching effect that is observed when ammonia is used to catalyse the hydrolysis and condensation of TEOS. This is particularly relevant to the silver nanoparticles discussed in Chapter 2, as the corners of the sharp triangles are known to be very sensitive to an etching process. Tests have shown only a small movement (approx. 7 nm) of the longitudinal band when sols are exposed to DMA solution without the presence of TEOS over a period of 30 minutes. When a sol is exposed to ammonia for the same period of time without the presence of TEOS, the particles are readily oxidized and form $Ag(NH_3)_2^+$ ions that are soluble and colourless.

The concentration of water in the reaction is very important. Under basic conditions it has been observed that the hydrolysis of TEOS has a zero-order

dependence on the water concentration.[19] However, if R is increased while maintaining a constant EtOH: silicate ratio, the silicate concentration is reduced, in turn reducing the hydrolysis and condensation rates. Also large values of R promote siloxane bond hydrolysis (reverse of Scheme 3.4 above). As the water concentration increases, dissociation of DMA and ionic strength increases, leading to the aggregation of silver particles and the formation of core free silica particles. It has been reported that a water concentration of 11.1 M, (4:1 EtOH to water) leads to uniformly coated silver particles with a negligible amount of core-free silica.[3, 9, 11]The concentration of catalyst is also important. When the concentration of DMA is too low the TEOS condensation will not go to completion and when it is too high, the ionic strength is increased and particle aggregation occurs leading to the particles precipitating out of solution.

The use of 3-mercaptopropyltriethoxysilane (MPTES) has previously been reported for the silica coating of AgI semiconductor nanoparticles.[21] This method also applies Stöber growth in the presence of the silane-coupling agent. DMA is also used as the catalyst for the hydrolysis. The addition of MPTES suppressed the generation of free silica particles and improved the uniformity of the shell thickness. It was proposed that the MPTES molecules possibly had a strong affinity for the AgI surface so that a condensation reaction between MPTES and TEOS was initiated on the surface.[21] It has also been used to prime the surface of citrate stabilized silver nanowires before a thicker silica shell was produced by the deposition of silica from sodium silicate.[22]When MPTES was used as a primer in the silica coating of the particles prepared by the 'added citrate' method, an inhomogeneous coating that bridged individual silver nanoparticles was produced. However, this was the first instance that silica coated silver nanoprisms were observed. The MPTES binds to the silver surface thus preventing etching and aggregation during the addition of the base, in this case DMA, required to catalyze the hydrolysis and condensation of TEOS. However, on closer inspection it is evident that the integrity of the silver nanoprism cores was not maintained completely and some etching of the edges of the particles can be seen. Because the synthesis devised after this procedure, involving a diaminopropane primer, appeared to be more successful a thorough investigation of all the parameters used in this synthesis using MPTES was not undertaken. However, the first step towards investigating this process further would be increasing the concentration of MPTES used to ensure complete monolayer coverage thus preventing etching of the particles during the coating process.

In the synthesis involving a diaminopropane primer silver nanoparticles with a discrete, homogeneous coat were produced. This is the first time that such a method has been used to prepare coated silver particles. Initially it was proposed that the diaminopropane, due to its bifunctional nature would prime the surface of the nanoparticles and also catalyse the hydrolysis and condensation of TEOS, thus preventing the nucleation of free silica. Unfortunately, this was found not to be the case. However, when additional catalyst was used in the form of DMA, silica coated nanoprisms were observed. A recent paper by Hu *et al.* has shown, through surface enhanced Raman experiments and DFT calculations, that ethanediamine adsorbs on a colloidal silver surface through the N atoms via lone pairs of electrons with the C-C bond parallel to the silver surface.[23] It is also proposed that the two N atoms bind to one silver atom rather than two. In the case of the system described above, the working pH is approximately 5.5 so that 1,3-diaminopropane would exist in its unprotonated form. It is therefore likely that it adsorbs onto the surface of the colloid in a similar fashion. So why does this encourage the silica to adsorb on to surface of the nanoparticles?

It is proposed here that the function of the diaminopropane is to provide a hydrophobic layer around the surface of the nanoparticle, thus preventing their etching or aggregation when exposed to the amine during the silica coating reaction. It must also be responsible for a 'tethering effect' because, as the concentration of diaminopropane is increased, the thickness of the silica shell is also increased, at the same TEOS concentration. The protection afforded by the diaminopropane was examined by varying the alkyl chain length and in the case when it was reduced (and ethylenediamine was used) the morphology of the particles was not maintained through the coating process. A representative TEM is shown above in Figure 3.19 and it can be seen that no prisms remain in the sample. However, the overall results from this batch of experiments were not as expected, as only a very thin silica shell (if any at all) was observed for the diaminopropane case. This result and the fact the method could not be carried out again reliably, with the same results highlights once more a recurrent theme throughout this thesis: reproducibility.

Numerous efforts were made to improve the reproducibility of the reaction as stated above. Unfortunately none were successful. As already highlighted above, the route used to prepare coated nanoparticles strongly depends on the method of

preparation of the nanoparticles *i.e* TSC *vs* PVP stabilized. As all external parameters such as the quality of reagents used *etc* were examined, it is suggested here that the source of the irreproducibility lies within small differences in the surface chemistry of the nanoparticles produced. This problem will be discussed again in Chapter 4, where different SERS spectra were obtained using nanoprisms prepared by the same method and using the same concentration of analyte. This is an area of nanochemistry that has not received a lot of attention probably due to the difficulties associated with characterizing the surface properties adequately.

During the time this work was being carried out a paper was published by Xue *et al.*[24]in which silver nanoprisms were coated with silica in a similar manner. In a typical experiment the nanoprisms were first passivated with a monolayer of 16-mercaptohexadecanoic acid via a Ag-S bond. This monolayer prevents the etching and aggregation of the silver nanoprisms upon exposure to the DMA used to catalyse the hydrolysis and condensation of TEOS.[24] In this paper, the authors cite 15 nm as the critical shell thickness because below this value, incomplete coatings are obtained. One advantage that the method described above has over this literature method by the Mirkin group is that thinner complete silica shells can be produced. This is an important factor to consider when thinking about the future use of such hybrid materials. For example, a thin coat would be an advantage when using these particles as spectral sensors because, the further the analyte is placed from the surface of the nanoparticle the smaller the spectral shift observed. This is because changes in the position of the plasmon band are only observed with changing dielectric constant around the surface of the nanoparticle.

3.1.3 Conclusions from the silica coating of silver nanoparticles:

The synthesis of silica coated silver nanoparticles has proved to be more difficult than originally anticipated. Different methods from the literature were used but were met with limited success. However, two new methods for the production of silica coated silver nanoprisms were developed. The first of these involves priming the surface of the silver nanoparticles with 3-mercaptopropyltriethoxysilane before carrying out the growth of the silica shells by the Stöber process. Inhomogeneous coats were observed but this was the first time, to the best of my knowledge that silica coated silver nanoprisms had been prepared. The second method is similar, in that Stöber growth is

also carried out however it uses a diamine as a primer molecule. In this case the shells were homogenous and the thickness could be varied in two ways, by changing the concentration of TEOS used and by changing the concentration of diaminopropane primer used at constant TEOS concentration. The one major drawback of this method is its limited reproducibility.

3.2 Other methods for functionalizing silver nanoparticle:

Another method that has been used in colloid science to functionalize nanoparticles is the layer-by-layer (LbL) technique. As the name suggests, this technique involves the assembly of polymer layers on the surface of a colloid. Typically the first layer of polymer is of opposite charge to that of the nanoparticle so the interaction is mainly electrostatic. It has been used to functionalize latex particles and in recent years has been adapted to coat gold nanoparticles.[1, 25-29] Under optimum conditions, Schneider and Decher have successfully coated gold colloids in concentrated suspension with up to 20 layers of the polyanion poly(styrene sulfonate) (PSSS) and the polycation poly(allylamine hydrochloride)(PAH).[27] This type of functional material has been used to investigate the phenomenon of Surface Enhanced Fluorescence.[28]

3.2.2 Results

It was decided to attempt to consecutively coat the silver nanoparticles prepared by the 'added citrate' method described in Chapter 2 with positively and negatively charged polymers. Some of the work described in the following section (Figure 3.21-21) was carried out by a summer student, Celine Mesclaux, working in the group under my supervision.

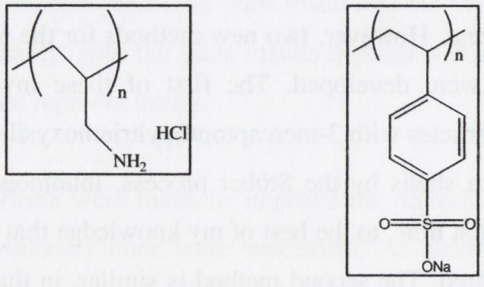


Figure 3.20: Structure of the positively charged poly(allylamine hydrochloride) and negatively charged poly(styrene sulfonate sodium salt).

A green sol prepared at 50°C using 0.7 mM TSC was centrifuged. The pellets were redispersed in an aqueous solution of poly(allylamine hydrochloride) (PAH) (1 mg/mL). As can be seen from the UV-vis spectra shown below, the sol was not stable in the presence of the PAH at this concentration, and the in-plane dipole resonance experienced a blue-shift with time. These results are similar to the case highlighted in Chapter 2, when the nanoparticles were redispersed in unpurified PVP solution. TEM analysis also confirms this, as after 1 day no sharp triangles remained in the sample, with the dominant morphology being circular discs.

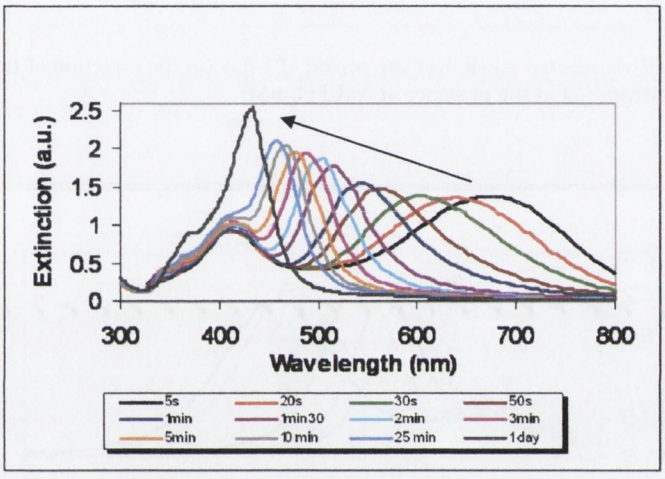


Figure 3.21: UV-vis spectra taken over the period of 1 day (in the direction of the arrow) of a green 'added citrate' sol redispersed in 1 mg/mL poly(allylamine hydrochloride).

This instability was attributed to the presence of the chloride counter-ion. For this reason it was decided to test the stability of a sol prepared by the same method in NaCl (1 mM). The study was also extended to include NaBr and NaI at the same concentration. The results are shown below in Figure 3.22, Figure 3.23 and Figure 3.24 respectively.

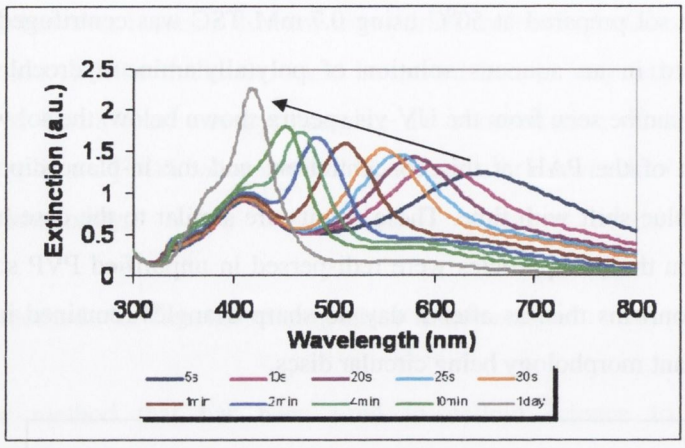


Figure 3.22: UV-vis spectra taken over the period of 1 day (in the direction of the arrow) of a green 'added citrate' sol in the presence of NaCl (1 mM).

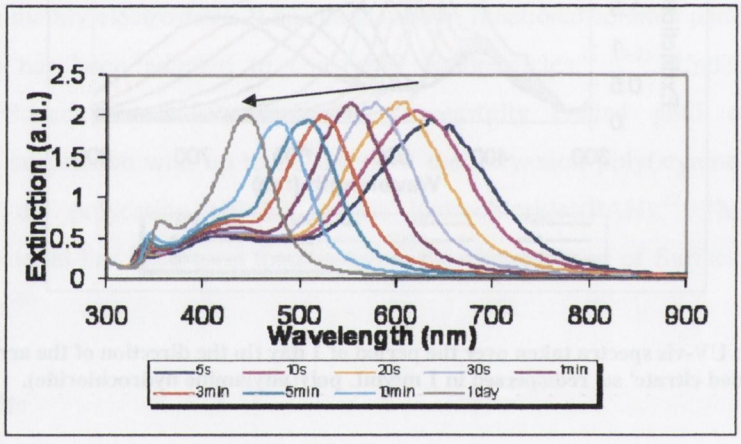


Figure 3.23: UV-vis spectra taken over the period of 1 day (in the direction of the arrow) of a green 'added citrate' sol in the presence of NaBr (1 mM).

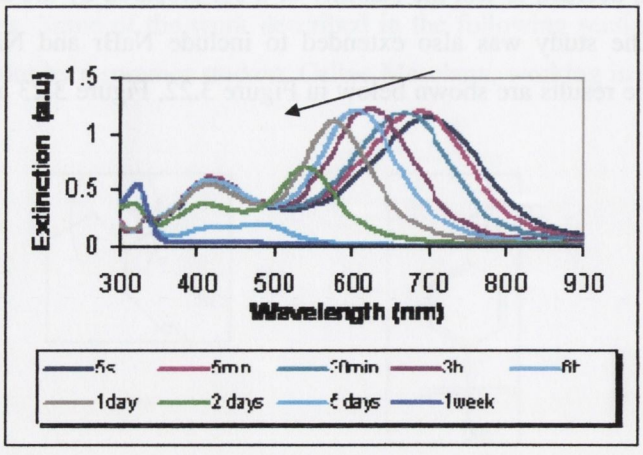


Figure 3.24: UV-vis spectra taken over the period of 1 day (in the direction of the arrow) of a green 'added citrate' sol in the presence of NaI (1 mM).

From the results above it can be clearly observed that the presence of halide ions is detrimental to the stability of the nanoparticles. By comparing the positions of the grey plots (spectra taken one day after redipsersion) in each of the above sets of spectra it can be seen that the halide ions etch the silver nanoparticles, prepared by the added citrate method in the following order: iodide < bromide < chloride. In the case of the NaI case, the emergence of a new band at ~320 nm after 2 days indicates the formation of silver iodide nanoparticles.

In addition to the halide anions a range of other anions were also tested at a concentration of 1 mM. The results are summarized in the table below. For the purpose of the documenting this results and in the discussion below, sols are defined as stable in the presence of the anions when no movement of the in-plane dipole resonance was observed over the period of 1 day.

Stable	*Unstable*
Sulfate	Chloride
Acetate	Bromide
Carbonate	Iodide
Hydroxide	Phosphate
Nitrate	
Nitrite	

Table 3.1: The stability of silver nanoparticles prepared by the added citrate method at 50°C using 0.7 mM TSC against various anions.

In light of these results it was decided that two approaches could be taken to modify the LbL procedure so that polyelectrolyte coated silver nanoparticles could be produced while still maintaining the morphology of the particles. Firstly, the poly(allylamine hydrochloride) could be subjected to ion exchange, so that the chloride ion could be replaced by one of the other anions that were found to be innocuous. Secondly, the surface of the nanoparticles could be modified so that the halide anions could not etch the particles. The first approach mentioned above was undertaken by another researcher in the group and it was decided that the work described in the proceeding section would concentrate on modifying the silver nanoparticles so that etching could be prevented.

Gelatin is a colourless, water-soluble glutinous protein that is produced by the partial hydrolysis of collagen and is extracted from processed bones, connective tissues and in some cases the organs of animals. It is a heterogeneous mixture of single or multi-stranded polypeptides with high percentages of glycine, proline and hydroxyproline residues and has been utilized in a wide variety of industries from pharmaceutical to adhesives. For over a century, it has been used to stabilize tabular silver halide micro and nanocrystals in nearly all photographic films and papers and no cheaper, synthetic alternate has been found.

It was decided to test if the surface of the silver nanoparticles prepared by the added citrate method could be modified post synthesis by the addition of gelatin. Silver nanoparticles were prepared as described in Chapter 2 by the added citrate method (using seeds prepared in the presence of PSSS). The sol was centrifuged, the supernatant removed and the pellets redispersed back to their original volume with 0.1 wt% gelatin. It was then left undisturbed overnight. An aliquot was then removed, centrifuged and the pellets were redispersed back to their original volume with water. The stability of this sol was tested against NaCl (10mM). A sample of a freshly prepared sol was also tested with NaCl (1 mM) as a reference. The results are shown below in Figure 3.25.

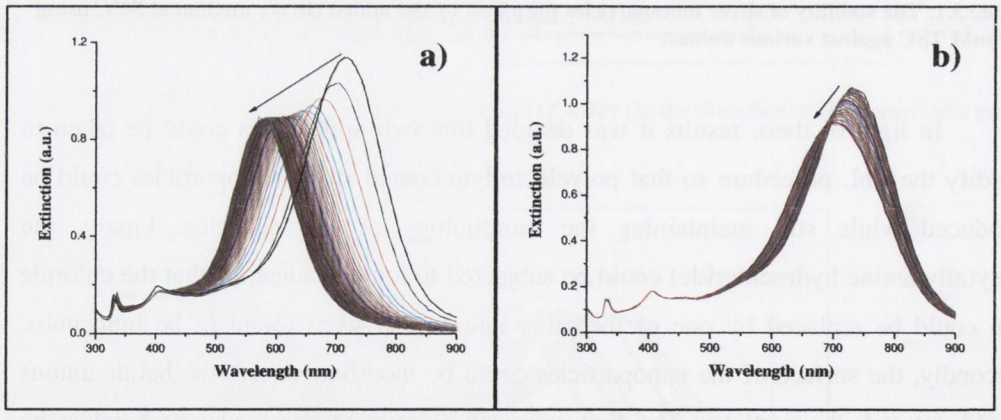


Figure 3.25: UV-vis spectra recorded at 30s intervals over the period of 15 minutes (in the direction of the arrow) of a sol prepared by the added citrate method (with seeds prepared in the presence of PSSS), a) as prepared tested with NaCl (1 mM) b) stabilized by 0.1 wt% gelatin, tested with NaCl (10 mM).

A blue-shift of the in-plane dipole of 135 nm was observed within the first 15 minutes after exposure to the salt solution for the as prepared sol while a shift of only 35 nm was experienced by the sol in the presence of gelatin. It must be noted that the concentration of NaCl used to test the gelatine stabilized nanoparticles was ten times greater than that used with the as prepared sol. It was then decided to test the same sol again 48 and 96 hours after redispersion in the gelatin. The results are shown below in Figure 3.26.

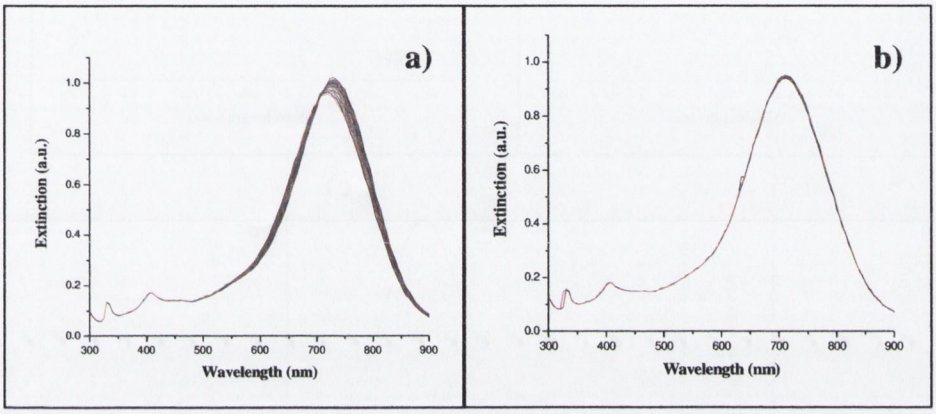


Figure 3.26: UV-vis spectra recorded at 30s intervals over the period of 15 minutes of a sol prepared by the added citrate method (with seeds prepared in the presence of PSSS) in the presence of gelatin after a) 48 hours b) 96 hours tested with 10 mM NaCl.

It can be observed from the sets of spectra shown above that, as the time during which the sol is left undisturbed in the presence of gelatin is increased, the stabilization afforded to the nanoparticles by the gelatin is also increased, up to the point where no etching of the particles is observed in the presence of 10 mM NaCl after 4 days.

The next stage in the process was to determine if there was a critical threshold concentration of gelatin below which protection of the particles against NaCl was not observed. To examine this, a similar sol to the one shown above was prepared. It was centrifuged, the supernatant removed and the pellets were redispersed in 0.1, 0.05, 0.01 and 0.005 wt% gelatin solutions. The sols were left undisturbed for 4 days after which they were centrifuged and the pellets redispersed back to their original volume in water. It was noted that as the concentration of gelatin was reduced, the quality of the pellets also deteriorated. It was necessary to subject the sol stabilized by 0.01 wt% gelatin to vortexing to ensure that all the pellets were redispersed. The nanoparticles in the

presence of 0.005wt% gelatine could not be redispersed even after vortexing and sonication. The results of the other three sols are shown below in Figure 3.27.

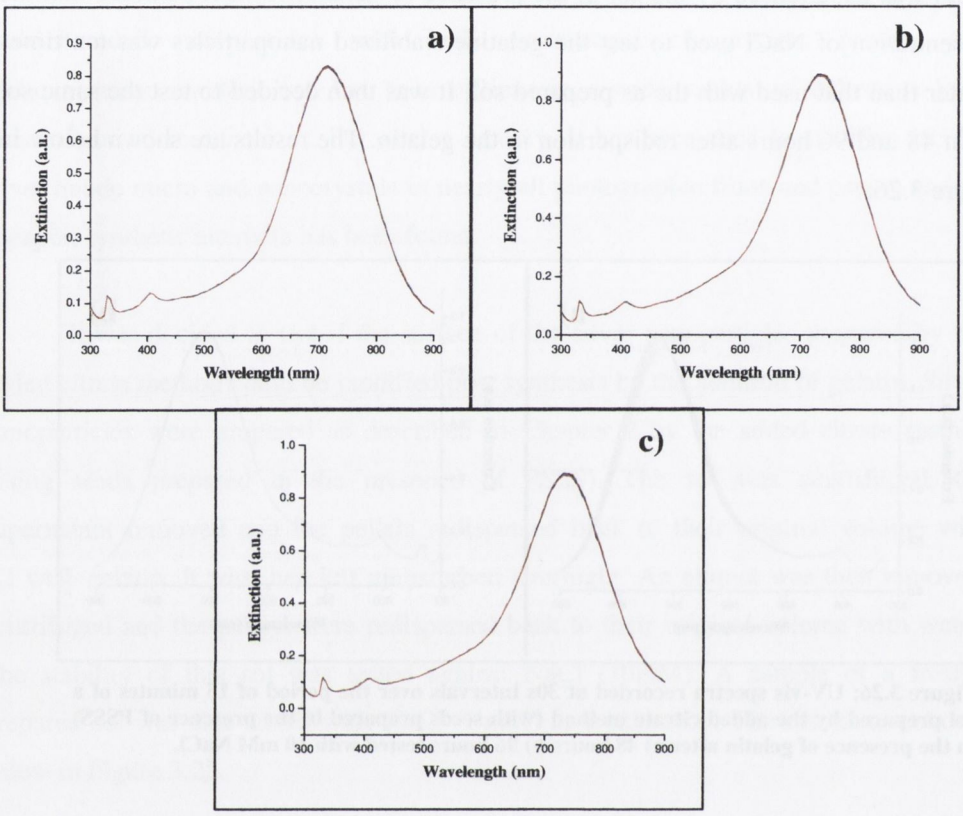


Figure 3.27: UV-vis spectra recorded at 30s intervals over the period of 15 minutes of a sol prepared by the added citrate method (with seeds prepared in the presence of PSSS) in the presence of a) 0.1 wt% b) 0.05 wt% and c) 0.01wt% gelatin and left to stand for 4 days, tested with 10 mM NaCl.

It can be clearly observed that enhanced stability of the nanoparticles was observed in the presence of gelatin to as low a concentration of 0.01 wt%. TEM analysis was also carried out on the above sols, 4 days after redispersion in the gelatin solution before the addition of NaCl. The particles do not appear to be encapsulated in a network of gelatine. In fact, no coating at all can be observed. This is not unexpected as the majority of biological samples need to be first stained with uranyl acetate in order for them to be observed clearly in TEM. It must also be noted that a significant red-shift of the in-plane dipole was not observed upon functionalization of the nanoparticles with gelatin. Zeta-potential measurements of a sol before (-45 mV) and after functionalization with gelatin (-17 mV) together with the enhanced stability of the

nanoparticles toward salt are the only indications that surface modification has occurred.

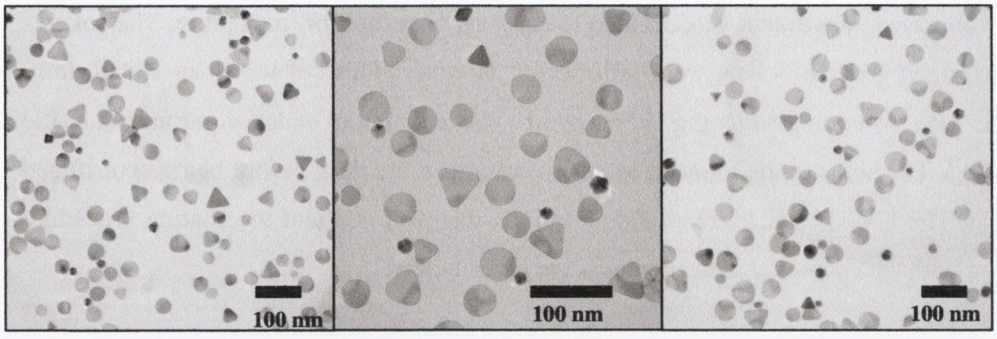


Figure 3.28: TEM images of the sols shown above in Figure 3.27 before stability testing with NaCl (10 mM) was carried out. a) 0.1 wt% b) 0.05 wt% c) 0.01 wt% gelatin.

At this stage in the work, a method had been devised to stabilize the nanoparticles. This was an important result as it meant that the LbL technique could be attempted again, in the knowledge that etching of the particles would not occur on exposure to the poly(allylamine hydrochloride) solution, where at a concentration of 1 mg/mL, the chloride concentration was estimated to be 0.1 mM.

A silver sol was prepared by the added citrate method using seeds that were prepared in the presence of PSSS (see Scheme 2.1). The sol was centrifuged and the pellets were redispersed in 0.1 wt% gelatin solution. It was then left to stand for 1 week without further disturbance. After this time, the sol was centrifuged again and the pellets were redispersed in water. The sol was then added drop-wise to a solution containing 5.56 mg/mL PAH solution under vigorous magnetic stirring. The sol was then allowed to stir overnight in the dark before being centrifuged again. At this stage, the sol which was originally blue in colour had become red indicating that etching of the particles had still occurred despite the presence of gelatin. It must be noted that an aliquot of the gelatin stabilized sol was tested with NaCl (10mM) prior to commencing the LbL procedure and no etching was observed.

It was then decided to ion exchange the chloride ion to nitrate in the PAH prior to carrying out the LbL procedure. This procedure had previously been optimized by another summer student, Dorota Mrozek under the supervision of Dr. Damian Aherne and is given in detail in Chapter 5. A similar procedure to the one described in the

previous paragraph was carried out using the modified PAH. After the overnight stirring the presence of the modified PAH it was noted that a colour change from blue to violet was observed, however it was decided to carry on with the LbL procedure. The sol was centrifuged and the pellets were redispersed in water. This sol was then added drop-wise to a solution containing 5.56 mg/mL PSSS solution under vigorous magnetic stirring. The sol was the allowed to stir overnight in the dark before being centrifuged again. The UV-vis spectra recorded at various stages throughout the coating procedure along with zeta potential measurements are given below.

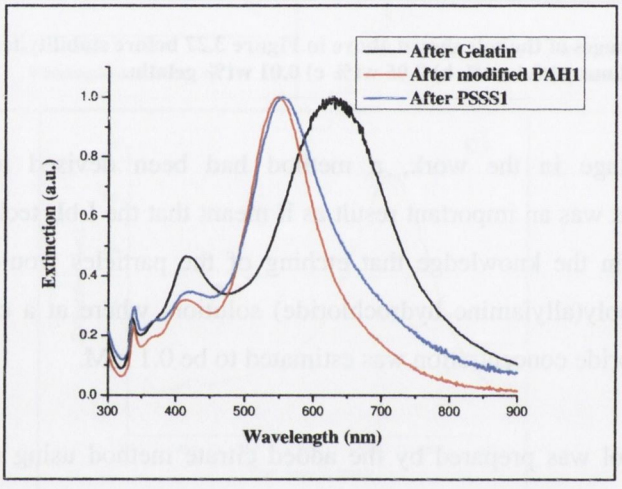


Figure 3.29: Normalized UV-vis spectra of a sol prepared by the added citrate method from seeds maded with PSSS after functionalization with gelatin (black), nitrate modified PAH (red), PSSS (blue).

Sample	*Zeta Potential (mV)*
After Gelatin	-15
After modified PAH1	+65
After PSSS 1	-54

Table 3.2: Zeta potential measurements of silver nanoparticles at various stages in theLbL coating procedure at pH 6.

Although there is an initial blue shift of the in-plane dipole resonance upon addition of the nitrate modified PAH , the zeta potential measurements suggest that

successful functionalization has occurred. Upon addition of the PSSS, a 10 nm red-shift was observed as expected. This, together with the zeta potential measurements suggests again that successful functionalization has occurred. However, this process is severely limited by the loss of particles through centrifugation. After two layer of polyelectrolyte had been deposited on the nanoparticles, the yield of recovered particles was deemed too low to continue with the deposition of further layers.

3.2.2 Discussion:

Initial investigations of the layer by layer (LbL) technique as a method for the functionalization of shaped silver nanoparticles revealed that the presence of chloride in the positively charged polymer poly(allylamine hydrochloride) was detrimental to the shape of the nanoparticles prepared by the added citrate method. When the particles were exposed to a 1 mg/mL aqueous solution of PAH, they experienced a morphological change from triangular to discal nanoplates. Upon further investigation it was observed that, halide ions in general have this sculpting effect, while other anions such as sulphate, acetate, carbonate, nitrate and nitrite do not cause the same effect at similar concentrations. The order of the reactivity of the halide ions with the silver nanoparticles was found to be as follows $I^- < Br^- < Cl^-$.

In order for the LbL layer procedure to be carried out without damaging the original morphology of the particles it was decided to investigate if it was possible to protect the surface of the nanoparticle from the effect of the halide ions. This was achieved by adsorption of gelatin at various concentrations. It was discovered that the stability of the nanoparticles in the presence of gelatin was optimized after 4 days. UV-vis analysis of the particles after functionalization with gelatin did not yield the expected shift of the in-plane dipole resonance associated with the change in the dielectric constant surrounding the particles and TEM analysis confirmed that the nanoparticles were not situated in a network of gelatin. However, a change in the zeta-potential of the particles after functionalization together with the enhanced stability of the particles towards NaCl confirmed that the gelatin had altered the surface chemistry of the nanoparticles.

Finally the LbL technique was carried out with the gelatin stabilized nanoparticles, and while etching was not observed in the presence of NaCl, it was observed upon addition of nitrate modified PAH, suggesting that the polymer itself can act as an etchant. Upon completion of the adsorption of 1 pair of layers (consisting of 1 layer of modified PAH and 1 layer of PSSS) it was noted that the zeta-potential of the nanoparticles had changed from negative (in the presence of gelatin) to positive (in the presence of modified PAH) to negative (in the presence of PSSS), indicating successful functionalization. However the yield of recovered particles at this stage in the process was so low that it was decided to discontinue any further attempts at further functionalization by this method.

The role of inorganic species in the control of nanoparticles has previously been reported, largely by the Xia group, for the control of particle morphology in the polyol process. As already highlighted in Chapter 1 they have reported that the Cl^-/O_2 pair can oxidatively etch twinned seed nanoparticles. By tuning the extent of this oxidative etching the morphology of the resulting nanoparticle can be tuned.[30, 31] So although the effect of chloride ions in the shape control of nanoparticles in the *seed-mediated growth* of silver nanoparticles has been investigated, up until recently the effect post-production had not been studied.

It has been proposed that the evolution from triangular plates to discs can reduce the total surface free energy through an atomic migration mechanism as the surface energy of different crystal faces for the fcc structure is : {111}<{100}<{110}.[32, 33] As already mentioned in Chapter 2, Mulvaney *et al.* investigated the dissolution of small spherical silver nanoparticles (~5 nm) in the presence of nucleophiles such as chloride, cyanide and thiolate ions.[34, 35] This process is proposed to be initiated by the adsorption of a nucleophile (N) onto the surface of the silver nanoparticle. Because of this donation of electron density to the nanoparticle, the Fermi level is raised. This creates a situation were it is energetically favourable for an oxidising agent such as the O_2 dissolved in water to convert the Ag(0) to Ag^+. A surface layer of δ^+Ag----Nδ^- is formed which eventually leaves the surface as AgN (for a schematic of this process see Figure 2.37.)

It is proposed here that the vertices of the triangular plates are stabilized less than the flat surfaces. As shown already in Chapter 2, these flat surfaces are comprised

of the {111} surface, which has the lowest surface energy. To date there is no consistent identity of the crystal faces at the edges of the nanoprisms within the literature but it is thought that they mainly consist of the higher energy {100} and {110} surfaces. It has been suggested that the difference of surface energy between the flat {111} faces and the {100} and {110} edge faces that leads to the transformation from triangular nanoplate to disc. Exposed silver atoms on these higher energy surfaces, can be easily attacked by the nucleophile, in this case halide ions.

But what happens then? What is the nature of the dissociated species? There are three possibilities.

1) Ag atoms aggregate to form small clusters
2) Ag atoms migrate onto the {111} surfaces thus increasing the thickness of the plates
3) They are oxidized and stay in solution as AgX.

Let us consider each one of these in turn.

The nanoparticles used in this section were prepared by the added citrate method from seeds prepared in the presence of PSSS. As shown in Chapter 2, the presence of spherical particles is greatly reduced in comparison to the standard added citrate preparation. Therefore, the surface plasmon resonance at 400 nm is also greatly reduced. This synthetic method was chosen intentionally, as if spherical nanoparticles were produced by the etching process, an increase of this band ~400 nm would be expected. As shown in Figure 3.25 above, as the in-plane dipole resonance blue-shifts rapidly in the presence of halide ions, a concommital increase in the band ~400 nm is not observed. Small silver nanoparticles are not observed under TEM analysis either so for these reasons, the aggregation of this displaced silver atoms into clusters is discounted.

A recent paper by An *et al.* has described the sculpting effect of chloride ions on silver nanoprisms that were prepared by a photochemical method.[36] They propose that the chloride ions can coordinate with the active silver atoms on the vertices and abstract them from the nanoprism. These silver atoms then aggregate to form silver clusters which are possibly stabilized by the Cl ions. Some of these Cl^- coated clusters might diffuse to and adsorb on the {111} surface of the nanoplates, thus increasing the

thickness of the disks. XPS measurements indicate that a trace of Cl is present on the {111} surface of the nanodisks. In the system discussed above in Section 3.2, when TEM analysis was carried out a decrease in the average size of the particles from 52±8 nm to 30±6 nm was observed after exposure to the salt solution. However, little or no increase in thickness was observed. Further exhaustive TEM studies need to be carried out to confirm this.

The third possibility involves the formation of AgX. In keeping with this mechanism, described by Mulvaney *et al.*[34, 35] the presence of AgCl precipitate should be observed. This is the case when the concentration of chloride ion is raised to over 100 mM. So how can the trend of etching associated with the different halide ions be explained? It is proposed here that it is simply dependent on the size of the ion. As you go down the group in the periodic table the size of the ion increases. Since smaller anions can get closer to the surface, they give rise to larger polarization of the metal and hence increased etching at the same concentrations is observed.

The trend observed above in Section 3.2 is opposite to that observed by Jiang and Yu in a recent paper, demonstrating the use of silver nanoplates as simple anion sensors.[37] In this report, although a blue-shift of the in-plane dipole resonance of the silver nanoplates was observed upon addition of the anions there was no shape change associated with the process. Instead, the blue-shift was attributed to surface electron charging of the particles. Similar to the case described above in Section 3.2, the authors report that the silver nanoplates were highly sensitive to the presence of chloride, bromide, iodide, phosphate and thiocyanate ions but not to the presence of fluoride, nitrate, perchlorate, acetate and sulphate ions. This phenomenon was explained in terms of the solubility product (K_{sp}) of the resultant AgX compound; the smaller the K_{sp}, the stronger the interaction tendency between the silver surface atoms and the injected ions. It must be noted that the nanoplates were prepared by a pseudo-seed-mediated synthesis in the presence of sodium bis(2-ethylhexyl) sulfosuccinate (NaAOT) and it had previously been reported that the undergo a morphological evolution from triangular plates to circular disks over time.[33] It therefore seems unlikely that the blue-shifting of the in-plane dipole resonance (by as much as 200 nm) is solely associated with surface electron charging of the particles.

The next aspect that needs to be discussed is the apparent stabilization afforded to the silver nanoplates by gelatin. Gelatin is a well-known, widely used stabilizer in the area of colloid chemistry. It is prepared by the hydrolysis of collagen which is made up of three polypeptide strands, each possessing the conformation of a left-handed helix. These three left-handed helices are twisted together into a right-handed coiled coil, a triple helix or "super helix", a cooperative quaternary structure stabilized by numerous hydrogen bonds. When it is partially hydrolysed, the triple helix is destroyed into globular, random coils producing gelatin. The fact that stability of the nanoparticles is increased upon aging in the presence of gelatin would indicate that it is not the gelatin that is interacting with the surface but actually its degradation product(s), as gelatin can be further hydrolysed to form collagen hydrolysate. As the above experiments were not carried out in proteinase free environment it is possible that this further degradation is occurring. SDS-PAGE analysis of the supernatant would confirm this. The fact that the stabilized nanoparticles still exhibit a negative zeta-potential can be explained by looking at the isoelectric points of gelatin and collagen hydrolysate which are 4.9 and 4.6 respectively. The pH of the sol prepared by the added citrate method from seeds prepared in the presence of PSSS is 5.5 so at this pH both gelatin and collagen hydrolysate carry a net negative charge.

Finally, the LbL coating procedure using the gelatin stabilized nanoparticles met with limited success. Although zeta-potential measurements indicate that successful functionalization had occurred, the yield of recovered particles was considered too low for the process to be continued. It is possible that the molecular weight of the polymers used was too small and as such the chain length was too small to ensure that complete encapsulation of the nanoparticles had occurred. It would also be advantageous to include a certain amount of salt with the polymers to ensure that they were in their extended conformation but for obvious reasons this was omitted. Although Au nanorods have been successfully functionalized by the LbL approach, to the best of my knowledge no silver nanoparticles shaped or otherwise have been used. Perhaps this is an indication of how sensitive this procedure is. It must also be noted that the LbL functionalization has only been carried out by a select number of research groups, also highlighting the sensitivity of this method. If it could be optimized, it would provide an ideal platform for investigating the phenomenon of surface or metal enhanced fluorescence as the distance of the fluorophore is placed from the surface of the

nanoparticle could be tuned to within 1 -2 nm, the reported thickness of the polyelectrolyte layers. Also as it is reported that polyelectrolytes can be labeled with fluorophores easily[28], it would lead to easy incorporation of the fluorophore into the shell.

3.3 General Conclusions on the Functionalization and Stability of Silver Nanoparticles:

The functionalization of silver nanoparticles prepared by the added citrate method (and variations there of) and the stability of these particles before and after functionalization were discussed in this chapter.

- Various routes for the synthesis of silica coated silver nanoparticles were attempted with two new methods for the production of coated particles being developed, albeit with limited reproducibility. Both new methods consisted of a modified Stöber growth procedure. The first consisted of priming the surface of the silver nanoparticles with 3-mercaptopropyltriethoxysilane while the second involved priming the surface with 1,3-diaminopropane. Different parameters in this second synthesis were investigated.
- The stability of the silver nanoparticles toward various anions was tested with the following results:

Stable	*Unstable*
Sulfate	Chloride
Acetate	Bromide
Carbonate	Iodide
Hydroxide	Phosphate
Nitrate	
Nitrite	

- The stability of nanoparticles was enhanced by redispersion in gelatin solution and aging over a four day period. The modification of the surface chemistry in the presence of gelatin was confirmed by zeta-potential measurements and stability tests with NaCl.
- The layer by layer approach was attempted, in order to functionalize the silver nanoparticles with polyelectrolytes of alternating charge.

In Chapter 4, Surface Enhanced Raman Spectroscopy (SERS) applications of the nanoparticles prepared by the methods discussed in Chapter 2 will be presented.

3.4 References:

1. F. Caruso, *Adv. Mater.*, 2001, **13**, 11-22.
2. L. M. Liz-Marzan, M. Giersig and P. Mulvaney, *Langmuir*, 1996, **12**, 4329-4335.
3. T. Ung, L. M. Liz-Marzan and P. Mulvaney, *Langmuir*, 1998, **14**, 3740-3748.
4. P. Mulvaney, L. M. Liz-Marzan, M. Giersig and T. Ung, *J. Mater. Chem.*, 2000, **10**, 1259-1270.
5. C. Graf, D. L. J. Vossen, A. Imhof and A. van Blaaderen, *Langmuir*, 2003, **19**, 6693-6700.
6. K. P. Velikov, G. E. Zegers and A. van Blaaderen, *Langmuir*, 2003, **19**, 1384-1389.
7. V. V. Hardikar and E. Matijevic, *J. Colloid Interface Sci.*, 2000, **221**, 133-136.
8. Y. Yin, Y. Lu, Y. Sun and Y. Xia, *Nano Lett*, 2002, **2**, 427-430.
9. E. Mine, A. Yamada, Y. Kobayashi, M. Konno and L. M. Liz-Marzan, *J. Colloid Interface Sci.*, 2003, **264**, 385-390.
10. D. D. Evanoff, R. L. White and G. Chumanov, *J. Phys. Chem. B*, 2004, **108**, 1522-1524.
11. Y. Kobayashi, H. Katakami, E. Mine, D. Nagao, M. Konno and L. M. Liz-Marzan, *J. Colloid Interface Sci.*, 2005, **283**, 392-396.
12. N. R. Jana, *Small*, 2005, **1**, 875-882.
13. K. Aslan, M. Wu, J. R. Lakowicz and C. D. Geddes, *J. Am. Chem. Soc.*, 2007, **129**, 1524-1525.
14. T. Li, J. Moon, A. A. Morrone, J. J. Mecholsky, D. R. Talham and J. H. Adair, *Langmuir*, 1999, **15**, 4328-4334.
15. M. Darbandi, R. Thomann and T. Nann, *Chem. Mater.*, 2005, **17**, 5720–5725.
16. Y. Han, J. Jiang, S. S. Lee and J. Y. Ying, *Langmuir*, 2008, **24**, 5842-5848.
17. N. R. Jana, C. Earhart and J. Y. Ying, *Chem. Mater.*, 2007, **19**, 5074-5082.
18. W. Stöber, A. Fink and E. Bohn, *J. Colloid Interface Sci.*, 1968, **26**, 62-69.
19. C. J. Brinker and G. W. Scherer, in *Sol-Gel Science: The Physics and Chemistry of Sol-Gel Processing,* Academic Press, Inc.: New York, 1990, pp. 97-234.

20. Y. Yin, Y. Lu, Y. Sun and Y. Xia, *Nano Lett.*, 2002, **2**, 427-430.
21. Y. Kobayashi, K. Misawa, M. Takeda, M. Kobayashi, M. Satake, Y. Kawazoe, N. Ohuchi, A. Kasuya and M. Konno, *Colloid Surface A*, 2004, **251**, 197-201.
22. S. E. Hunyadi and C. J. Murphy, *J. Phys. Chem. B*, 2006, **110**, 7226-7231.
23. G. Hu, Z. Feng, J. Li, G. Jia, D. Han, Z. Liu and C. Li, *J. Phys. Chem. C*, 2007, **111**, 11267-11274.
24. C. Xue, X. Chen, S. J. Hurst and C. A. Mirkin, *Adv. Mater.*, 2007, **19**, 4071-4074.
25. D. I. Gittins and F. Caruso, *Adv. Mater.*, 2000, **12**, 1947-1949.
26. D. I. Gittins and F. Caruso, *J. Phys. Chem. B*, 2001, **105**, 6846-6852.
27. G. Schneider and G. Decher, *Nano Lett.*, 2004, **4**, 1833-1839.
28. G. Schneider, G. Decher, N. Nerambourg, R. Praho, M. H. V. Werts and M. Blanchard-Desce, *Nano Lett.*, 2006, **6**, 530-536.
29. A. Dorris, S. Rucareanu, L. Reven, C. J. Barrett and R. B. Lennox, *Langmuir*, 2008, **24**, 2532-2538.
30. B. J. Wiley, S. H. Im, Z. Y. Li, J. McLellan, A. Siekkinen and Y. A. Xia, *J. Phys. Chem. B*, 2006, **110**, 15666-15675.
31. B. Wiley, Y. Sun and Y. Xia, *Acc. Chem. Res.*, 2007, **40**, 1067-1076.
32. X. Jiang, Q. Zeng and A. Yu, *Nanotech.*, 2006, **17**, 4929-4935.
33. X. C. Jiang, Q. H. Zeng and A. B. Yu, *Langmuir*, 2007, **23**, 2218-2223.
34. P. Mulvaney, T. Linnert and A. Henglein, *J. Phys. Chem.*, 1991, **95**, 7843-7846.
35. T. Linnert, P. Mulvaney and A. Henglein, *J. Phys. Chem.*, 1993, **97**, 679-682.
36. J. An, B. Tang, X. Zheng, J. Zhou, F. Dong, S. Xu, Y. Wang, B. Zhao and W. Xu, *J. Phys. Chem. C*, 2008, **112**, 15176-15182.
37. X. C. Jiang and A. B. Yu, *Langmuir*, 2008, **24**, 4300-4309.

Chapter 4:
Surface Enhanced Raman Scattering

4.1 Introduction to Surface Enhanced Raman Spectroscopy

Raman spectroscopy is concerned with the study of molecular vibrations. When radiation of a particular frequency falls on a molecule, some radiation is scattered. This can occur in two ways

1) Elastic scattering or Rayleigh scattering involves radiation of the same frequency as that of the incident light being scattered.

2) Inelastic scattering or Raman scattering involves radiation of frequencies $\nu_0 \pm \nu$ where ν is a fundamental frequency of a vibrational mode of the molecule. If the transfer of energy in the virtual state is from the photon to the molecule, the scattered photon will be lower in energy than that of the incident photon and is referred to as Stokes Raman scattering. Conversely, if the transfer of energy is from the molecule to the photon, the scattered photon is higher in energy than the incident photon and is referred to as anti-Stokes Raman scattering. Most observed Raman peaks result from Stokes scattering. Anti-Stokes peaks have the same wavenumber shift as Stokes but as they involve energy transfer from a molecule already in a vibrational excited state are much rarer. A schematic of these processes is shown below in Figure 4.1.

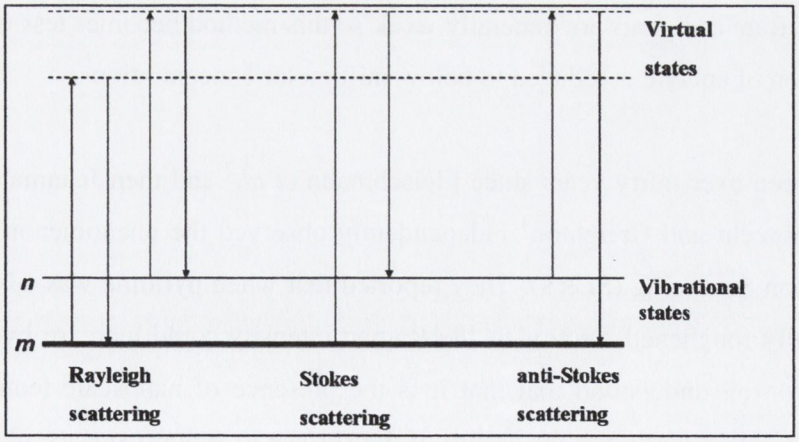


Figure 4.1: Schematic of the scattering processes. Adapted from reference [1].

The Raman effect is a relatively weak one. Light that is not absorbed by the molecule of interest is only weakly inelastically scattered off the vibration in the molecule. As is the case in IR spectroscopy, Raman spectroscopy is governed by a fundamental selection rule. It states that the polarizability of the molecule must change during the course of the vibration. (The fundamental selection rule for infrared spectroscopy is that the dipole moment of the molecule must change during the vibration.)

The distortion of a molecule in an electric field is determined by its polarizability. When a molecule is placed in an electric field, it acquires an induced dipole moment of magnitude

$$\mu = \alpha E \qquad \textbf{Equation 4.1}$$

in addition to any permanent dipole moment it may have. If the same distortion is induced whatever the direction of the applied field, then the molecule is anisotropically polarisable and is therefore Raman active.

The resulting Raman spectrum is very informative as it provides a good vibrational fingerprint of the molecule. Also one major advantage that it has over the more commonly used infrared spectroscopy is that the O-H bond is only weakly Raman active so spectra can be recorded in aqueous solution with less interference from water. However as stated above the intensity of Raman signals are generally weak so this method becomes less useful when the concentration of analyte is reduced to below millimolar concentrations.

It has been over thirty years since Fleischmann *et al.*[2] and then Jeanmaire and Van Duyne[3] and Albrecht and Creighton[4] independently observed the phenomenon of Surface Enhanced Raman Scattering (SERS). They reported that when pyridine was adsorbed onto electrochemically roughened electrodes, the Raman intensity could increase by a factor of $\sim 10^6$. It is now well understood that that it is the presence of nanoscale features on the metallic surface and in particular the ability of the surface to support surface plasmons that is responsible for this SERS effect. However, despite the fact that with the development of this technique high sensitivity could now be coupled with high molecular specificity, SERS

has not become a routinely used analytical tool. The reasons for this are two-fold. Firstly the reproducibility of the technique was poor due to lack of control over the fabrication of suitable SERS substrates and secondly, the high cost of the equipment needed. However, in recent years there has been resurgence in the development of SERS as the cost of optoelectronic equipment has fallen and the development of nanofabrication techniques such that well defined substrates can be produced consistently. The ultimate aim of work in this area is to provide a highly sensitive analytical tool that will be able to compete with the more established techniques.

A measure of the renewed interest in this area is the volume of review articles recently published on this topic. While some of the important aspects of SERS will be discussed below, it is beyond the scope of this chapter to provide an exhaustive review. For further information the reader is directed towards the following references.[5-23]

4.1.1 Factors affecting Surface Enhanced Raman Scattering (SERS)

To begin with it is necessary to explain the mechanism of the enhancement of the Raman spectra of molecules that are in close proximity to the surface of noble metal nanoparticles. The exact nature of this phenomenon is still a topic of great debate in the literature but to date two main explanations have been agreed upon. The first is the electromagnetic (EM) enhancement mechanism while the second is known as the chemical (CHEM) enhancement mechanism. The same selection rules that are associated with Raman scattering apply but additional factors must also be considered.

4.1.1.1 Electromagnetic enhancement mechanism:

The intensity of Raman scattering is directly proportional to the square of the induced dipole which in turn is (as shown above in Equation 4.1) the product of the Raman polarizability and the magnitude of the incident electric field. As a consequence of exciting the localized surface plasmon resonance (LSPR), the local electromagnetic field is enhanced. It has been shown, that for a metal sphere the Raman scattering scale as E^4.

Therefore if the local electric field is enhanced by a factor of 10 by the nanoparticle, the Raman scattering will be enhanced by 10^4.[24]

It is now widely accepted that the presence of 'hot spots' gives rise to enormous enhancement of the electromagnetic field.[13] These 'hot spots' have been attributed to two basic phenomena

1) Lightning rod effect
2) Coupling of SPRs

The lightening rod effect is not associated with surface plasmons. It occurs when the incident electromagnetic field does not penetrate inside the metal nanoparticles that are next to each other. In essence the electric field is compressed or focussed into the gap between nanostructures. As this event is purely dependent on the geometry of the nanoparticles concerned it is no surprise that it has been reported as the key to SERS for nanoparticles such as nanorods. The coupling of SPRs occurs when the SPRs on adjacent nanoparticles interact and hybridise giving rise to extremely intense electromagnetic fields.

The most important aspects of the EM model are

1) Excitation of a SPR of nanoparticles or aggregates of nanoparticles
2) As discussed in Chapter 1, the position of the plasmon resonances are determined by various factors such as size, shape, dielectric properties of the metal and dielectric properties of the medium surrounding the nanoparticles.
3) The E^4 enhancement discussed above has been calculated from theory based on a spherical metal nanoparticle model. However, as also shown in Chapter 1, as the shape of the nanoparticle is changed the number of plasmon resonances is also changed so in practice, multiple plasmon resonances must be considered.

4.1.1.2 Chemical Enhancement Mechanism:

Although it is now widely accepted that the electromagnetic enhancement mechanism is the dominating contributing factor to SERS, the chemical enhancement mechanism must also be considered. There are two methods by which a molecule can interact with a surface. When the energy of interaction is more positive than ~25 $kJmol^{-1}$,

the interaction is classified as physisorption and when the interaction is very negative and comparable to chemical bond energies chemisorption is the term used.[24] It is important to understand which of these two regimes are in action as for physisorbed species the pattern of relative intensities within the observed SERS spectrum may differ from that of the reference molecule as adsorption may induce a fixed molecular orientation. However, when dealing with chemisorbed species a completely different vibrational spectrum might be evident. It is also thought that the presence of the metal nanoparticle aids in charge transfer (CT) interactions between the highest occupied molecular orbital (HOMO) and the lowest unoccupied molecular orbital (LUMO) of the adsorbate.[8]

In general SERS is dependent on a number of factors which need not be considered when dealing with Raman spectroscopy. These include the

- Size of the nanoparticle
- Shape of the nanoparticle
- Dielectric function of the nanoparticle
- Dielectric function of the surrounding medium
- Surface coverage of the analyte
- Adsorption of the target molecule
- Metal-molecule interactions
- Molecular orientation of the analyte
- Polarization effects

However two generic factors should always be optimized in any SERS experiment. Firstly, the plasmon resonance of the nanoparticles (usually aggregates) should be in tune with the laser line used for excitation of Raman scattering. And secondly, the adsorption of the target molecule on the surface must be maximised. The aim of the work reported in the following section was to investigate in detail, the dependence of the Raman enhancement of the position of the main absorption of the nanoparticle substrate with fixed laser excitation.

4.2 Results

4.2.1 Preliminary results using 'added citrate' nanoparticles

All of the SERS experiments described in this section were carried out in Dr. Steven Bell's laboratory, in the School of Chemistry and Chemical Engineering, Queen's University Belfast. Initial experiments were carried out to investigate the presence of trisodium citrate on the surface of the nanoparticles prepared by the 'added citrate' method, described in Chapter 2. A green sol was prepared using 0.7 mM TSC at room temperature. The UV-vis spectrum is shown below in Figure 4.2.

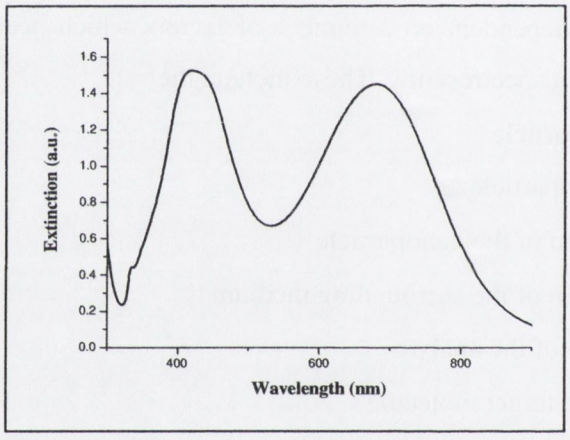


Figure 4.2: UV-vis spectrum of a green sol prepared by the 'added citrate' method using 0.7 mM TSC at room temperature.

The Raman spectra were collected on a home built spectrometer using a *532 nm laser source*. The spectrometer was calibrated using the standard Raman band positions of acetonitrile. The samples were held in microtitre plates and the results come from 30 accumulations. 200 μL sol was placed in the well however no Raman signals were observed. The sol was then aggregated using magnesium chloride (50 μL, 0.1 M). An aliquot of the sol was also centrifuged at 4,000 rpm, the coloured supernatant removed and the pellets redispersed in distilled water. Again no Raman signals were detected before aggregation. The results of this experiment are shown below in Figure 4.3. It must be noted that the maximum concentration of TSC is 0.7 mM.

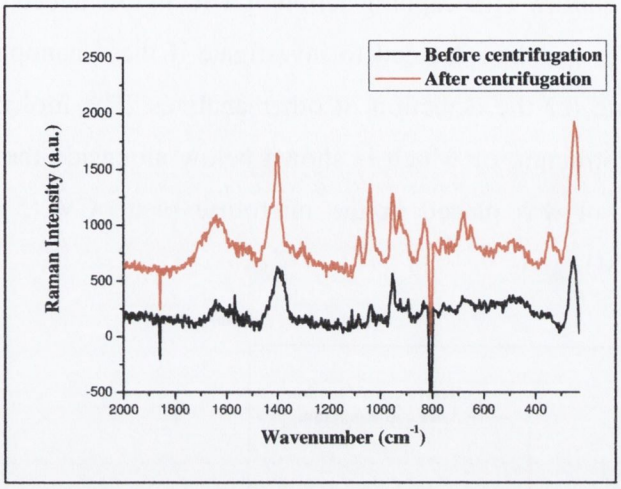


Figure 4.3: SERS spectra of the green added citrate sol shown above in Figure 4.2, after aggregation with $MgCl_2$ before (black) and after (red) centrifugation.

The peaks shown below in Table 4.1 were attributed to the presence of TSC.[25, 26] Another point to be noted is that there were no signals associated with the poly(vinylpyrrolidone) (PVP) present. After centrifugation, the intensity of the SERS signals increased, despite the fact that pellets were small and the majority of nanoparticles remained in the supernatant. This is consistent with the idea that the PVP is not adsorbed onto the nanoparticle, but acts only to prevent the aggregation of the nanoparticles. When some of the PVP is removed by centrifugation, the particles present are more easily aggregated by the same concentration of $MgCl_2$, giving rise to a more enhanced SERS spectrum.

Frequency (cm^{-1})	*Assignment*
1401	ν_s (COO)
1303	
1085	
1040	
953	ν (C-COO)
922	ν (C-COO)
830	ν_s (CCCC-O)
681	δ (COO)
650	
345	
247	Ag-Cl

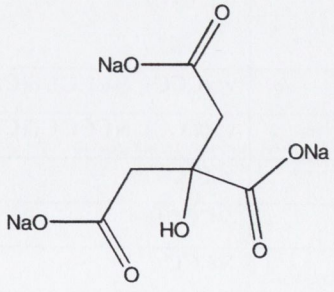


Table 4.1: Assignment of the Raman signals observed in Figure 4.3, from a green added citrate sol prepared at room temperature using 0.7 mM TSC.

The above result confirms the capping action of TSC in the 'added citrate' synthesis of silver nanoparticles. It was then decided to investigate if these nanoparticles could be used as a SERS substrate for the detection of other analytes. The molecule chosen was crystal violet (CV), the structure of which is shown below alongside the resulting SERS spectra. Again 200 μL sol was placed in the microtitre plate. CV (5 μM) was added followed by $MgCl_2$ (0.1 M).

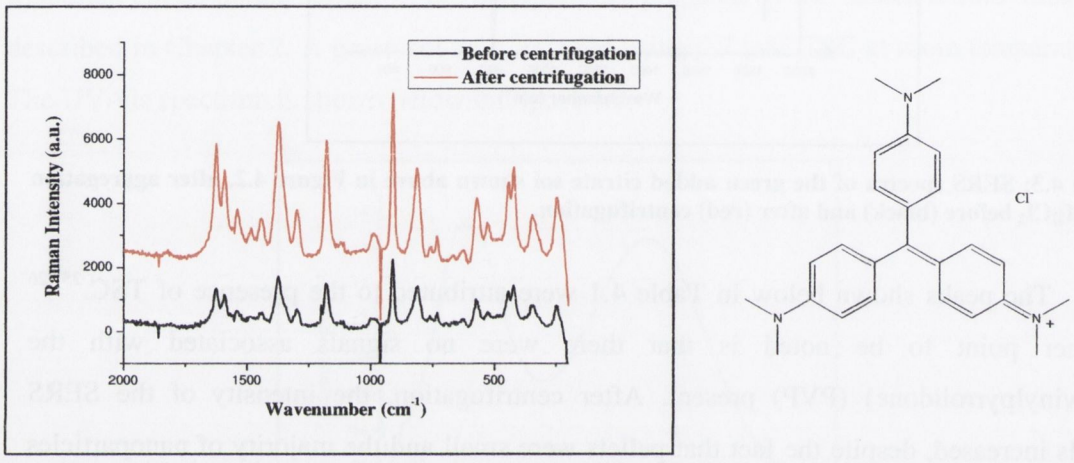


Figure 4.4: SERS spectra of crystal violet (5 μM) using nanoparticles before (black) and after (red) centrifugation. Also shown is the structure of crystal violet.

Position of band (cm^{-1})	*Assignment*	*Position of band (cm^{-1})*	*Assignment*
1627	-	813	
1593	-	761	ν_s(CCC), ν(CN)
1541	ν(CN), δ_s (CH_3)	731	ν(CN)
1483	δ_{as} (CH_3)	626	
1445	δ_{as} (CH_3)	573	γ(CCC), δ(CNC), δ(CCC)
1376	ν_{as}(CCC), δ(CCC), δ(CH)	531	δ(CNC)
1300	ν_{as}(CCC), δ(CCC), δ(CH)	443	δ(CNC)
1182	ν_{as}(CCC)	423	δ(CNC), δ(CCC),
990	δ(CCC)	348	γ(CNC)
912	δ(CCC),		

Table 4.2: Assignments of SERS signals of crystal violet from ref[20] δ= bending, ν=stretching γ = out-of-plane deformation.

Similar to the case described above with TSC, when the PVP was removed by centrifugation, the intensity of the SERS signals increased, even though there is a lower concentration of nanoparticles present. In this case, the laser excitation wavelength overlaps with an electronic absorption band of the dye. (CV λ_{max}= 590nm). The intensities of the Raman scattering of the vibrational modes of the CV are enhanced so Surface Enhanced Resonance Raman scattering (SERRS) is observed.

In summary these preliminary experiments

1) confirmed the presence of TSC on the surface of the nanoparticles prepared by the added citrate method.
2) demonstrated the ability of silver nanoparticles prepared by this method, once aggregated, to act as useful SERS substrates.

4.2.2 Detailed study using 'no added citrate' nanoparticles

4.2.2.1 Part 1: Nanoprisms with λ_{max} between 485-615 nm

Based on the positive results achieved during the preliminary studies it was decided to carry out an extended study. At the time when this was considered, the third method described in Chapter 2, the 'no added citrate' method had been well developed such that monodisperse, well-defined silver nanoprisms of varying edge length could be routinely produced. Another advantage associated with particles prepared by this method is that there is no polymer present to prevent the adsorption of the analyte onto the nanoparticle surface. The Raman spectrometer used in the series of experiments described below was also different. The SERS spectra were recorded on an Avalon Instruments RamanStation with an excitation wavelength of 785 nm. The laser power was 100 mW and the resolution of the Raman instrument was 4 cm^{-1}. An exposure time of 10 s was used with two exposures to record each spectrum. All experiments were carried out in a 96 well polypropylene microtitre plate. The final volume in each of the wells was 300 µL, consisting of 200 µL sol + 50 µL analyte + $MgSO_4$ (1 M, 50 µL).

Sols were prepared as follows. In a typical experiment, silver seeds are produced by combining aqueous trisodium citrate, aqueous poly(sodium styrenesulphonate) and aqueous $NaBH_4$ followed by addition of aqueous $AgNO_3$ while stirring vigorously. The nanoprisms were produced by combining 5 mL distilled water, aqueous ascorbic acid and various quantities of seed solution, followed by addition of aqueous $AgNO_3$. After synthesis, aqueous trisodium citrate is added to stabilize the particles. The detailed synthesis is given in Chapter 5.

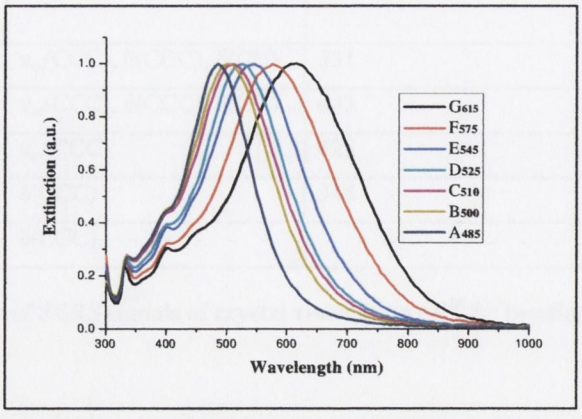


Figure 4.5: Sols prepared by the 'no added citrate' method using, from A-G, 1 mL, 800 µL, 750 µL, 600 µL, 500 µL, 400 µL and 250 µL seeds.

4.2.2.1.1 Crystal Violet

Some initial experiments were carried out using crystal violet (5 μM) as the analyte. Each well contained sol (200 μL), $MgSO_4$ (0.1 M) followed by CV (5 μM)

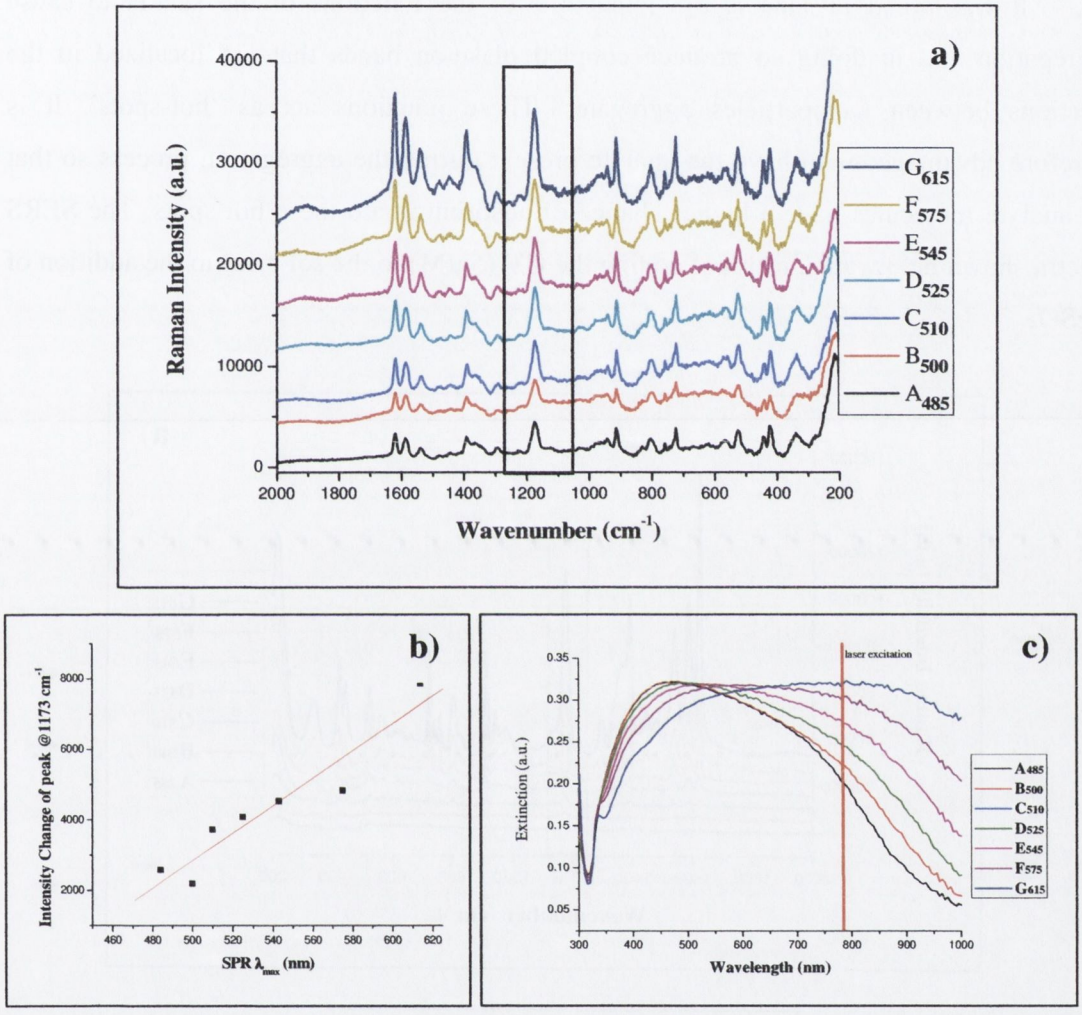


Figure 4.6: a) SERS spectra of crystal violet added to each of the sols shown above in Figure 4.5, after aggregation with $MgSO_4$ b) a plot of the change in intensity of 1173cm^{-1} peak against the initial SPR λ_{max} of each sol c) UV-vis spectra of each of the sols shown above in Figure 4.5 after aggregation with $MgSO_4$.

From Figure 4.6 above it is clear to see that the intensity of the SERS spectrum is dependent on the sol used. As the SPR λ_{max} moves more into the red, the intensity of the SERS spectrum increases. Also from Figure 4.6c above (UV-vis spectra of the aggregated sols) it can be noted that as the λ_{max} of the aggregates becomes more red-shifted, and as a

consequence the absorbance of the sol at 785nm increases, the SERS spectrum is further enhanced.

It was noted in Jana *et al.*[27], that one of the functions of the salt is to cause aggregation and in doing so produce coupled plasmon bands that are localized in the junctions between nanoparticles aggregates. These junctions act as 'hot-spots'. It is therefore advantageous to have the analyte present during the aggregation process so that the analyte molecules have a higher chance of adsorbing onto these hot-spots. The SERS spectra shown below are a result of adding the CV (5 μM) to the sol prior to the addition of $MgSO_4$.

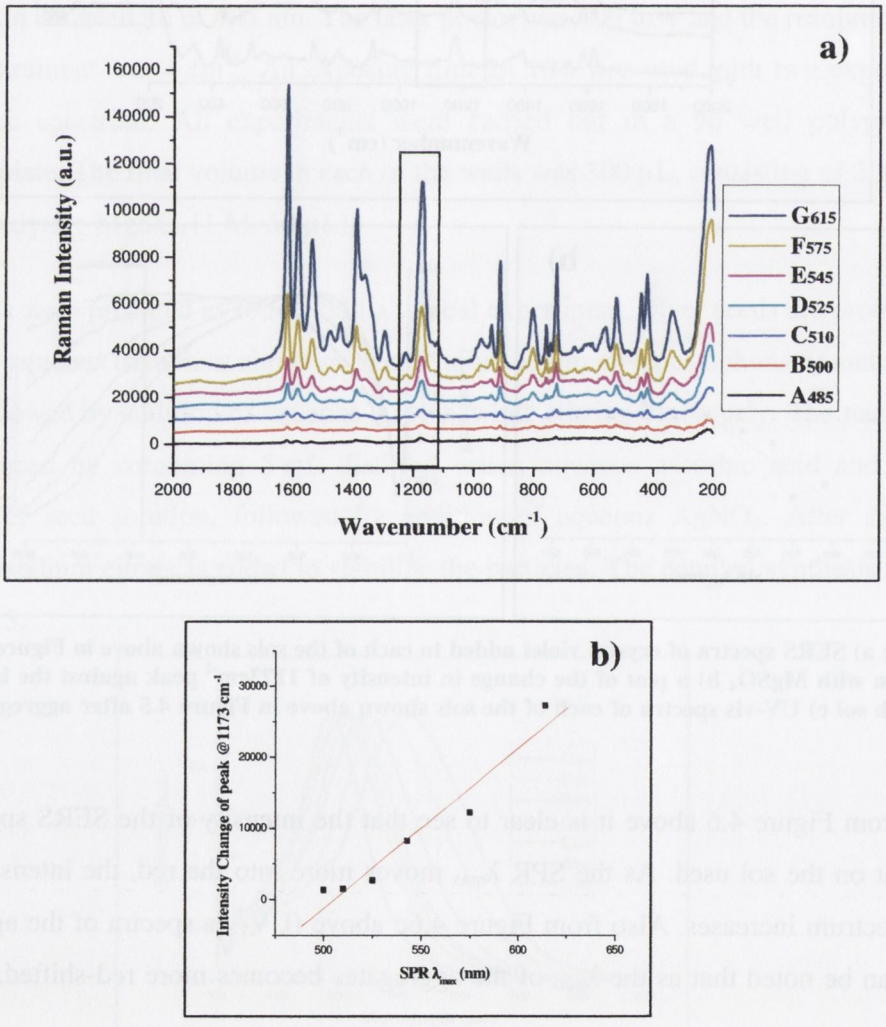


Figure 4.7: SERS spectra of CV added before aggregation and plot of the change in intensity of 1173cm^{-1} peak against the initial SPR λmax.

As can been seen from the above result the intensity of the SERS bands increased when the analyte was present prior to aggregation. To quantify the importance of adding the analyte before aggregation, a direct comparison was carried out between the SERS intensities in Figure 4.6 and Figure 4.7. The results confirm that the intensity of the SERS signal is increased by 66±10 % if the analyte is present during the aggregation process.

To summarize the above results, SERS spectra were obtained using crystal violet (5 μM) as an analyte and silver nanoprisms of varying edge length as substrates. The intensity of the SERS signal was dependent on the wavelength, $\lambda_{max,}$ of the nanoprisms. As the aggregated sols start absorbing further into the red, the resulting Raman intensities are enhanced. It is important to include the analyte before aggregation, as this increases the likelihood of the analyte adsorbing onto the hot spots created during aggregation.

Crystal violet is quite a common SERS analyte. It is positively charged and will easily stick to the negatively charged (zeta potential -39±5 mV) silver nanoprisms. It was decided to investigate other analytes to determine the suitability of these nanoprisms as a universal SERS substrate. The molecules chosen were 4-mercaptopyridine, again another common SERS analyte from the literature and adenine and adenosine, important biological molecules.

4.2.2.1.2 4-Mercaptopyridine

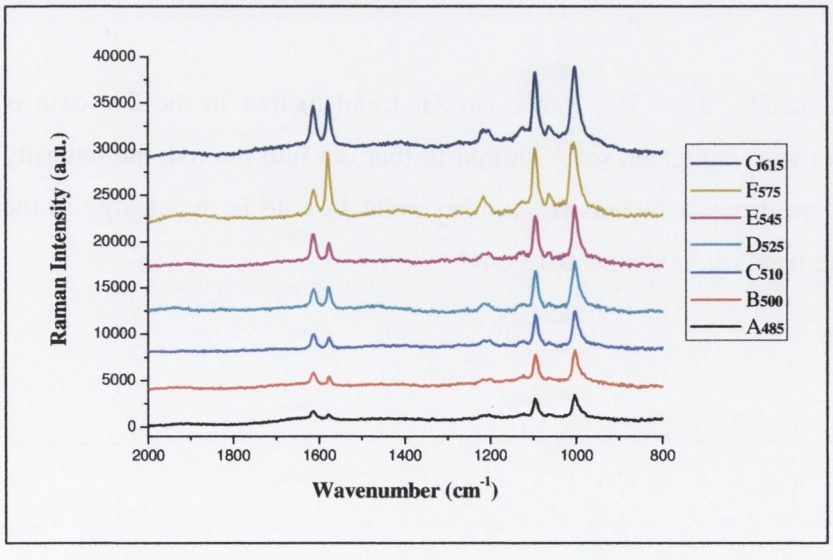


Figure 4.8: SERS spectra of 4-mercaptopyridine (30 μM) using sols from Figure 4.5 as substrates.

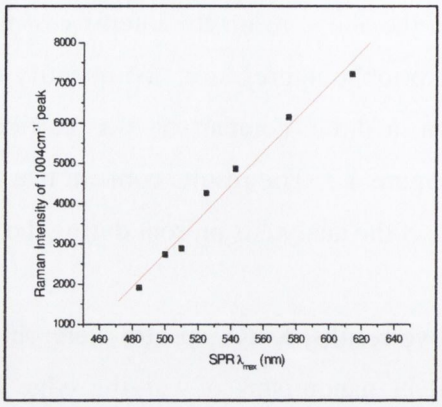


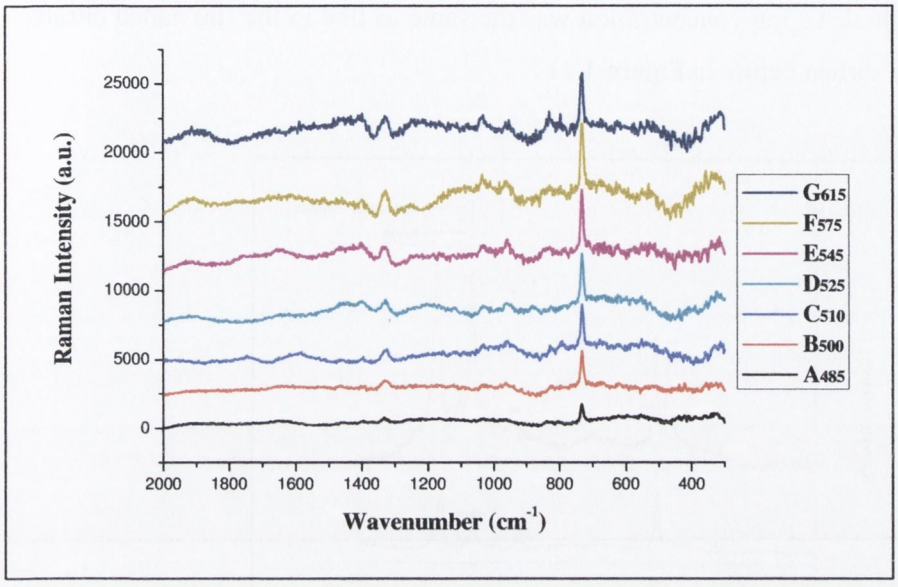
Figure 4.9: Plot of the Raman intensity of the 1004 cm^{-1} band of 4-mercaptopyridine in Figure 4.8 against SPR λ_{max}.

Position of band (cm^{-1})	*Assignment*
1003	ν(C-C)$_{ring}$
1065	δ(C-H)
1096	ν(C-C)$_{ring}$, C-S
1217	δ(C-H), δ(N-H)
1580	ν(C-C)$_{ring}$
1615	ν(C-C)$_{ring}$

Table 4.3: Assignments of SERS signals of 4-mercaptopyridine from refs[28-30] δ= bending, ν=stretching, ring=ring breathing.

From the above results it is clear that a similar trend to that in the CV case is observed. As the λ_{max}, of the aggregated sol is shifted further out into the red, the intensity of the observed SERS spectrum is increased. Another point to note is the change in the relative intensities of the bands at 1580 and 1615 cm^{-1}.

4.2.2.1.3 Adenine



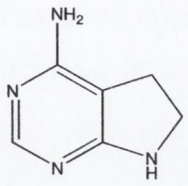


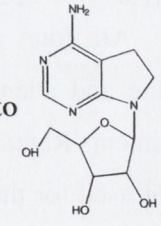
Figure 4.10: SERS spectra of adenine using sols shown above in Figure 4.5 as substrates.

Position of band (cm^{-1})	*Assignment*
734-738	Ring breathing

Again a similar trend to that observed for the previous analytes is observed. However a shift in the position of the ring breathing mode from 734-738 $cm^{-1}$is also observed. This has been previously reported but only when the concentration of the analyte has been varied.[31]

4.2.2.1.4 Adenosine

It was attempted to use adenosine as an analyte in a similar manner to adenine. However no enhanced spectrum was obtained.



4.2.2.1.5 Comparison with Lee and Meisel colloids

One of the standard SERS substrates commonly used is silver colloid prepared by the Lee and Meisel method.[32] This involves the reduction of silver nitrate by a boiling solution of TSC. A batch of Lee and Meisel colloid was prepared by the Bell group and

was tested with 4-mercaptopyridine. So a direct comparison could be made, the sol was diluted so that the initial Ag ion concentration was the same as that in the 'no added citrate sols'. The results are shown below in Figure 4.11.

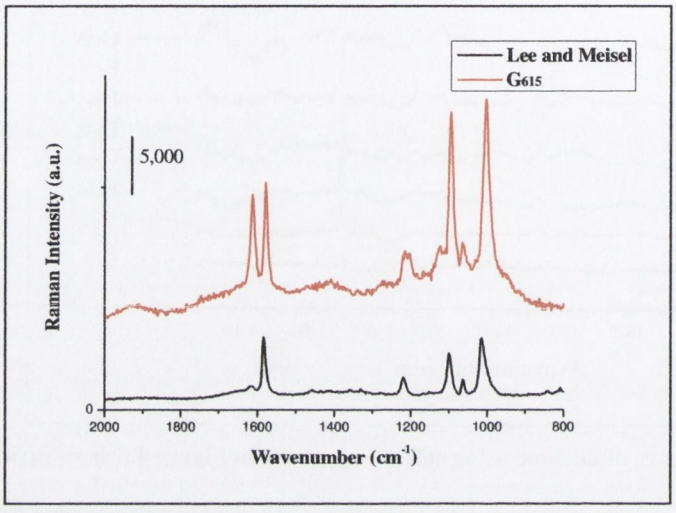


Figure 4.11: SERS spectra of 4-cerpatopyridine (30 μM) using Lee and Meisel colloid (black) and $SolG_{615}$ from Figure 4.5 (red) as the substrates.

It can be seen that nanoprisms prepared by the 'no added citrate' method can act as a good alternative to the Lee and Meisel colloid as the intensity of the peaks observed when $SolG_{615}$ was used as the SERS substrate were up to three times as intense as when standard colloid was used.

4.2.2.1.6 532 nm laser excitation

All four analytes discussed above namely crystal violet, 4-mercaptopyridine, adenine and adenosine were then tested with 532 nm laser excitation using an Avalon Instruments RamanMicro-EZ. Experiments were carried out using the same microtitre plate as that used for the 785 nm excitation experiments. However only signals for crystal violet were observed. In this case, the laser excitation wavelength overlaps with an electronic absorption band of the dye. (CV λ_{max}= 590 nm). The intensities of the Raman scattering of the vibrational modes of the CV are enhanced resulting in Surface Enhanced Resonance Raman scattering (SERRS). This also explains why a SERS spectrum was not observed for the other analytes, as they do not absorb strongly in the visible region.

In general the following points can be drawn from the above experiments.

1) Silver nanoprisms prepared by the 'no added citrate' method can be used as SERS substrates.
2) The intensity of the SERS spectrum is increased (by ~66%) when the analyte is added before the aggregation process, probably due to the increased probability of it adsorbing onto the hot spots as they are formed.
3) As the λ_{max} of the SPR is shifted further into the red (therefore as the λ_{max} of the aggregated sol is shifter further in to the NIR) the enhancement factor increases.
4) The nanoprisms are negatively charged. CV adsorbs electrostatically to the nanoparticles giving rise to the enhanced spectrum. 4-Mercaptopyridine chemisorbs to the nanoparticles through a Ag-S bond giving rise to the enhanced spectrum. Both adenine and adenosine are neutral molecules, with N atoms available for bonding. These do not form as strong a bond with the Ag surface as thiols do and as such give rise to poor SERS signals.

4.2.2.2 Part 2: Nanoprisms with λ_{max} between 510-925 nm

Sols were prepared by the 'no added citrate' method. This time the range of the λ_{max} of the sols prepared was varied from 510-920 nm (see Figure 4.12). The purpose of this was to investigate if the SERS intensities of the analytes could be increased even further by pushing the λ_{max} of the SERS substrate further into the near infrared region of the spectrum.

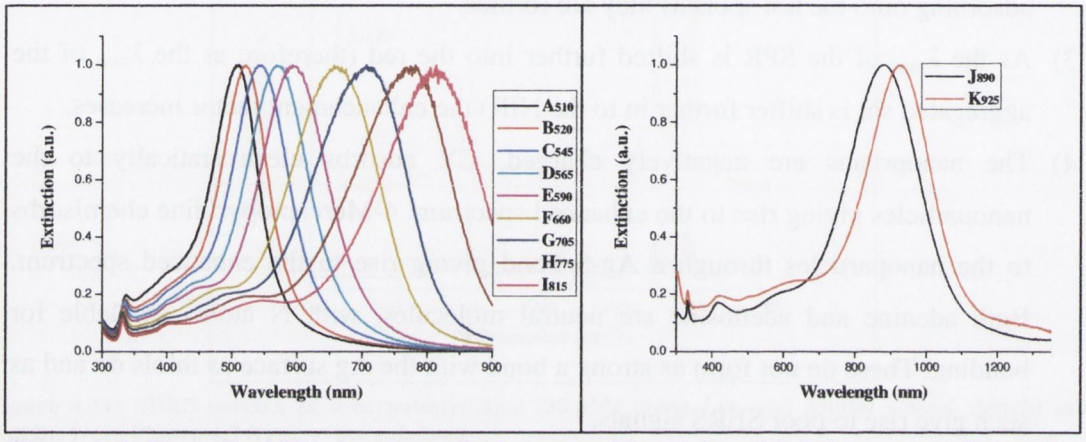


Figure 4.12: Normalized UV-vis spectra of sols prepared by the 'no added citrate method' from A-K with 650 µL, 500 µL, 400 µL, 260 µL, 200 µL, 120 µL, 90 µL, 60 µL, 40 µL, 20 µL, 10 µL seeds.

4.2.2.2.1 Study of the aggregation process

As the aggregation process, is key to the observation of SERS, it was decided to monitor it by both UV-vis spectroscopy and TEM prior to carrying out further SERS experiments. Figure 4.13 below shows the UV-vis spectra of Sols A-H, 10 minutes after aggregation with $MgSO_4$ (0.1 M).

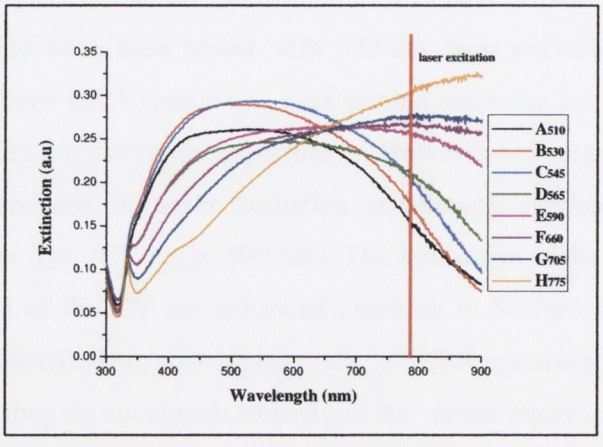


Figure 4.13: UV-vis spectra of sols A-H after aggregation with $MgSO_4$.

TEM images of sols before and after aggregation with 0.1 M $MgSO_4$ are shown below. It must be noted that the images taken of the sols before aggregation are a result of centrifuging 1 mL of sol, removing the supernatant and redispersing the pellet in 100 µL distilled water. The sols after aggregation were not preconcentrated before being dropped on the TEM grid.

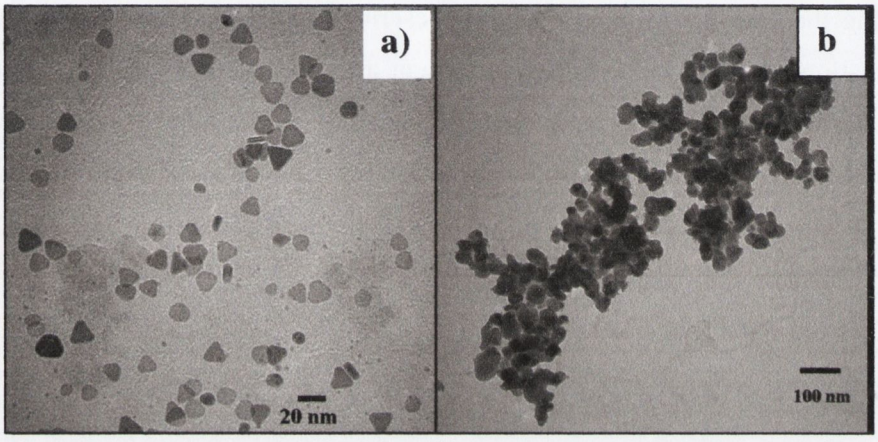


Figure 4.14: TEM images of Sol B520 from Figure 4.12 a) before b) after aggregation with $MgSO_4$ (0.1 M).

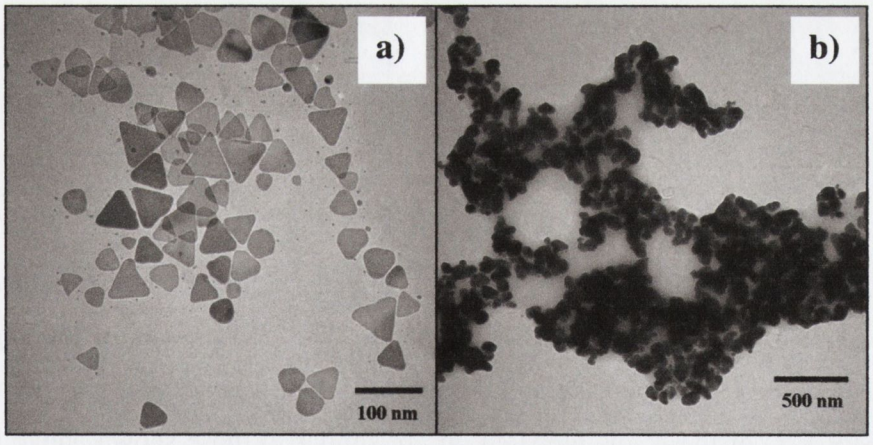


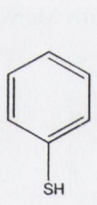
Figure 4.15: TEM images of Sol H775 from Figure 4.12 a) before b) after aggregation with $MgSO_4$ (0.1 M)

One important aspect that needs to be commented on at this stage is that on aggregation of the nanoprisms with $MgSO_4$, the original morphology of the particles was not maintained. As can been seen from the TEM images above in Figure 4.14 and Figure

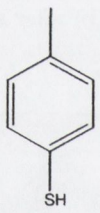
4.15, the nanoprisms have 'melted' and the resulting nanoparticles do not appear to have any specific morphology. This is an important aspect to consider when choosing an aggregating agent, as in this case the SERS substrate after aggregation with $MgSO_4$ does not resemble the initial nanoparticles in any way and thus could negate the advantage of using anisotropically shaped silver nanoparticles over the standard Lee and Meisel colloid.

During the course of the experiments described in this section, it was noted that some aggregation of the nanoparticles was evident after the addition of the analyte alone. For this reason it was decided to monitor the aggregation of the sols by the analytes alone without the addition of $MgSO_4$. The analytes chosen for these series of experiments were

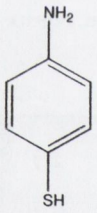
1) thiophenol
2) 4-methylthiophenol
3) 4-aminothiophenol
4) 4-mercaptopyridine



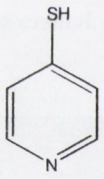
(1)



(2)



(3)



(4)

The TEM data shown below corresponds directly to the original sols shown above in Figure 4.12 and the SERS spectra shown below. The UV-vis data of the aggregation process was recorded at a later date and because of this it was necessary to prepare fresh sols. The SPR λ_{max} of these sols prepared on are similar to those shown above in Figure 4.12.

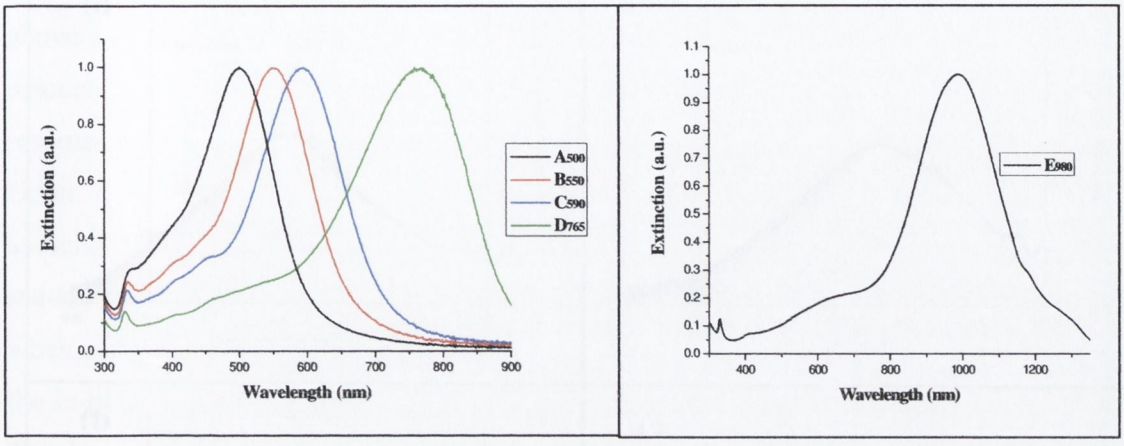


Figure 4.16: Normalized UV-vis spectra of sols prepared by the 'no added citrate' method from A-E with 650 µL, 400 µL, 200 µL, 60 µL and 10 µL seeds.

Effect of the addition of 30 µM 4-aminothiophenol:

The main section of the work in examining the aggregation process of the sols was carried out with 4-aminothiophenol. It will be shown in proceeding paragraphs that this system gave rise to the best SERS spectra. The aggregation of the five sols shown above in Figure 4.16 was examined by UV-vis spectroscopy. 200 µL of the sol to be analyzed was placed in a 1 mm quartz cuvette. The spectrum was recorded. The analyte was then added to the required concentration and the contents of the cuvette were agitated with the pipette. Spectra were then recorded every 30 seconds for 15 minutes. No additional aggregating agent was used. TEM images of the $SolE_{590}$ from Figure 4.12 with each analyte are also shown. It must be noted again that sols were not concentrated prior to dropping on the TEM grid. Analytes caused sufficient aggregation, without causing the nanoparticles to crash out of solution, for analysis by TEM without preconcentrating the sample.

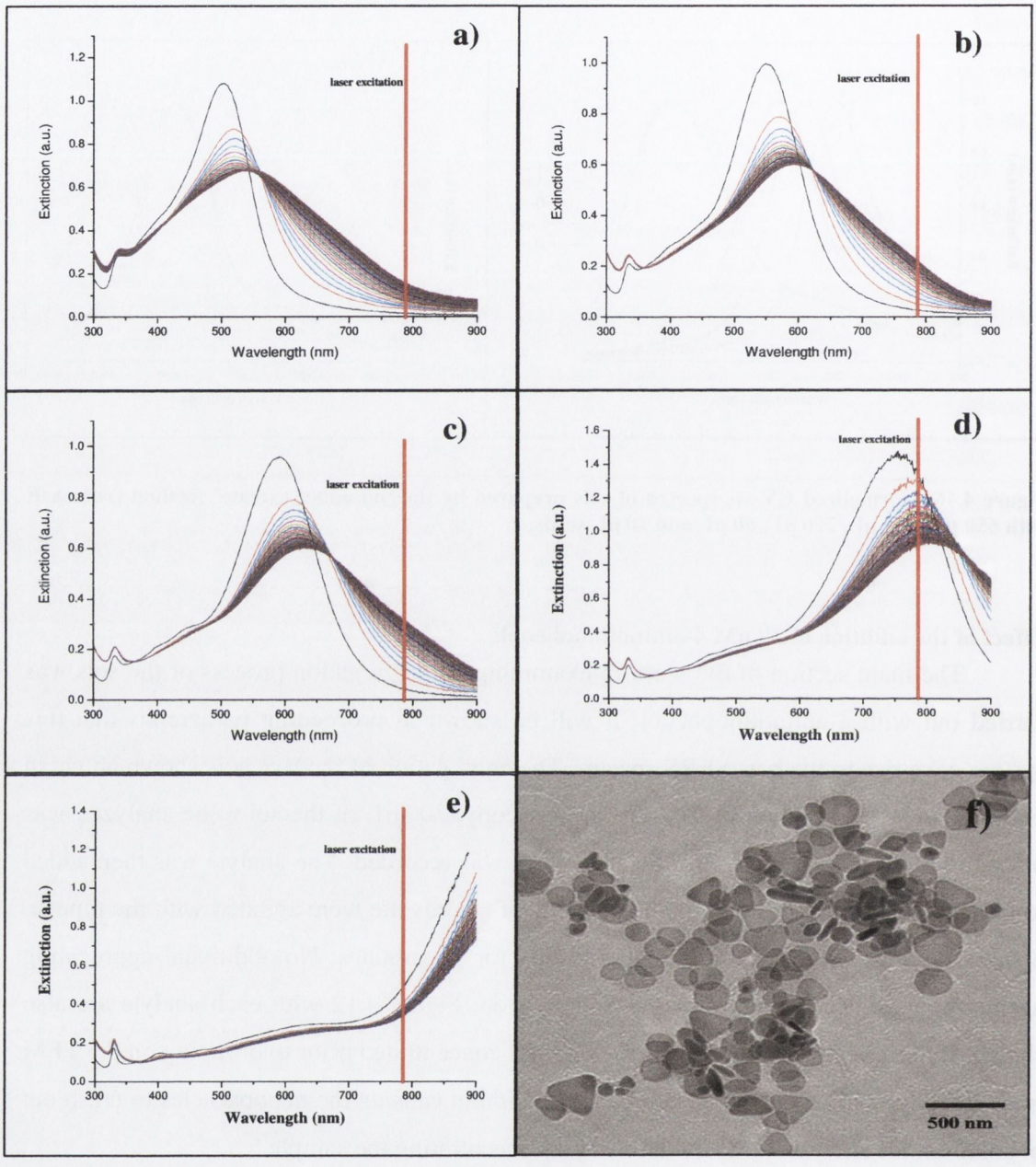


Figure 4.17: UV-vis spectra monitoring the aggregation process of sols in the presence of 4-aminothiophenol (30 μM). Spectra were recorded every 30 seconds for 15 minutes. a)A_{500} b) B_{550} c) C_{590} d) D_{765} e) E_{980} f) TEM image of Sol E_{595} from Figure 4.12 in the presence of 30 μM 4-aminothiophenol. Red lines indicate the laser excitation wavelength.

The two dominant peaks observed in the UV-vis spectra of the nanoprisms shown above are the in-plane dipole resonance (at lower energy) and the out-of-plane quadrupole resonance, typically at 334 nm. Both the out-plane dipole and in-plane quadrupole resonances are present but are only seen as shoulder, in between the two main resonances. Upon aggregation with the 4-aminothiophenol, the main change in the spectrum is associated with the in-plane dipole. The out-of –plane quadrupole does experience a small red-shift, accompanied by a small change in intensity however these are not remarkable when compared with the movement of the in-plane dipole. During the aggregation process, the in-plane dipole resonance, shifts to longer wavelengths and broadens out significantly. This broadening also occurs mainly on the longer wavelength side of the resonance.

This aggregation process, initiated by the presence of the 4-aminothiophenol alone, is completely different to the aggregation process that occurs in the presence of $MgSO_4$. From Figure 4.13 above, it can be seen that 10 minutes after the addition of $MgSO_4$ to the sol a broad absorption of the whole of the visible spectrum is recorded. The TEM images of the sols aggregated with 4-aminothiophenol and $MgSO_4$ are also remarkably different. Upon aggregation with 4-aminothiophenol, while some change in morphology of the particles is evident *i.e.* truncation from prisms to disks, in general the particles are merely brought closer to each other. This is in contrast to aggregation with $MgSO_4$ when the integrity of the initial nanoprisms is not maintained.

Effect of the addition of 30 µM 4-methylthiophenol and thiophenol:

The aggregation of $SolC_{590}$ from Figure 4.16 with 4-methylthiophenol and thiophenol are shown below in Figure 4.18 and Figure 4.19 respectively.

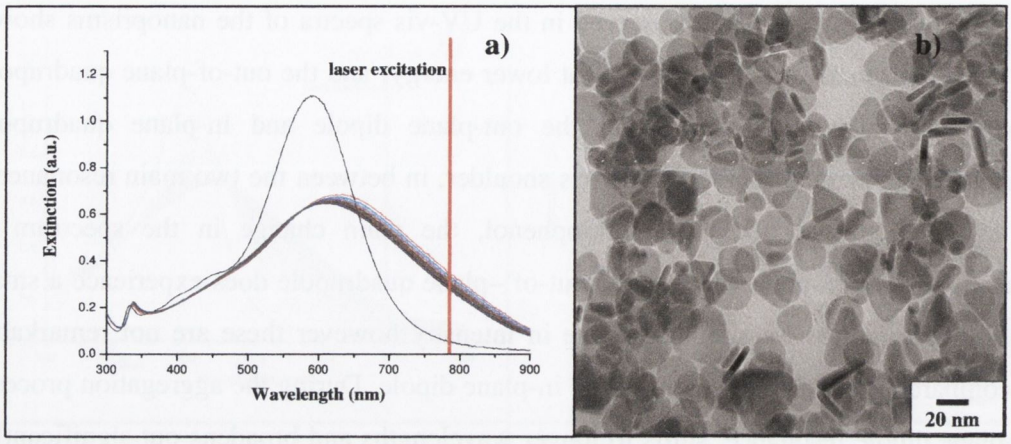


Figure 4.18: a) UV-vis spectra monitoring the aggregation process of $SolD_{590}$ from Figure 4.16 in the presence of 4-methylthiophenol (30 μM). Spectra were recorded every 30 seconds for 15 minutes. b) TEM image of $SolE_{595}$ from Figure 4.12 after aggregation. Red lines indicate the laser excitation wavelength.

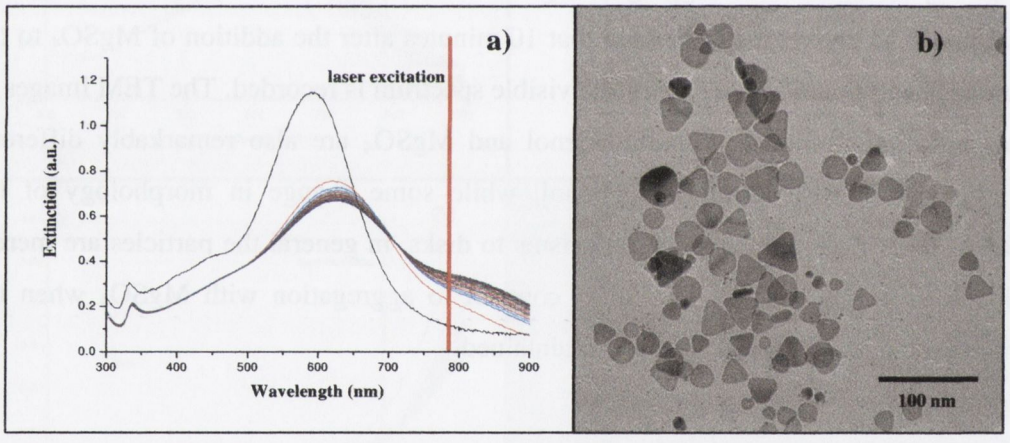


Figure 4.19: a) UV-vis spectra monitoring the aggregation process of $SolD_{590}$ from Figure 4.16 in the presence of thiophenol (30 μM). Spectra were recorded every 30 seconds for 15 minutes. b) TEM image of $SolE_{595}$ from Figure 4.12 after aggregation. Red lines indicate the laser excitation wavelength.

It can be seen that the two aggregation processes shown above are slightly different to that of 4-aminothiophenol shown above in Figure 4.17. Firstly, the extent of aggregation (from the UV-vis spectra) is less for 4-methylthiophenol and thiophenol. Also in the case of thiophenol, as the aggregation proceeds a new absorption band at the longest wavelength side appears. It must be noted that the extent of aggregation cannot be ascertained from the TEM images as in some cases the drying process alone is enough to induce aggregation.

The purpose of the TEM analysis is to confirm the morphology of the SERS substrates and it can be seen that the integrity of the nanoprisms is, on the whole, maintained during the aggregation process.

Effect of the addition of 30 μM 4-mercaptopyridine

Of the four analytes shown above, 4-mercaptopyridine was the only molecule which did not cause aggregation of the nanoprisms itself and in order for SERS spectra to be recorded, $MgSO_4$ was required. The aggregation of $SolC_{590}$ (from Figure 4.16) is shown below in Figure 4.20. It can be seen that upon addition of 4-mercaptopyriidne to the sol, a small red-shift of the in-plane dipole was observed. The sol was monitored for 15 minutes but no significant broadening was observed, $MgSO_4$ was then added and the sol was again monitored for 15 minutes. The UV-vis spectra after the addition of the $MgSO_4$ are similar to those shown above in Figure 4.13 in that a broad absorption over the entire visible region of the spectrum is evident. However from the TEM analysis it can be seen that the extent of 'melting' experienced by the nanoprisms in the presence of 4-mercaptopyridine is not as great as that experienced by the as prepared nanoprisms. This suggests, along with the red-shift of the in-plane dipole resonance after the addition of the 4-mercaptopyriine, that the molecule adsorbs onto the nanoparticles and protects them to some extent from the $MgSO_4$.

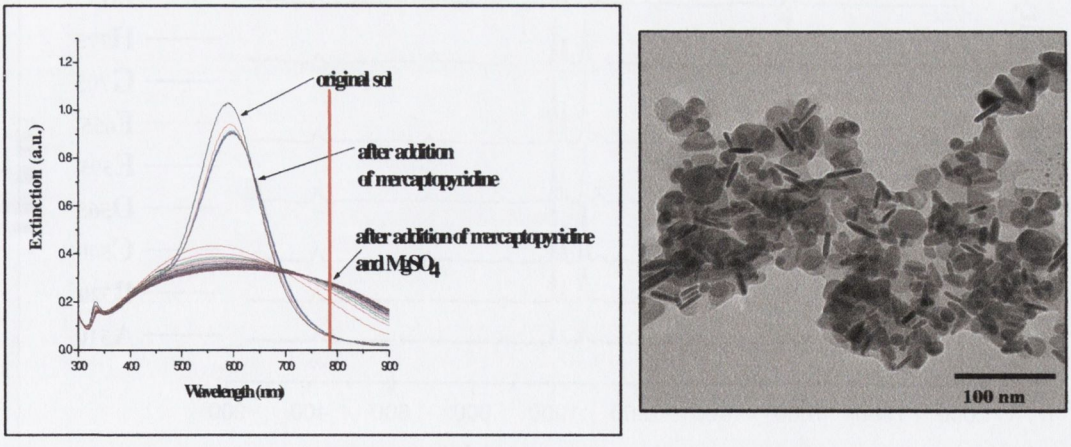


Figure 4.20: a) UV-vis spectra monitoring the aggregation process of SolD590 from in the presence of 4-mercaptopyridine (30 μM) and $MgSO_4$ (0.1 M). Spectra were recorded every 30 seconds for 15 minutes. b) TEM image of SolE595 from Figure 4.12 after aggregation. Red lines indicate the laser excitation wavelength.

4.2.2.2.2 SERS study

As previously mentioned in Section 4.2.2.1, the SERS spectra were recorded on an Avalon Instruments RamanStation with an excitation wavelength of 785 nm. The laser power was 100 mW and the resolution of the instrument was 4 cm^{-1}. An exposure time of 10 s was used with two exposures to record each spectrum. All experiments were carried out in a 96 well polypropylene microtitre plate. The final volume in each of the wells was 250 µL (200 µL sol + 50 µL analyte). It was found that the addition of an external aggregating agent, such as $MgSO_4$ was unnecessary, as the analytes alone induced enough aggregation for a SERS spectrum to be recorded. *The exception to this was the case of 4-mercaptopyridine. $MgSO_4$ (0.1 M) was added after the analyte. Therefore the total volume in the well was 300 µL.*

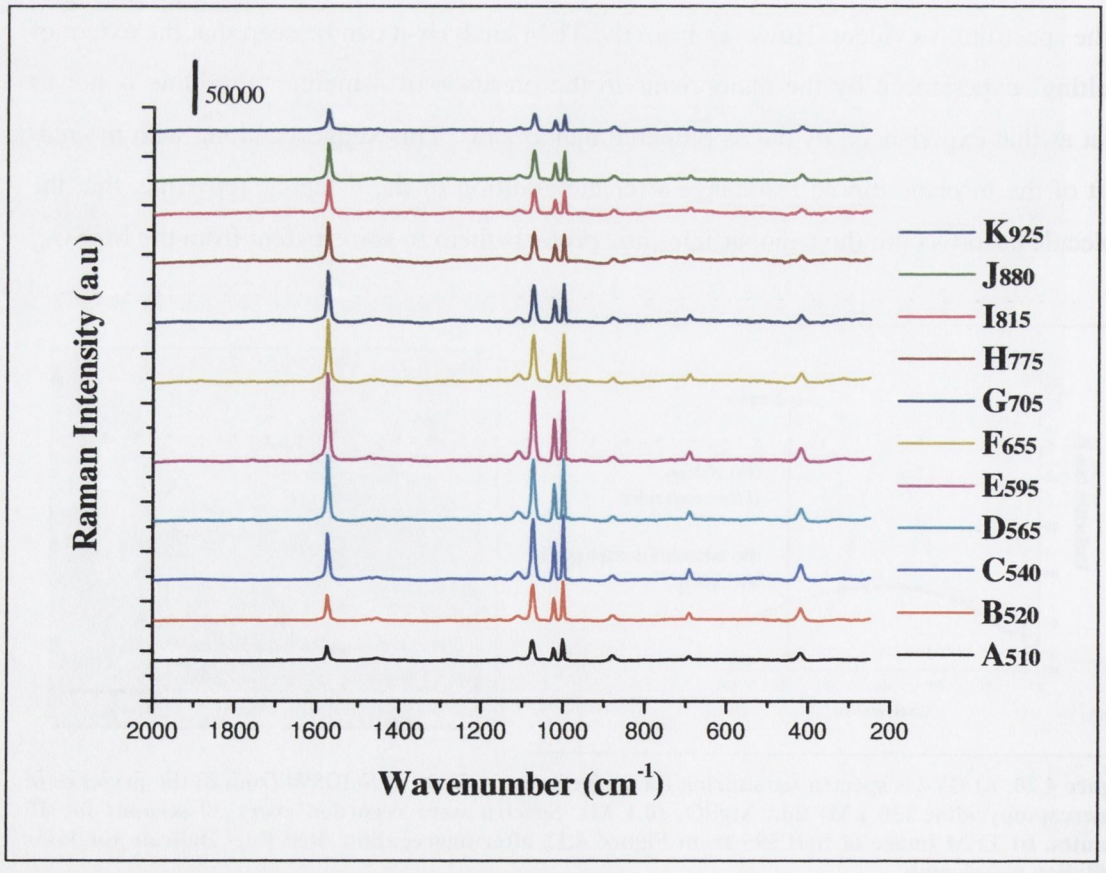


Figure 4.21: SERS spectra of thiophenol (30 µM) using the sols from Figure 4.12 as substrates.

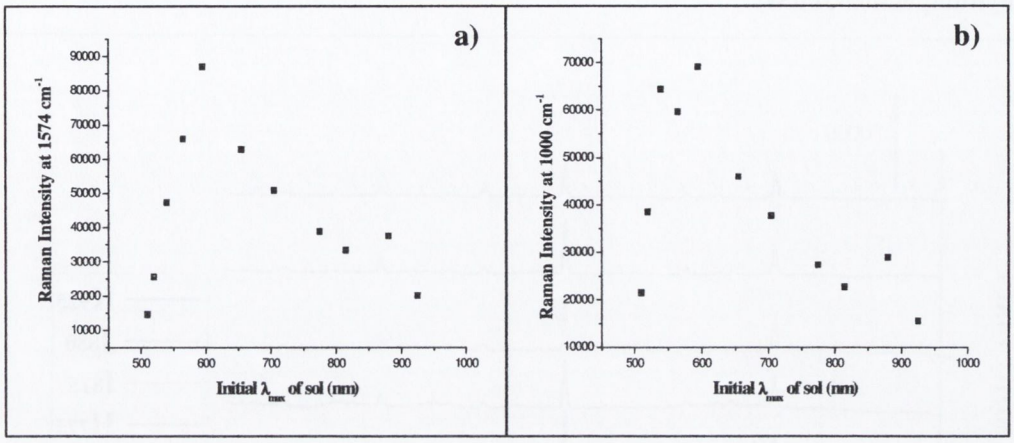


Figure 4.22: Raman intensities of the band at a) 1574 b) 1000 cm^{-1} of thiophenol versus the initial λ_{max} of each sol.

Position of band (cm^{-1})	*Assignment*
419	ν(CS), δ(CC)ring
691	ν(CS), δ(CC)ring
878	*EtOH*
1000	δ(CC)ring
1020	δ(CH)
1073	δ(CH)
1111	δ(CH)
1456	*EtOH*
1575	ν(CC)ring, ν(CS)

Table 4.4: Assignment of the Raman intensities of thiophenol above in Figure 4.21 from references[33-35]

4-Methylthiophenol (30μM)

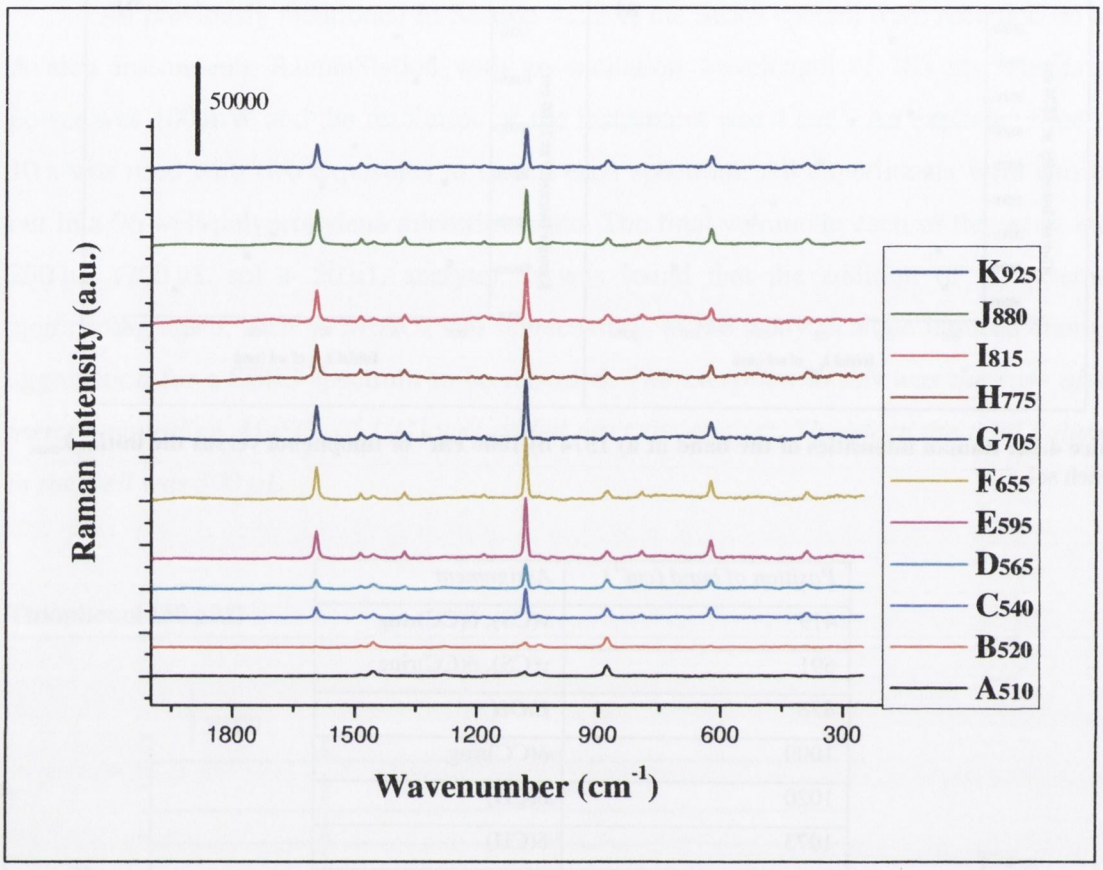


Figure 4.23: SERS spectra of 4-methylthiophenol (30 μM) using the sols from Figure 4.12 as substrates,

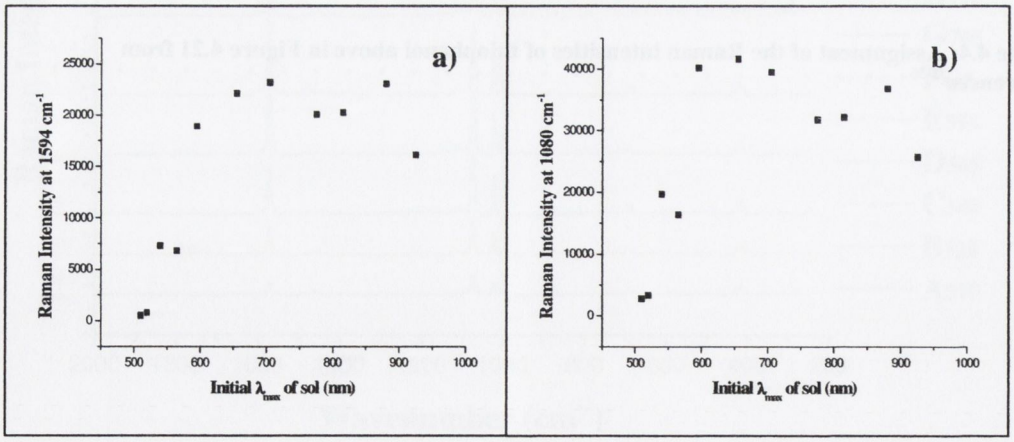


Figure 4. 24: Raman intensities of the band at a) 1594 b) 1080 cm^{-1} in 4-methylthiophenol versus the initial λ_{max} of each sol.

Position of band (cm^{-1})	*Assignment*
440	γ (CC)ring
625	δ(CC)ring
795	γ (CH)
880	*EtOH*
1080	ν(CC)ring, ν(CS)
1184	δ(CH)
1379	ν(CC)ring
1456	*EtOH*
1484	ν(CC)ring
1594	ν(CC)ring

Table 4.5: Assignment of the Raman intensities of 4-methylthiophenol above in Figure 4.23 from references[36]

4-Aminthiophenol (30 µM)

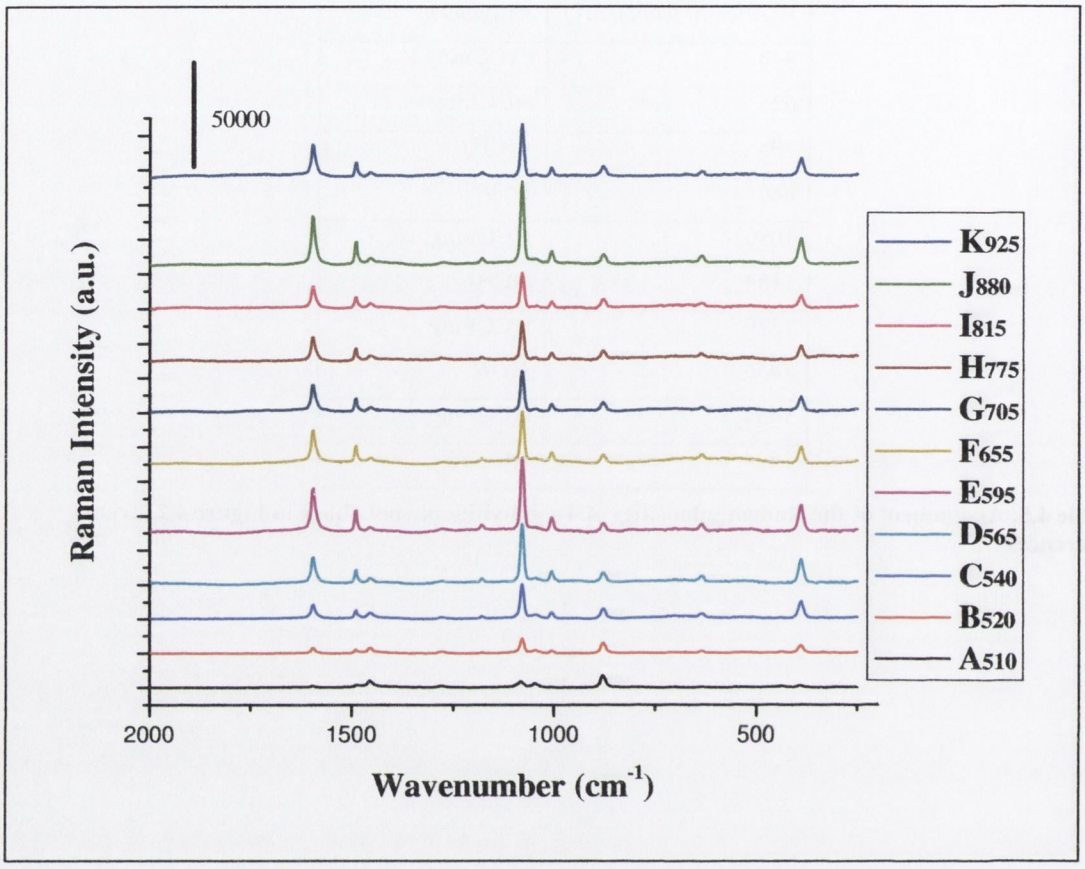


Figure 4.25: SERS spectra of 4-aminothiophenol (30 µM) using the sols from Figure 4.12as substrates.

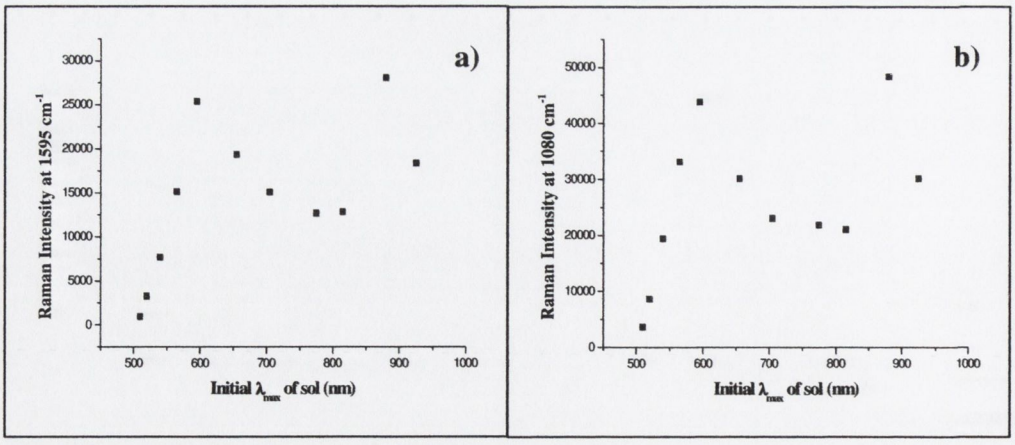


Figure 4.26: Raman intensities of the band at a) 1594 b) 1080 cm^{-1} of 4-aminothiophenol versus the initial λ_{max} of each sol.

Position of band (cm^{-1})	*Assignment*
389	δ (CS)
435	γ (CC)ring
636	δ (CC)ring
879	*EtOH*
1006	δ(CH)
1046	δ(CH)
1080	ν(CC)ring, ν(CS)
1178	δ(CH)
1276	δ(CH)
1454	*EtOH*
1489	ν(CC)ring
1595	ν(CC)ring

Table 4.6: Assignment of the Raman intensities of 4-aminothiophenol above in Figure 4.25 from references[37-39]

4-mercaptopyridine (30 μM)

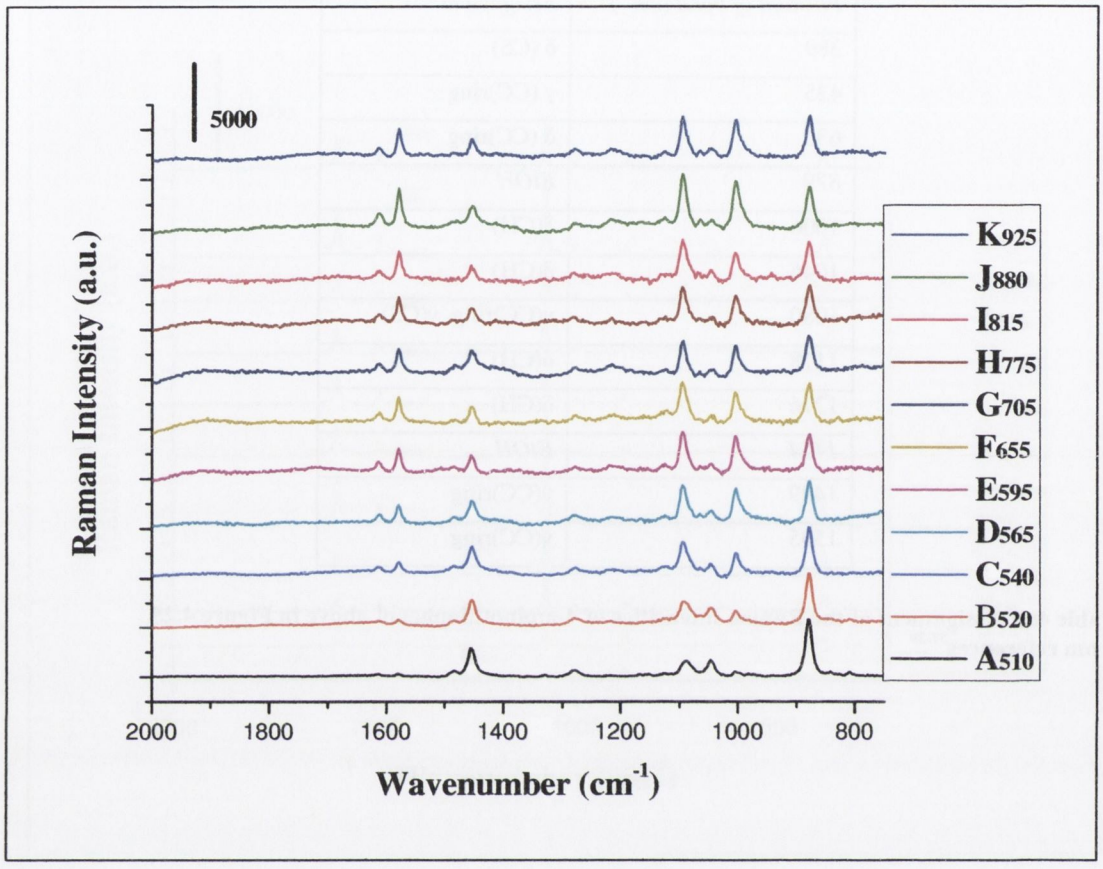


Figure 4.27: SERS spectra of 4-mercaptopyridine (30 μM) using the sols from Figure 4.12 as substrates. Sols were aggregated with $MgSO_4$ (0.1M) after the addition of the analyte.

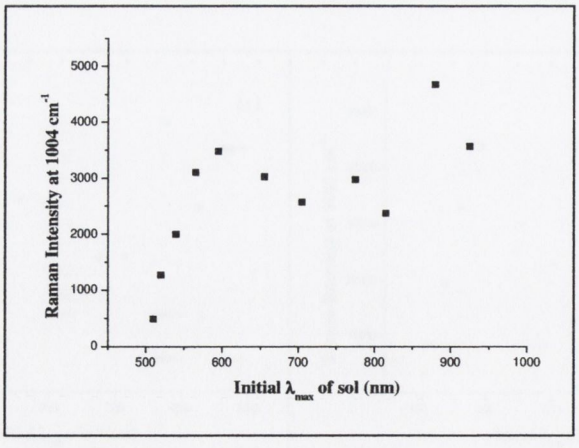


Figure 4.28: Raman intensities of the band at 1004 cm^{-1} of 4-mercaptopyridine versus the initial λmax of each sol.

Position of band (cm^{-1})	*Assignment*
878	*EtOH*
1004	γ (CC)ring
1044	δ (CH)
1096	γ (CC)ring , γ (CS)
1280	δ (CH)
1456	*EtOH*
1580	ν(CC)ring
1612	ν(CC)ring

Table 4. 7: Assignment of the Raman intensities of 4-mercaptopyridine above in Figure 4.27 from references[28-30]

The purpose of the experiments described in this section was to investigate if the SERS intensities of the analytes could be increased even further than seen in Part 1 by pushing the λ_{max} of the SERS substrate further into the near infrared region of the spectrum. From the spectra shown above it is clear that a similar trend to that seen in Part 1 was again observed for sols with λ_{max} less than 600 nm. As the λ_{max} of the SPR is shifted further into the red (therefore as the λ_{max} of the aggregated sol is shifter further in to the NIR) the enhancement factor increases. However, as the λ_{max} is pushed out further than 600 nm the enhancement decreases again or at best a levelling off is observed. This phenomenon is independent of the analyte used.

Ethanol peaks

Another point to be noted from the above SERS spectra is that peaks from ethanol can be observed. All of the above analytes were in ethanolic solution. EtOH peaks were not observed in previous SERS experiments (see Figure 4.8). It is particularly significant in the case of 4-mercaptopyridine where the intensities of the EtOH are comparable to the intensities of the analyte peaks. The spectrum of EtOH is given below in Figure 4.29.

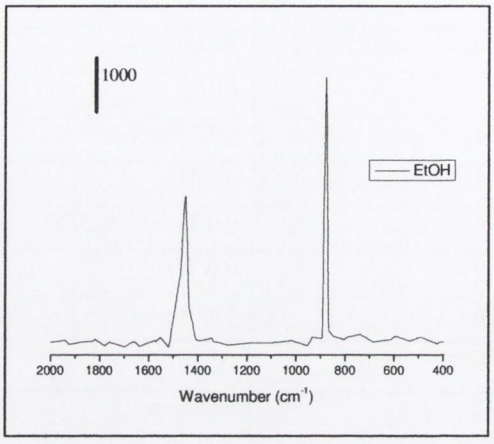


Figure 4.29: Spectrum of ethanol (3.4M)

Varying the substrate concentration

One final experiment that was carried out was to investigate the importance of the nanoprism concentration on the resultant SERS spectra. In Figure 4.30 and Figure 4.31 below, only the concentration of the nanoprisms was varied. The analyte concentration remained at 30 μM.

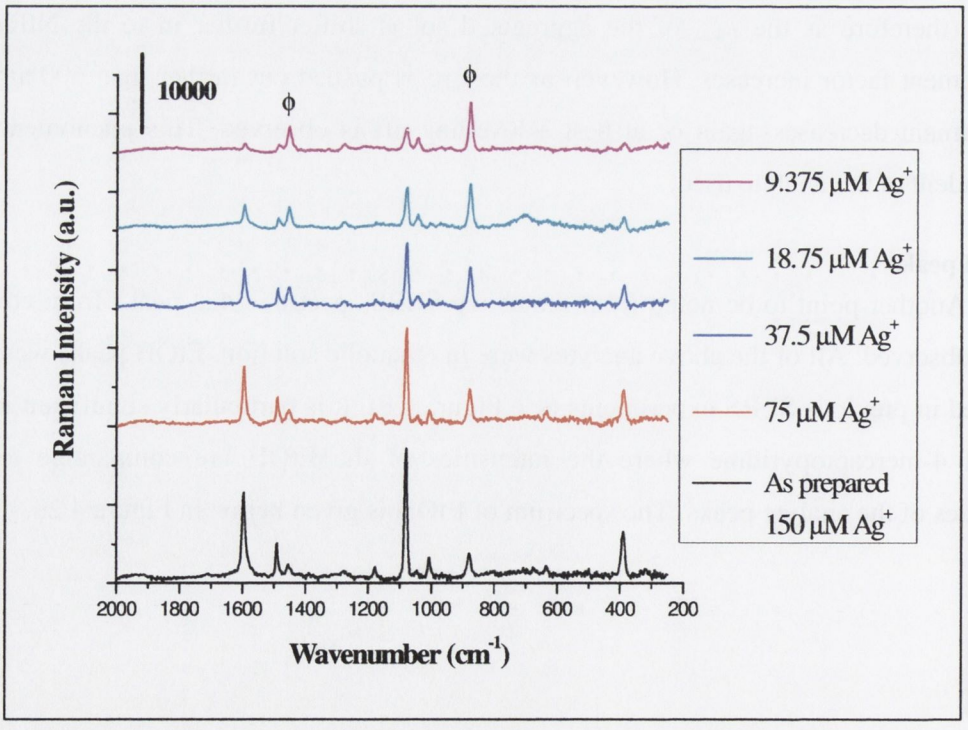


Figure 4.30: SERS spectra of 4-aminothiophenol (30 μM) when the concentration of substrate was lowered. Φ denotes the EtOH peaks.

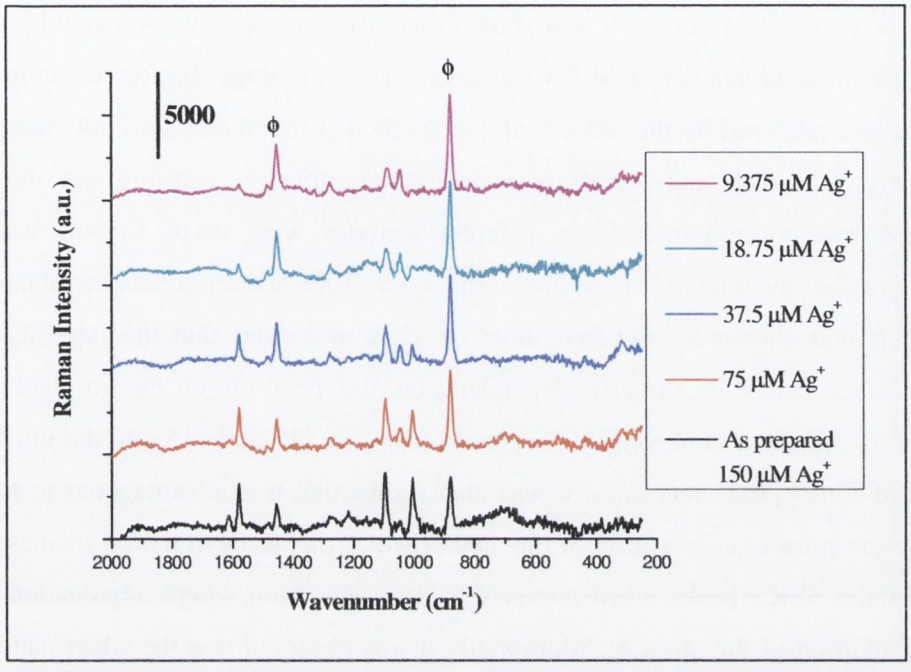


Figure 4.31: SERS spectra of 4-mercaptopyridine (30 μM) when the concentration of substrate was lowered. Φ denotes the EtOH peaks.

It can be seen from both of the above spectra, that as the concentration of nanoprism was decreased by dilution, the intensity of peaks associated with the analytes decreased. However, the intensity of the peaks attributed to EtOH was enhanced. As the surface area of the particles was reduced, the intensity of the EtOH peaks was increased, to such an extent that in the 4-mercaptopyridine case the EtOH peaks dominate the spectra.

4.3 Discussion:

To begin with it is useful to give an overview of the results shown above in Section 4.2. Preliminary experiments using nanoparticles prepared by the 'added citrate' method confirmed the presence of TSC on the surface of the nanoparticles. There were no SERS signals present due to the poly(vinylpyrrolidone) (PVP), again confirming that it acts only to prevent the aggregation of the nanoparticles and is not adsorbed onto the surface of these nanoparticles. Experiments using crystal violet as an analyte confirmed that silver nanoparticles prepared by such a method had the ability to act as useful SERS substrates.

In Section 4.2.2.1 above, it was shown that silver nanoprisms prepared by the 'no added citrate' method can act as SERS substrates. The advantage that these nanoparticles have over those prepared by the 'added citrate' method is that there is no polymer present during the growth step and therefore centrifugation prior to carrying out the SERS experiments was not required. Four different analytes were used; Crystal Violet, 4-mercaptopyridine, adenine and adenosine, although a SERS spectrum was not obtained for adenosine. It was shown for the first three of these molecules that the intensity of the observed SERS peaks is strongly dependent on the position of the in-plane dipole resonance. As this band is moved in increments between 485 and 615 nm, the intensity of the observed SERS peaks increases. It was also shown that it is advantageous to have the analyte present prior to aggregation of the nanoprism as this leads to a 66% increase in the intensity of the SERS peaks when compared with a situation where aggregation occurs before the addition of the analyte. Additionally it was observed that the silver nanoprisms prepared by this method compare favourably with the standard SERS substrate prepared by the Lee and Meisel method.

In Section 4.2.2.2, the study was extended. Sols with their in-plane dipole resonances varying between 500 and 925 nm were used. In this instance the four analytes chosen were thiophenol, 4-methylthiophenol, 4-aminothiophenol and 4-mercaptopyridine. It was found that the intensity of the SERS spectra again increased with increasing λ_{max} of the nanoprisms up to 600 nm. After this point the SERS intensities decreased with increasing λ_{max}. The aggregation process of these sols was examined in detail by UV-vis spectroscopy and TEM. It was found that the aggregation can occur upon addition of the analyte alone, rendering the addition of an external aggregating agent unnecessary. The exception to this case was 4-mercaptopyridine, where SERS spectra could not be observed without the addition of $MgSO_4$. SERS spectra were also taken after $MgSO_4$ had been added to the nanoprisms that had been preaggregated with the analytes, however a reduction in the SERS intensity was observed. This was attributed to the fact that large unstable agglomerates were formed in the presence of MgSO4 which settled out of solution after a short time period (less than 5 minutes). Various points that have been raised during the presentation of the results above will now be discussed.

4.3.1 Discussion of the Preliminary study:

The first SERS experiment that was carried out involved the use of a green 'added citrate' sol prepared at room temperature using 0.7 mM TSC (as described in Scheme X). The sol was aggregated with $MgCl_2$ and a SERS spectrum that has been assigned to trisodium citrate was recorded.[25, 26] It has been reported previously by Munro *et al*[25]. that the ν_s(COO) in the Raman spectrum of TSC consists of a narrow band at 1417 cm^{-1}, and that when the citrate is adsorbed on the surface of silver colloid, this band is shifted to 1390 cm^{-1} indicating interactions between the carboxylates and the silver surface. In the case described above in Figure 4.3, the observed shift in this band is less with ν_s(COO) at 1401 cm^{-1}. It would have been useful to characterize the nanoparticles prepared at higher temperature by the added citrate method to see if this could give any insight into the increased stability. However, due to time constraints this was not carried out.

The intensities of the observed SERS peaks were increased by at least a factor of two by removing the poly(vinylpyrrolidone) (PVP), despite the fact that the concentration of nanoparticles in the redispersed sol was less, as many of the nanoparticles remained in the supernatant. The fact that no peaks associated with the PVP were observed in the SERS spectra of the nanoparticles, confirms again the idea that PVP plays no role in the growth of the nanoparticles prepared by the 'added citrate' method and merely acts as an agent to prevent their aggregation. The increased intensity of the SERS peaks after centrifugation can be explain by the removal of the polymer making the particles more susceptible to aggregation, creating more 'hot-spots' or SERS active regions in the sol. A similar trend was observed when crystal violet (CV) was used as the analyte. It must be noted that the observed phenomenon here is Surface Enhanced Resonance Raman Scattering (SERRS) as CV absorbs strongly (molar extinction coefficient = 112,000 $M^{-1}cm^{-1}$ at 510 nm) in the visible region of the spectrum with λ_{max} = 590 nm. SERRS combines the advantage of surface enhancement with the use of a resonant chromophore so that molecular resonance enhancement as well as surface enhancement is obtained with scattering from the chromophore dominating the spectrum.[1] The disadvantage of this method of analysis is that with fixed excitation wavelength the number of analytes is limited, as it is not always

possible to find a suitable chromophore and without further functionalization or derivitization it is not suitable for the analysis of many substances.[18]

4.3.2 Discussion of the Detailed Study: Part 1: Nanoprisms with λ_{max} between 485-615 nm

In Section 4.2.2.1 (Detailed study: Part 1), crystal violet (CV) was again used as an analyte. In this case the aggregating agent was changed from $MgCl_2$ to $MgSO_4$. The reason for this was two-fold. Firstly it was reported by the Bell group that some aggregating agents can adsorb to the surface of the colloid particles and in doing so prevent the adsorption and detection of the incoming analytes.[26] This is particularly important when $MgCl_2$ is used as the aggregation agent, as it was reported that the chloride has the ability to displace the citrate on the surface of Lee and Meisel colloids during the aggregation process and in doing so change the binding affinity of analytes on the surface. In contrast to this when $MgSO_4$ is used, only aggregation is observed and the citrate is displaced only by the analyte of interest leading to an optimized SERS spectrum. Secondly, as shown in Chapter 2, the addition of halide ions to silver sols can etch the sharp corners of the nanoprisms. Therefore the nanoparticles giving rise to the SERS spectra would more than likely be of a different morphology to that of the original nanoparticles.

In this section it was also demonstrated that it is advantageous to have the analyte present during the aggregation process (see Figure 4.7). It is now widely accepted that it is the presence of 'hot-spots' that give rise to the large enhancement factors associated with SERS. As mentioned in Section 4.1.1.1 these hot spots have been attributed to two basic phenomena 1) the lightning rods effect and 2) the coupling of surface plasmons on nearby nanoparticles. Regardless of the explanation of these phenomena, the presence of extremely intense electromagnetic fields is required for SERS to be observed. Theoretical calculations have been reported in which these intense electromagnetic fields have been shown to exist in the junctions between nanoparticles.[40] It therefore makes sense that if the analyte is present before the aggregation of the nanoparticles, it is likely that more of the analyte molecules will get trapped in these junctions and therefore will be SERS active than if the analyte is introduced after the aggregation process.

Three other analytes were also examined: 4-mercaptopyridine, adenine and adenosine. It was found with the first two of these molecules that as the λ_{max} was varied from 485-615 nm, the intensity of the observed SERS spectrum was increased. This will be discussed further below in the discussion of Part 2. At this stage let us look in detail at the observed SERS spectra of 4-mercaptopyridine. There are three possibilities for the adsorption of 4-mercaptopyridine onto a metal surface namely via participation of the lone pair of electrons of the sulphur, via participation of the lone pair of electrons of the nitrogen or via interaction with the π aromatic electrons. It is proposed here that the S-H bond is cleaved and there is then interaction of the S atom with the silver surface. The aromatic ring is then perpendicular or tilted with respect to the silver surface. This is confirmed by the disappearance of the 2575 cm^{-1} S-H band and is consistent with finding in the literature.[41, 42] Depending on the working pH of the solution the 4-mercaptopyridine molecules can then exist in the protonated or deprotonated form and the ν(CC) and δ(CH) bands are found to be sensitive this. As such the position and intensity of the bands at 1580 and 1217 cm^{-1} are characteristic of the N-deprotonated form of the adsorbed 4-mercaptopyridine molecules while bands at 1615 , 1217 and 1004 cm^{-1} are characteristic of the N-protonated form. Values similar to these have been reported previously.[43] It was noted above that a change in the relative intensities of the bands located at 1580 and 1615 cm^{-1} was observed as the λ_{max} of the substrate was varied from 485 nm to longer wavelength. As these bands are indicative of the deprotonated and protonated form respectively, this variation in the relative intensities is associated with variation in the pH.[41, 42] However as all the sols used above were stabilized by excess TSC and had a pH of 5.8 it is unlikely that variations of the pH is the cause of the observed fluctuations in intensity. It is proposed here that the change in the relative intensities of the bands at 1580 and 1615 cm^{-1} is due to an orientation change of the adsorbed 4-mercaptopyridine molecules as the edge length of the nanoprisms is varied. As the loading of the analyte per particle is varied with increasing or decreasing edge length (smaller number of bigger nanoparticles present) there is a variation in the intermolecular interactions of the analyte. Because of decreased π-π stacking of the aromatic rings, the pyridine ring may adopt a parallel orientation to the metal surface, leading to a strong interaction between the pyridine N atom and the nanoprism surface. The coordination of the nitrogen atom to the silver metal would cause a decrease in the electron

density of the nitrogen (as more electron density is donated to the metal) consequently weakening the ability of the adsorbed 4-mercaptopyridine to be protonated. This has been reported previously by Chao *et al.* when the SERS of 4-mercaptopyridine adsorbed on electrochemically roughened silver electrodes was investigated.[43]

Now consider the observed SERS spectra of adenine. A shift in the position of the ring breathing mode from 734 to 738 $cm^{-1}$was observed. This has been previously reported when the concentration of the analyte has been varied and has also been attributed to a change in the orientation of the adenine on the surface of the nanosubstrate.[31] At low concentrations the adenine molecules lie in such a way so that the bases lie flat on the substrate and as the concentration is increased the molecules become aligned in a perpendicular orientation. This causes the ring breathing mode to shift to lower wavenumbers. In the case above the concentration of the adenine was kept constant and only the edge length of the nanoprisms was varied. A small shift to higher wavenumbers was observed as the edge length of the nanoprism was increased so it is proposed here (again that a similar case to that observed for 4-mercaptopyridine) that as the loading of the analyte per particle is varied with increasing edge length the orientation of the adenine changes from the bases being perpendicular to the surface to the bases lying flat on the surface.

It was attempted to use adenosine as an analyte in a similar manner to adenine. However no enhanced spectrum was obtained. Background fluorescence was the major contributor to the spectrum. This could indicate a number of factors:

a. The orientation of the molecule on the surface is important. With adenosine is it possible that the sugar is blocking the adsorption of the base onto the surface
b. There are two N atoms available for bonding with the surface in adenine, but only one in adenosine.
c. Intermolecular hydrogen bonding of the molecules may be preventing them from adsorbing onto the surface.

4.3.3 Discussion of the Detailed Study: Part 2: Nanoprisms with λ_{max} between 510-925 nm

The first important aspect that must be discussed with regard to the results reported above in Section 4.2.2.2 is the difference observed in the aggregation process when $MgSO_4$ is used as the aggregating agent as opposed to when the analyte alone is used. As shown above in Figure 4.15 when nanoprisms prepared by the 'no added citrate' method are exposed to a solution of $MgSO_4$, a dramatic change in morphology is observed. From the TEM analysis it can be seen that the nanoprisms appear to have 'melted' and the resulting nanoparticles do not resemble the starting material in anyway. A similar phenomenon has been reported by Novo and Mulvaney for gold nanorods that have been exposed to ascorbic acid or sodium borohydride.[44] Concentration dependent shape changes caused by charge induced fragmentation were observed. In the case of the silver nanoprisms described above it must be noted that the concentration of $MgSO_4$ was 0.1 M and is almost 10^4 times higher than the concentration of Ag^0 (assuming complete reduction of Ag^+ in the growth of the nanoprisms) so although the sulphate anions was shown not to displace citrate from the surface of Lee and Meisel colloids[26] it is not surprising that it appears to have done so in the case shown above when considering the relative concentrations.

It was found during the course of the experiments described above that the presence of an external aggregation such as $MgSO_4$ was in fact unnecessary in three out of the four analyte cases examined. The presence of thiophenol, 4-methylthiophenol and 4-aminothiophenol alone were adequate to induce sufficient aggregation of the nanoprisms, such that SERS spectra were obtained. This is different to the results of a study carried out by Zou and Dong in the SERS activity of aggregated silver nanoplates in aqueous solution.[45] It was reported there that the addition of 2-aminothiophenol to silver nanoplates slightly dampened the absorption maximum but was unable to aggregate them. The addition of NaCl was required to induce aggregation so that detectable SERS of 2-ATP was observed. The advantage that the results presented in this thesis have over the system examined by Zou and Dong is that TEM analysis of the SERS substrates after aggregation is presented, so that the nature of the substrate giving rise to SERS has been well characterized and it has been shown that although small changes in the morphology of the

particles acting as the SERS substrate were observed upon aggregation on the whole the integrity of the nanoplates is maintained throughout the SERS experiment. Also because an additional aggregating agent is not required, there is one less variable to be considered when designing a successful SERS experiment.

However, there was one exception to these observations. The addition of 4-mercaptopyridine did not induce the aggregation of the nanoprisms. As shown above in Figure 4.20 a slight red-shift of the in-plane dipole resonance accompanied by a damping in the extinction intensity was observed upon addition of this analyte to the sol. This indicates that the 4-mercaptopyridine is adsorbed onto the surface of the nanoprisms. $MgSO_4$ was then added to induce aggregation so that a SERS spectrum could be recorded. From the TEM analysis of the aggregates (Figure 4.20) it is clear that although the shape of the nanoprisms has changed upon aggregation with the $MgSO_4$, the interaction of the salt is less severe than that observed in Figure 4.14 and Figure 4.15 and a melting process has not occurred. This is presumably evidence that the 4-mercaptopyridine adsorbs onto the surface of the nanoprisms, protecting them to some extent from the $MgSO_4$. It must be noted also, that inversion of the relative intensities of the bands at 1580 and 1615 cm^{-1}discussed above in Section 4.3.2. This can only be attributed to different surface chemistry of the nanoprisms used as substrates. However as discussed in Chapter 2 this is an area in the preparation of nanoparticles by aqueous based methods that has not been well characterized probably due to the difficulty associated with it.

Another result that requires discussion is the increase and subsequent decrease in the SERS intensities observed as the in-plane dipole resonance is shifted from 510 to 925 nm. The correlation between the surface plasmon resonance and laser excitation wavelength reveals that in general higher SERS intensities can be achieved when the excitation wavelength is coincident or slightly to the red side of the absorption maximum of the aggregated sols.[1, 8, 24, 45, 46]As seen in Figure 4.17 as the position of the in-plane dipole resonance is shifted further into the red region of the spectrum, the position of the aggregated absorption maximum is also shifted in a similar manner. Thus the degree of overlap of the absorption band with the excitation wavelength first increases and then

decreases with the threshold position of the in-plane dipole of the original sol at ~600 nm. If the laser excitation was varied to1064 nm (another common laser excitation wavelength) this observed trend would also change.

Another aspect of these results to be discussed is the apparent change in the relative intensities of the SERS of both 4-aminothiophenol and 4-mercaptopyridine upon lowering the concentration of nanoprisms used (Figure 4.30 and Figure 4.31). Upon closer inspection of the SERS spectra it was found that the intensity of the analyte peaks decreases with decreasing substrate concentration, as expected (as the number of SERS active sites or 'hot spots' is decreased) while it is the intensity of the EtOH peaks increases. Again on closer inspection of the SERS spectra of the four analytes, it was noted that while the intensities of the analyte peaks were varying as the substrate was changed, the intensity of the EtOH peaks remained constant. This would indicate that the observed ethanol peaks are in fact Raman and not SERS peaks. The increase in the intensity of the peaks can be explained by an 'inner filter effect'. In essence, the nanoprisms reabsorb the Raman scattering from the EtOH. This process was not complete in Figure 4.21- Figure 4.27 and as such the Raman bands were observed. Upon decreasing the concentration of the nanoprisms used in the SERS experiments, this inner filter effect was reduced and the intensity of the Raman bands increased.

One final aspect that needs to be addressed that is perhaps conspicuous by its absence is the calculation of enhancement factors. The SERS enhancement factor (EF) arguably one of the most important numbers for characterizing the SERS effect, however the wide discrepancies in quoted EF arises from the wide variety of definitions of the EF and also the many assumptions and estimates that are involved in its calculation. In fact a recent article has been dedicated to this subject.[20] The relative enhancement factors for the thiophenol from Figure 4.21 are shown below in Table 4.8 with the caveat that these values can only be compared truly with EF values calculated by the same method.

The following equation was used[20, 45]:

$$EF = \frac{(I_{SERS} / C_{SERS})}{(I_{normnal} / C_{bulk})} \quad \textbf{Equation 4.1}$$

where C_{SERS} is the concentration of the adsorbed molecules on the silver surface and C_{bulk} is the concentration of molecules in the bulk samples and I_{SERS} and I_{normal} are the intensities of a certain vibration in SERS and normal Raman respectively. For the complete calculation see Chapter 5. The total surface area of the nanoprisms in each sol is assumed to remain constant as the same concentration of silver ion is used to prepare all of the sols and it has been found that the thickness does not vary with edge length.[47] Therefore the total surface area was estimated to be 7.56 nm^2/10 mL sol. The footprint of thiophenol was estimated to be 0.28 nm^2, similar to that of 2-aminothiophenol from reference[45]. Considering that 200 µL sol was used for each experiment, the concentration of thiophenol required to achieve monolayer coverage is calculated to be 0.45 µM. Using equation 4.2 above, the enhancement factors for thiophenol on the different substrates were calculated.

Sol	*Enhancement Factor*
A_{510}	7.4×10^6
B_{520}	1.3×10^7
C_{540}	2.2×10^7
D_{565}	2.0×10^7
E_{595}	2.4×10^7
F_{655}	1.6×10^7
G_{705}	1.3×10^7
H_{775}	9.4×10^6
I_{815}	7.8×10^6
J_{880}	9.9×10^6
K_{510}	5.3×10^6

Table 4.8: Enhancement factors calculated by equation 4.2 above for the band at 1000 cm^{-1} in the SERS spectrum of thiophenol (from Figure 4.21)

These values are an order of magnitude greater than those reported for 2-ATP on similar aggregated silver nanoplates.[45] However as stated above, these values must be treated with caution and all the assumptions used in the calculations must be taken into consideration.

4.4 Conclusions

The suitability of silver nanoparticles prepared by the 'added citrate' and 'no added citrate' (as discussed in Chapter 2) as good SERS substrates was investigated. Initial experiments confirmed the presence of citrate on the surface of nanoparticles prepared by the 'added citrate' method at room temperature. It was also noted that the intensity of the observed SERS spectrum was increased by removing the poly(vinylpyrrolidone). For this reason the majority of the experiments that were carried out used silver nanoprism prepared by the 'no added citrate' method, as these substrates could be used as prepared, without further purification.

Aggregation of the nanoparticles in aqueous solution is a key process in the observation of SERS spectra. It was demonstrated that is desirable to have the analyte of interest present during the aggregation process, as in this scenario it is more likely that the analyte molecules will get trapped in the 'hot spots' that are known to give rise to very intense electromagnetic fields when in turn are one of the most important factors responsible for the SERS phenomenon.

The method of aggregation of the nanoparticles was found to be important. When $MgSO_4$ was used, the nanoprism experienced a change in morphology so that the SERS substrate did not resemble the original nanoprisms in anyway. It was found that in three out of four cases that the presence of the analyte alone was enough to cause sufficient aggregation so that SERS spectra could be recorded. TEM analysis of these aggregates confirmed that the morphology of the nanoprism remained largely intact upon aggregation.

It was found that the position of the absorption maximum of the aggregated silver nanoprisms relative to the position of the laser excitation was important. Maximum SERS intensities were observed when there was an overlap between excitation wavelength and the maximum absorbance of the substrate.

Using thiophenol as the analyte, large enhancement factors was obtained for aggregated silver nanoprisms in solution. The ease with which the in-plane dipole

resonance of the silver nanoprisms can be tuned across the visible into the near-infrared region of the spectrum makes nanoprisms prepared by this method desirable as substrates for SERS measurements with varying laser excitation wavelength.

4.5 References

1. E. Smith and G. Dent, *Modern Raman Spectroscopy - A Practical Approach*, John Wiley and Sons, 2005.
2. M. Fleischmann, P. J. Hendra and A. J. McQuillan, *Chem. Phys. Lett.*, 1974, **26**, 152.
3. D. L. Jeanmaire and R. P. Van Duyne, *J. Electroanal. Chem.*, 1977, **84**, 1-20.
4. M. G. Albrecht and J. A. Creighton, *J. Am. Chem. Soc.*, 1977, **99**, 5215-5217.
5. A. Campion and P. Kambhampati, *Chem. Soc. Rev.*, 1998, **27**, 241-250.
6. S. Abdali and E. W. Blanch, *Chem. Soc. Rev.*, 2008, **37**, 980-992.
7. E. Bailo and V. Deckert, *Chem. Soc. Rev.*, 2008, **37**, 921-930.
8. M. J. Banholzer, J. E. Millstone, L. D. Qin and C. A. Mirkin, *Chem. Soc. Rev.*, 2008, **37**, 885-897.
9. S. E. J. Bell and N. M. S. Sirimuthu, *Chem. Soc. Rev.*, 2008, **37**, 1012-1024.
10. I. Chourpa, F. H. Lei, P. Dubois, M. Manfait and G. D. Sockalingum, *Chem. Soc. Rev.*, 2008, **37**, 993-1000.
11. R. M. Jarvis and R. Goodacre, *Chem. Soc. Rev.*, 2008, **37**, 931-936.
12. J. Kneipp, H. Kneipp and K. Kneipp, *Chem. Soc. Rev.*, 2008, **37**, 1052-1060.
13. S. Lal, N. K. Grady, J. Kundu, C. S. Levin, J. B. Lassiter and N. J. Halas, *Chem. Soc. Rev.*, 2008, **37**, 898-911.
14. R. C. Maher, C. M. Galloway, E. C. Le Ru, L. F. Cohena and P. G. Etchegoin, *Chem. Soc. Rev.*, 2008, **37**, 965-979.
15. N. P. W. Pieczonka and R. F. Aroca, *Chem. Soc. Rev.*, 2008, **37**, 946-954.
16. M. D. Porter, R. J. Lipert, L. M. Siperko, G. Wang and R. Narayanana, *Chem. Soc. Rev.*, 2008, **37**, 1001-1011.
17. X. M. Qian and S. M. Nie, *Chem. Soc. Rev.*, 2008, **37**, 912-920.
18. W. E. Smith, *Chem. Soc. Rev.*, 2008, **37**, 955-964.

19. D. Y. Wu, J. F. Li, B. Ren and Z. Q. Tian, *Chem. Soc. Rev.*, 2008, **37**, 1025-1041.
20. E. C. Le Ru, E. Blackie, M. Meyer and P. G. Etchegoin, *J. Phys. Chem. C*, 2007, **111**, 13794-13803.
21. J. P. Camden, J. A. Dieringer, J. Zhao and R. P. Van Duyne, *Acc. Chem. Res.*, **doi:10.1021/ar800041s**.
22. K. A. Willets and R. P. Van Duyne, *Annu. Rev. Phys. Chem.*, 2007, **58**, 267-297.
23. P. L. Stiles, J. A. Dieringer, N. C. Shah and R. P. Van Duyne, *Annu. Rev. Anal. Chem.*, 2008, **1**, 601-626.
24. R. F. Aroca, *Surface Enhanced Vibrational Spectroscopy*, John Wiley and Sons, 2006.
25. C. H. Munro, W. E. Smith, M. Garner, J. Clarkson and P. C. White, *Langmuir*, 1995, **11**, 3712-3720.
26. S. E. J. Bell and N. M. S. Sirimuthu, *J. Phys. Chem. A*, 2005, **109**, 7405-7410.
27. N. R. Jana and T. Pal, *Adv. Mater.*, 2007, **19**, 1761-1765.
28. C. J. Orendorff, L. Gearheart, N. R. Jana and C. J. Murphy, *Phys. Chem. Chem. Phys.*, 2006, **8**, 165-170.
29. J. A. Baldwin, B. Vlckova, M. P. Andrews and I. S. Butler, *Langmuir*, 1997, **13**, 3744-3751.
30. J. Baldwin, N. Schuhler, I. S. Butler and M. P. Andrews, *Langmuir*, 1996, **12**, 6389-6398.
31. S. K. Kim, T. H. Joo, S. W. Suh and M. S. Kim, *J. Raman Spectrosc.*, 1986, **17**, 381-386.
32. P. C. Lee and D. Meisel, *J. Phys. Chem.*, 1982, **86**, 3391-3395.
33. C. A. Szafranski, W. Tanner, P. E. Laibinis and R. L. Garrell, *Langmuir*, 1998, **14**, 3570-3579.
34. K. T. Carron and L. G. Hurley, *J. Phys. Chem.*, 1991, **95**, 9979-9984.
35. Tai Ha Joo, M. S. Kim and K. Kim, *J. Raman Spectrosc.*, 1987, **18**, 57-60.
36. T. O. Deschaines and K. T. Carron, *Appl. Spectrosc.*, 1997, **51**, 1355-1359.
37. Y. Bae, N. H. Kim, M. Kim, K. Y. Lee and S. W. Han, *J. Am. Chem. Soc.*, 2008, **130**, 5432-5433.
38. Y. Chen, C. Wang, Z. Ma and Z. Su, *Nanotech.*, 2007, **18**, 325602.

39. Q. Zhou, G. Zhao, Y. Chao, Y. Li, Y. Wu and J. Zheng, *J. Phys. Chem. C*, 2007, **111**, 1951-1954.

40. H. Xu and M. Käll, *Phys. Rev. Lett.*, 2002, **89**, 246802.

41. J. Hu, B. Zhao, W. Xu, B. Li and Y. Fan, *Spectrochim. Acta A*, 2002, **58**, 2827-2834.

42. L. Zhang, Y. Bai, Z. Shang, Y. Zhang and Y. Mo, *J. Raman Spectrosc.*, 2007, **38**, 1106-1111.

43. Y. Chao, Q. Zhou, Y. Li, Y. Yan, Y. Wu and J. Zheng, *J. Phys. Chem. C*, 2007, **111**, 16990-16995.

44. C. Novo and P. Mulvaney, *Nano Lett.*, 2007, **7**, 520-524.

45. X. Zou and S. Dong, *J. Phys. Chem. B*, 2006, **110**, 21545-21550.

46. X. Li, W. Xu, J. Zhang, H. Jia, B. Yang, B. Zhao, B. Li and Y. Ozaki, *Langmuir*, 2004, **20**, 1298-1304.

47. D. Aherne, D. M. Ledwith, M. Gara and J. M. Kelly, *Adv. Funct. Mater.*, 2008, **18**, 2005-2016.

Chapter 5: Experimental

5.1 Chemicals used in the preparation and functionalization of silver nanoparticles.

The following chemical were purchased from Sigma Aldrich and were used without further purification unless otherwise stated.

Name	*Purity*
1,3-Acetonedicarboxylic acid	technical grade
1,3-Diaminopropane	Puriss., ≥99.0% (GC) (Fluka)
1,4-Diaminobutane	Puriss., ≥99.0% (GC) (Fluka)
2-pyrrolidone	≥99%
3-aminopropyltriethoxysilane	≥98%
3-mercaptopropyltriethoxysilane	≥80% (GC), technical
4-aminothiophenol	97%
4-mercaptopyridine	95%
4-methylthiophenol	98% (Aldrich)
Acetone	HPLC grade
Ammonium hydroxide solution	Puriss., 30-33% NH_3 in H_2O (Sigma-Aldrich)
Ascorbic acid	ACS reagent, ≥99%
Crystal violet	ACS reagent (Sigma-Aldrich)
D_2O	99.9 atom% D
Dimethylamine	40 wt% in H_2O (Aldrich)
Ethanol	Absolute alcohol
Ethylene diamine	ReagentPlus®, ≥99% (Sigma-Aldrich)
Gelatin	Ph Eur (Fluka)
Hydrogen peroxide solution	35 wt% in H_2O
Magnesium sulphate	Reagent grade, ≥97%
N-methylpyrrolidone	ACS reagent, ≥99%
N-vinylpyrrolidone	≥99%
Poly(allylamine hydrochloride)	Average Mw ~ 15,000 (Aldrich)
Poly(4-styrene sulfonate)	Average Mw ~ 15,000 powder
Poly(4-styrene sulfonate)	Average Mw ~ 1,000,000 powder
Poly(vinyl alcohol)	Average Mw ~ 89,000-98,000, 99+% hydrolysed
Poly(vinylpyrrolidone)	K15, mol wt ~ 10,000 (Fluka)
Poly(vinylpyrrolidone)	K15, mol wt ~ 55,000 (Fluka)
Potassium bromide	ACS reagent, ≥99%
Silver nitrate	ACS reagent, ≥99%

Sodium borohydride	ReagentPlus®, ≥99%
Sodium bromide	ACS reagent, ≥99%
Sodium chloride	ACS reagent, ≥99%
Sodium dodecylsulfate	ReagentPlus®, ≥98.5% (GC) (Sigma-Aldrich)
Sodium iodide	ACS reagent, ≥99.5%
Sodium silicate solution	Reagent grade (Sigma-Aldrich)
Sucrose	For molecular biology, ≥99.5% (GC)
Tetraethylorthosilicate	99.999% trace metals basis (Aldrich)
Thiophenol	≥99% (Aldrich)
Trisodium citrate	ACS reagent, ≥99%

All water used throughout was first distilled before being purified further by passing through a Millipore Synergy 185 unit. All glassware was rinsed with aqua regia (three parts concentrated hydrochloric acid to one part concentrated nitric acid) and then thoroughly with water and finally Millipore water before use.

5.2 Instrumentation/Characterization

Ultraviolet-visible (UV-vis) spectroscopy was used to follow the reaction process and to characterize the optical properties using 1 cm quartz cuvettes. The following spectrometers were used through the course of this work: Cary Varian, Shimadzu UV-2401PC spectrometer and a Cary 6000i UV-vis-NIR spectrometer.

Transmission electron microscopy (TEM) prior to DATE was performed with a Hitachi H-7000 scanning electron microscope operating at 100 kV using Formvar coated copper grids. It was then carried out on a Jeol 2100 transmission electron microscope operating at 200 kV using Agar® Carbon film grids. UTHSCA Image Tool software was used for measuring the particle dimensions.

Particle sizing and zeta potential measurements were carried out on a Malvern Zetasizer Nano ZS. Sols were first passed through 0.2 μm filters a number of times prior to measurement.

Particles were centrifuged in an Eppendorf 5415D microcentrifuge.

A Bruker Avance 400 NMR was used.

5.3 Preparation of 'added citrate' silver nanoplates

5.3.1 Preparation of seed particles

$AgNO_3$ (5 mg) and TSC (7.4 mg) were dissolved in 100 mL Millipore water. 20 mL of this solution was placed in a 50 mL beaker, in an ice-bath. $NaBH_4$ (600 µL, 0.01 M) was added drop-wise by hand using a micropipette. The seeds were then aged for 3 hours before use in the next step.

5.3.2 Growth from seeds

PVP (1 wt%, 10 mL, Mw = 10,000), seed solution (100 µL), ascorbic acid (50 µL, 0.1 M) and TSC (300 µL, 2.5 x 10^{-2} M) were placed in a 50 mL beaker and stirred together for 3 minutes. $AgNO_3$ (5 x 50 µL, 0.01 M) was added in aliquot with 30 seconds between each addition. The sol was allowed to stir for 5 minutes after the last addition of $AgNO_3$ before being decanted into a foil cover sample tube.

5.4 Acetone precipitation of PVP

PVP (MW 10,000, 2 g) was dissolved in 10 mL H_2O. Acetone (200 mL, HPLC grade) was added drop wise using a dropping funnel. When the acetone addition was complete, the resulting mixture was filtered on 0.45 µm Sartorius filters. The resulting off-white precipitate was dissolved in a small volume of water and then evaporated a reduced pressure. The resulting oil was washed three times with acetone. Any residual solvent was removed under vacuum. The resulting product was an off-white powder.

The acetone washings from the above purification were also evaporated under reduced pressure to yield slightly pink oil.

5.5 Preparation of seed particles by other methods from the literature

From Jana et al.[1]

$NaBH_4$ (10 mM, 600 µL) was added all at once to a 20 mL aqueous solution of $AgNO_3$ and TSC (0.25 mM). Stirring was stopped after 30s and the seeds were used 4 hours later.

From Maillard et al.[2]

Ice-cold $NaBH_4$ (25 mM, 500 µL) was added to a stirring solution of TSC (10 mM, 20 mL) and $AgNO_3$ (5 mM, 500 µL). The solution was stirred fro 5 minutes and aged for 24 hours before use.

From Chen et al.[3]

$NaBH_4$ (10 mM, 600 µL) was rapidly injected into a stirring mixture containing $AgNO_3$ (10 mM, 500µL) and TSC (1.25 mM, 20 mL). The resultant sol was stirred for 3 hours and aged for 6 days under ambient laboratory conditions before use.

From Lu et al.[4]

An aqueous solution of $AgNO_3$ (0.25 mM, 100 mL) was rapidly mixed with TSC (30 mM, 1 mL). Ice-cold $NaBH_4$ (10 mM, 3 mL) was added under vigorous stirring. The stirring was stopped after 30 seconds and the seeds were used after 2 hours.

From Ni et al.[5]

Silver dodecyl sulphate (AgDS) was precipitated from sodium dodecyl sulphate (0.1442 g in 5 mL H_2O) and $AgNO_3$ (0.5 g in 5 mL H_2O) at room temperature. The white solid of AgDS was filtered, dried and recrystallized from warm water to remove any remaining sodium salt.

AgDS (5.5 mg) was dissolved in Millipore water (50 mL). $NaBH_4$ (0.1 M, 600 µL) was added dropwise to 20 mL of this solution under vigorous stirring. A colour change

from colourless to yellow to dark yellow was observed. The sol was allowed to age at 35°C for 2 hours prior to use.

5.6 Preparation of silver nanoparticles by the PVA method

5.6.1 Preparation of seeds

Seeds were prepared as described above in Section 5.3.1

5.6.2 Growth from seeds:

PVA (1 %w/v. 89-98 kDa, 50 mL) and silver nitrate (0.01 M, 1.25 mL) were placed in a beaker and heated to 40°C and kept at this temp for 30 minutes in the dark. Silver seeds (0.5 mL) were added with vigorous stirring followed by ascorbic acid (0.1 M, 0.25 mL). A colour change from colourless to red was observed immediately after the addition of ascorbic acid.

5.7 Sols prepared by the added citrate method and PVA method in the presence of PSSS:

5.7.1 Preparation of seed particles

$AgNO_3$ (5 mg) and TSC (7.4 mg) were dissolved in PSSS (20 mg/L, 100 mL). 20 mL of this solution was placed in a 50 mL beaker, in an ice-bath. $NaBH_4$ (600 µL, 0.01 M) was added drop-wise by hand using a micropipette. The seeds were then aged for 3 hours before use in the next step.

5.7.2 Growth from seeds:

Carried out as detailed above in Sections 5.3.2 and 5.6.2. PSSS was not included in the growth stage.

5.8 Preparation of silver nanoprisms by the 'no added citrate' method.

Distilled H_2O is used throughout the preparation of nanoparticles by this method.

5.8.1 Preparation of seed particles:

Aqueous TSC (5 mL, 2.5 mM), poly(sodium styrenesulphonate) (PSSS; 0.25 mL, 500 mg/L; 1,000 kDa) and $NaBH_4$ (0.3 mL, 10 mM) were combined with vigorous stirring followed by addition of $AgNO_3$ (5 mL, 0.5 mM) at a rate of 2 mL/min using a syringe pump, while stirring continuously.

5.8.2 Growth from seeds

5 mL distilled water, ascorbic acid (75 μL, 10 mM) and various quantities of seed solution were combined followed by addition of $AgNO_3$ (3 mL, 0.5 mM) at a rate of 1 mL/min with vigorous stirring. After synthesis, TSC (0.5 mL, 25 mM) is added to stabilize the particles and the sample is diluted with distilled water as desired.

5.9 Silica coating procedures

5.9.1 Ung *et al*[6].

5.9.1.1 Preparation of the silver sol:

$NaBH_4$ (10 mL, 1 mM) was added to TSC (89 mL, 0.30 mM) in a round bottomed flask. The flask was placed in an ice-bath and left to cool. $AgNO_3$ (1 mL, 0.01 M) was added to the ice-cold solution with vigorous magnetic stirring. The solution turned bright yellow immediately indicating the presence of silver nanoparticles.

5.9.1.2 Priming of the surface with APTES:

APTES (150 μL, 1 mM) was added to the sol under stirring. The sol was then left to stir for 30 minutes to ensure complete complexation of the amine groups with the particle surface.

5.9.1.3 Coating with sodium silicate:

Sodium silicate solution (3 mM, 1.2 mL) was added to the reaction vessel, with vigorous magnetic stirring. The resultant dispersion was than allowed to stand for at least one day to ensure complete polymerisation of the silica onto the particle surface. The particles were then transferred into ethanol (ethanol/water volume ratio of 4:1). TEOS (300 μL) followed by ammonia (2 mL, 28 %) was then added with stirring and the sol was allowed to stir gently for 12 hours overnight. It was then centrifuged at 6,000 rpm for 30 minutes and the pellets were redispersed in EtOH.

5.9.3 Graf *et al.*[7]

5.9.3.1 Synthesis of the particles:

PVP (1.5 g, MW 10,000) was dissolved in ethylene glycol (75 mL) at room temperature. $AgNO_3$ (50 mg) was added with stirring. The suspension was then stirred at room temperature until complete dissolution of the silver nitrate. The system was heated up to 120°C and kept at this temperature for 1 hour. The suspension changed colour in this time from clear to brown to orange. At the end of this period, the reaction vessel was allowed to cool at room temperature in a water bath. 500 mL acetone was added followed by centrifugation at 3000 rpm for 30 minutes. The resultant precipitates were redispersed in the minimum volume of EtOH (~15ml). The solution was left to stand overnight. It was then centrifuged again at 3000 rpm for 40 minutes, to ensure precipitation of the maximum amount of particles. The supernatant was removed.

5.9.3.2 Synthesis of the Silica Shell:

The sediments were redispersed in a solution of ammonia in ethanol. (4.2 vol% ammonia {33wt% NH_3 in water} in ethanol) (9.9 mL). Immediately after this, a TEOS solution (10 vol% in EtOH, 100 μL) was added and the reaction mixture was left to stir for a minimum of 12h to ensure complete condensation of the silica.

5.9.3.3 Volhard titration[8]

This involved the titration of the supernatant removed by centrifugation against ammonium thiocyanate, using ammonium iron sulphate as the indicator. At first a white precipitate was produced giving the liquid a milky white appearance. As each drop of thiocyanate was introduced, it produced a reddish brown cloud, which quickly disappeared on shaking. When all the silver(I) has been precipitated as white silver thiocyanate, the first excess of titrant and the iron(III) indicator react and form a soluble red complex- this is taken as the endpoint.

$$Ag^+ + SCN^- \leftrightarrow AgSCN \qquad \textbf{Equation 5.1}$$

$$Fe^{3+} + SCN^- \leftrightarrow Fe(SCN)^{2+} \qquad \textbf{Equation 5.2}$$

5.9.4 Kobayashi et al[9]

5.9.4.2 Preparation of the nanoparticles

A green 'added citrate' sol (10 mL) using 0.7 mM TSC was prepared at 50°C using the method described above in Section 5.3. The sol was centrifuged at 13,200 rpm for 30 minutes and the pellets were redispersed in water.

5.9.4.3 Coating procedure

To 10 mL sol, EtOH (40 mL) was added with stirring, TEOS (1 mM, 500 µL) was then added followed by DMA (25 wt%, 100 µL). The sol was left to stir overnight before being centrifuged at 6,000 rpm for 30 minutes and the pellets redispersed in EtOH.

5.9.5 Mercaptopropyltriethoxysilane (MPTES) primed method

5.9.5.1 Preparation of the nanoparticles

A green 'added citrate' sol (10 mL) using 0.7 mM TSC was prepared at 50oC using the method described above in Section 5.3. The sol was centrifuged at 13,200 rpm for 30 minutes and the pellets were redispersed in water.

5.9.5.2 Coating procedure

To 10 mL redispersed sol, MPTES (1.35 mM, 200 μL) was added and allowed to stir for 30 minutes. EtOH (40 mL) was the added followed by TEOS (0.1 M, 500 μL). DMA (25%, 100 μL) was then added and the sol was allowed to stir overnight before being centrifuged at 6,000 rpm for 30 minutes and the pellets redispersed in EtOH.

5.9.6: Diaminopropane primed method

5.9.6.1 Preparation of the nanoparticles

A green 'added citrate' sol (10 mL) using 0.7 mM TSC was prepared at 50°C using the method described above in Section 5.3. The sol was centrifuged at 13,200 rpm for 30 minutes and the pellets were redispersed in water.

5.9.6.2 Coating procedure

To 10 mL redispersed sol, diaminopropane in water (10 mM, 200 μL) was added and allowed to stir for 30 minutes. EtOH (40 mL) was the added followed by TEOS (0.1 M, 500 μL). DMA (25%, 100 μL) was then added and the sol was allowed to stir overnight before being centrifuged at 6,000 rpm for 30 minutes and the pellets redispersed in EtOH.

5.10 Anion etching experiments

A 1 mL aliquot of the sol to be examined was placed in a 2 mm quartz cuvette and the UV-vis spectrum was recorded. A nominal volume of NaCl was then added (to avoid dilution of the sol). The cuvette was stoppered, shaken and then replaced in the spectrometer. A number of scans over a set period of time were then recorded using the Scan software on the Cary 50 spectrometer.

[NaCl]	Volume added
100 mM	40 μL, 2.5 M
10 mM	40 μL, 0.25 M
1 mM	4 μL, 0.25 M

5.11 Functionalization with Gelatin

A sol was prepared as described above in Section 5.7. It was then centrifuged at 13,200 rpm for 30 minutes, the supernatant was removed and the pellets were redispersed in 0.1 wt% gelatin solution. It was then decanted into a sample tube, capped and left undisturbed under ambient laboratory conditions for the required period of time. The sol was then centrifuged at 13,200 rpm for 30 minutes and the pellets were redispersed back to their original volume with H_2O.

5.12 LbL functionalization

Gelatin stabilized silver nanoparticles were prepared as described above in Section 5.11. A 5.56 mg/mL aqueous poly(allylamine hydrochloride) (PAH) solution was prepared. This solution was sonicated and then stirred for 1 hour at room temperature prior to use. 5 mL of this PAH solution was placed in a 50 round bottomed flask. 5 mL of the gelatin functionalized sol was added slowly drop-wise with vigorous magnetic stirring. The sol was then allowed to stir overnight in the dark for 12 hours, before being centrifuged at 8,000 rpm for 30 minutes. The coloured supernatant was removed and the pellets were redispersed back to their original volume with H_2O. A 5.56 mg/mL aqueous poly(sodium 4-styrenesulfonate) (PSSS) solution was prepared. This solution was sonicated and then stirred for 1 hour at room temperature prior to use. 5 mL of this PSSS solution was placed in a 50 round bottomed flask. 5 mL of the gelatin functionalized sol was added slowly dropwise with vigorous magnetic stirring. The sol was then allowed to stir overnight in the dark for 12 hours, before being centrifuged at 8,000 rpm for 30 minutes.

5.13 Ion exchange of the poly(allylamine hydrochloride)

6 mL, 55.6 mg/mL aqueous solution of PAH was prepared. 3 x 10 cm length of Spectra/Por Biotech Regenerated Cellulose Dialysis Membranes MWCO:3,500 were left to soak in distilled water for 4 hours. After this time the membranes were filled with 2 mL of the PAH solution. They were left to stir in $NaNO_3$(1 mM) solution for 4 hours. The buffer

was the replaced and the filled membranes were left to stir for 8 hours. The buffer was then replaced a second time and the filled membranes were allowed to stir for a further12 hours. The polymer was the recovered by evaporation under reduced pressure. A yield of 96 mg was recorded. Due to the unstable nature of this nitrated polymer the resultant solid was quickly dissolved in 17 mL distilled H2O to create a stock solution.

5.14 SERS experiments

All SERS experiments were carried out in the laboratory of Dr. Steven Bell in the School of Chemistry and Chemical Engineering, Queen's University Belfast.

5.14.1 785 nm laser excitation

The SERS spectra were recorded on an Avalon Instruments RamanStation-FS with an excitation wavelength of 785 nm. The laser power was 100 mW and the resolution of the instrument was 4 cm^{-1}. An exposure time of 10 s was used with two exposures to record each spectrum. All experiments were carried out in a 96 well polypropylene microtitre plate. 200 µL of the required sol was used.

5.14.2 532 nm laser excitation

The SERS spectra were recorded on an Avalon Instruments Raman*Micro*-EZ with an excitation wavelength of 532 nm. The laser power was 100 mW and the resolution of the instrument was 4 cm^{-1}. An exposure time of 10 s was used with two exposures to record each spectrum. All experiments were carried out in a 96 well polypropylene microtitre plate. 200 µL of the required sol was used.

5.15 References:

1. N. R. Jana, L. Gearheart and C. J. Murphy, *Chem. Commun.*, 2001, 617-618.
2. M. Maillard, P. Huang and L. Brus, *Nano Lett.*, 2003, **3**, 1611-1615.
3. S. Chen and D. L. Carroll, *J. Phys. Chem. B*, 2004, **108**, 5500-5506.
4. L. Lu, A. Kobayashi, K. Tawa and Y. Ozaki, *Chem. Mater.*, 2006, **18**, 4894-4901.
5. C. Ni, P. A. Hassan and E. W. Kaler, *Langmuir*, 2005, **21**, 3334-3337.
6. T. Ung, L. M. Liz-Marzan and P. Mulvaney, *Langmuir*, 1998, **14**, 3740-3748.
7. C. Graf, D. L. J. Vossen, A. Imhof and A. van Blaaderen, *Langmuir*, 2003, **19**, 6693-6700.
8. J. Mendham, R. C. Denney, J. D. Barnes and M. J. K. Thomas, *Vogel's Qualitative Inorganic Analysis*, 6th edn., Prentice Hall, 2000.
9. Y. Kobayashi, H. Katakami, E. Mine, D. Nagao, M. Konno and L. M. Liz-Marzan, *J. Colloid Interface Sci.*, 2005, **283**, 392-396.

Chapter 6:
Conclusion and Future Work

The aims of the work presented in this thesis were:

1. To develop new aqueous based methods for the preparation of well-defined, monodisperse silver nanoparticles.
2. To functionalize these nanoparticles with a view towards further biofunctionalization
3. To examine some applications of the prepared nanoparticles.

6.1 Preparation of silver nanoparticles

The synthesis of silver nanoparticles of tuneable colour via a seed mediated method involving trisodium citrate and a polymer such as poly(vinylpyrolidone) (PVP) has been described. The effects of different parameters for example time, temperature and concentration of citrate have been investigated. The colour of the sols may be tuned by varying the concentration of citrate. Sols prepared at room temperature exhibit a blue- shift of the in-plane dipole resonance with time. As the temperature at which the reaction is carried out is increased from room temperature, well-defined triangular plates with enhanced stability are produced. However the procedure does lead to mixture of shapes being produced. The presence of the polymer PVP was not found to be an important factor in determining the final morphology of the nanoparticles produced. However, the purity of the PVP used was found to be crucial to the stability of the sols produced. An impurity was isolated from commercially available PVP which caused etching the particles. The reliability of the method described above was found to be very dependent on the structure of the seed particles. As such, a growth mechanism highlighting both the role of the underlying structure of the seed particles and the presence of an organic molecule capable of adsorbing selectively onto certain crystallographic faces of the seeds has been suggested.

Experiments carried out to improve the reproducibility of an existing synthesis of silver nanoparticles developed within the group which employed poly(vinylalcohol), have been outlined. Two key factors which greatly enhance the batch to batch reproducibility have been identified namely the exclusion of light from the growth step of the synthesis and

the inclusion of the anionic polymer poly(4-styrene sulfonate) sodium salt (PSSS) during the synthesis of the seed particles.

The role of PSSS in the seed preparation was explored in the two syntheses described above and also a third 'no added citrate' method. It was concluded that the presence of PSSS before or during the growth of the seed particles was necessary to prevent the formation of nanoparticles with a diversity of shapes and sizes. Possible explanations as to why the presence of PSSS in the growth of the seed particles is so important have been proposed

6.2 Functionalization of silver nanoparticles

The functionalization of silver nanoparticles prepared by the added citrate method (and variations there of) and the stability of these particles before and after functionalization were investigated. Various routes for the synthesis of silica coated silver nanoparticles were attempted with two new methods for the production of coated particles being developed, albeit with limited reproducibility. Both new methods consisted of a modified Stöber growth procedure. The first consisted of priming the surface of the silver nanoparticles with 3-mercaptopropyltriethoxysilane while the second involved priming the surface with 1,3-diaminopropane. Different parameters in this second synthesis were investigated and it was found that the thickness of the silica shells could be tuned in two different ways, firstly by varying the concentration of alkoxide precursor and secondly by adjusting the concentration of the 1,3-diaminopropane used. The disadvantage of this method is its limited reproducibility. However when silica does occur the advantage that this method presents is that very thin, uniform silica coats (~7 nm) could be produced.

The stability of the silver nanoparticles was found to be sensitive to the present of various different anions, in particular the halide anions. This stability was enhanced by redispersion in gelatin solution and aging over a four day period. The modification of the surface chemistry in the presence of gelatin was confirmed by zeta-potential measurements

and stability tests with NaCl. The layer by layer approach was attempted, in order to functionalize the silver nanoparticles with polyelectrolytes of alternating charge.

6.3 Applications of shaped silver nanoparticles

The suitability of silver nanoparticles prepared by the 'added citrate' and 'no added citrate' (as discussed in Chapter 2) as good SERS substrates was investigated. Initial experiments confirmed the presence of citrate on the surface of nanoparticles prepared by the 'added citrate' method at room temperature.

Aggregation of the nanoparticles in aqueous solution is a key process in the observation of SERS spectra and it was demonstrated that is desirable to have the analyte present before aggregation of the SERS analytes in order to maximise the intensity of the observed SERS spectrum. The nature of the aggregating agent used was also found to be important as TEM experiments confirmed that when $MgSO_4$ was used the integrity of the initial particles was destroyed.

Large SERS enhancements were found for aggregated silver nanoprisms in solution. The ease with which the in-plane dipole resonance of the silver nanoprisms can be tuned across the visible into the near-infrared region of the spectrum makes nanoprisms prepared by this method desirable as substrates for SERS measurements with varying laser excitation wavelength as it was found that maximum SERS intensities were observed when there was an overlap between excitation wavelength and the maximum absorbance of the substrate.

6.4 Future work

With respect to the synthesis of silver nanoparticles a tremendous amount of progress has been made. The holy grail of nanoparticle synthesis is the production of 'one size, one shape' by a rapid environmentally friendly method. The 'added citrate' method has been developed into the 'no added citrate method' so that the concentration of spherical nanoparticles produced is minimal and the dominant morphology is silver nanoprisms. It

has been proposed, based on TEM analysis of the nanoprisms, that it is the defect structure of the seed that is the most important factor in determining the end morphology of the nanoparticles produced.[1] It has also been shown that poly(sodium styrenesulphonate) (PSSS) is a key ingredient in the production of nanoprisms although at present we have no information on precisely how PSSS influences the defect structure of the seeds. Future work in this area would involve investigating other molecules with a sulfonate moiety to see if they have a similar effect. The study could also be extended to examine other anionic polymers. Also if it is the defect structure of the seed nanoparticle that determines the final morphology of the nanoprisms, it would be interesting to investigate if a similar synthetic procedure could be used to prepared nanoprisms of other fcc metals such as gold, platinum and palladium.

In the area of the functionalization of silver nanoparticles, although significant progress has been made, in that silica coated silver nanoprisms have been produced, this achievement has been marred by the limited reproducibility of the procedure. Future work in this area would involve improving this batch to batch reproducibility. The ultimate aim of the work described in Chapter 3 was to functionalize these nanoparticles with a view towards further biofunctionalization. It is my opinion that the area of in-situ functionalization needs to be explored further as an alternative to post-synthetic modification of the nanoparticles. This work would be an extension of the investigation of different molecules that could be used to control the defect structure of the seed particles, as mentioned above. PSSS has been know as a cheap alternative to DNA so it would be interesting to investigate if this approach could be used to both control the defect structure of the seeds while also biofunctionalizing the resulting nanoparticles

It has been shown that shaped silver nanoparticles can be used as good SERS substrates and are in fact superior to the Lee and Meisel colloid that is at present used as the standard substrate. However, as shown above the interaction of analyte molecule with the substrate is an important factor in determining the intensity of the SERS spectrum observed. In order for these nanoparticles to be used as a generic SERS substrate the surface chemistry needs to be adjusted to suit the analyte. For example, of the current

samples it is unlikely that negatively charged molecules would adsorb onto the nanoparticle surface so that a SERS spectrum could be recorded. Work also needs to be carried out on the original system as it stands so that the limit of detection can be lowered significantly.

At present, the area of silver nanoparticles is an exciting one to be working in. The past decade has seen an explosion in the uses of silver nanoparticles in areas such as hygiene (from socks to washing machines to refrigerators), medicine (wound dressings) and electronics (conductive inks). However to date, extensive toxicological data has not been collected. This is an important aspect to be considered if the use of silver nanoparticles and indeed nanoparticles in general is to become commonplace.

In conclusion, the next few years will see important progress being made in the area of nanotechnology and as such there has been a lot done but there's more to do!

6.5 References

1. D. Aherne, D. M. Ledwith, M. Gara and J. M. Kelly, Adv. Funct. Mater., 2008, 18, 2005-2016.